Paul Johann Fasching, MSc ETH

Natural Gas as Fuel for Monovalent and Dual Fuel Combustion Engines – an Experimental and Numerical Study

DISSERTATION

to attain the degree of

Doktor der technischen Wissenschaften

submitted to the

Technische Universität Graz

Examiner

Univ.-Prof. Dipl.-Ing. Dr.techn. Helmut Eichlseder
Institute of Internal Combustion Engines and Thermodynamics

Co-Examiner

Prof. Dr. Christopher Onder
Institute for Dynamic Systems and Control, ETH Zürich

Graz, October 2017

Institut für Verbrennungskraftmaschinen und Thermodynamik
Head: Univ.-Prof. Dipl.-Ing. Dr.techn. Helmut Eichlseder

Vorwort

Viele Menschen haben zum Gelingen dieser Arbeit beigetragen, an die ich meinen Dank richten möchte. An erster Stelle bedanke ich mich bei meinen Eltern und meiner Familie für die Unterstützung in unterschiedlichster Form über all die Jahre hinweg. Ohne euch hätte ich das Bisherige nicht erreichen können und es hätte auch nicht dieselbe Bedeutung. Ich bedanke mich auch ganz herzlich bei Prof. Helmut Eichlseder für das Ermöglichen meiner Dissertation am Institut für Verbrennungskraftmaschinen und Thermodynamik, die Unterstützung und die fachlichen Diskussionen, sowie für die Infrastruktur am Institut, die ihresgleichen sucht. Weiters danke ich herzlich Peter Grabner und Eberhard Schutting für die unzähligen Diskussionen, Hilfestellungen und Anmerkungen zu meiner Arbeit, sowie Prof. Christopher Onder für die Bereitschaft meine Dissertation zu begutachten.

Die experimentellen Untersuchungen zur Dual Fuel Verbrennung habe ich gemeinsam mit meinem Kollegen Florian Sprenger durchgeführt. Wir haben lange Tage gemeinsam am Prüfstand verbracht, Probleme gelöst, Ergebnisse diskutiert und Veröffentlichungen verfasst, danke für die gute Zusammenarbeit und die gegenseitige Unterstützung. Sehr herzlich danke ich auch Stefan Kammerstätter, unserem Ansprechpartner bei BMW Steyr, für das große Engagement, Michael Barth für seinen großen Einsatz am Prüfstand und Josef Pfeifer für die tatkräftige Hilfe während seiner Diplomarbeit.

Auch im HDGAS Projekt wurde ich von mehreren Seiten unterstützt. Ich bedanke mich ganz herzlich bei Stefano Golini von FPT Industrial, für die angenehme und unkomplizierte Zusammenarbeit, Anton Arnberger von AVL Graz für die gute Zusammenarbeit und die fachlichen Diskussionen, sowie Lukas Nenning für seinen Beitrag im Rahmen seiner Bachelorarbeit.

Abschließend möchte ich mich noch bei meinen Arbeitskollegen am Institut für die schöne Zeit und das gute Arbeitsklima bedanken. Die Kollegialität und die gegenseitige Unterstützung, die ich am Institut erleben durfte ist wirklich bemerkenswert.

Eidesstattliche Erklärung
Affidavit

Ich erkläre an Eides statt, dass ich die vorliegende Arbeit selbstständig verfasst, andere als die angegebenen Quellen/Hilfsmittel nicht benutzt, und die den benutzten Quellen wörtlich und inhaltlich entnommenen Stellen als solche kenntlich gemacht habe.

I declare that I have authored this thesis independently, that I have not used other than the declared sources/resources, and that I have explicitly indicated all material which has been quoted either literally or by content from the sources used.

Graz, am 24.10.2017 Paul Fasching

Abstract

One viable possibility to achieve a reduction in the CO_2 emissions from transportation is to reduce the carbon-intensity of the vehicle fuel. Natural gas (NG) consists mainly of methane (CH_4) which has the lowest carbon-intensity among all fossil fuels. When NG is used CO_2 emissions can be reduced by approx. 25 % compared to diesel and gasoline if the fuel efficiencies are equal. In this context two different concepts for internal combustion engines which utilise natural gas as a fuel were studied both experimentally and numerically.

The first concept is a novel natural gas-diesel dual fuel (DF) combustion process for passenger car engines. The conventional NG-diesel DF concept features NG port fuel injection and direct injection of a diesel pilot quantity to ignite the mixture. This concept suffers from high unburned CH_4 emissions in part load operation due to over-lean air-NG mixtures. The novelty of the proposed concept is a low-pressure direct injection of NG to stratify the air-NG mixture. Thereby, the local air-NG equivalence ratio can be reduced and a significant reduction of the CH_4 emission is achieved. The concept was named DDI – *Dual Direct Injection* and investigated experimentally on the engine test bench. The influence of the main application parameters on the combustion and the results of a variation of the compression ratio are presented. Based on these results, the calibration of the DDI concept was optimised in four stationary load points and an operating strategy was developed for the engine operating map. Along with the DDI concept three more combustion processes were realised on the same base engine: conventional diesel compression ignition, NG spark ignited operation and conventional NG-diesel DF combustion with port fuel injection. The optimised DDI concept is compared with these combustion processes and with a gasoline spark ignited engine. Engine-out pollutant emissions on the level of modern gasoline engines are achieved with the DDI concept. Compared to conventional DF combustion the unburned hydrocarbon emissions are reduced by up to 75 % at light loads. A CO_2 reduction of between 20 % and 29 % is achieved in comparison to the diesel and the gasoline engine. Despite these significant achievements, the exhaust gas aftertreatment of the remaining CH_4 emissions is an unsolved challenge with current technology as the exhaust gas temperature is too low for the catalytic oxidation of CH_4.

The second concept studied is a novel monovalent and stoichiometric NG spark ignited engine with direct injection for heavy duty commercial vehicles. These investigations were conducted numerically by means of 1D engine simulations. The heavy duty NG engines available today are derivations of existing diesel engines. This results in penalties in fuel efficiency besides other disadvantages such as the emission performance, since the base engines are optimised for diesel compression ignition. Thus, as part of the EU project HDGAS for the first time a modern heavy duty engine was developed dedicatedly for NG operation together with partners. The engine features a combustion chamber design optimised for NG spark ignition comprising of a pent roof combustion chamber, angular valves and tumble charge motion. Furthermore, NG direct injection, high-frequency (*Corona*) ignition, cam phasing, cooled exhaust gas re-

circulation (EGR) and a waste gate turbocharger are deployed. By the introduction of these novel technologies in heavy duty engines a 10 % increase in torque and rated power and a 10 % reduction in greenhouse gas emissions in the WHTC should be achieved compared to existing heavy duty NG engines of the model year 2013. The thermodynamic layout for this engine was performed by means of the 1D engine simulations. Essential engine components were defined and the efficiency potential of several of the introduced technologies was investigated. In this work the influence of EGR in a heavy duty NG spark ignited engine in part load and full load operation is discussed. Early and late Miller valve timing in the presence of external EGR is reviewed and contrasted with conventional valve lift profiles. Furthermore, the potential of cam phasing in combination with EGR is analysed for standard and early Miller valve lift profiles and indications for the operating strategy are given. Finally, the simulation results are confirmed with single-cylinder engine measurements performed by a project partner and the combined effect of these three measures is assessed. The introduction of EGR, early Miller timing and cam phasing raises the net indicated efficiency by $3\,\%_{\mathrm{Pt.}}$ respectively reduces the specific fuel consumption by 7.2 % in the important part load operating point relevant for highway driving.

Kurzfassung

Eine Möglichkeit um die CO_2 Emissionen zu senken, die durch den Verkehr verursacht werden, ist, die Kohlenstoffintensität des Kraftstoffs zu reduzieren. Erdgas besteht großteils aus Methan (CH_4), das die geringste Kohlenstoffintensität aller fossilen Kraftstoffe aufweist. Dadurch können die CO_2 Emissionen im Vergleich zu Diesel- und Benzinmotoren um ca. 25 % reduziert werden unter der Voraussetzung gleicher Wirkungsgrade. Aus diesem Zusammenhang heraus wurden zwei verschiedene Konzepte für Verbrennungsmotoren mit Erdgas als Kraftstoff experimentell und numerisch untersucht.

Bei dem ersten Konzept handelt es sich um ein neues Erdgas-Diesel Dual Fuel (DF) Brennverfahren für PKW Motoren. Bei konventionellen Erdgas-Diesel DF-Konzepten wird Erdgas in das Saugrohr eingebracht und durch Direkteinspritzung einer Dieselpilotmenge entzündet. Dieses Konzept führt zu hohen CH_4 Emissionen im Teillastbetrieb durch ein zu mageres Erdgas-Luftgemisch. Die Neuheit des vorgestellten Konzepts ist eine Niederdruck-Direkteinblasung von Erdgas um eine Schichtung des Erdgas-Luftgemisches zu erreichen. Dadurch kann das örtliche Luftverhältnis des Erdgas-Luftgemisches reduziert und somit die CH_4 Emissionen stark gesenkt werden. Das Konzept wurde DDI – *Dual Direct Injection* genannt und experimentell am Motorenprüfstand untersucht. Der Einfluss der wichtigsten Applikationsparameter auf die Verbrennung und die Ergebnisse einer Variation des Verdichtungsverhältnisses werden gezeigt. Basierend auf diesen Ergebnissen wurde der Betrieb des DDI-Konzepts in vier stationären Betriebspunkten optimiert und eine Betriebsstrategie für das Motorkennfeld entwickelt. Neben dem DDI-Konzept wurden mit dem gleichen Grundmotor noch drei weitere Brennverfahren realisiert: normaler Dieselbetrieb, ein Erdgasottomotor mit Fremdzündung sowie das konventionelle DF-Konzept mit Saugrohreinblasung von Erdgas. Das optimierte DDI-Konzept wird mit diesen Brennverfahren verglichen, sowie mit einem Benzinottomotor. Mit dem DDI-Konzept können Abgasrohemissionen auf dem Niveau moderner Benzinottomotoren realisiert werden. Im Vergleich zum konventionellen DF-Konzept werden mit dem DDI-Konzept bei niedriger Last die unverbrannten HC Emissionen um bis zu 75 % reduziert. Die CO_2 Emissionen werden zwischen 20 % und 29 % im Vergleich zum Diesel- und dem Benzinottomotor gesenkt. Trotz dieser eindrucksvollen Ergebnisse ist die Abgasnachbehandlung der verbleibenden CH_4 Emissionen mit heutiger Technologie ein ungelöstes Problem, da die Abgastemperaturen zu niedrig sind für eine katalytische Oxidation von CH_4.

Bei dem zweiten Konzept handelt es sich um einen neuen monovalenten und stöchiometrischen Erdgasottomotor mit Direkteinblasung für schwere Nutzfahrzeuge (NFZ). Diese Untersuchungen wurden numerisch mit Hilfe von 1D Motorsimulationen durchgeführt. Derzeitige Erdgasmotoren für schwere NFZ werden von bestehenden Dieselmotoren abgeleitet. Dies führt zu Einbußen im Wirkungsgrad, sowie anderen funktionalen Nachteilen wie das Emissionsverhalten, da die Grundmotoren für den Dieselbetrieb optimiert sind. Im Rahmen des EU-Projekts HDGAS wurde daher gemeinsam mit Partnern zum ersten Mal ein moderner Erdgasmotor für

schwere NFZ entwickelt, der von Grund auf für den Betrieb mit Erdgas ausgelegt ist. Dieser Motor verfügt über einen für Ottomotoren optimierten Brennraum mit kuppelförmigem Brennraumdach, schräg stehenden Ventilen und Tumble Ladungsbewegung. Weiters kommen Direkteinblasung, eine Hochfrequenzzündung (*Corona*), variable Steuerzeiten, gekühlte Abgasrückführung (AGR) und ein Wastegate-Turbolader zum Einsatz. Durch diese im NFZ-Segment neuen Technologien soll eine Steigerung des Drehmoments und der Nennleistung um 10 % erzielt werden, sowie eine Reduktion der Treibhausemissionen um 10 % im WHTC im Vergleich zu bestehenden Erdgasmotoren aus dem Modelljahr 2013. Mittels der 1D Motorsimulation wurde die thermodynamische Auslegung dieses Motors durchgeführt. Es wurden wesentliche Komponenten des Motors definiert und das Potenzial der eingesetzten Technologien bewertet, den Kraftstoffverbrauch zu senken. Es wurden dabei folgende Schwerpunkte gewählt: Der Einfluss von AGR in der Teillast und an der Volllast wird gezeigt. Frühe und späte Miller Steuerzeiten werden bei gleichzeitigem Einsatz von externer AGR analysiert und mit konventionellen Steuerzeiten verglichen. Schließlich wird das Potenzial variabler Steuerzeiten in Kombination mit AGR für konventionelle und frühe Miller Ventilhubkurven bewertet und Richtwerte für eine Betriebsstrategie gegeben. Abschließend werden die Simulationsergebnisse mit Messungen am Einzylindermotor verifiziert, die von einem Partner durchgeführt wurden und der gemeinsame Einfluss der drei untersuchten Maßnahmen bewertet. Die Kombination von AGR mit variablen Steuerzeiten und frühen Miller Ventilhubkurven steigert den indizierten Wirkungsgrad um 3 $\%_{\text{Pkt.}}$, beziehungsweise reduziert den spezifischen Verbrauch um 7.2 % im wichtigen Teillastbetriebpunkt der die Autobahnfahrt widerspiegelt.

Contents

Symbols and Abbreviations

Latin Symbols

$I_{w,s}$	MJ/m^3	Upper Wobbe Index
L_{st}	kg/kg	Stoichiometric air-fuel ratio
M	Nm	Brake torque
m	kg	Mass
n	min^{-1}	Engine speed
p_{Diesel}	bar	Diesel rail pressure
$p_{exhaust}$	bar	Exhaust manifold pressure
p_{intake}	bar	Intake manifold pressure
p_{NG}	bar	Natural gas injection pressure
Q_{LHV}	kJ/kg	Lower heating value
T_{intake}	°C	Intake manifold temperature
V_c	dm^3	Clearance volume
V_d	dm^3	Displacement
x_{NG}	%	Natural gas energy fraction

Greek Symbols

ε	–	Compression ratio
$\Delta\zeta_{IC}$	%	Unburned species
η_e	%	Brake thermal efficiency
$\eta_{i,g}$	%	Gross indicated efficiency
$\eta_{i,n}$	%	Net indicated efficiency
λ_{bowl}	–	Air-natural gas equivalence ratio in the piston bowl
λ_{global}	–	Global air-fuel equivalence ratio
λ_{local}	–	Local air-fuel equivalence ratio
λ_{NG}	–	Air-natural gas equivalence ratio
φ_e	°CA	Exhaust cam phasing angle
φ_i	°CA	Intake cam phasing angle

Abbreviations

BDC	Bottom dead centre	DDI	Dual direct injection
BEV	Battery electric vehicle	DF	Dual fuel
BMEP	Brake mean effective pressure	DI	Direct injection
CFD	Computational fluid dynamics	DOE	Design of experiments
CH_4	Methane	ECU	Engine control unit
CNG	Compressed natural gas	EAS	Exhaust aftertreatment system
CO	Carbon monoxide	EGR	Exhaust gas recirculation
CO_2	Carbon dioxide	EGT	Exhaust gas temperature
COV	Coefficient of variation	EVO	Exhaust valve opening

FMEP	Friction mean effective pressure in bar
FSN	Filter smoke number
FTP	Federal Test Procedure
GHG	Greenhouse gas
GWP	Global warming potential
HC	Hydrocarbon
H/C	Hydrogen-carbon
HCCI	Homogeneous charge compression ignition
HD	Heavy duty
HDV	Heavy duty vehicle
HPDI	High-pressure direct injection
HRR	Heat-release rate
IVC	Intake valve closing
IMEP	Indicated mean effective pressure in bar
LNG	Liquefied natural gas
LNT	Lean nitrogen oxide trap
MFBxx	xx % conversion point of the net heat-release in °CA
MOC	Methane oxidation catalyst
N_2	Nitrogen
NEDC	New European Driving Cycle
NO_x	Nitrogen oxide
NG	Natural gas
NMHC	Non-methane hydrocarbon
PC	Passenger car
PCCI	Premixed charge compression ignition
PFI	Port fuel injection
PHEV	Plug-in hybrid electric vehicle
PMEP	Pumping mean effective pressure in bar
PoliMi	Politecnico di Milano
PPCI	Partially premixed compression ignition
RCCI	Reactivity controlled compression ignition
RCEM	Rapid compression expansion machine
RDE	Real driving emissions
SCE	Single-cylinder engine
SCR	Selective catalytic reduction
SI	Spark ignited
SOI	Start of injection in °CA
TDC	Top dead centre
TWC	Three-way catalyst
VNT	Variable nozzle turbine
WHTC	World Harmonised Transient Driving Cycle
WLTC	Worldwide Light Duty Test Cycle

1 Introduction

The influence of human activities on our environment should be kept to a level that is as low as possible. Global warming has been observed over the past century as Figure 1.1 demonstrates. It is reported that the average surface temperature of the Earth in the period of 1850 – 1900 and 2003 – 2012 increased by 0.78 °C. There is high confidence that more than half of the temperature increase from 1951 to 2010 was caused by an anthropogenic increase in greenhouse gas (GHG) concentration in the atmosphere and other anthropogenic effects such as changes in land use [94].

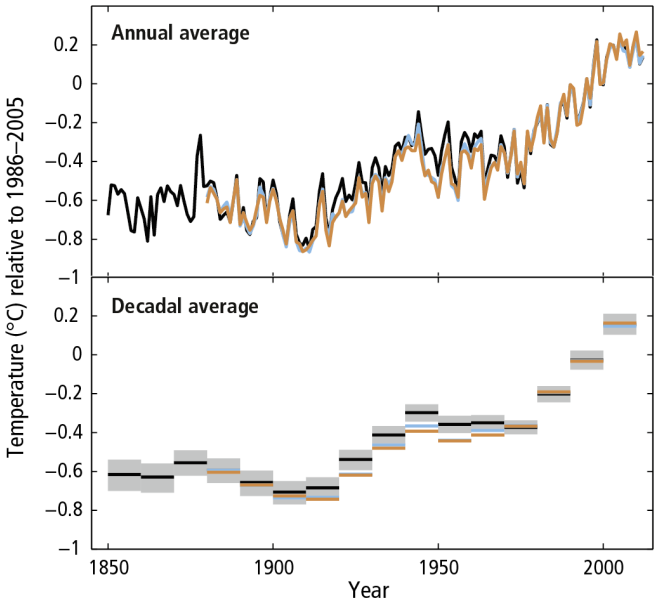

Figure 1.1: The observed globally averaged combined land and ocean surface temperature [94]. The colours indicate different datasets and the grey bars the uncertainty of the decadal average for one dataset.

Figure 1.2 a gives measurements of the carbon dioxide (CO_2) concentration in the atmosphere from 1500 until 2016. In pre-industrial eras the CO_2 concentration was stable at approx. 280 ppm. Since 1750 it has increased exponentially by more than 40 % to 400 ppm. Figure 1.2 b displays estimates of the yearly CO_2 emissions due to the use of fossil fuels. This also exhibits an exponential growth from near zero in 1751 to 35.8 Gt CO_2 in 2013. It is estimated that CO_2 accounts for 78 % of total GHG emissions making it the most important GHG. Models predict that without additional mitigation efforts the global surface temperature will rise by 3.7 °C to 4.8 °C by 2100 compared to pre-industrial levels. This is likely to increase the frequency and intensity of extreme weather events such as heat waves and extreme precipitation, threatening our ecological system. If the GHG concentration is kept below the equivalent of 500 ppm CO_2

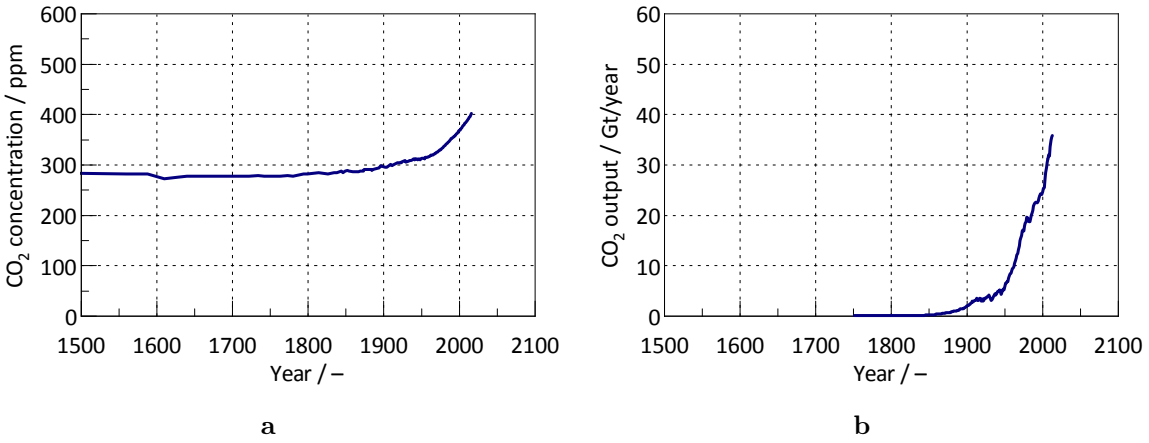

Figure 1.2: **(a)** CO_2 concentration in the atmosphere since 1500 [66, 80] and **(b)** estimates of the yearly CO_2 output due to the use of fossil fuels from 1751 to 2013 [14].

it is likely that global warming can be limited to 2 °C in 2100. This requires a reduction of GHG emissions of 40 % to 70 % by 2050 compared to 2010 [94]. This ambitious target was accepted in the *Paris Agreement* during the United Nations Climate Change Conference in Paris in 2015 [127].

Figure 1.3 states the distribution of GHG emissions in 2010. Transportation accounts for 14 % of the world's total GHG emissions which is the fourth largest share after electricity and heat production, agriculture and industry. Transport consumes 28 % of the total end-use energy and is responsible for 53 % of the global primary oil consumption. It is the fastest growing share among all energy end-use sectors, doubling output since 1970 [27]. Reducing the carbon intensity of transportation thus represents an important step. The Intergovernmental Panel on Climate Change lists four principal pathways to reduce the GHG emissions of transport [27]:

- Reducing the carbon intensity of the fuel (e.g. gasoline, natural gas, renewable energy)
- Reducing the energy intensity of transport (e.g. increasing the efficiency of vehicles, promoting an economic driving style or raising vehicle occupancy)
- Reducing the number of journeys or the distances travelled
- Changing the share of various modes of transport (e.g. aircraft, private passenger car, public transport, cycling, walking)

70 % of transport related GHG emissions result from road vehicles with light duty and heavy duty vehicles being the major contributors [27]. It is thus vital to reduce the GHG emissions caused by road vehicles and laws have been enacted in all key markets to limit the CO_2 emission of passenger cars (PCs). Through this significant incentives have been created to increase the efficiency of passenger cars and to reduce the carbon intensity of the fuel. In 2012 the European Union started to limit the corporate average CO_2 emissions of newly registered passenger cars of each manufacturer. The CO_2 emission are determined in the New European Driving Cycle (NEDC). Since 2015 the limit is 130 g CO_2/km and it will be lowered to 95 g/km

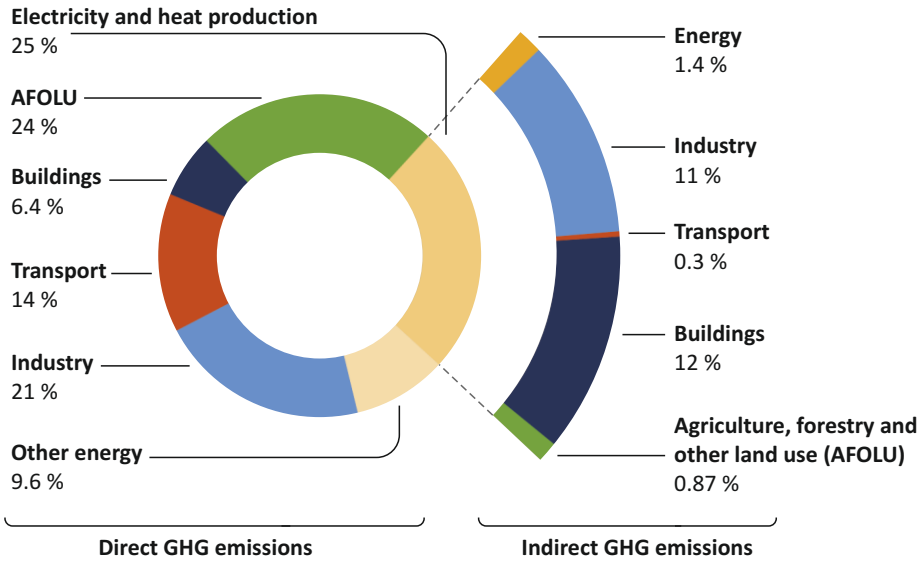

Figure 1.3: The sources of global GHG emissions in 2010 [94].

in 2020 [35]. In order to achieve this ambitious target manufacturers need to invest in advanced engine technologies, in the electrification of the powertrain and alternative and renewable fuels.

Figure 1.4 a displays the CO_2 emissions in the NEDC plotted against the vehicle weight of all cars registered in Germany in 2015 of Europe's five top selling manufacturers. It shows that the majority of available models are powered by gasoline and diesel and that diesel vehicles tend to be more efficient. Gasoline vehicles in particular are still relatively far from the 2020 limit. It also shows that natural gas (NG) vehicles emit less CO_2 than gasoline vehicles. This results from different carbon intensities of the fuels. Natural gas consists mainly of methane (CH_4) which has a hydrogen-carbon-ratio (H/C-ratio) of 4 while the H/C-ratio of gasoline is approx. 1.89 [97]. Under the condition of equal brake thermal efficiencies the tank-to-wheel CO_2 emissions are approx. 25 % lower with methane. The use of natural gas as fuel is therefore the most effective single measure to cut the tank-to-wheel CO_2 emissions of combustion engines until renewable energy sources become available on a large scale for passenger cars. Furthermore, it is cost-effective as the technology is proven and it can be realised short-term since a well-developed infrastructure for natural gas already exists in many European countries. Despite these proven advantages NG vehicles are a minority in manufacturers' portfolios as Figure 1.4 a demonstrates. Accordingly, only 0.6 % of all registered passenger cars in Europe were powered by natural gas in 2015 [34]. Also [27] refers to natural gas as a measure to mitigate the impact of transport on global warming.

Novel combustion concepts for passenger cars and heavy duty engines which utilise natural gas are thus investigated in this thesis. Generally, combustion engines can be classified by the number of fuels used. Monovalent engines operate on one fuel and represent the vast majority of engines deployed in road vehicles. Natural gas spark ignited (SI) engines for heavy duty vehicles are also usually monovalent engines. Bivalent engines are designed to switch between two fuels, but run on one fuel at a time. The majority of NG engines in passenger cars are bivalent engines and can switch between NG and gasoline. By contrast with this dual fuel (DF) engines run on two fuels simultaneously. The most common approach in dual fuel combustion

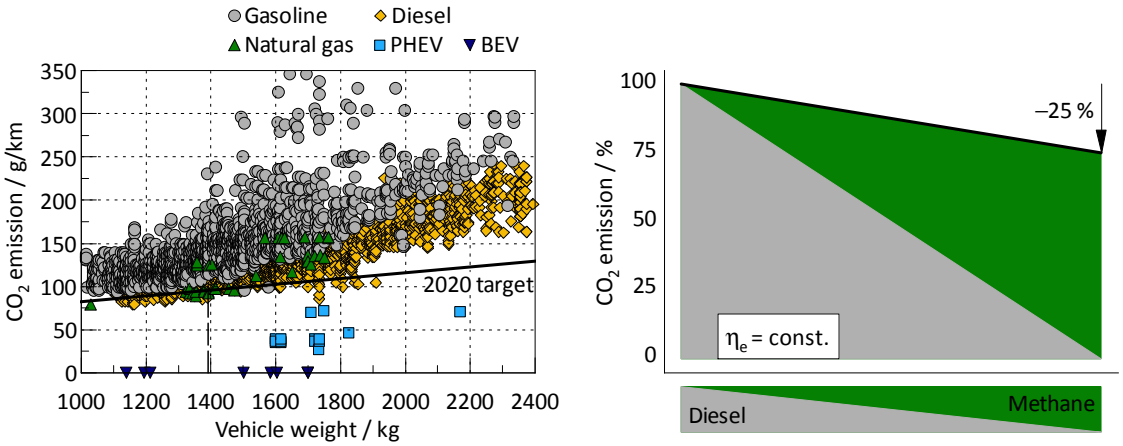

Figure 1.4: **(a)** The CO_2 emissions plotted against the vehicle weight of all new cars registered in Germany in 2015 of the five highest selling manufacturers in Europe [33] and **(b)** the feasible CO_2 reduction with dual fuel combustion in dependency on the share of methane in the total fuel energy.

is the combination of NG and diesel. Dual fuel engines are state of the art for large engines in marine applications and power generation. However, they are not widespread in road vehicles so far. Each concept has benefits and disadvantages. Monovalent and bivalent NG spark ignited engines use tried and tested technology and feature effective exhaust gas aftertreatment when operated stoichiometrically. However, spark ignited engines exhibit a lower fuel efficiency compared to diesel engines, especially bivalent engines as the design for two different fuels results in compromises. Dual fuel engines have the potential for higher fuel efficiency, but the exhaust gas aftertreatment is difficult as the exhaust gas is lean. In addition, dual fuel engines are prone to emit high hydrocarbon (HC) emissions in low load operation. In order to realise high CO_2 reductions with DF engines high shares of NG are necessary as Figure 1.4 b illustrates.

The aim of this thesis is the development and investigation of two novel combustion processes which use natural gas and enable high CO_2 reductions compared to conventional diesel and gasoline engines. The work is divided into two sections and consists of an experimental and a numerical part. In the first section the development of a dual fuel combustion process for passenger car engines is discussed. Compressed natural gas (CNG) and diesel are used as fuels. In the literature a thoroughly studied concept is the combination of port fuel injection (PFI) of CNG and direct injection (DI) of diesel. In this work a new configuration which features low-pressure direct injection of CNG and direct injection of diesel is investigated experimentally. This layout enables a stratification of the natural gas-air mixture and thus mitigates the problem of high HC emissions during part load operation. The measurements were conducted in four stationary load points on the engine test bench. The chosen load points are characteristic for the operation of a passenger car engine in day-to-day use. The influence of the application parameters (injection timing, exhaust gas recirculation, air-fuel equivalence ratio, rail pressures, etc.) on the combustion was investigated and the main influencing factors on

fuel efficiency and emissions were identified. In addition, the influence of the compression ratio was investigated. Subsequently, the combustion was optimised and an operating strategy for the whole engine map was derived. Natural gas spark ignited operation was also realised on the same base engine to allow for a comparison of the dual fuel combustion with conventional spark ignition. Finally, the developed dual fuel combustion process was compared with measurements of conventional diesel and gasoline engines. This work was carried out at the Institute of Internal Combustion Engines and Thermodynamics (IVT) at Graz University of Technology together with my colleague Florian Sprenger who also wrote his PhD thesis on these investigations [115]. Portions of the results obtained have been published at several conferences and in journal papers. A list of my publications is provided in Appendix D. This project was realised in co-operation with BMW Motoren GmbH in Steyr, Austria and received public funding of the Austrian Research Promotion Agency (FFG). The injectors for CNG direct injection were supplied by Delphi.

In the second part of this thesis the thermodynamic layout of a monovalent NG spark ignited engine for heavy duty commercial vehicles by means of 1D engine simulations is conducted. The potential of several novel technologies in heavy duty NG engines and their combinations to raise the fuel efficiency are reviewed. This work was part of the EU project *HDGAS* (www.hdgas.eu) and received funding from the European Union's Horizon 2020 research and innovation program. Within this framework four different and novel natural gas engine concepts for heavy duty vehicles (HDVs) are developed. No up-to-date data on cumulated registrations of NG powered HDVs in Europe has been published. However, the numbers are low as the data from Germany indicates. In 2015 a total of 317 518 new commercial vehicles, heavy duty trucks and buses were registered in Germany. Among these 938 vehicles were powered by natural gas of which 801 exhibited a payload below 1 000 kg [71]. This indicates that the majority of newly registered natural gas commercial vehicles are light duty vehicles with a permissible total weight below 3 500 kg. It has thus not been profitable for commercial vehicle manufacturers to develop dedicated natural gas engines for heavy duty vehicles. Diesel engines from their existing portfolio are modified for natural gas operation instead. This results in penalties in fuel efficiency as the NG engines are spark ignited engines and the base engines were developed for compression ignition. These are two fundamentally different combustion processes with different requirements.

HDGAS was launched to promote the development of dedicated heavy duty NG engines. The *HDGAS* consortium consists of 20 partners. The engine concept which is investigated in this thesis was developed in close collaboration with FPT Industrial, AVL Graz and the Internal Combustion Engines Research Group of Prof. Angelo Onorati at Politecnico di Milano. It is for the first time that a modern heavy duty NG engine is developed dedicatedly for NG operation. The engine follows a stoichiometric concept and comprises of several novel technologies in heavy duty engines. In this engine low-pressure direct injection of liquefied natural gas (LNG), high-frequency (*Corona*) ignition, a waste gate turbocharger with fixed turbine size and cooled high-pressure exhaust gas recirculation (EGR) is realised. In addition, a combustion chamber design optimal for SI engines is implemented featuring a pent roof combustion chamber, angular valves and a flat piston. Furthermore, cam phasing is implemented to realise variable valve timing. By means of this technology mix a 10 % reduction in GHG emissions in the World Harmonised Transient Driving Cycle (WHTC) and 10 % higher torque and rated power should be achieved compared to existing heavy duty NG engines of the model year 2013.

At first the turbocharger matching was performed and different EGR layouts were examined. The subsequent investigations focused on maximising the fuel efficiency of this engine concept. For this purpose, the effect of EGR in part load and full load operation was investigated. Early and late Miller timing in the presence of external EGR was contrasted with conventional valve timing and the interdependencies between turbine size, EGR, valve timing, gas exchange work and fuel efficiency were analysed. Furthermore, the potential of cam phasing was analysed for conventional and early Miller valve timing in combination with EGR and indications for the operating strategy were derived. Finally, the simulation results were confirmed with single-cylinder measurements performed by a project partner and the combined effect of the investigated technologies (EGR, Miller timing and cam phasing) on the fuel efficiency was quantified.

In Chapter 2 of this thesis characteristics of natural gas in comparison to the conventional fuels gasoline and diesel are reviewed. The state of the art in monovalent NG spark ignited engines and dual fuel combustion is discussed in Chapter 3. Chapter 4 covers the experimental investigation of dual fuel combustion. The cause of the high HC emission is highlighted, the examined concept is explained in detail and the followed methodology is reviewed. The results focus on the investigation of the most important application parameters, the influence of the compression ratio and the optimisation of the dual direct injection (DDI) combustion process. Furthermore, the comparison with CNG SI operation is stated, which was realised on the same base engine. Finally, the optimised DDI combustion is compared with conventional diesel and gasoline combustion processes, as also with conventional dual fuel combustion with natural gas PFI.

In Chapter 5 the numerical analysis of the NG spark ignited engine is discussed. At first the methodology, the model building and the model matching are explained. Afterwards the effect of EGR in part load and full load operation and the influence of different EGR layouts is reviewed. Early and late Miller timing is investigated and the influence of cam phasing on the gas exchange is analysed. Finally, a comparison of simulation results and single-cylinder engine measurements is given. Chapter 6 summarises the findings and the work as carried out.

2 Natural Gas Fundamentals

2.1 Characteristic Fuel Properties

Natural gas (NG) is a fossil fuel which is gaseous under standard conditions. It consists of several chemical species. The main component is methane (CH_4), but also other alkanes, nitrogen (N_2) and CO_2 are present in natural gas. Table 2.1 gives a typical composition for NG of high quality. The composition can vary considerably depending on where the natural gas is extracted. Especially the CH_4 and N_2 shares vary substantially. CH_4 shares vary between 80 % and 98 % and N_2 shares vary between 0.6 % and 18 % [19]. Obviously, high shares of inert gas affect the lower heating value (Q_{LHV}) negatively.

Table 2.1: Typical composition of natural gas of grade H [19].

	$\mathbf{CH_4}$	$\mathbf{C_2H_6}$	$\mathbf{C_3H_8}$	$\mathbf{C_4H_{10}}$	$\mathbf{CO_2}$	$\mathbf{N_2}$
Molar fraction ν_i / %	93.0	3.0	1.3	0.6	1.0	1.1

In Germany the specification of natural gas is regulated in DVGW-G 260. It defines two grades (L and H) which differentiate in the upper Wobbe Index ($I_{w,s}$). Grade H is the higher quality and thus exhibits higher shares of CH_4 and less inert gases [19]. Recently a European standard (EN 16726) was developed for NG [32] to ease the cross-border trade of NG. Also the maximum sulphur content is regulated and the maximum content of the toxic and corrosive hydrogen sulfides (H_2S). NG as specified in these standards is odourless. It is odorised to detect leakages in gas lines easier.

For the use as fuel in vehicles natural gas is specified in DIN 51624. The CH_4 share must be above 80 % and for grade H the lower heating value has to be higher than 46 MJ/kg. The total sulphur content is required to be below 10 mg/kg [22].

Methane is a very stable molecule with high activation energy. The benefit it brings is that natural gas is more knock resistant than gasoline and from this point of view it is a suitable fuel for SI engines with the potential for higher fuel efficiency than gasoline engines. The drawback is that the conversion of unburned HC emissions is more difficult since the HC emissions also consist mainly of methane. In lean operation the light-off temperature for CH_4 oxidation in an oxidation catalyst is approx. 450 °C [48].

Table 2.2 gives the characteristic fuel properties of methane, natural gas, diesel and gasoline. The properties of natural gas are valid for the composition stated in Table 2.1. The properties of methane and natural gas are similar. Both state H/C-ratios being twice as high as the ones of gasoline and diesel. The lower heating value (Q_{LHV}) of CH_4 and NG is higher compared to the liquid fuels, but the energy density is lower by a factor of 1000. This is relevant for the storage on a vehicle. With compressed natural gas (CNG) or liquefied natural gas (LNG) the

Table 2.2: Fuel properties of methane, natural gas, diesel and gasoline [19, 97].

	Methane	**Natural gas**[1]	**Diesel**	**Euro Super**
Molar mass / g/mol	16.04	17.49	≈ 170	≈ 98
H/C-ratio / –	4.0	3.82	1.89	1.99
Density[2]/ kg/m^3	0.72	0.78	815...855	730...780
Q_{LHV} / MJ/kg	50	47.5	43	41
Energy density / MJ/m^3	35.9[2]	37.2[2]/ 8733[3]/ 21458[4]	35905[2]	30955[2]
Q_{LHV} of mixture[2]/ MJ/m^3	3.39[5]/ 3.75[6]	3.41[5]/ 3.75[6]	3.80[6]	3.66[6]
Flammability limits / –	0.7 / 2.1	–	0.48/1.35	0.4/1.4
$(\mathrm{A/F})_{\mathrm{stoich.}}$ / kg/kg	17.2	16.4	14.5	14.5
CO_2 reduction[7]	25.4 %	23.5 %	–	–

[1] Composition stated in Table 2.1
[2] At 0 °C and 1.013 bar
[3] CNG at 20 °C and 200 bar calculated according to ISO 12213-2:2006 using [128]
[4] LNG at -163.5 °C and 1.013 bar calculated according to ISO 6578 using [128]
[5] Port fuel injection and $\lambda = 1$
[6] Direct injection and $\lambda = 1$
[7] Compared to diesel and equal brake thermal efficiency

energy density can be increased. However, at constant tank capacity the energy contained is still lower than gasoline by 30 % to 70 %. The lower heating value of the mixture refers to a stoichiometric air-fuel mixture and standard conditions of air. It is an indication for the feasible power density of an engine, if the intake manifold conditions remain constant and the influence of the fuel on knocking is not considered. It indicates that without additional measures the power density of natural gas engines with PFI is approx. 7 % lower than of a gasoline DI engine. Similar values are stated in [12]. The feasible reduction of tank-to-wheel CO_2 emissions by 25.4 % results from the higher H/C-ratio of CH_4. With NG consisting also of longer hydrocarbon chains, the H/C-ratio is reduced and along with this the feasible CO_2 potential is also reduced to 23.5 %. These values are calculated under the assumption of equal brake thermal efficiency and in comparison to diesel. The derivation of this CO_2 potential is stated in Section 2.2. The tank-to-wheel consideration excludes emissions arising from the fuel production. A more complete review provides the well-to-wheel approach and ultimately the 'cradle-to-grave' life cycle assessment which considers all GHG emissions from the production of a vehicle through to the recycling. It enables a holistic comparison of various powertrain concepts. More information on the well-to-wheel CO_2 emissions of NG vehicles and the influence of renewable NG in comparison to other propulsion concepts can be found in [3, 15, 20, 132]. A life cycle assessment of NG vehicles which incorporates the vehicle production is stated in [92]. In most European countries the taxation of passenger cars is based on tank-to-wheel CO_2 emissions. In Switzerland the taxation has already been shifted to well-to-wheel CO_2 emissions, which is a more integral approach [18].

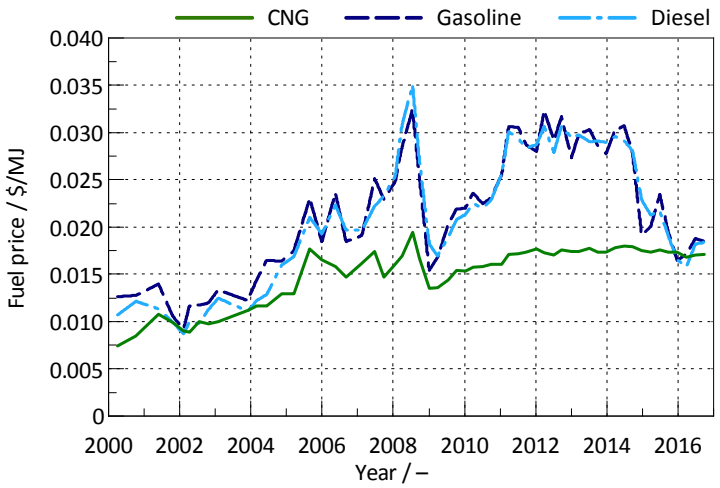

Figure 2.1: Fuel retail prices in the United States since 2000 [129].

With the information of this section in mind the drawbacks of bivalent natural gas and gasoline powered vehicles already become apparent. Today, these vehicles feature NG port fuel injection and gasoline port fuel or direct injection. The compression ratio of the engine must be chosen for the less knock resistant fuel which is gasoline. The potential of natural gas to raise the fuel efficiency of the engine thus remains unused. In addition, in naturally aspired engines the lower heating value of the mixture cannot be compensated by a higher boost pressure resulting in a power loss compared to gasoline operation. This is particularly characteristic for retrofit solutions for passenger cars.

Finally, Figure 2.1 provides the trend of average fuel prices in \$/MJ in the United States since 2000. Over long periods CNG was considerably cheaper and the price fluctuation was notably less. While fuel prices may not be the main criterion for consumers when deciding on a fuel type, for fleet operators of commercial vehicles the total cost of ownership is critical. Therefore, more predictable and lower fuel prices are an argument in favour of NG.

2.2 The Potential of Natural Gas to Reduce the Tank-to-Wheel CO_2 Emissions

In the literature a 25 % reduction of tank-to-wheel CO_2 emissions is stated when using CH_4 instead of gasoline and diesel. Since the reason for this is not frequently discussed in detail, a derivation is provided below. For the sake of simplicity but without loss of generality a hypothetical natural gas grade is assumed which consists only of methane (CH_4) and ethane (C_2H_6). The chemical reaction equation for complete combustion of this hypothetical grade is as stated below:

$$\nu_1 CH_4 + \nu_2 C_2H_6 + (2\,\nu_1 + \frac{7}{2}\,\nu_2)O_2 \longrightarrow \underbrace{(\nu_1 + 2\nu_2)}_{\nu_{CO_2}} CO_2 + (2\,\nu_1 + 3\,\nu_2)H_2O \tag{2.1}$$

ν_1 and ν_2 are the stoichiometric coefficients of methane and ethane and equal to their mole fractions in the assumed natural gas grade. ν_{CO_2} is the stoichiometric coefficient of the CO_2 produced. The oxidation of 1 mol of natural gas produces ν_{CO_2} mol of CO_2. If natural gas consists of more species than methane and ethane the calculation of ν_{CO_2} must be adapted accordingly. The total amount of CO_2 $n_{CO_2,NG}$ is calculated according to Equation 2.2 with n_{NG} being the total number of moles of natural gas.

$$n_{CO_2,NG} = \nu_{CO_2} \cdot n_{NG} \tag{2.2}$$

The total mass of CO_2 $m_{CO_2,NG}$ which results from the combustion of NG is given in Equation 2.4. It is derived from the molar mass of CO_2 M_{CO_2} and natural gas M_{NG} and is a combination of Equation 2.2 with 2.3.

$$n_{NG} = \frac{m_{NG}}{M_{NG}} \tag{2.3}$$

$$m_{CO_2,NG} = n_{CO_2,NG} \cdot M_{CO_2} = \nu_{CO_2} \cdot m_{NG} \cdot \frac{M_{CO_2}}{M_{NG}} \tag{2.4}$$

Diesel and gasoline consist of long hydrocarbon chains. The calculation of the CO_2 emission resulting from complete combustion of diesel is stated below. The CO_2 emission from gasoline is calculated analogue to this. Usually the fuel analysis delivers the mass fractions μ_i of atomic carbon (C), hydrogen (H) and oxygen (O). Equation 2.5 defines the mass fraction of carbon μ_c as ratio of the mass of carbon atoms m_c and the total fuel mass m_{Diesel}. In complete combustion every C-atom leads to a CO_2 molecule which is expressed in Equation 2.6. M_c is the molar mass of carbon.

$$\mu_c = \frac{m_c}{m_{Diesel}} \tag{2.5}$$

$$n_{CO_2,Diesel} = n_c = \frac{m_c}{M_c} \tag{2.6}$$

Combining Equation 2.5 and 2.6 the mass of CO_2 resulting from the combustion of diesel $m_{CO_2,Diesel}$ can be calculated.

$$m_{CO_2,Diesel} = n_{CO_2,Diesel} \cdot M_{CO_2} = \mu_c \cdot m_{Diesel} \cdot \frac{M_{CO_2}}{M_C} \tag{2.7}$$

The masses of CO_2 resulting from natural gas and diesel combustion are set into relation.

$$\frac{m_{CO_2,NG}}{m_{CO_2,Diesel}} = \frac{\nu_{CO_2} \cdot m_{NG} \cdot M_c}{\mu_c \cdot m_{Diesel} \cdot M_{NG}} \tag{2.8}$$

Under the condition of equal brake thermal efficiencies and equal load the fuel energy is the same. Thus, the fuel masses are related according to Equation 2.9.

$$m_{NG} \cdot Q_{LHV_{NG}} = m_{Diesel} \cdot Q_{LHV_{Diesel}} \tag{2.9}$$

Combining Equations 2.8 and 2.9 results in Equation 2.10 which states the feasible CO_2 reduction.

$$\frac{m_{CO_2,NG}}{m_{CO_2,Diesel}} = \frac{Q_{LHV_{Diesel}}}{Q_{LHV_{NG}}} \cdot \frac{\nu_{CO_2} \cdot M_c}{\mu_c \cdot M_{NG}} \tag{2.10}$$

With the fuel properties stated in Table 2.2 and a carbon mass fraction μ_c of 86.3 % methane results in a CO_2 reduction potential of 25.4 % compared to diesel. Natural gas of a composition as stated in Table 2.1 results in a CO_2 reduction potential of 23.5 %. These values increase by 1.5 $\%_{Pt.}$ with gasoline as reference. This means the feasible tank-to-wheel CO_2 reduction depends on the lower heating values and the carbon intensities of the two fuels involved. In this calculation the H/C-ratio does not arise explicitly.

Equation 2.11 can be derived in order to calculate the CO_2 reduction directly from the lower heating values and the H/C-ratios. The disadvantage is that also the mass fractions of nitrogen and oxygen μ_n and μ_o appear in this equation. With the assumption that the sum of these mass fractions is approximately equal in both fuels Equation 2.12 is derived.

$$\frac{m_{CO_2,NG}}{m_{CO_2,Diesel}} = \frac{Q_{LHV_{Diesel}}}{Q_{LHV_{NG}}} \cdot \frac{(h/c)_{Diesel} + 12}{(h/c)_{NG} + 12} \cdot \frac{(1 - \mu_o - \mu_n)_{NG}}{(1 - \mu_o)_{Diesel}} \tag{2.11}$$

$$\approx \frac{Q_{LHV_{Diesel}}}{Q_{LHV_{NG}}} \cdot \frac{(h/c)_{Diesel} + 12}{(h/c)_{NG} + 12} \tag{2.12}$$

3 State of the Art

This overview of current research and series applications of natural gas engines focuses on passenger car and heavy duty (HD) engines. The fact should not be discounted, however, that natural gas is also a common fuel for large engines.

3.1 Monovalent and Bivalent Natural Gas Engine Concepts

All major manufacturers of heavy duty commercial vehicles have natural gas vehicles in their portfolio. Since fuel efficiency is of great importance in commercial vehicles the engines are designed as monovalent engines to avoid the penalty in fuel efficiency of bivalent engines. All available engines are turbocharged and feature NG port fuel injection and spark ignition. The engines on the European market are five-cylinder and six-cylinder engines. The displacement ranges from 6.9 litres to 12.8 litres and the rated power is in the range between 162 kW and 294 kW [57, 77, 89, 117]. A factor these engines have in common is that they are derivations of existing diesel engines [2, 57, 77, 89, 99] since the sales volume of NG vehicles has not so far allowed for the development of dedicated NG engines. CNG is used for buses and urban distribution trucks. Due to the higher energy density of LNG first LNG applications for long haul trucks above 18 t were reported in Europe [77]. In China and in the United States [101] both a network of LNG filling stations and LNG trucks are also available.

While many Euro 5 engines were operated lean most of the Euro 6 engines (since 2013) are operated stoichiometrically due to the stricter emission limits. Lean operated natural gas engines would require selective catalytic reduction (SCR) exhaust gas aftertreatment and a methane oxidation catalyst (MOC) to comply with Euro 6 emission limits. The durability of the MOC specifically is critical. In stoichiometric operation a three-way catalyst (TWC) is sufficient [2, 39, 46].

Stoichiometric SI engines have a disadvantage compared to diesel engines in fuel efficiency due to the higher gas exchange work in part load operation, the lower compression ratio, higher wall heat losses and different gas properties, to only name a few of the differences. Miller valve timing and EGR in part load and full load operation were proposed to reduce the gas exchange work, enable a higher compression ratio, decrease the knock probability and to reduce the thermal strain on the engine [2, 39, 46, 99, 112]. Experimental investigations of the Miller cycle in combination with cooled high-pressure EGR indicated promising results [68] and a series application has already been reported [57].

Variable valve timing is another technology to raise the fuel efficiency of SI eninges, especially during part load operation. While variable valve timing is state of the art in gasoline SI passenger car engines [98, 118] a series introduction has not been reported in heavy duty NG engines. There are a few studies on variable valve timing in heavy duty diesel engines [21, 28] and natural gas-diesel dual fuel engines [84]. Usually the focus of variable valve timing in diesel engines is a different one. While in SI engines the main motivation is a reduction of the gas

exchange losses during part load operation the focus in diesel engines is on a rapid heat-up of the exhaust gas aftertreatment system and a reduction of the engine-out pollutant emissions. Literature on variable valve timing in heavy duty natural gas engines is scarce and does not cover cam phasing on both cam shafts. In [137] variable intake valve closing was investigated numerically in order to decrease the gas exchange losses during part load operation. In [5] the effect of variable exhaust valve opening on the turbolag was analysed by means of 1D engine simulations. The application of cam phasing on both cam shafts in a passenger car SI engine with CNG direct injection was reported in [7].

In PCs all natural gas engines are equipped with port fuel injection. There are turbocharged and naturally aspired engines available [88, 131, 134]. They are designed as bivalent engines to enable customers to bridge areas with a scarce network of NG filling stations. However, this functionality comes at the cost of lower fuel efficiency. All engines run on CNG, LNG applications have not been reported in passenger cars. The engines are spark ignited and are derivations of gasoline engines. This means unlike the situation for heavy duty vehicles the layout of the base engine is more favourable to natural gas operation. In [38, 50, 119] the potential was investigated of what a monovalent NG passenger car engine offers compared to an existing bivalent engine. The rated torque was increased by 55 Nm or 24 % and the fuel consumption was reduced by 7 % in the NEDC. An elaborate review of existing technologies for NG passenger cars and heavy duty vehicles as also further potentials is given in [12].

Direct injection of compressed natural gas has been investigated for PC engines, but no series application has been reported yet. Delphi is developing an injector for low-pressure direct injection of NG for rail pressures up to 16 bar [60, 102]. The main motivation for direct injection is to raise the low-end torque to a level comparable to gasoline DI engines. PFI of natural gas reduces the volumetric efficiency compared to gasoline DI engines due to the volume of the NG and the necessity to avoid scavenging. Deteriorations of the low-end torque of up to 50 % were reported [12]. Both causes can be avoided by natural gas direct injection. Furthermore, charge stratification and multiple injection events become feasible with direct injection, the latter one being beneficial for catalyst heating after cold-start. The effects of CNG direct injection with homogeneous and stoichiometric charge were investigated mainly experimentally in [43, 52, 58, 108, 110] relying on injector equipment of Bosch, Delphi and Siemens VDO. Lean and stratified operation was investigated optically and numerically in [6, 42, 87].

3.2 Dual Fuel Combustion

Dual fuel (DF) combustion is not a recent development but was already investigated several decades ago. An early series application was the IFA W50, a truck built in East-Germany from 1965 onwards [62]. For this truck a conversion kit for natural gas-diesel dual fuel operation existed [47]. In academia, the ignition mechanisms of dual fuel combustion were investigated at this institution in 1968 [96]. Different fuel combinations have been investigated. Apart from the combination of natural gas and diesel which is discussed in detail in the following section, also the combination of NG and gasoline was studied in the literature mainly with a focus on avoiding knocking [40, 49, 95]. Blends of natural gas and hydrogen were studied in [29]. Dual fuel combustion of gasoline and diesel with the focus on high fuel efficiency was reviewed in [53, 75]. Hydrogen and diesel DF engines for passenger car and HD engines were investigated

in [10, 31, 120]. Diesel ethanol dual fuel combustion was examined in [54]. Finally, octane on demand concepts as studied in [17] use two fuels with different knock resistance. These concepts have a different focus than the natural gas diesel dual fuel combustion introduced below.

3.2.1 Natural Gas-Diesel Dual Fuel Combustion

NG and diesel is likely to be the most widely studied fuel combination in dual fuel combustion. Various combustion concepts in NG-diesel dual fuel combustion exist which are introduced below. The terminology associated with it and used in this work is also defined. Subsequently the current research on NG-diesel dual fuel combustion is reviewed. Figure 3.1 schematically illustrates the injection events of various DF combustion processes during the compression stroke. The most common concept is the combination of port fuel injection (PFI) of natural gas and direct injection of diesel. It also is the easiest DF concept to realise as a conventional diesel engine can be adapted by retrofitting NG port fuel injection. This concept is referred to as *Conventional DF* concept. The NG injection must take place before intake valve closing (IVC), which means it has to occur before bottom dead centre (BDC). The diesel is injected late in the compression stroke close to firing top dead centre (TDC) in order to ignite the air-NG mixture. Figure 3.1 depicts a case with a diesel pilot injection. However, the ratio of diesel and NG can vary substantially between pure diesel operation and DF combustion with only a diesel pilot injection as depicted.

The concept investigated in this thesis is referred to as *Dual Direct Injection* (DDI). It features low-pressure DI of NG and direct injection of diesel. The NG injection occurs in the compression stroke after IVC. The injection occurs early or later in the compression stroke, depending on whether a homogeneous or stratified operation is desired. Again, the diesel is injected close to TDC to initiate the combustion. Like in conventional diesel engines the diesel injection timing is used to trigger the desired combustion phasing. There is an unambiguous correlation between the start of diesel injection (SOI_{Diesel}) and the 50 % conversion point of the net heat-release (MFB50).

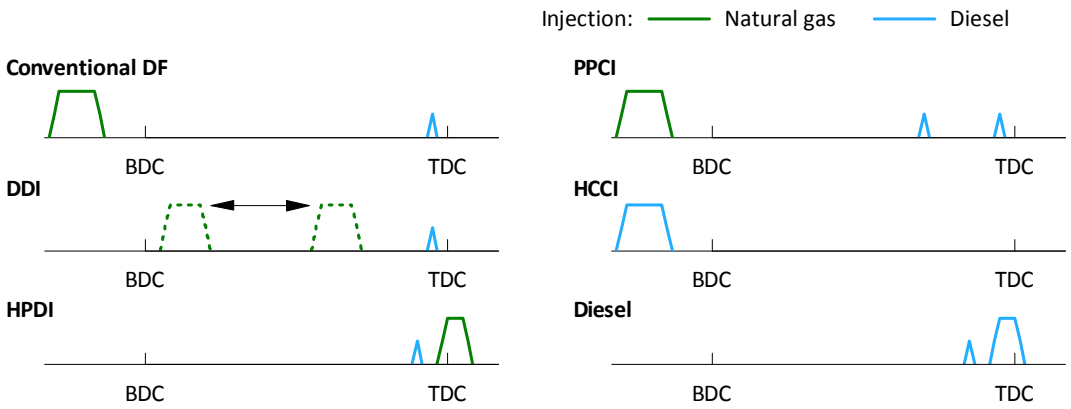

Figure 3.1: The injection events of various dual fuel combustion processes and their delimitation against HCCI and diesel compression ignition.

The concept of *high-pressure direct injection* (HPDI) follows an approach of non-premixed natural gas combustion. A diesel pilot quantity is injected close to TDC which ignites itself. In the flames of the diesel pilot spray the NG is injected which then burns in a non-premixed manner too. *Partially premixed compression ignition* (PPCI) is another approach in dual fuel combustion which will be discussed later.

These four DF combustion processes have in common that the combustion phasing is controlled by the injection timing. In contrast to that there are combustion processes as HCCI, reactivity controlled compression ignition (RCCI) or premixed charge compression ignition (PCCI). Some of these processes also use two different fuels, but usually they are not referred to as dual fuel combustion. The difference is that in HCCI combustion and alike processes there is no direct control of the combustion phasing via the ignition timing. The start of combustion only depends on the evolution of pressure and temperature during the compression stroke and the reactivity of the mixture in the combustion chamber. Exemplarily the injection pattern of diesel HCCI combustion is displayed in Figure 3.1. The diesel is injected close to BDC and forms a homogeneous mixture with air and possible dilutants. After the diesel is injected and the intake valves are closed there is no control on the ignition anymore. Finally, Figure 3.1 also illustrates the injection pattern of conventional diesel compression ignition with a diesel pilot injection and a main injection.

Dual Fuel Combustion with Natural Gas Port Fuel Injection – Conventional DF

NG-diesel dual fuel combustion is state of the art for large engines in marine applications and power generation [124]. However, no widespread application for road vehicles has been reported yet. A few aftermarket solutions for Euro 5 heavy duty commercial vehicles are available to convert diesel engines for dual fuel operation [104, 116]. These solutions rely on port fuel injection of NG (*Conventional DF*) and were reviewed in [13, 116]. A significant increase of CH_4 emissions was observed, resulting in reduced brake thermal efficiency especially in low load operation. The engine-out CO_2 emissions were found to be reduced with some systems, however considering the global warming potential (GWP) of methane this reduction was offset

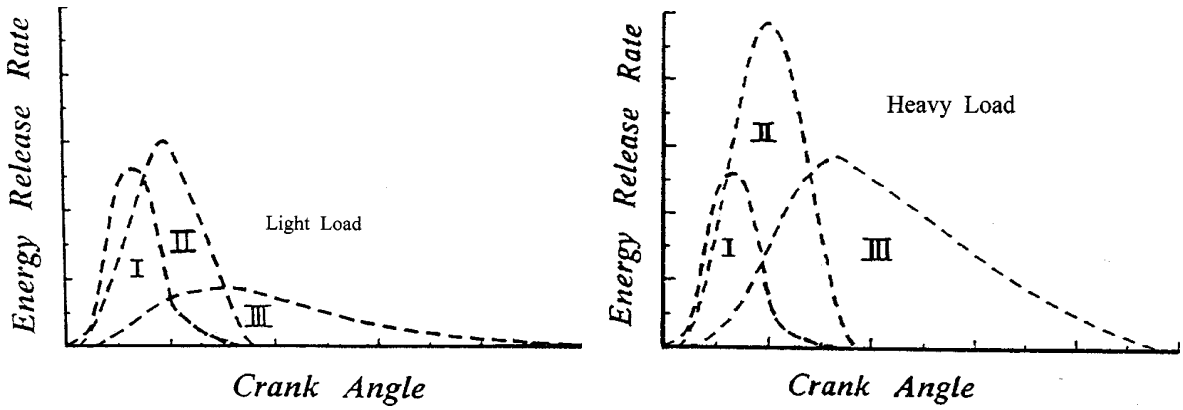

Figure 3.2: Model of conventional dual fuel combustion developed by Karim [65] and valid for various gaseous fuels.

leading to an overall increase of total engine-out GHG emissions between 18 % and 129 % in the transient Federal Test Procedure (FTP) cycle [13].

In 2011 Volvo launched a small batch series of a dual fuel HD truck running on LNG and diesel. It also followed the conventional DF concept and achieved Euro 5 emission standards [81, 130]. Investigations indicated that Euro 6 emission limits are very challenging to achieve with this concept [81] and so far no Euro 6 version of this vehicle has been released.

Apart from these series applications there has been extensive research on the conventional dual fuel concept, both for heavy duty and passenger car engines. Karim developed a model for conventional DF combustion which is valid for a wide range of gaseous fuels and has been referred to by many authors [65]. According to Figure 3.2 he divided the *energy release rate* into three components:

I. Combustion of the diesel pilot

II. Combustion of the gaseous fuel which is in the immediate vicinity of the ignition and combustion centres of the diesel pilot

III. Combustion due to a turbulent flame propagation within the premixed air-gas mixture and possible pre-ignitions in the end gas

At light loads the premixed air-gas mixture is very lean and a flame propagation cannot develop. Therefore the main energy release results from modes I and II and large portions of the air-gas mixture remain unburned. Most of the researcher confirm the lean and premixed air-NG mixture as the root cause for high CH_4 emissions [44, 45, 70, 79, 83, 109] at low loads. This is consistent with the findings of this work. At high loads good results are reported.

Various mitigation strategies were developed to attribute the high CH_4 emissions. In [109] EGR was introduced to reduce the stoichiometry of the air-NG mixture. Positive effects were reported, but it was concluded that EGR alone is not sufficient to reduce the CH_4 emissions satisfactorily. Garcia et al. investigated the effect of intake manifold pressure and temperature on the CH_4 emissions [45]. Throttled operation resulted in a reduction of CH_4 emissions at low loads. It was estimated that above 5 bar indicated mean effective pressure (IMEP) the legislative HC limit may be achieved. Below these load the HC emission remained critical. It might be noted that dual fuel passenger cars are not considered in the European legislation. Therefore, researcher take the emission limits of diesel and gasoline PCs as indication for what the limit could be. Specific legislation does exist for heavy duty DF vehicles.

A split diesel injection has been suggested and reviewed in many publications as a means of introducing some kind of stratification to decrease the local air-fuel equivalence ratio in the piston bowl and thus reduce the CH_4 emissions. Many researcher refer to this approach as PPCI (see Figure 3.1). Investigations were carried out by [23, 44, 63, 70, 85]. The experimental set-ups varied considerably due to differences in the combustion chamber geometries, the piston shapes and the port designs, which influence the charge motion. The range of the injection timings also varied. The charge motion potentially has an influence on the mixture formation and the stratification. Thus, the magnitude of the observed effects varied and different conclusions were drawn. In general, at least slight improvements were observed, but the majority reported, however, that the HC emission reduction was not effective enough to solve the problem.

This finding is consistent with the understanding developed during the investigation of the DDI concept. A split diesel injection introduces a charge stratification, but the air-NG mixture

in the background remains homogeneous. The CH_4 emission results from an air-NG mixture being too lean. Thus, a split diesel injection might improve the ignition of the air-NG mixture and extend the flame propagation to some extent. However, the portions of the air-NG mixture which are not penetrated by the diesel spray and which are above the upper flammable limit remain unburned. As a consequence, to effectively reduce the CH_4 emissions the stoichiometry of the air-NG mixture has to be shifted towards unity or a stratification of the air-NG mixture itself is required. Garcia et al. suggested that NG direct injection could be an enabler for a further reduction of the CH_4 emissions at low load operation [44].

In [23] a variation of the compression ratio was investigated by increasing the bowl volume. A reduction of the compression ratio was found to be beneficial for the CH_4 emissions in particular at low load operation. It was argued that this decrease results from a reduction of air-methane mixture in the crevice volume as the bowl/crevice ratio increases when the compression ratio is reduced. This finding is not in-line with own investigations which indicated that a high compression ratio is advantageous as detailed in Section 4.5. The different results probably arise from different experimental set-ups. In [23] a natural gas energy fraction of only 50 % in combination with a split diesel injection and natural gas PFI was investigated. The own investigations as presented in Section 4.5 feature direct injection of natural gas and a stratified air-NG mixture. Therefore less mixture in the crevices is expected independent of the compression ratio. Furthermore, a single diesel pilot injection and high natural gas energy fractions are used.

Optical investigations of conventional dual fuel combustion were carried out in single-cylinder engines in [25, 83]. A consistent finding was that the combustion starts near the piston bowl walls and moves towards the centre of the bowl. Furthermore, it was consistently reported that if the premixed air-NG mixture is too lean, even the mixture in the centre of the bowl remains unburned. This indicates that the high CH_4 emission at low load operation results not only from crevices, but also from large unburned zones in the piston bowl. A detailed study of the phenomena and mechanisms occurring during DF combustion is given in [25]. Measurements of the natural luminosity and the OH* chemiluminescence were made to visualise the flame front propagation, but also PLIF measurements were conducted to determine the fuel distribution during the start of combustion. In [103] optical investigations with a rapid compression expansion machine (RCEM) are presented. The penetration length of the diesel spray and the ignition delay were studied for various conditions as also the flame front development by measurements of the OH* chemiluminescence.

In [100] a methodology is presented to divide the heat-release rate (HRR) according to the modes described in [65] and depicted in Figure 3.2 and to quantify the contribution of the individual regimes to the total heat-release. Evidence was found that even if a large share of the air-NG mixture in the piston bowl is combusted, CH_4 emissions remain which are indifferent to a further enhancement of the flame propagation. The assumption was stated that these CH_4 emissions result from crevices [100]. Furthermore, an infrared absorption sensor was used by the same research group to study the local air-fuel equivalence ratio in the combustion chamber [135] and optical investigations on a transparent single-cylinder engine were conducted [67]. Depending on the diesel injection pressure different flame front propagation directions were observed as depicted in Figure 3.3. At high injection pressures of 1300 bar the start of combustion was found to be in the vicinity of the piston bowl walls. Subsequently the flame front propagated towards the centre of the bowl. However, at lower injection pressures (300 bar)

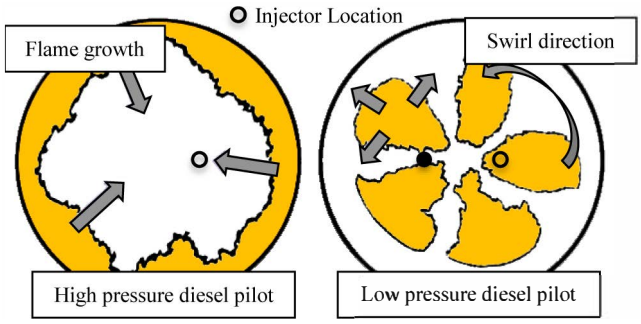

Figure 3.3: Flame propagation in the piston bowl in dependence of the diesel injection pressure [67, 135]; yellow: burned mixture, white: unburned mixture.

a different mechanism was described. The ignition started in the centre of the bowl near to the diesel spray and sequentially, the flames propagated away from these ignition sites [67]. These observations are consistent with optical investigations in [83, 103] which were conducted at 1350 bar ([83]) and 400 bar ([103]), but they contradict the investigations in [25]. In [25] a flame propagation from the piston bowl wall towards the centre was also observed, although the injection pressure was 400 bar. It would thus appear that other mechanisms exist apart from the diesel injection pressure, which influence the nature of the flame front propagation.

Conventional dual fuel combustion was studied by Ott [91] from a controls perspective. A feedback control was developed for the centre of combustion and the maximum pressure rise rate. The transient operation of a passenger car dual fuel engine was experimentally studied in the NEDC and the Worldwide Light Duty Test Cycle (WLTC). Furthermore, a hybrid electric vehicle with DF engine was emulated by hardware-in-the-loop experiments and the performance was assessed in the NEDC and WLTC in terms of fuel consumption and CO_2 reduction.

More fundamental work by optical measurements in RCEMs was conducted by [105, 125] with a focus on large engines.

Dual Fuel Combustion with Dual Direct Injection – DDI

No literature was found on the concept of Dual Direct Injection as depicted in Figure 3.1. Even research on dual fuel combustion with NG direct injection and a premixed combustion of the air-NG mixture is scarce. Only a few publications exist in which similar concepts to DDI were investigated. The injection patterns are displayed in Figure 3.4. In [138] a concept was examined which consists of a late direct injection of NG and a diesel injection before and afterwards. This process was investigated numerically by means of computational fluid dynamics (CFD) simulations for a heavy duty engine. The concept was developed as a measure to control the heat release of reactivity controlled compression ignition (RCCI) by stratification of the air-CH_4 mixture. The influence of the start of NG injection (SOI_{NG}) was investigated for a range from −26 °CA to −20 °CA. This injection is considerably later than in the investigated DDI concept where in the case of stratification SOI_{NG} was in the range from −100 °CA to −70 °CA.

The same injection strategy as proposed with the DDI concept was also investigated in [41] and named *co-direct injection of natural gas and diesel* (DI^2). One motivation for the exper-

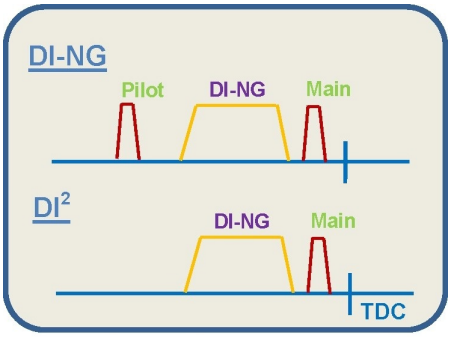

Figure 3.4: The dual fuel combustion processes investigated in [41, 138] (Figure modified from [41]).

imental investigation of DI^2 on a heavy duty single-cylinder engine was to reduce the power demand of the fuel system which results from high NG injection pressures as the HPDI system requires it. However, injection pressures of 210 bar were still investigated with DI^2. CNG is not applicable in this case as typical tank systems are designed for a maximum system pressure of 200 bar and feed the injection system directly without using an intermediate compressor. NG injection timings in the range of −35 °CA to −5 °CA were investigated, however without publishing the CH_4 emission, which is the major challenge in the development of DF combustion systems.

Dual Fuel Combustion with High Pressure Direct Injection – HPDI

An injector for *high-pressure direct injection* (HPDI) of NG was developed and tested by Westport. A single injector features two needles and is responsible for the NG and the diesel injection. The injector was developed for heavy duty engines. The injection pattern is presented in Figure 3.1. The natural gas burns in a non-premixed manner. This has the major advantage that high CH_4 emissions during low load operation are circumvented as no lean and premixed air-NG mixture is present in the combustion chamber. The disadvantage is that high NG injection pressures are required making it difficult to use CNG and increasing the power demand of the fuel system. In most of the publications LNG is used. As in conventional diesel engines where injection pressures of up to 2000 bar are standard, it was found that a high NG injection pressure is beneficial for combustion. Experiments with NG injection pressures up to 600 bar were reported. Extensive literature is available on HPDI combustion research reporting a diesel-like fuel efficiency at a significant CO_2 reduction and low particulate emissions [51, 86]. A series application in Europe has not been reported yet.

Also Bosch published research on the HPDI combustion using own injection equipment [8]. The results are consistent with work conducted with the Westport system verifying the need for high NG injection pressure particularly at full load operation. Fundamental optical investigations of non-premixed NG combustion were conducted by Takasaki et al. with a focus on large engines [122]. A RCEM with optical access was used for this purpose.

4 DDI Dual Fuel Combustion

4.1 Definitions

A few definitions are introduced which are consecutively used during the investigation of dual fuel combustion. Equation 4.1 defines the natural gas energy fraction x_{NG}. It characterises the fraction of NG on the total fuel energy in the combustion chamber. The fuel energy of each fuel is calculated by multiplying the injected fuel mass (m_{NG} and m_{Diesel}) with the corresponding lower heating value of the fuel ($Q_{\mathrm{LHV_{NG}}}$ and $Q_{\mathrm{LHV_{Diesel}}}$).

$$x_{\mathrm{NG}} = \frac{m_{\mathrm{NG}} \cdot Q_{\mathrm{LHV_{NG}}}}{m_{\mathrm{NG}} \cdot Q_{\mathrm{LHV_{NG}}} + m_{\mathrm{Diesel}} \cdot Q_{\mathrm{LHV_{Diesel}}}} \tag{4.1}$$

The air-natural gas equivalence ratio λ_{NG} describes the stoichiometry of the air-NG mixture (Equation 4.2). m_{air} is the inducted air mass and $L_{\mathrm{st_{NG}}}$ is the stoichiometric air-fuel ratio of natural gas. The injected diesel is not considered meaning that λ_{NG} describes the charge in which the diesel is injected. It is a key parameter to influence the CH_4 emissions.

$$\lambda_{\mathrm{NG}} = \frac{m_{\mathrm{air}}}{m_{\mathrm{NG}} \cdot L_{\mathrm{st_{NG}}}} \tag{4.2}$$

The global air-fuel equivalence ratio characterises the stoichiometry of the total mixture in the cylinder considering both natural gas and diesel (Equation 4.3).

$$\lambda_{\mathrm{global}} = \frac{m_{\mathrm{air}}}{m_{\mathrm{NG}} \cdot L_{\mathrm{st_{NG}}} + m_{\mathrm{Diesel}} \cdot L_{\mathrm{st_{Diesel}}}} < \lambda_{\mathrm{NG}} \tag{4.3}$$

Since stratification is a crucial measure in the DDI concept, it is necessary to have an indication of what the influence on the stoichiometry is. Therefore, λ_{bowl} is calculated, the air-natural gas equivalence ratio in the piston bowl, if perfect stratification was achieved as depicted Figure 4.4. It is not a measurement quantity, but a hypothetical value which indicates the stoichiometry in the piston bowl, if perfect stratification was achieved. For the calculation of λ_{bowl} it is assumed that all injected NG is captured in the piston bowl. The remaining bowl volume not occupied by NG is occupied by air ($m_{\mathrm{air,bowl}}$). λ_{bowl} is smaller than λ_{NG} and smaller than the global air-fuel equivalence ratio $\lambda_{\mathrm{global}}$ in case of diesel pilot quantities.

$$\lambda_{\mathrm{bowl}} = \frac{m_{\mathrm{air,bowl}}}{m_{\mathrm{NG}} \cdot L_{\mathrm{st_{NG}}}} < \lambda_{\mathrm{global}} < \lambda_{\mathrm{NG}} \tag{4.4}$$

Equation 4.5 defines the unburned species $\Delta\zeta_{\mathrm{IC}}$. It relates the energy retained in the engine-out HC and carbon monoxide (CO) emissions to the total fuel energy. It is an indicator for the completeness of the combustion. The subscript *IC* stands for *incomplete combustion*. In typical gasoline SI engines the HC emission alone accounts for 1 % to 2.5 % of the fuel energy [55].

$$\Delta\zeta_{\mathrm{IC}} = \frac{m_{\mathrm{CO}} \cdot Q_{\mathrm{LHV_{CO}}} + m_{\mathrm{HC}} \cdot Q_{\mathrm{LHV_{HC}}}}{m_{\mathrm{NG}} \cdot Q_{\mathrm{LHV_{NG}}} + m_{\mathrm{Diesel}} \cdot Q_{\mathrm{LHV_{Diesel}}}} \tag{4.5}$$

4.2 CH_4 Emission in Dual Fuel Combustion

Since the CH_4 emissions are of crucial importance and the major obstacle for the introduction of natural gas-diesel dual fuel combustion in road vehicles their origin and the metrics influencing them are highlighted. A mitigation strategy is developed which leads to the DDI concept which is described in detail subsequently.

In conventional dual fuel combustion a premixed air-NG mixture is present in the combustion chamber, therefore it seems reasonable to review the HC sources in homogeneously operated SI engines as also performed in [70]. In [55] four mechanisms for the origination of HC emissions are mentioned:

- flame quenching at the walls (wall quenching)
- unburned HC from crevices
- unburned HC resulting from poor combustion quality (bulk quenching)
- adsorption and desorption in the engine oil and in deposits.

The adsorption and desorption mechanisms were ruled out in [70]. Deposits of significant magnitude are only present in engines with a high operating time as highlighted in [55] which is not the case for research engines. Therefore, this mechanism is not relevant either. The first three mechanisms remain as potential sources of the high HC emission, they are displayed in Figure 4.1. Their significance is assessed by means of measurement data for conventional dual fuel combustion.

Figure 4.2 demonstrates a variation of the air-natural gas equivalence ratio λ_{NG} in conventional DF combustion (i.e. port fuel injection of NG) in the load point $n = 1750\,min^{-1}$ / BMEP = 5 bar. λ_{NG} is varied by reducing the intake manifold pressure p_{intake} by means of the throttle valve of the engine starting from ambient pressure. The compression ratio ε of the engine is 16.5. The natural gas energy fraction x_{NG} is set to 85 %. EGR is not deployed and MFB50 is kept constant at 11 °CA. The diesel rail pressure p_{Diesel} is set to 400 bar. Figure 4.2 depicts in the lower right part the correlation between the intake manifold pressure p_{intake}, λ_{global} and λ_{NG}. At atmospheric conditions the stoichiometry of the homogeneous air-NG mixture (λ_{NG}) exceeds the upper flammable limit (Table 2.2). At 0.7 bar the global air-fuel

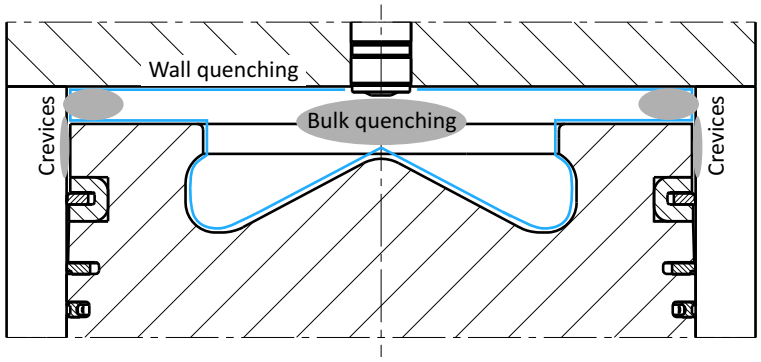

Figure 4.1: Potential sources of HC emission in dual fuel combustion.

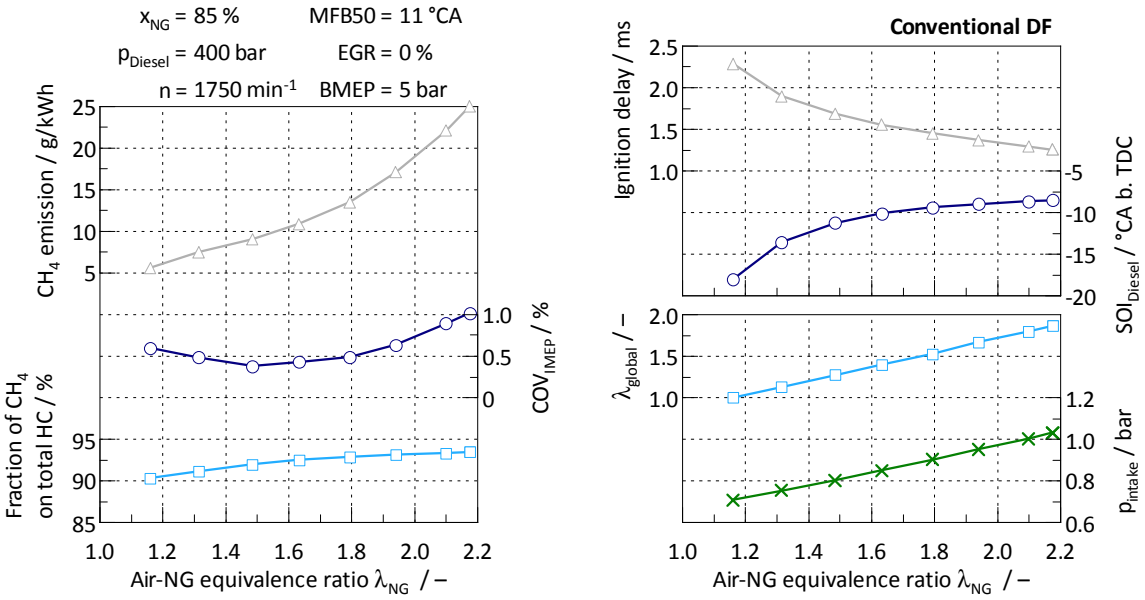

Figure 4.2: Variation of the air-NG equivalence ratio in conventional dual fuel combustion.

equivalence ratio reaches unity while λ_{NG} equals 1.14. The measurement demonstrates that by reducing λ_{NG} the CH_4 emission decreases almost by a factor of 5. Furthermore, the CH_4 emissions account for more than 90 % of the total HC emissions on a molar basis. This shows that the air-NG equivalence ratio is a significant parameter influencing the CH_4 emissions. This was also stated by several other researchers, for example [44, 67, 79]. Furthermore, it is observed that the trend of reducing CH_4 emissions flattens out and although the premixed air-NG mixture is close to stoichiometry a significant amount of CH_4 remains unburned. A similar observation was made by Rochussen et al. [100]. It is assumed that these remaining CH_4 emissions result from crevices and wall quenching, which is also assumed by Rochussen [100]. Possibly areas of the combustion chamber which are not reached by the flame due to the ragged combustion chamber (e.g. the squish area of the piston) are also a source of HC emissions.

If this theory proves correct these remaining CH_4 emissions can be attributed by stratification of the air-NG mixture. In the event that the natural gas is captured in the piston bowl to a large extent, less fuel is located in crevices, in the proximity of walls and in the squish area of the piston reducing the HC emissions. The soaring CH_4 emissions at high air-NG equivalence ratios in Figure 4.2 are attributed to the third mechanism mentioned. Flame quenching occurs in the bulk gas due to the over-lean mixture exceeding the upper flammable limit. Thus, a propagating flame front cannot develop and the flame does not capture the whole volume of the combustion chamber. This was also confirmed by optical investigations in [25, 67, 83].

To conclude, the main reason for excessive CH_4 emissions is flame quenching due to the poor combustion quality of lean air-NG mixtures. If this is avoided the mechanisms of wall quenching and HC emissions from crevices are likely to dominate.

Figure 4.2 also demonstrates that the ignition conditions of the diesel pilot injection (2.7 mg at 400 bar rail pressure) worsen with reducing intake manifold pressure. The ignition delay rises

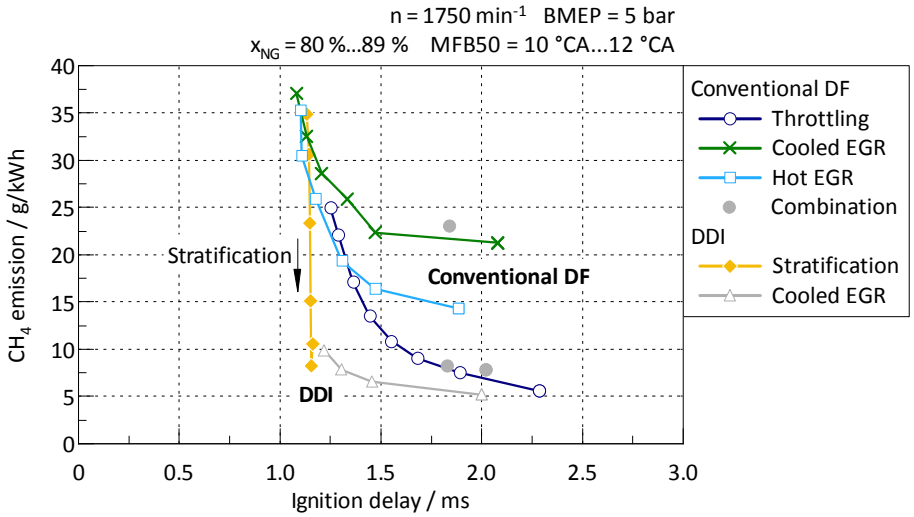

Figure 4.3: The trade-off between the ignition delay and the CH_4 emission in conventional dual fuel combustion.

significantly and SOI_{Diesel} must be advanced to keep MFB50 constant. The ignition delay rises exponentially, because an advancement of the injection means that pressure and temperature in the combustion chamber at SOI are further lowered. The effect of temperature and pressure on the ignition delay is discussed for example in [55]. Figure 4.2 demonstrates that there is a trade-off between the flammability of the air-NG mixture and the ignition conditions of the diesel spray. While the CH_4 emissions reduce with reducing λ_{NG} the ignition delay rises. The discussed results refer to a load of BMEP = 5 bar. At lower loads this trade-off worsens as the air-NG mixture becomes even leaner. The ignition conditions of the diesel spray deteriorate to such an extent that the combustion phasing cannot be controlled by means of SOI_{Diesel} anymore when the intake manifold pressure is reduced. This trade-off prevents stable dual fuel operation at $\lambda_{global} = 1$ and light engine loads and causes the excessive HC emissions.

Another possibility to reduce λ_{NG} without reducing the intake manifold pressure is EGR. However, similar relations as demonstrated in Figure 4.2 exist. Also the combination of EGR and reduced intake manifold pressure is not successful, especially at loads below BMEP = 5 bar. In [113] the effect of throttling and EGR on the CH_4 emission and the diesel ignition conditions is discussed for operation at BMEP = 3 bar.

Figure 4.3 displays the explained trade-off. It is a different representation of the same measurement data depicted in Figure 4.2 and is complemented by measurements of a variation of cooled and hot high-pressure EGR and the combination of throttling and EGR. Furthermore, measurements of the DDI concept are depicted. A SOI sweep of the NG direct injection displays the effect of stratification. The CH_4 emissions are significantly reduced while the ignition delay remains constant. The trade-off is considerably improved. The addition of EGR further decreases the CH_4 emissions, however the ignition delay rises as Figure 4.3 shows.

The observed correlation with DDI can be explained by reviewing the conceptual representation of charge stratification. Figure 4.4 states the mixture preparation of air and NG directly before the diesel injection in conventional dual fuel and DDI combustion. PFI of natural gas

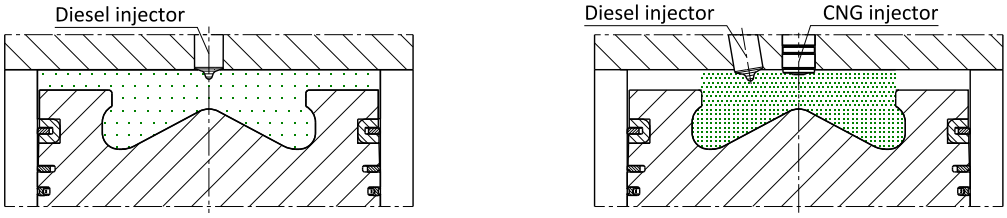

Figure 4.4: Conceptual representation of the distribution of the air-NG mixture in conventional dual fuel combustion (left) and with DDI and charge stratification (right).

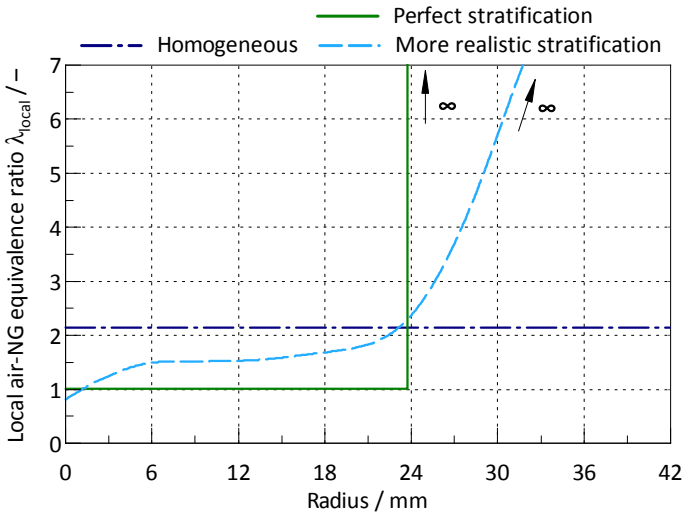

Figure 4.5: Trends of the local air-NG equivalence ratio λ_{local} over the cylinder radius for homogeneous and stratified mixtures.

leads to a homogeneous air-NG mixture and thus to HC emissions from crevices, wall quenching and also bulk quenching if the mixture is over-lean.

With DDI the attempt is made to capture the NG in the piston bowl leading to a stratified air-NG mixture to prevent over-lean mixtures at low loads. Thus, bulk quenching is avoided, but also HC emissions from crevices as no fuel is present in the region of the crevices. The DDI concept is operated unthrottled resulting in a short ignition delay which remains unaffected by increased stratification. Figure 4.4 displays perfect stratification with a sharp transition from mixture to pure air. In a real engine there is of course a gradient thus at the borders of the air-NG mixture over-lean regions exist which are a source of HC emissions also creating a 'floor' of emissions which is an inevitable development. Figure 4.5 displays schematically the local air-NG equivalence ratio λ_{local} over the cylinder radius for a homogeneous mixture, perfect stratification and a more realistic stratification, likely to occur in a real engine. Compared to the conventional DF combustion the operating limit is shifted towards lower loads as throttling is not required with DDI. The HC emissions are reduced as less NG is trapped in crevices and over-lean mixtures are avoided while maintaining favourable ignition conditions of the diesel spray. This results in improved efficiency.

4.2.1 Oxidation of Engine-Out CH_4 Emissions

The aftertreatment of engine-out CH_4 emissions is critical due to their magnitude and their global warming potential (GWP) in relation to CO_2 which is reported to be between 21 and 28 based on a horizon of 100 years and in reference to the literature [27, 94]. Due to its high activation energy CH_4 is particularly difficult to oxidise in an oxidation catalyst and high exhaust gas temperatures are required in comparison to non-methane hydrocarbons (NMHCs). Light-off temperatures of approx. 400 °C are reported for new methane oxidation catalysts (MOCs) [4, 48, 58] and of approx. 450 °C to 560 °C for aged catalysts and in the presence of sulphur [48, 93]. The exhaust gas aftertreatment in NG-diesel dual fuel combustion was investigated in [115]. Figure 4.6 depicts the conversion of various hydrocarbons in an oxidation catalyst in dependence of the temperature.

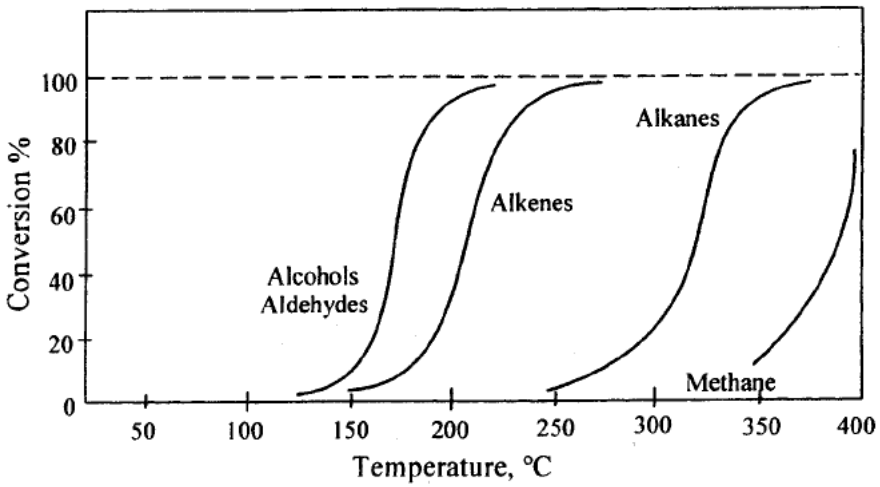

Figure 4.6: Conversion of various hydrocarbons in an oxidation catalyst in dependence on the temperature [11].

4.3 The DDI Concept

To the author's knowledge, natural gas-diesel dual fuel combustion featuring low-pressure direct injection of NG has not previously been studied experimentally for a passenger car engine. In this section the concept, the mechanical realisation, the experimental setup on the engine test bench and the studied variants are discussed. Table 4.1 states characteristics of the BMW B47C20O0 diesel engine which was adapted for the investigations. It is a modern 4-cylinder engine which fulfils the Euro 6 emission standards. The engine features a swirl charge motion. The intensity of the swirl motion can be altered by a swirl flap in one of the two intake ports. The exhaust aftertreatment system (EAS) in the vehicle consists of a lean nitrogen oxide trap (LNT) which also acts as a diesel oxidation catalyst and a diesel particulate filter. On the engine test bench the EAS was not installed though. The series engine is calibrated for low engine-out nitrogen oxide (NO_x) emissions to achieve Euro 6 emission limits with only a LNT installed on the vehicle.

Table 4.1: Parameters of the BMW B47C20O0 diesel engine which was adapted for the investigations [1].

Cylinder	4
Displacement	1995 cm^3
Bore / Stroke	84 mm / 90 mm
Compression ratio	16.5
Valves per cylinder	4
Rated power	140 kW at 4000 min^{-1}
Rated torque	400 Nm at 1750 min^{-1}
Technology	Common-rail system with 2000 bar
	VNT turbocharger with intercooler
	Cooled and hot high-pressure EGR
	Swirl flap
	Throttle valve
	Euro 6 certified

A new and dedicated cylinder head was designed and machined with support of the manufacturer to realise the DDI concept with low-pressure direct injection of natural gas. Other components such as the crank case, the crank train and the piston remained unchanged. The CNG injectors were supplied by Delphi. They are designed for a maximum injection pressure of 16 bar [38, 60, 102] and feature a hollow cone nozzle. Figure 4.7 depicts the fourth generation of Delphi's CNG DI injector.

Figure 4.7: The fourth generation of Delphi's CNG DI injector [60].

Figures 4.8, 4.9 and 4.10 display the mechanical realisation of the DDI concept. The CNG injector is located centrally, the diesel injector is installed eccentrically and inclined. In order to accommodate botch injectors one exhaust valve per cylinder must be omitted. The configuration with central CNG injector was chosen due to mechanical constraints. The series diesel injectors were replaced by injectors with a reduced flow rate of 200 cm^3/30s, six nozzle holes and an asymmetric spray pattern to account for the altered orientation. The asymmetric spray pattern was required to ensure that all six jets penetrate the piston bowl.

Low-pressure direct injection was chosen, because of the intention to use CNG. For passenger car applications CNG is preferred over LNG due to its higher availability and the easier refuelling. Tank systems of available CNG vehicles operate at a maximum tank pressure of 200 bar. The CNG injection system of available vehicles is directly fed from the tank without a compressor in between as all available vehicles feature PFI of CNG with an injection pressure

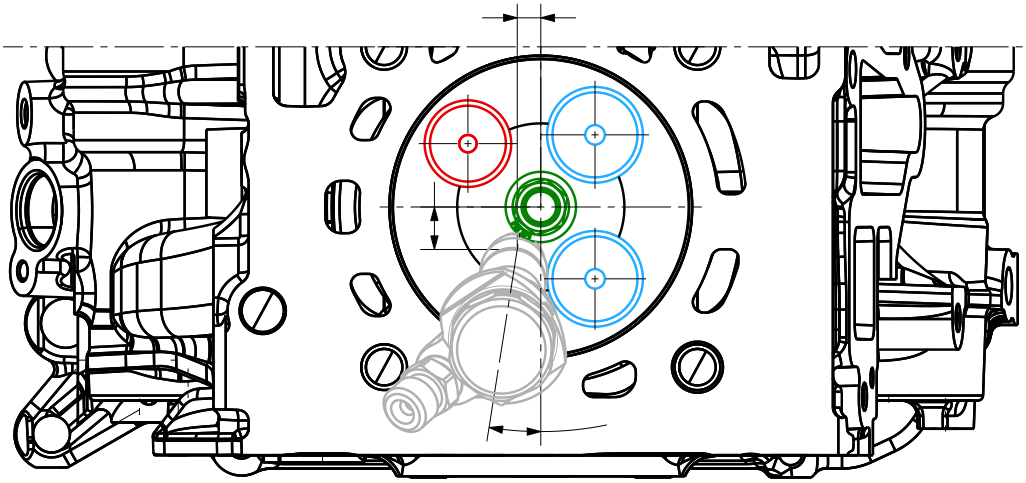

Figure 4.8: Top view of the crank case of the DDI concept. The valves and injectors are added to this view (blue – intake valves, red – exhaust valve, green – NG injector, grey – diesel injector).

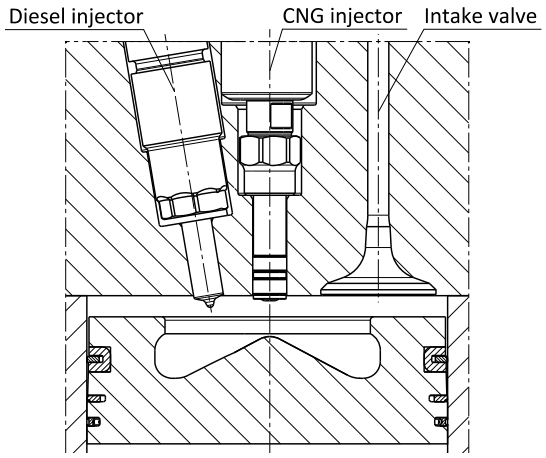

Figure 4.9: Cross-section of the combustion system of the DDI concept.

of maximum 10 bar. This makes a compressor between tank and injection system obsolete [88]. This means, however, that the injection pressure is affecting the cruising range of the vehicle. Once the tank pressure approaches the injection pressure the tank needs to be refilled although it is not fully depleted. A low-pressure system with a maximum injection pressure of 16 bar was decided on for this reason. However, the injection pressure also affects the degree of charge stratification which can be achieved as Figure 4.11 demonstrates. For a stable and repeatable NG injection the pressure gradient across the injector nozzle must be supercritical. According to [19] the critical pressure ratio for methane is 0.542 which means the cylinder pressure must be below 8.7 bar during the injection. This value is reached at −46 °CA for average intake manifold conditions of 1.2 bar and 80 °C. Thus the latest possible SOI_{NG} is approx. −70 °CA for typical injection durations of 20 °CA. This means with low-pressure DI moderate charge stratification becomes feasible.

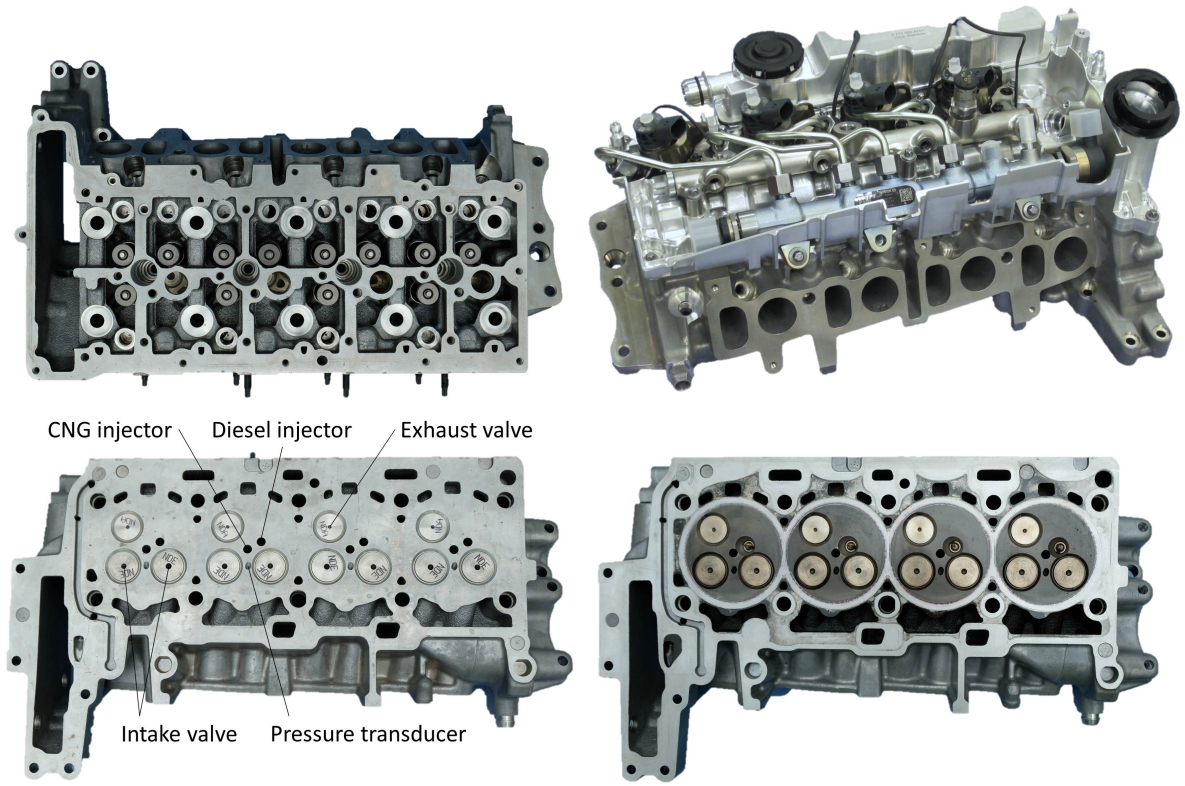

Figure 4.10: Top: The DDI cylinder head. Bottom left: Bottom view of the DDI cylinder head. Bottom right: Bottom view of the SI cylinder head.

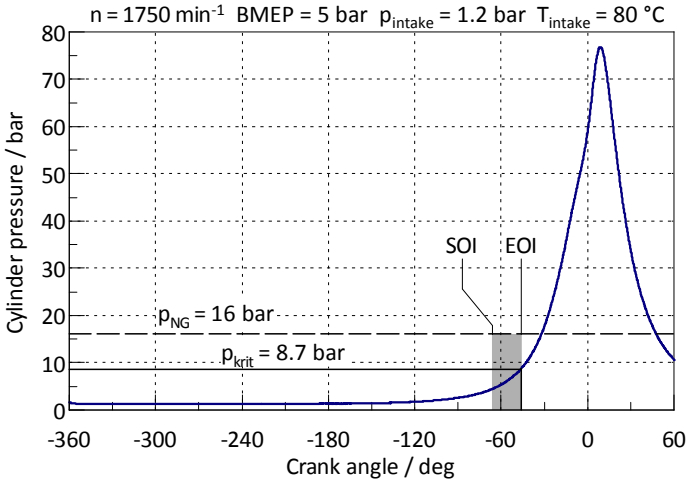

Figure 4.11: The latest possible NG injection timing in dependence of the injection pressure and the cylinder pressure.

4.4 Methodology

The approach followed to investigate the DDI combustion process and the experimental setup is outlined in this section. The investigations were carried out on the engine test bench by measurements in four stationary load points as stated in Table 4.2. Since the challenge in dual fuel combustion is to improve the low load operation two low load and two medium load operating points were chosen. Figure 4.12 depicts the investigated load points and the frequency of load points during a trip with a BMW 320d (F31) according to the specifications of the future real driving emissions (RDE) legislation. The load points 1500/3 and 1750/5 in particular are characteristic for real world driving. The RDE measurements processed in Figure 4.12 were conducted at this institute and kindly provided.

Table 4.2: Examined load points and the corresponding short form.

BMEP / bar	**Engine speed / min^{-1}**	**Short form**
3	1500	1500/3
5	1750	1750/5
11	2000	2000/11
15	1750	1750/15

Outline

The conducted work can be subdivided in six steps:

1. At first variations of the individual application parameters were performed to investigate basic correlations of the DDI concept. The most important application parameters were thus identified.

2. Subsequently the calibration in the four stationary load points was optimised with regard to fuel efficiency, CO_2 emissions and engine-out pollutant emissions. Due to the vast number of parameters design of experiments (DOE) was used to narrow the space of optimal operation. The final optimisation was performed manually starting from the DOE optimum.

3. In a next step hardware parameters as the compression ratio were manipulated to identify their influence on the combustion process. The calibration was optimised for each hardware variation again.

4. For the best hardware configuration an operating strategy was developed for the relevant area of the engine operating map (see Figure 4.12).

5. One of the most interesting questions to answer is the benefit of DDI over other (conventional) combustion processes. Thus, also the series diesel operation, conventional dual fuel combustion and monovalent natural gas spark ignited operation with direct injection were examined on the same base engine (see Table 4.3).

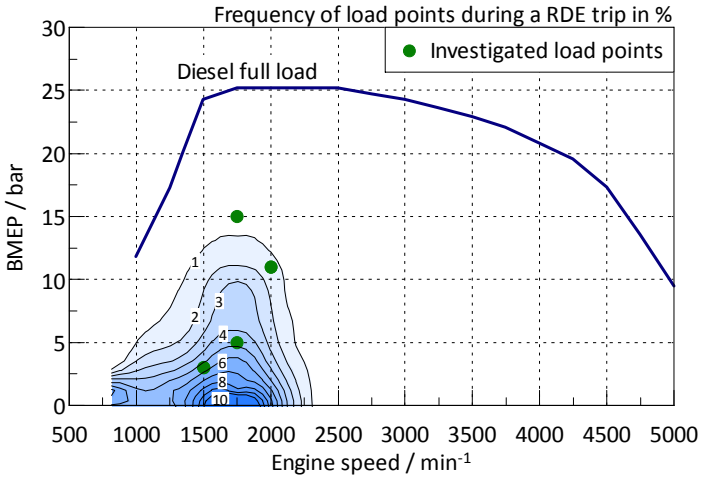

Figure 4.12: The investigated load points and the frequency of load points during an RDE trip.

6. Finally, the optimised DDI combustion process was compared with these combustion processes.

Analysed Combustion Processes

Apart from the DDI concept also other combustion processes were investigated on the same base engine. This has the advantage that the boundary conditions and main parameters of the engine remain identical to ensure the comparability of the results. Table 4.3 lists all examined setups. In addition to the series diesel operation and the DDI concept conventional DF combustion was also investigated. The series diesel cylinder head was installed in combination with a prototype intake manifold for these investigations. The intake manifold was equipped with eight Bosch NGI2 injectors for port fuel injection of natural gas. The injectors are designed for a maximum rail pressure of 10 bar. The investigations of conventional DF combustion were conducted by my colleagues Florian Sprenger and Rudolf Wichtl. Furthermore, spark ignited monofuel operation with CNG direct injection was investigated. The diesel injectors (Figures 4.8 and 4.9) were replaced by conventional spark plugs of the type Bosch ZMR5TPP330 for this purpose.

Table 4.3: Overview of the combustion processes investigated on the identical base engine.

	Diesel	**Conventional DF**	**DDI**	**CNG DI SI**
Compression ratio	16.5	16.5	16.5 / 14.5	14.5
Fuel	Diesel	Diesel & CNG	Diesel & CNG	CNG

Experimental Setup

Figure 4.13 depicts the setup on the engine test bench. The oil temperature, the coolant temperature and the air temperature at the intercooler outlet were conditioned on the test bench. A torque transducer was used to determine the engine torque. The CNG and diesel flow rates were measured by Coriolis flow and density meters. The engine was equipped with cylinder pressure indication on all four cylinders, indication of the intake and exhaust manifold pressure and the CNG rail pressure. Furthermore, the engine-out emissions were analysed by an emission bench. The soot was also characterised by determining the opacity of the exhaust gas. In order to determine the amount of EGR the CO_2 concentration in the intake manifold was also measured. A list of all the measurement devices is given in Appendix A. Furthermore, access was provided to the internal measurands of the engine control unit (ECU). The CNG injectors were actuated by a separate engine timing unit and a driver unit. The diesel injectors and all other actuators (variable nozzle turbine, throttle valve, EGR,...) were manipulated by write access to the series ECU.

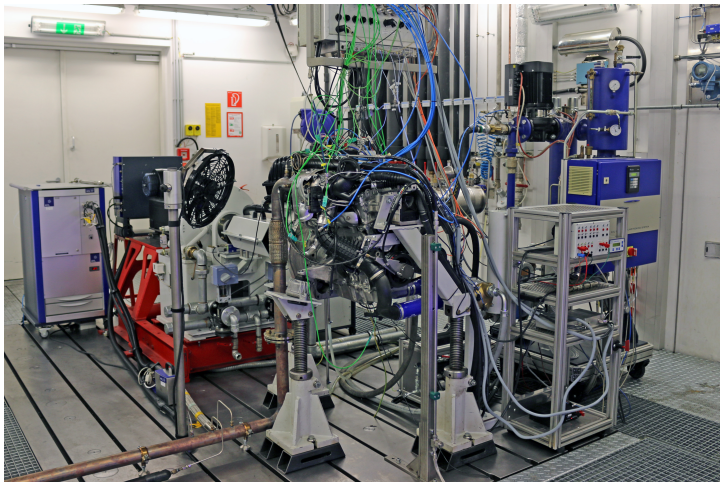

Figure 4.13: The experimental setup on the engine test bench.

For all experiments CNG with a CH_4 share between 96 % and 99 % was used. The CNG was provided by cylinder bundles of 600 litre and 200 bar. The composition of each lot was analysed with a gas chromatograph to determine the lower heating value. Table 4.4 gives the average composition of the natural gas used, the average lower heating value was 48.9 MJ/kg. By means of a pressure regulator the CNG pressure was reduced to 16 bar and fed to the engine. It was kept constant at 16 bar throughout all measurements of the DDI system to enable maximum stratification. The net heat-release rates, where stated, were calculated from the measured cylinder pressure traces with the software *AVL Concerto*.

Table 4.4: The average composition of the used natural gas.

	CH_4	C_2H_6	C_3H_8	C_4H_{10}	CO_2	N_2
Mole fraction ν_i / %	97.9	0.6	0.2	0.15	0.15	1.0

4.5 Results

The most important findings are reviewed in this section. The results are discussed in the same sequence as stated in the outline in Section 4.4.

4.5.1 Influence of Application Parameters

As DDI is a new concept and no literature exists about how to build on it, the essential issue here was to investigate the fundamental correlations between the application parameters and the combustion process. Subsequently, only those parameters are reviewed which exhibit a significant influence. Their effect on the HC emission was published to some extent earlier in [36]. In this section a more detailed analysis is given.

Natural Gas Energy Fraction x_{NG}

One of the obvious parameters to study in natural gas-diesel dual fuel combustion is the ratio between the two fuels. It is expressed by the natural gas energy fraction x_{NG}. Figure 4.14 displays a variation of x_{NG} between 0 % (diesel only) and 90 % which corresponds to a diesel injection of 1.7 mg. The results are depicted for the load point 1750/5 and intake manifold pressures of 1030 mbar and 1200 mbar. The measurements are conducted without EGR. The commanded start of NG injection SOI_{NG} is set to −160 °CA which means the charge is not stratified. SOI_{Diesel} is adjusted to keep MFB50 constant at 11 °CA. A single diesel injection is used throughout the investigations of the DDI concept. This remains valid also for the case of $x_{NG} = 0\,\%$.

The air-NG equivalence ratio λ_{NG} is reduced as the mass of natural gas increases. This relation is very basic, but it already illustrates that high NG energy fractions are necessary. Firstly to facilitate a high CO_2 reduction potential (Figure 1.4 b) and secondly to reduce λ_{NG} which is imperative for low CH_4 emissions as discussed in Section 4.2. The reduction of λ_{NG}, however, is not sufficient. The upper flammable limit of 2.1 is exceeded independent of x_{NG} at an intake manifold pressure of 1200 mbar and barely achieved at 1030 mbar. Consequently, the HC emissions rise with increasing x_{NG} as the air-NG mixture is too lean. The more NG is introduced the more NG remains unburned. This trend ends at close to 30 g/kWh, because the measurement range of the emission bench is exceeded at this point. The HC emissions rise with less strength at the lower intake manifold pressure, because λ_{NG} is also lower.

The CO emissions exhibit a similar trend, however they peak at $x_{NG} = 70\,\%$ and reduce again at higher NG energy fractions. The soot emissions are expressed by the filter smoke number (FSN) which ranges from 0 to 10. The soot is reduced to almost zero as with increasing x_{NG} the injected diesel quantity is reduced and together with this the significance of the non-premixed diesel combustion decreases. At the same time the NO_x emissions rise only moderately. This indicates that the soot-NO_x trade-off which exists in conventional diesel engines does not apply to DF combustion if the injected diesel quantity is small.

The combustion duration is calculated as the difference between MFB90 and MFB05. The ignition delay is the difference between the commanded SOI_{Diesel} and MFB05. The combustion duration reduces with increasing x_{NG} while the coefficient of variation of the IMEP (COV_{IMEP}) rises. It is assumed that the cause of both observations is the decreasing diesel mass. Thus the combustion regime shifts from the mixing-controlled and non-premixed diesel combustion

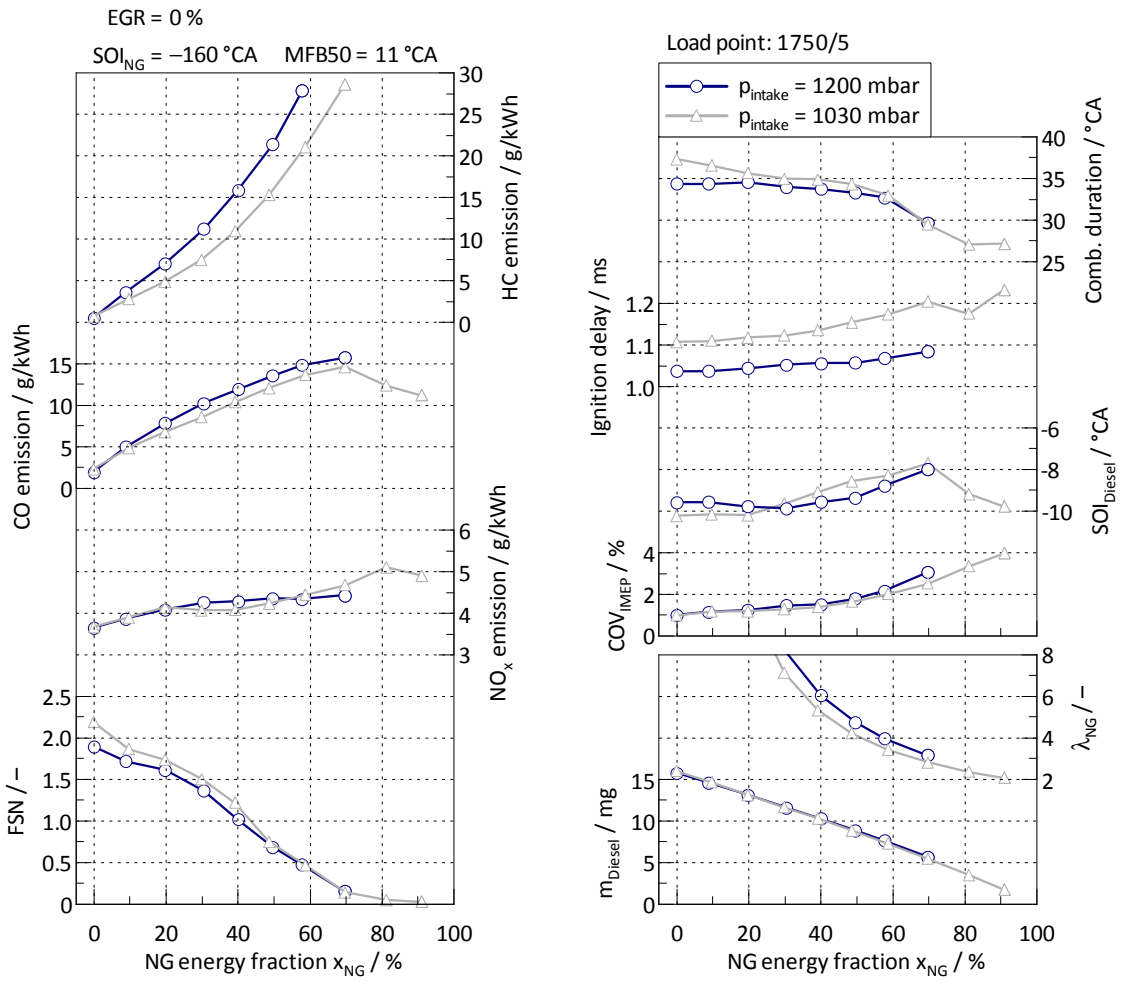

Figure 4.14: Variation of the NG energy fraction x_{NG} in the load point 1750/5 at two different intake manifold pressures.

towards a premixed combustion of natural gas (modes II and III in Figure 3.2), which is controlled by the reaction kinetics and in general evolves faster. Furthermore, with decreasing diesel mass the ignition energy reduces proportionally and bulk quenching due to the over-lean air-NG mixture becomes more dominant. Both effects result in an increase of $\mathrm{COV_{IMEP}}$. The rise of the ignition delay is assumed to be caused by the reduction in λ_{NG}. The concentration of oxygen in the charge reduces and thus the diffusion and reaction of oxygen and diesel slow down.

Figure 4.15 depicts the net heat-release rate, the electric signal of the diesel injection and the cylinder pressure for the case of $p_{\mathrm{intake}} = 1030\,\mathrm{mbar}$ and NG energy fractions of 0 %, 70 % and 90 %. The large peak of the premixed combustion (mode I in Figure 3.2) is well observed for a NG energy fraction of 0 % and 70 % since only a single diesel injection is used. The peak is higher at 70 % because of the larger ignition delay. At 0 % the asymmetric shape of the heat-release rate characteristic for non-premixed combustion is distinctive. At 70 % a

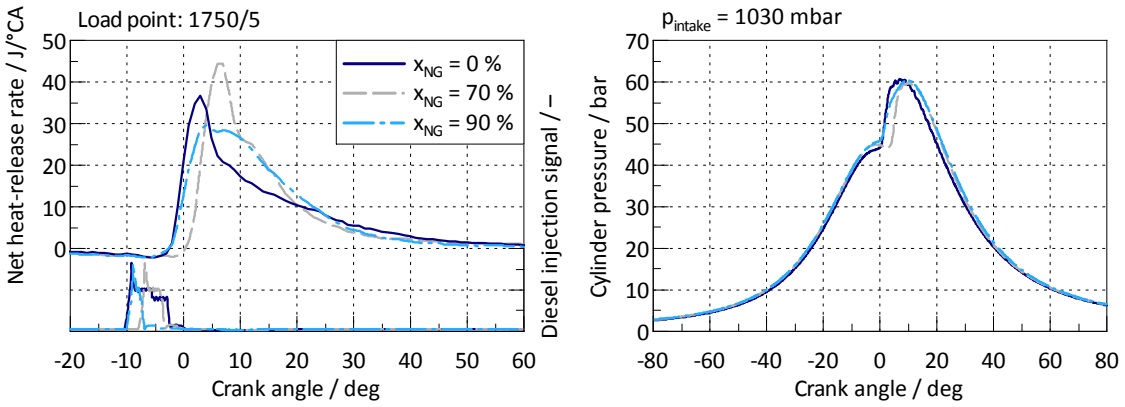

Figure 4.15: The net heat-release rates and cylinder pressure traces for natural gas energy fractions x_{NG} of 0 %, 70 % and 90 % at an intake manifold pressure of 1030 mbar.

small second increase at 12 °CA is observed while the general shape still resembles the shape of non-premixed combustion. At a NG energy fraction of 90 % the premixed peak is barely distinguishable due to the small amount of diesel injected and the shape is more symmetric indicating the dominance of premixed combustion.

To conclude, the variation of the NG energy fraction x_{NG} reveals the importance of high NG shares to lower the air-NG equivalence ratio λ_{NG}. Furthermore, the soot emissions are reduced to almost zero in natural gas-diesel dual fuel combustion if the diesel quantity is small. The shape of the heat-release rate is similar to the heat-release rate in premixed combustion, indicating that the regime of premixed combustion is prevailing if the diesel quantity is small. Finally, the major challenge in DF combustion are high HC emissions resulting from an over-lean air-NG mixture.

Start of NG Injection $\mathrm{SOI_{NG}}$

Another obvious parameter to investigate is the injection timing of NG described by the commanded start of NG injection $\mathrm{SOI_{NG}}$. This affects the mixture preparation of the air-NG mixture. By altering $\mathrm{SOI_{NG}}$ a homogeneous or stratified charge can be realised.

Charge stratification as a measure to reduce the local stoichiometry is only meaningful at globally lean mixtures. If there is a choice between stoichiometric, homogeneous operation and lean, stratified operation, the stoichiometric operation is beneficial in dual fuel combustion from an emissions point of view. In stoichiometric operation a three-way catalyst can be used and the exhaust gas temperature is high enough to convert potential engine-out $\mathrm{CH_4}$ emissions.

The challenge of high $\mathrm{CH_4}$ emissions only exists in operating points where a stoichiometric operation is not feasible as detailed in Section 4.2. Thus, before investigating the effects of charge stratification it is first necessary to determine at which load points stratification is in any case required. Figure 4.16 gives the global air-fuel equivalence ratio $\lambda_{\mathrm{global}}$ and the intake manifold pressure without EGR and throttling in the four investigated load points (Table 4.2). If p_{intake} equals the ambient pressure the mixture is globally lean only in the load points 1500/3 and 1750/5. At 2000/11 and 1750/15 the intake manifold pressure must be raised to avoid rich conditions. Thus only at 1500/3 and 1750/5 charge stratification for a reduction of the local

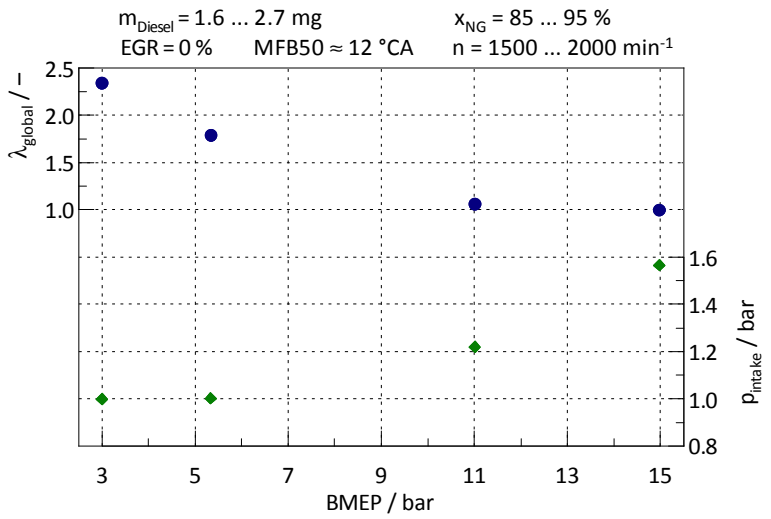

Figure 4.16: The global air-fuel equivalence ratio λ_{global} without throttling and EGR in dependence of the load.

stoichiometry is required while at 2000/11 and 1750/15 a stoichiometric mixture is feasible without additional measures such as EGR.

Figure 4.17 demonstrates a variation of SOI_{NG} between $-300\,°\text{CA}$ and $-90\,°\text{CA}$ for the load points 1750/5 and 2000/11. The load point 1750/5 is first discussed. Results without EGR and an intake manifold pressure of 880 mbar and with 35 % EGR and $p_{\text{intake}} = 1015\,\text{mbar}$ are depicted. Without EGR the air-NG equivalence ratio is approx. 1.9, with EGR it is approx. 0.5 units lower. As detailed in Section 4.2 retarding the NG injection is a measure to stratify the air-NG mixture and thus the local air-NG equivalence ratio is reduced. Thereby, a remarkable reduction of the HC emission is achieved. Without EGR the HC emission is reduced from 19 g/kWh to 7 g/kWh, which is a reduction of 63 %. At $\text{SOI}_{\text{NG}} = -90\,°\text{CA}$ λ_{bowl} is 1.67 which is 0.4 units lower than the air-NG equivalence ratio. This gives an indication for the reduction of the local equivalence ratio. The relative reduction is almost independent of EGR. At $\text{SOI}_{\text{NG}} = -100\,°\text{CA}$ the HC emission is reduced by another 3 g/kWh with EGR. In this case λ_{bowl} is lowered to 1.18. The results confirm the positive effect of NG direct injection on the HC emission at low load operation. An interesting effect occurs at SOIs between $-200\,°\text{CA}$ and $-180\,°\text{CA}$. An increase of the HC emission is observed in both cases. It is assumed that this rise results from unfavourable mixing or from unfavourable conditions during the diesel injection. For a detailed investigation of the observed effect, 3D CFD simulations would be required.

The reduction of the HC emission is achieved without reducing the intake manifold pressure. Thus, the ignition conditions of the diesel spray remain unchanged and the ignition delay remains constant. Consequently, the trade-off between CH_4 emissions and ignition delay is improved significantly as depicted in Figure 4.3. The reduction of the HC emission also reflects in the net indicated efficiency $\eta_{\text{i,n}}$. The air-NG equivalence ratio λ_{NG} rises slightly as less natural gas is injected with increasing efficiency. The smoke emission also peaks at $-180\,°\text{CA}$, but overall remains on a low level.

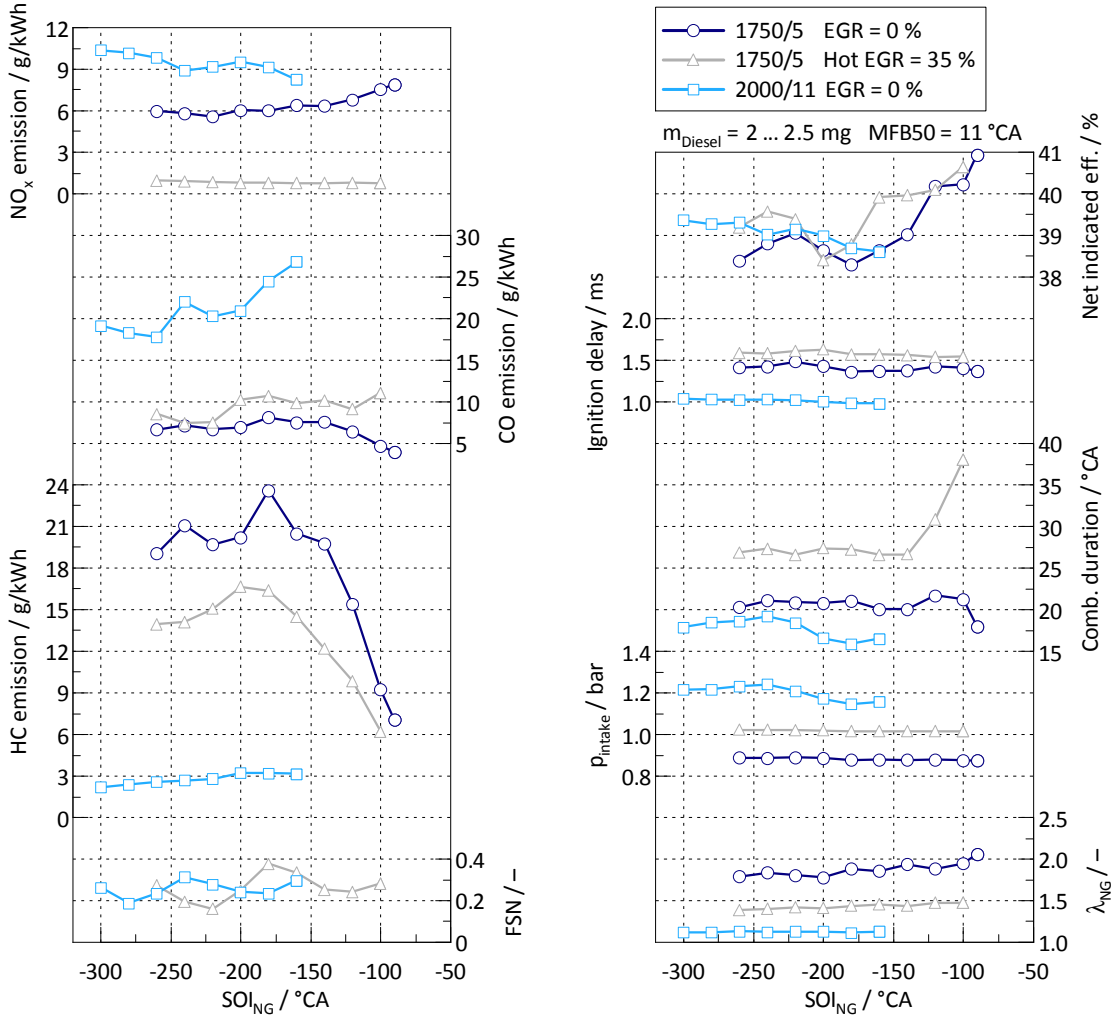

Figure 4.17: The influence of the start of NG injection SOI_{NG} on combustion characteristics in the load points 1750/5 and 2000/11.

The effect of stratification on the CO emissions is ambivalent. Starting from a comparable level they reduce by 40 % in the case of no EGR. In case of EGR they increase by 30 %. The increase is an indication for fuel rich zones in the combustion chamber as the air-NG equivalence ratio is lower by approx. 0.5 with EGR. The NO_x emission is below 1 g/kWh with EGR. It increases by 30 % without EGR as the injection is retarded and the local air-fuel equivalence ratio is reduced. The trend of the combustion duration supports the previous statements. The combustion duration decreases without EGR which indicates an improved combustion. The combustion is slower with EGR resulting from a lower combustion temperature and increases significantly after −140 °CA. This rise is again assumed to result from fuel rich zones.

Figure 4.18 depicts the net heat-release rate and the cylinder pressure at three injection timings for the measurement without EGR. The shape of the heat-release rate is similar to an SI combustion process and the combustion accelerates up with retarded SOI_{NG}. This is another indication that with increasing stratification the combustion improves. Compared to

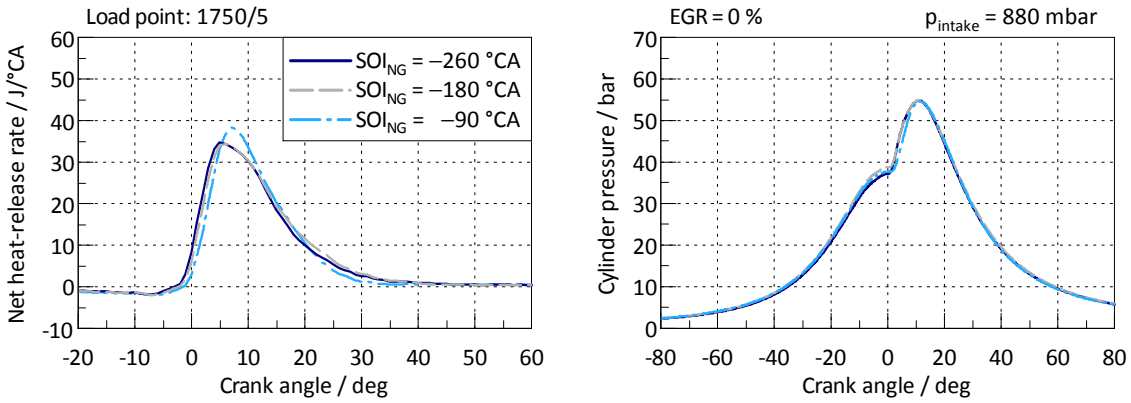

Figure 4.18: The net heat-release rate and the cylinder pressure for different NG injection timings in the load point 1750/5 without EGR.

the case of $x_{\mathrm{NG}} = 90\,\%$ in Figure 4.15 the shape of the heat-release rate is more symmetrical and the heat-release is faster. This is caused by the lower intake manifold pressure and thus the lower air-NG equivalence ratio. Evidence for this correlation will be given in the next section.

The correlations are fundamentally different in the load point 2000/11 in which a stoichiometric and homogeneous operation is pursued. The intake manifold pressure is adapted in order to achieve a global air-fuel equivalence ratio of unity. EGR is not applied. All characteristics indicate that best homogeneity of the air-NG mixture is achieved with the earliest $\mathrm{SOI_{NG}}$ of $-300\,°\mathrm{CA}$. At later injection timings the net indicated efficiency reduces and the HC and CO emissions rise.

Exhaust Gas Recirculation

It was demonstrated that high natural gas energy fractions are required and in lean operated load points late NG injection is also necessary to stratify the charge and reduce the local air-NG equivalence ratio. EGR is another measure to further reduce the air-NG equivalence ratio. The effect of cooled and hot EGR is investigated. An alternative measure to reduce λ_{NG} is the reduction of the intake manifold pressure by means of throttling. In order to compare these two approaches with each other the results in Figure 4.19 are plotted against the air-NG equivalence ratio. The measurements are conducted with stratified air-NG mixture at $\mathrm{SOI_{NG}} = -100\,°\mathrm{CA}$. MFB50 is set to 11 °CA. In the lower right part of Figure 4.19 the influence on the stoichiometry is displayed. With 35 % EGR resp. 680 mbar intake manifold pressure λ_{bowl} is approx. 1.1. It must be assumed that under this condition NG rich zones exist in the piston bowl as λ_{bowl} describes an idealised situation. In the lower left part the pollutant emissions are depicted. Throttling is the most effective measure to reduce the HC emission. A decrease from above 15 g/kWh to 4 g/kWh is achieved. With hot EGR a reduction to 6 g/kWh is achieved. Cooled EGR is less effective regarding the reduction of HC emissions. A minimum HC emission of 10.5 g/kWh is achieved at $\lambda_{\mathrm{NG}} = 1.65$ which corresponds to 30 % EGR. At higher EGR rates a steep increase in the HC emission is observed. The trend of the CO emissions is similar for all three variants. The CO emissions remain almost constant at around 5 g/kWh and soar at air-NG equivalence ratios smaller than 1.6. The rise in HC as also CO emissions is an indication

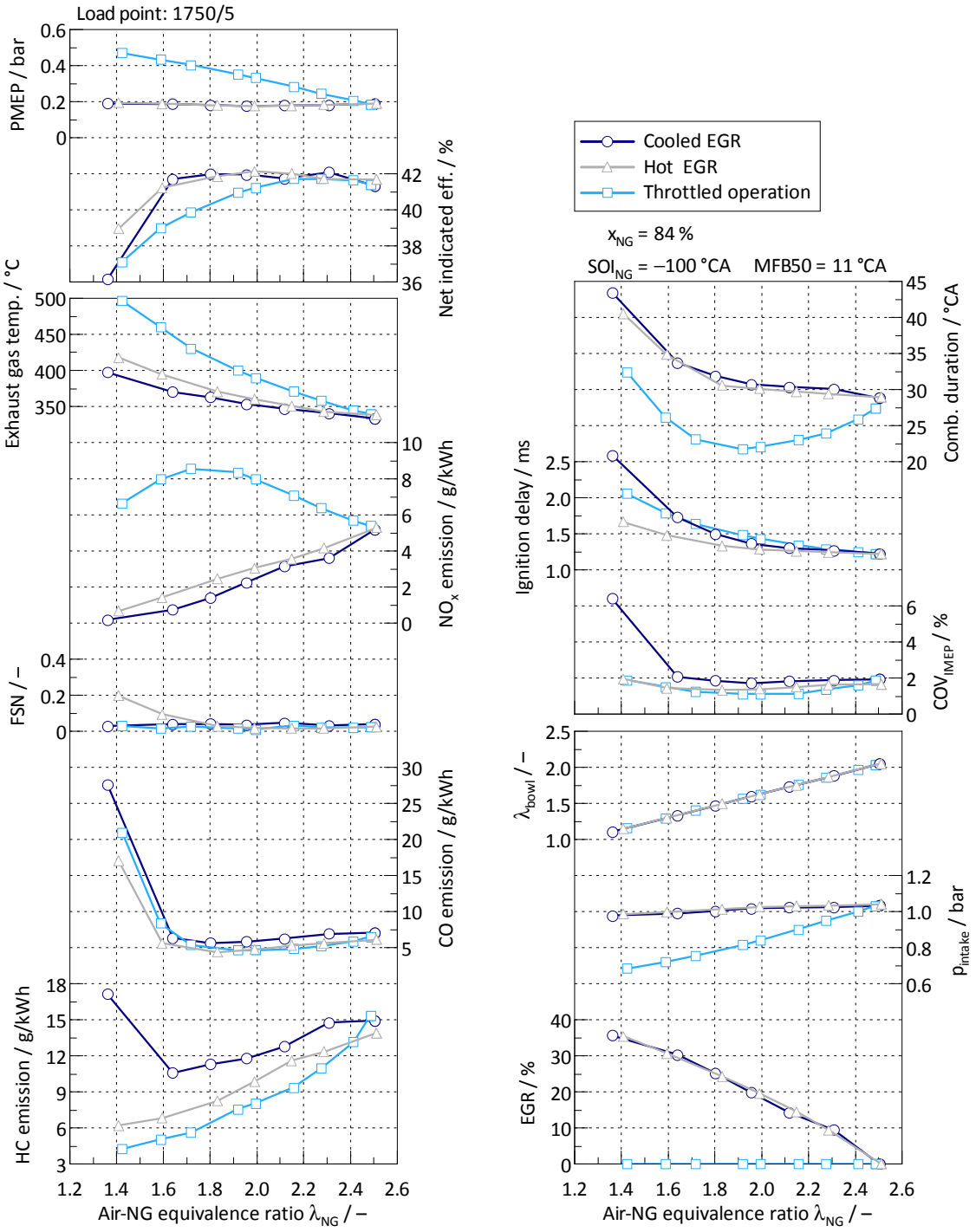

Figure 4.19: The influence of EGR and a reduced intake manifold pressure on the combustion in the load point 1750/5.

for NG rich zones which start to occur in the piston bowl. This means in stratified operation at an injection timing of $SOI_{NG} = -100\,°CA$ the limit of reducing the air-NG equivalence ratio is reached at approx. 1.6 which corresponds to $\lambda_{bowl} = 1.3$. In the load point 1500/3 (data not depicted) this rise is not observed, because at 40 % EGR and $p_{intake} = 1000\,mbar$ the air-NG equivalence ratio is still 2.0 due to the lower load.

Soot is almost not present at high air-NG equivalence ratios. The soot emission starts to rise at air-NG equivalence ratios below 1.8 only in the case of hot EGR. The trend is related to the decreasing oxygen concentration. Due to the lean operation oxygen is also present in the exhaust gas which is recirculated during EGR and influences the air-fuel equivalence ratio in the combustion chamber. The density of hot EGR is lower than of cooled EGR which means that for a given intake manifold pressure and a given mass of fresh air less exhaust gas is recirculated. This entails less oxygen being recirculated with hot EGR resulting in a lower air-fuel equivalence ratio in the combustion chamber. It explains why the soot emissions start to rise only in the case of hot EGR. Another possible cause is an uneven distribution of EGR among the cylinders due to changes in the flow field when the EGR cooler is bypassed.

A significant difference between throttling and the addition of EGR is clearly observed in the NO_x emissions. These are reduced to below 1 g/kWh with EGR while by throttling the NO_x emission increases to a maximum of 8.5 g/kWh. This trend results from a higher combustion temperature with throttling as the amount of inert mass in the cylinder is lower compared to EGR and the heat-release evolves faster. The rise of the exhaust gas temperature (EGT) is explained in a similar manner. By reducing p_{intake} the in-cylinder mass is reduced and therefore the temperature rises during combustion. The rise due to the addition of EGR is attributed to different causes. Firstly, the charge temperature increases which also affects the exhaust gas temperature. Secondly, the in-cylinder mass reduces, as higher temperatures at constant pressure result in lower mass. Thirdly, the more complete combustion also adds to the rise of the exhaust gas temperature.

The pumping mean effective pressure (PMEP) and the net indicated efficiency are presented in the top left of Figure 4.19. While the gas exchange losses remain almost unaffected by EGR they increase considerably by throttling as the intake manifold pressure is lowered. This affects the net indicated efficiency negatively which continuously decreases although the completeness of the combustion increases. At equivalence ratios smaller than 1.65 also with EGR a reduction of $\eta_{i,n}$ is observed. This reduction is related to the presence of NG rich zones and all its consequences as explained above.

Finally, in the top right part COV_{IMEP}, the ignition delay and the combustion duration are depicted. The COV_{IMEP} confirms that at the investigated NG injection timing no stable operation is feasible at air-NG equivalence ratios below 1.65 with cooled EGR. With hot EGR and throttling, however, the variation also starts to rise. The trend of the ignition delay is explained by a deterioration of the ignition conditions of the diesel spray due to the lower oxygen availability. In the case of throttling the ignition conditions worsen additionally due to the lower p_{intake}. The rise of the ignition delay is less pronounced with hot EGR than with cooled EGR, because of the higher charge temperature.

The combustion duration is influenced by the combustion temperature, the oxygen concentration and the turbulence intensity. The trend is inverse to the trend of the NO_x emission. The overall cylinder charge is reduced with throttling and therefore the combustion temperature rises, which reduces the combustion duration until two other effects dominate. With

increasing throttling the turbulence intensity and the oxygen availability are reduced, both of which factors prolong the combustion duration. In case of EGR the reduction of the oxygen availability seems to dominate from the beginning as the combustion temperature is less affected.

To conclude, the investigation shows that a reduction of the intake manifold pressure and hot EGR are effective measures to reduce the HC emission by means of a reduction of the air-NG equivalence ratio. However, the reduction of p_{intake} entails negative effects on the gas exchange losses and the NO_x emission which is particularly critical due to the globally lean operation. Depending on the degree of stratification a lower limit for the air-NG equivalence ratio exists below which NG rich zones start to exist. This appears in a steep rise of CO and HC emissions and ultimately in unstable engine operation.

Combustion Phasing – MFB50

The influence of the combustion phasing in stratified DDI combustion is investigated in this paragraph. The combustion phasing is described by MFB50. Figure 4.20 displays a variation of MFB50 in the load point 1750/5. Measurements without EGR and with 20 % cooled EGR are displayed. The start of NG injection is set to −100 °CA. The intake manifold pressure is constant at 1030 mbar in both cases thus the air-NG equivalence ratio with EGR is lower by approx. 0.5 units. EGR does not influence the general trends, but due to the lower oxygen concentration and the lower total in-cylinder mass (due to a higher charge temperature) the absolute values differ.

Both, the HC and the CO emission reduce almost linearly with advancing MFB50. Two effects are assumed to be responsible for the exhibited trend. The stratification of the air-NG mixture deteriorates with more time elapsing between the end of the NG injection and SOI_{Diesel}. This results in larger zones with over-lean mixtures leading to an increase in HC emissions. Furthermore, since the mixture is lean high temperature and pressure are crucial for the oxidation of the fuel. Due to the downwards piston movement in the expansion stroke pressure and temperature reduce as the piston moves downwards. Advancing MFB50 thus means the combustion evolves closer to TDC where pressure and temperature are higher. In addition the peak cylinder pressure also rises (top right part of Figure 4.20), which leads to an even stronger increase of pressure and temperature [55]. This effect can also be observed in the decreasing combustion duration and the reducing cycle-to-cycle variations. The lower HC and CO emission with EGR is attributed to the lower air-NG equivalence ratio. The NO_x emission rises steadily with advancing MFB50 due to the higher cylinder temperature during the combustion.

The exhaust gas temperature decreases with earlier MFB50 as the combustion evolves earlier. The influence of EGR on the exhaust gas temperature was already discussed in the section of exhaust gas recirculation. Due to the higher charge temperature with EGR the total in-cylinder mass reduces as the intake manifold pressure is maintained. This results in a higher combustion temperature. The gross indicated efficiency $\eta_{\text{i,g}}$ is a quantity characteristic for the combustion efficiency. With earlier MFB50 a rise in $\eta_{\text{i,g}}$ is observed before a flat optimum is reached at approx. 5 °CA and 45 %. The increase results from a reduction of the HC emission, but also from the influence of the combustion phasing on the brake torque [55].

In the load point 2000/11 (data not depicted) the influence of MFB50 on the HC emission

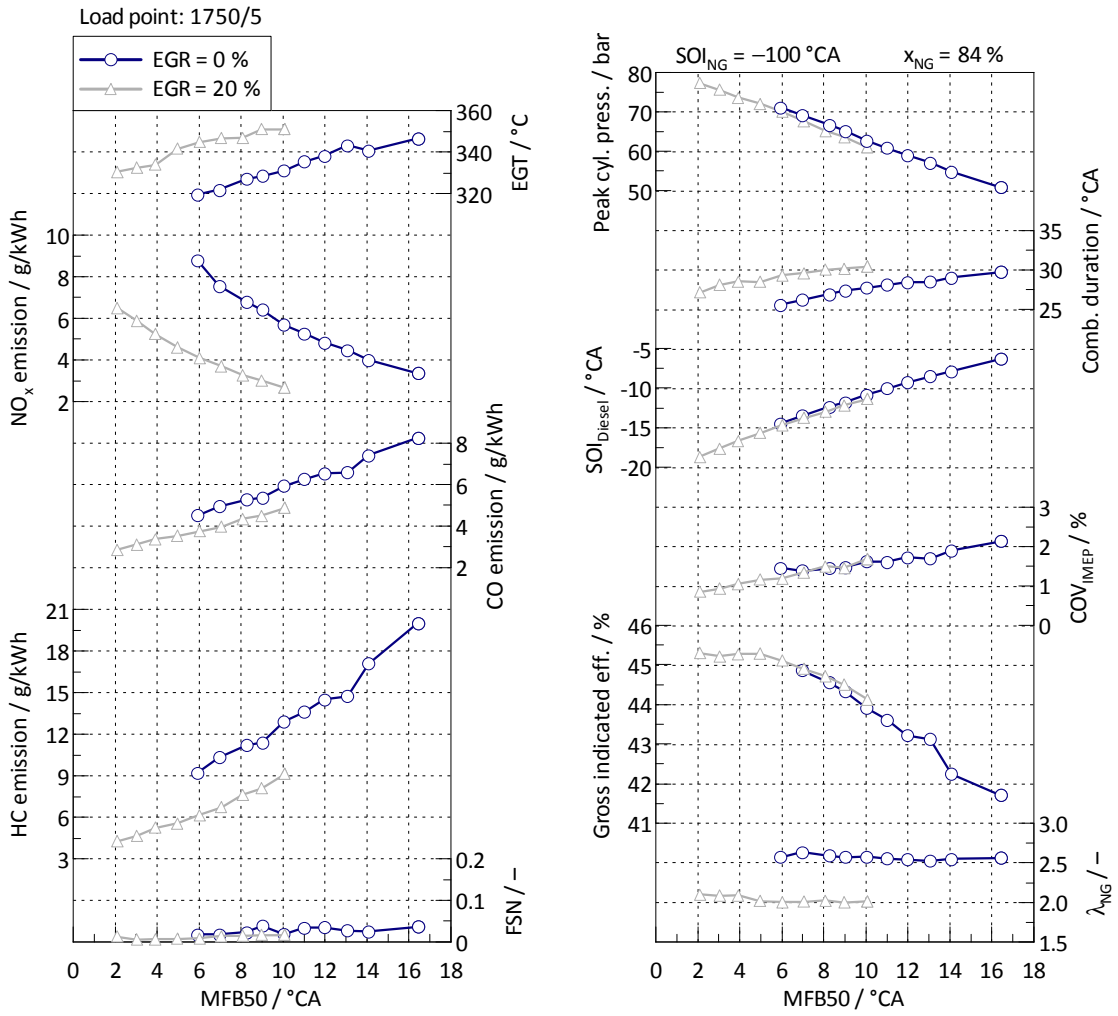

Figure 4.20: Variation of the combustion phasing described by MFB50 in the load point 1750/5 with and without cooled EGR.

and therefore the fuel efficiency is less pronounced as the DDI engine is operated stoichiometrically and homogeneously at 2000/11 and the conditions for the fuel oxidation are thus more favourable.

Diesel Rail Pressure

The diesel rail pressure (p_{Diesel}) has a considerable influence on the penetration length of the diesel spray, the jet breakup and the atomisation, the diesel evaporation and thus the mixture formation and ignition of the air-fuel mixture. It is therefore another obvious parameter to investigate. Figure 4.21 shows a variation of the diesel rail pressure between 400 bar and 800 bar. The injected diesel quantity remains constant at 2.7 mg. Analogue to the correlations in conventional diesel combustion [55] and consistent with findings in conventional dual fuel combustion [105] an increase of the diesel rail pressure reduces the ignition delay. It is attrib-

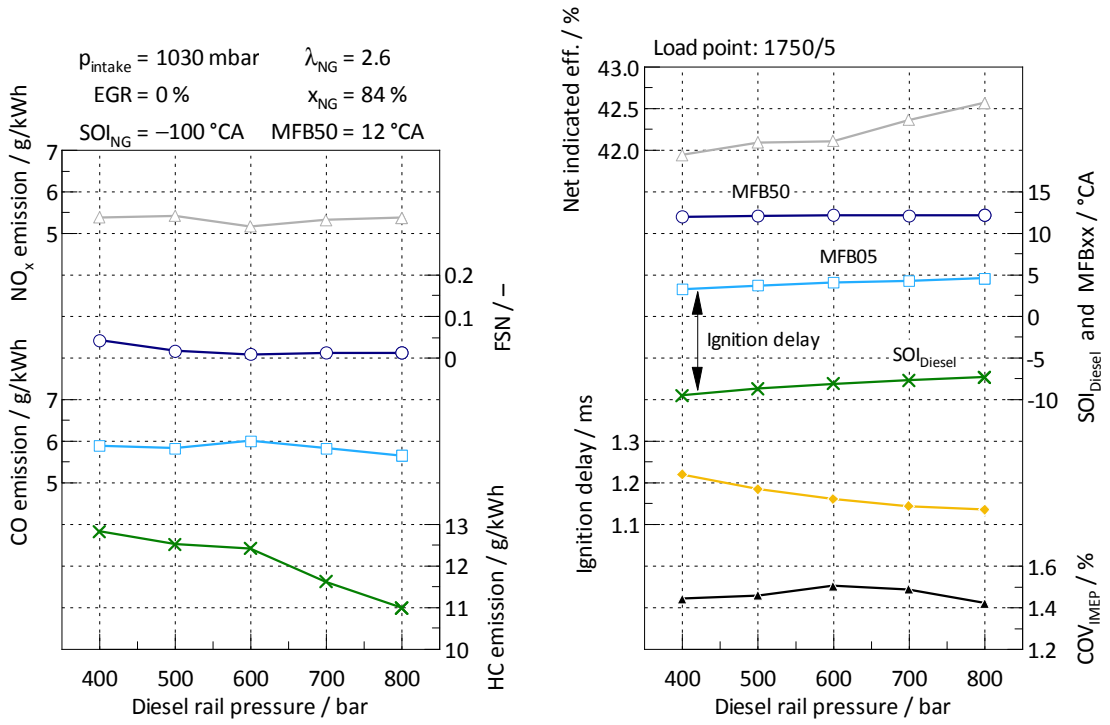

Figure 4.21: Variation of the diesel rail pressure in the load point 1750/5.

uted to improved entrainment of air, smaller droplets and thus a faster evaporation. A second effect amplifies the reduction of the ignition delay. SOI_{Diesel} must be retarded to maintain a constant MFB50 of 12 °CA as the ignition delay reduces. This means the diesel injection is shifted towards higher pressure and temperature in the cylinder which further reduces the ignition delay. Figure 4.22 displays the net heat-release rate and the electric diesel injection signal for 400 bar and 800 bar rail pressure. It is observed that only the first part of the heat-release rate is accelerated with increasing rail pressure. After 20 °CA the heat-release rates evolve identically. Furthermore, the first peak of the heat-release rate is more pronounced and higher. According to the combustion model stated in [65] and discussed in Section 3.2.1 this implies that the combustion of the diesel pilot injection (mode I) is enhanced while the subsequent combustion of NG which depends on flame propagation (mode III) is not significantly influenced. This finding converges with results in [100] where a method was developed to quantify the shares of the three combustion modes. It was demonstrated that an increase of the rail pressure increases the fraction of the pilot combustion due to a faster evaporation of the diesel and increased entrainment of air and natural gas and thus improved mixing. The acceleration of the initial part of the heat-release rate is also observed in Figure 4.21 as the duration between MFB05 and MFB50 decreases. A distinct trend of the cycle-to-cycle variations is not identified.

The influence on the emissions is depicted in the left part of Figure 4.21. A significant influence on the NO_x and the CO emission is not observed. The soot emission reduces further with increasing rail pressure from an already very low level. This indicates that soot results from the combustion of diesel. An increase of the rail pressure is an established method to

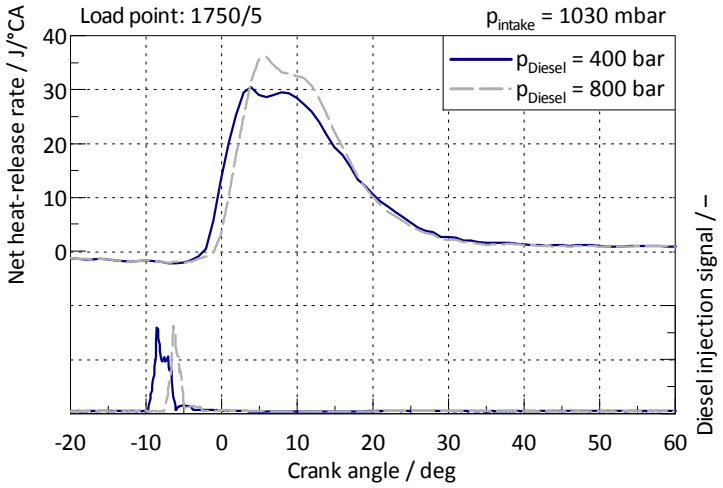

Figure 4.22: The net heat-release rate and the electric diesel injection signal for different diesel rail pressures.

reduce soot in conventional diesel combustion as the mixture formation and the entrainment of air is enhanced [55]. It is also a viable measure to reduce soot in the DDI concept due to the same mechanisms. However, due to the small diesel quantity the level of soot in DF combustion is lower by one order of magnitude compared to diesel combustion.

Furthermore, a distinct reduction of the HC emission from 13 g/kWh to 11 g/kWh is noted. Again due to the improved mixture formation of diesel larger quantities of NG are entrained and more NG is located in the vicinity of the premixed fraction. Optical measurements conducted in [105] for different rail pressures with an air-NG equivalence ratio of 2.7 confirm that with higher rail pressures larger areas of the piston bowl are covered by the combustion. It is attributed to larger ignition sites caused by the improved diesel evaporation. Furthermore, observations made in [135] suggest that the rail pressure influences the location of the ignition sites and the direction of the subsequent flame propagation fundamentally (Figure 3.3). This may also impact the size and location of unburned zones.

Charge Motion

The base diesel engine has two intake ports. One is designed as helical (filling) duct for high volumetric efficiency and one as tangential swirl duct for high swirl motion. The intake air can be directed to the swirl duct by closing a flap located before the filling duct. With open flap the air flows through both ducts. By closing the flap more air is flowing through the swirl duct. Thus, the in-cylinder swirl motion is adjusted to the particular requirements. Furthermore, due to the piston bowl and the large squish area, a squish motion is superimposed on the swirl motion as the piston moves towards TDC. This means the charge is forced into the piston bowl which has a smaller radius than the cylinder bore. Due to the equilibrium of momentum the angular velocity increases with decreasing radius, intensifying the swirl motion around TDC. Figure 4.23 displays a variation of the swirl flap position in the operating point 1750/5. Higher values correspond to an increase of the swirl motion. The air-NG mixture is stratified as SOI_{NG}

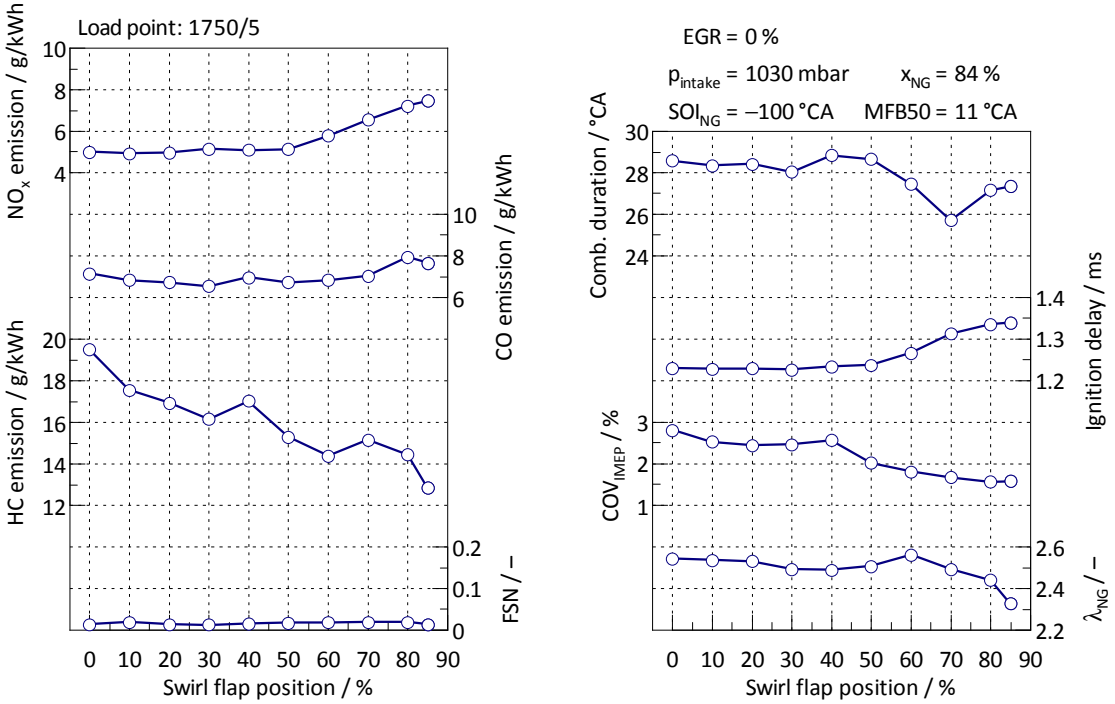

Figure 4.23: Variation of the swirl flap position in the load point 1750/5.

is set to −100 °CA. The intake manifold pressure is constant at 1030 mbar.

The smoke emission remains unaffected and close to zero. The CO and NO_x emissions exhibit an increase at swirl flap positions higher than 50 %. The increase in CO is weak while the increase in NO_x is significant. Simultaneously, the HC emission decreases remarkably by 35 % or almost 7 g/kWh. In addition, the combustion duration and the cycle-to-cycle variation reduce while the ignition delay rises with increasing swirl. The air-NG equivalence ratio λ_{NG} reduces, because the volumetric efficiency is reduced by closing the swirl flap. This is also expected to influence the HC emission positively. Thus the reduction in HC results not only from an increase in swirl. The influence of swirl on the HC emission is confirmed, however, as λ_{NG} is affected only at positions above 60 % while the HC emission is already reduced previously.

It is noticeable that for all quantities depicted an influence of the swirl flap is only observed for positions higher 50 % except for the HC emission. This results from the chosen load point and the characteristic of the flap. The air mass flow is low as the engine speed and the load are low also. In addition, the cross-section of the filling duct does not reduce linearly with the swirl flap position. Thus significant quantities of air are redirected and channelled through the swirl port and intensifying the swirl motion only above 50 %. The increase in NO_x as also the reduction in HC is attributed to improved mixing and a faster combustion due to the increased charge motion and turbulence. This is confirmed by the reduction of the combustion duration and the cycle-to-cycle variation.

The trend of the combustion duration with a minimum at 70 % is discussed by reference to the net heat-release rates displayed in Figure 4.24 for swirl flap positions of 0 %, 70 % and 85 %.

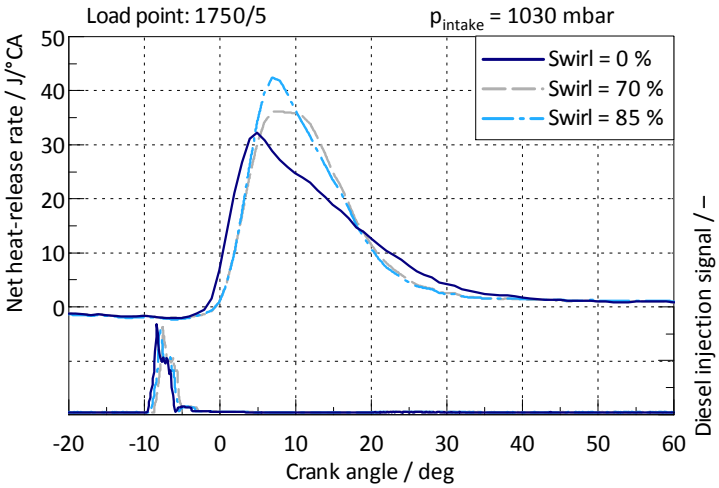

Figure 4.24: The influence of different swirl levels on the net heat-release rate.

The level of swirl significantly influences the shape of the heat-release rate, as also its peak. The ignition delay is prolonged with higher swirl which leaves more time for the evaporation of diesel and mixing with air and NG. This increases the fraction of pilot combustion (mode I) and leads to a higher peak of the heat-release rate. Even more pronounced is the effect on the subsequent combustion of NG, which is significantly accelerated and results in an almost symmetric shape of the heat-release rate. The higher calculated combustion duration with 85 % swirl compared to 70 % results from a slightly lower heat-release rate after 10 °CA and is not relevant as the heat release-rates illustrate.

In conclusion it can be stated that a positive influence of swirl on the combustion is observed. It is emphasised, however, that on the basis of this investigation it is not yet understood if swirl is the optimal charge motion pattern for the DDI concept. More information on the influence of different charge motion patterns on the combustion of the DDI concept is given in [115].

4.5.2 Optimised Parameter Set

As demonstrated in Section 4.5.1 there are more than six application parameters to optimise in stratified operation thus opening up a large design space. In order to find the optimum efficiently DOE was used. The optimisation is demonstrated on an exemplary basis for the load point 1750/5. Using the response surface methodology (RSM) a D-optimal quadratic model was created with five input factors and several responses by means of the software *MODDE* v9.1. D-optimal means that the experimental design is created in a way to maximise the information for a given number of experiments and thus reducing the number of required measurement points. Another advantage is that constraints can be added to exclude certain areas of the design space [126]. In order to assess the reproducibility of the measurements additional measurement points were added for validation. The input factors and their domain are: cooled EGR (0 %...40 %), SOI_{NG} (−260 °CA...−80 °CA), p_{intake} (800 mbar...1200 mbar), swirl (30 %...90 %) and MFB50 (6 °CA...12 °CA). The model is valid for a NG energy fraction of 85 %. A constraint was added to limit the amount of EGR in dependency of the intake manifold

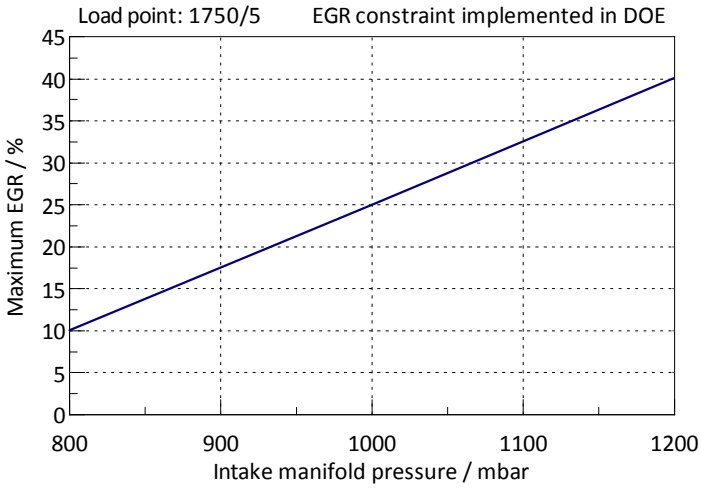

Figure 4.25: The constraint of EGR in dependency of the intake manifold pressure implemented in the DOE model.

pressure as depicted in Figure 4.25 to avoid instable operation due to excessive cycle-to-cycle variations. The most important responses of the DOE model are the unburned species $\Delta\zeta_{\mathrm{IC}}$ and the NO_x emission. The unburned species are chosen over the HC emission as they aggregate the HC and CO emissions and describe the total losses due to incomplete combustion. The model generally considers all quadratic terms and all two-factor interactions for each response. The chosen fitting method was multiple linear regression (MLR). The algorithm minimises the sum of squares of the residuals and fits one response at a time. It assumes the responses to be independent from each other [126]. The significance of each model term was then assessed by comparing its influence and the calculated confidence interval. Non-significant terms were excluded.

The created model states minimum $\Delta\zeta_{\mathrm{IC}}$ at maximum NG stratification as also demonstrated in the previous section. Figure 4.26 depicts the $\Delta\zeta_{\mathrm{IC}}$ response of the DOE model over EGR and MFB50 for intake manifold pressures of 1000 mbar and 1200 mbar. $\mathrm{SOI_{NG}}$ is set to $-80\,°\mathrm{CA}$ and the swirl flap is set to 60 %. Two different optimisation criteria are employed. The first criterion is minimum $\Delta\zeta_{\mathrm{IC}}$. Minimum unburned species are achieved at early combustion phasing and low intake manifold pressure in combination with highest permissible EGR which results in the lowest air-NG equivalence ratio for a given p_{intake} (Figure 4.26). However, since the charge is globally lean in this load point also the NO_x emission is of importance, as the exhaust gas aftertreatment of NO_x in lean operation is critical. In a second step thus the unburned species are optimised under the condition of a maximum permissible NO_x emission of 0.4 g/kWh. This approximately equals the engine-out NO_x of the base diesel engine in this load point. The minimum NO_x emission occurs at maximum charge dilution (40 % EGR and 1200 mbar intake manifold pressure) and late combustion phasing. Hence, the optimum of the second criterion is found in the area spanned by the points of minimum $\Delta\zeta_{\mathrm{IC}}$ and minimum NO_x (green triangle in Figure 4.26). It is located at maximum charge dilution and early combustion phasing.

The parameter combinations found by means of DOE were validated and fine-tuned experimentally on the engine test bench. Figure 4.27 displays the measurement results of these

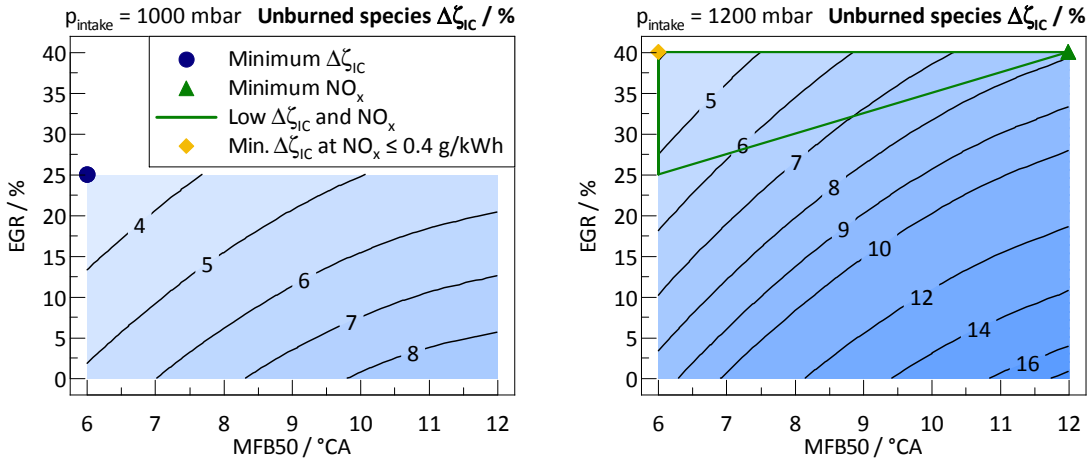

Figure 4.26: The unburned species $\Delta\zeta_{\mathrm{IC}}$ calculated with the DOE model in the load point 1750/5 with $\mathrm{SOI_{NG}} = -80\,°\mathrm{CA}$, 60 % swirl and $x_{\mathrm{NG}} = 85\,\%$.

final optima in the load point 1750/5. The corresponding application parameters are stated in Table B.1 in Appendix B. The DOE optima prove very to be accurate. The biggest difference compared to the DOE optimisation is that in the case of minimum $\Delta\zeta_{\mathrm{IC}}$ hot EGR is deployed instead of cooled EGR, but this differentiation was not included in the DOE model.

Minimum unburned species of 1 % are achieved in this load point. This corresponds approximately to HC and CO emissions of 2 g/kWh each. However, the NO_x emission reaches almost 5 g/kWh. Limiting the NO_x to 0.4 g/kWh requires a reduction larger than one magnitude. As a consequence the unburned species double to 2 %. This is still within the range of typical gasoline SI engines. The HC emissions alone of gasoline SI engines are reported to account for 1 % to 2.5 % of the fuel energy [55]. The net indicated efficiency $\eta_{\mathrm{i,n}}$ reaches 42.5 % and 43 % respectively. These results demonstrate the remarkable potential of the DDI concept to improve natural gas-diesel dual fuel combustion in low load operation. The exhaust gas temperature is low and between 305 °C and 355 °C, owing to high EGR, the lean charge and the high compression ratio of 16.5. The effect of hot EGR is observed in the combustion duration which is considerably shorter than with cooled EGR.

The same optimisation was performed for the load point 1500/3. Again Table B.1 states the application parameters for the derived calibration. Figure 4.28 displays a comparison of the operation calibrated for minimum $\Delta\zeta_{\mathrm{IC}}$ at low NO_x in the load points 1500/3 and 1750/5. At 1500/3 the NO_x emission is 0.6 g/kWh which equals the engine-out NO_x emission of the base diesel engine in this load point. At 1500/3 the HC emission increases by 3 g/kWh to 6.5 g/kWh. Also the CO emission rises by 3 g/kWh to 8 g/kWh. Thus, the unburned species increase from 2 % to 3.5 %. The main reason is the leaner charge at this load point. The air-NG equivalence ratio rises from 1.6 to 2.1. This corresponds to λ_{bowl} of 1.3 resp. 1.7 under the condition of ideal charge stratification. This reveals that low load operation remains critical also with the DDI concept, however the effects are mitigated. The net indicated efficiency remains high at 41.6 %. The exhaust gas temperature decreases further to 250 °C which is regarded as large challenge for any kind of exhaust gas aftertreatment.

As discussed in Section 4.5.1 in dual fuel combustion charge stratification is only meaningful

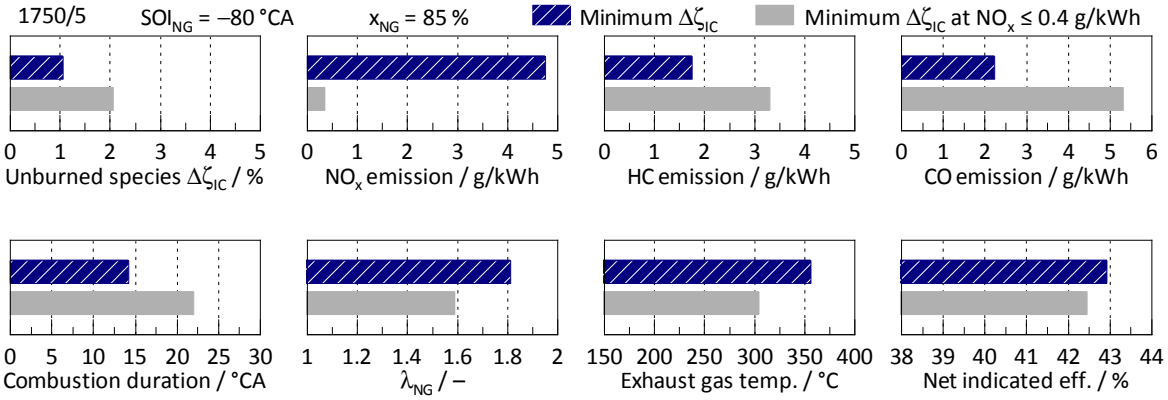

Figure 4.27: Measurement results of the optimised DDI operation in the load point 1750/5.

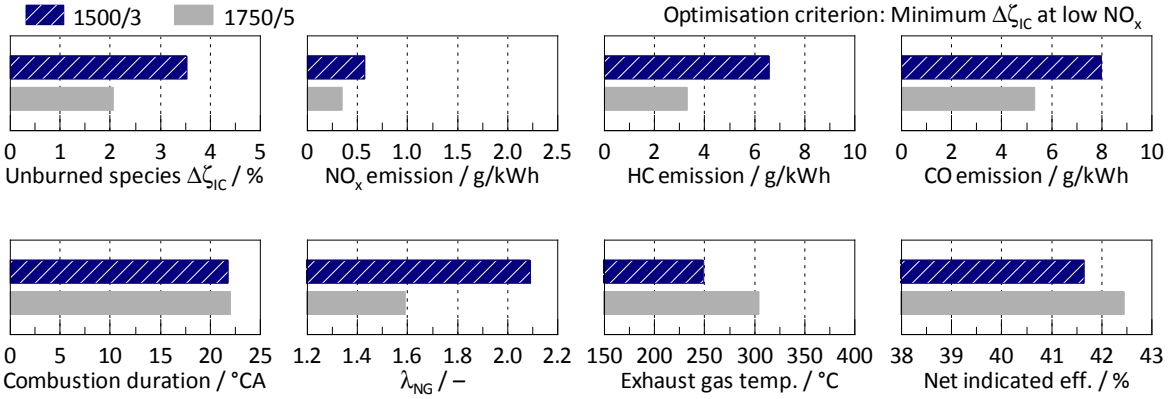

Figure 4.28: Comparison of the operation in the load points 1500/3 and 1750/5 optimised for minimum $\Delta\zeta_{\mathrm{IC}}$ at low NO_x.

if homogeneous and stoichiometric operation is not feasible. Since in the load point 2000/11 homogeneous and stoichiometric operation is achieved without throttling (Figure 4.16) the optimisation criterion is a different one. In stoichiometric operation the exhaust gas temperature is higher and a three-way catalyst can be deployed for the exhaust gas aftertreatment. This means both the HC and the NO_x emission can be converted effectively, no longer being the main criterion for optimum engine operation. The optimisation criterion is instead the maximum net indicated efficiency $\eta_{\mathrm{i,n}}$. Of course this requirement corresponds to an operation with low HC emission as the losses of incomplete combustion directly affect the fuel efficiency. Figure 4.29 depicts the measurement results of the optimised stoichiometric and homogeneous calibration in load point 2000/11. The results are contrasted with the lean and stratified operation in load point 1750/5 optimised for minimum $\Delta\zeta_{\mathrm{IC}}$ and low NO_x. The corresponding application parameters are stated in Table B.1. The HC emission is lower at 2000/11 than at 1750/5. However, characteristic for stoichiometric operation the NO_x and the CO emissions increase significantly. Overall, the unburned species increase by 0.6 $\%_{\mathrm{Pt.}}$ in the load point 2000/11. Furthermore, the exhaust gas temperature reaches 600 °C facilitating the exhaust gas aftertreatment even of

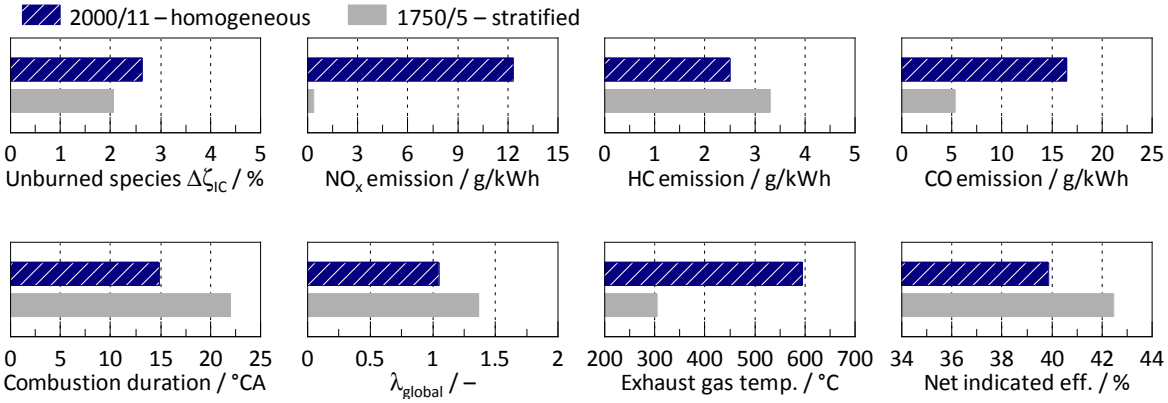

Figure 4.29: Measurement results of the stoichiometric operation optimised for maximum net indicated efficiency in the load point 2000/11 and the calibration for minimum $\Delta\zeta_{\mathrm{IC}}$ and low NO_x in the load point 1750/5.

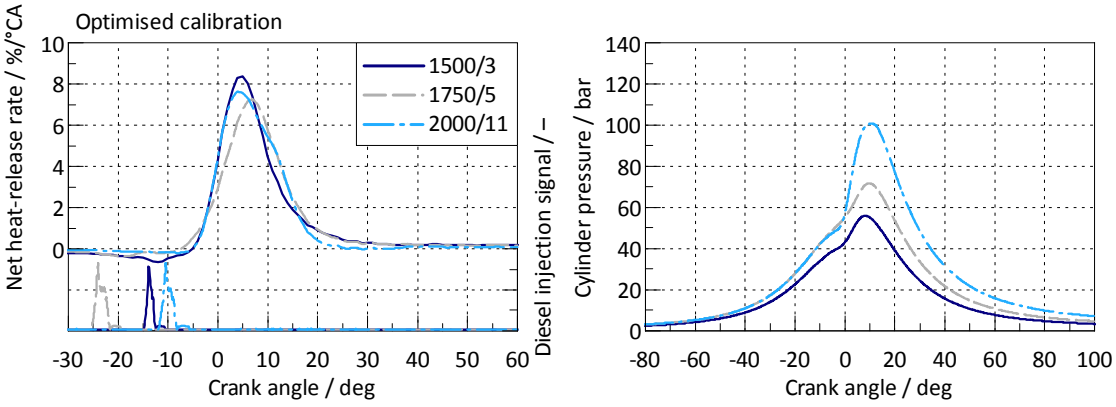

Figure 4.30: The net heat-release rates and the cylinder pressure traces of the optimised operation in the load points 1500/3, 1750/5 and 2000/11.

methane. The combustion duration is longer in the lean and stratified operation due to the use of EGR. The net indicated efficiency reaches 40 % at 2000/11. It is 2.6 $\%_{\mathrm{Pt.}}$ lower than at 1750/5 due to higher wall heat losses, higher losses due to incomplete combustion and a different composition of the charge resulting in different thermodynamic properties.

Finally, Figure 4.30 shows the cylinder pressure traces and the net heat-release rates corresponding to the optimised calibration of the load points 1500/3, 1750/5 and 2000/11. The heat-release is normalised to 100 % to allow for a qualitative comparison between the three load points. Overall, the heat-release rates are almost symmetric and resemble the heat-release of premixed SI combustion. The asymmetric shape of non-premixed combustion (Figure 4.15 $x_{\mathrm{NG}} = 0\,\%$) is no longer distinguishable, indicating good mixture preparation and a combustion of the air-NG mixture by flame propagation immediately after the ignition of the diesel pilot spray. Furthermore, the effect of EGR on the heat-release can be well studied. In 1750/5 high amounts of cooled EGR are used, resulting in the longest ignition delay (also in the time domain) and a shallower rise of the heat-release rate. The shape of the heat-release rates is

quite different to the shape in non-optimised operation points (e.g. Figure 4.15, 4.22). This holds true for the results published of many other researchers. To a large extent the published heat-release rates are asymmetric and feature a distinct premixed peak while in a few operating points an almost symmetric heat-release rate is observed, e.g. [25, 70, 85]. It would appear that the mixture preparation, the ignition conditions and the conditions for a subsequent flame propagation are favourable, the boundaries between the different combustion regimes in dual fuel combustion as stated in [65] blur increasingly.

4.5.3 Operating Strategy

An operating strategy for the DDI concept can be developed with the knowledge of optimised calibration in the investigated load points. Figure 4.31 displays the derived operating strategy which divides the engine operating map into three operating regimes. During idling and at very light loads conventional diesel operation is inevitable. Significant improvements are demonstrated with the DDI concept to limit the HC emission at light loads and the boundary for stable dual fuel combustion is shifted towards lower loads. However, conceptual constraints exist for DF combustion as explained in Section 4.2. These constraints cannot be suspended with the DDI concept, making diesel operation necessary at lightest load also with the presented concept. However, it is vital to limit the diesel operation to an area as small as possible. Otherwise the CO_2 reduction diminishes in real world driving. Especially, as in urban driving the average engine load is low.

At high loads when stoichiometric operation becomes feasible without considerable throttling stoichiometric and homogeneous dual fuel operation is preferred as demonstrated in the previous section for the load point 2000/11. Thus, effective exhaust gas aftertreatment becomes feasible using a three-way catalyst. At loads in between the stratified and lean operation is pursued as demonstrated for the load points 1500/3 and 1750/5. The loads at which the operating regimes are switched are only estimations. It was not part of the investigations to identify exact delimitations between the individual operating regimes. Furthermore, a possible

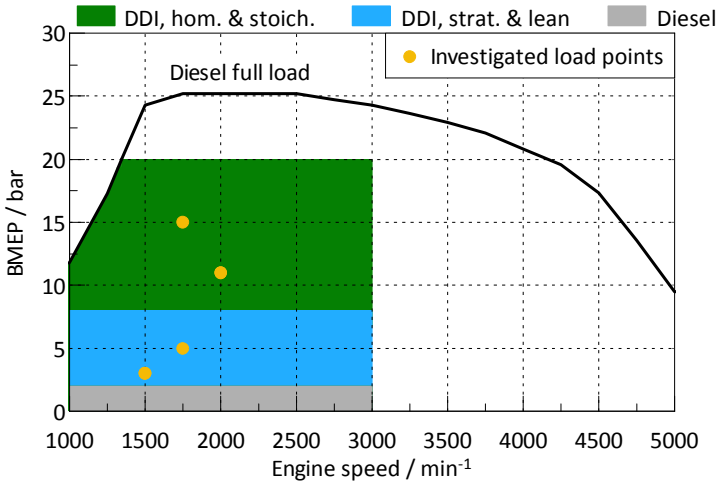

Figure 4.31: The developed operating strategy for the DDI concept.

influence of the engine speed on the boundaries was also not studied.

Dual fuel operation was not studied at engine speeds higher than 3000 min^{-1} thus no statement is made on operation in this part of the engine map. Results of dual fuel combustion at engine loads up to 19 bar BMEP were published earlier in [114]. Knocking was avoided even though a compression ratio of 16.5 was used. However, the question of whether the same maximum load is achievable compared to the base diesel engine was not investigated in detail. In general DF combustion is prone to knocking and related combustion anomalies. Therefore, the area above 20 bar BMEP is not marked in Figure 4.31. The phenomenon of low speed preignition in DF combustion was studied in [136]. Methods to predict knocking in DF combustion were developed in [111]. The knock limit also depends on the fuel. The knock resistance of natural gas is high due to the high methane share, but it can vary substantially depending on the composition of natural gas.

An operating strategy for conventional DF combustion was developed in [123]. Similarly, an operation in diesel mode was suggested at light engine loads. The effect of the operating strategy on the CO_2 emission and the fuel efficiency in the NEDC was estimated and compared to a diesel engine. In order to avoid knocking at high loads, diesel operation was suggested also close to full load.

4.5.4 Variation of the Compression Ratio

The influence of hardware parameters was also studied in addition to the application parameters. The results of these studies were published in [37]. One of the most important hardware parameters is the compression ratio ε. The compression ratio was reduced from 16.5 to 14.5 to study its effects on the DDI combustion and to investigate the limits of the combustion process. In view of the interrelated topics of power density, knocking and varying NG qualities a lower compression ratio might be desirable, despite the fact that the fuel efficiency would be reduced. Equation 4.6 states the compression ratio, V_d is the displacement and V_c is the clearance volume in TDC.

$$\varepsilon = \frac{V_c + V_d}{V_c} \tag{4.6}$$

The compression ratio was reduced by increasing the clearance volume. This was achieved by increasing the volume of the piston bowl. The ω-shape of the bowl was maintained. Figure 4.32 displays the two pistons bowls. The following analysis is performed in the load points 1500/3 and 2000/11.

Figures 4.33 and 4.34 display a comparison of measurements with a compression ratio of 16.5 and 14.5 in the load point 1500/3. In both cases the operation is optimised for minimum

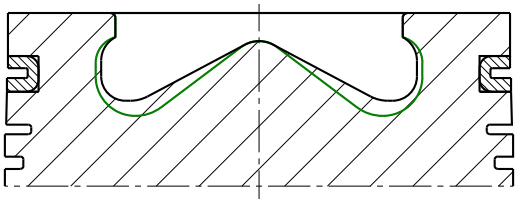

Figure 4.32: The standard piston (black) with $\varepsilon = 16.5$ and the modified piston bowl (green) for $\varepsilon = 14.5$.

unburned species at NO_x emissions on the level of the base diesel engine in this load point. Different engine calibrations are required to achieve this. In case of $\varepsilon = 16.5$ the calibration is the same as depicted in Figure 4.28 and stated in Table B.1. A different calibration had to be developed for the engine with reduced compression ratio. Not only that the calibration for $\varepsilon = 16.5$ was not optimal, but an engine operation was not even feasible. The reason is that the ignition conditions of the diesel spray deteriorate with a reduced compression ratio and thus without countermeasures the cycle-to-cycle variations increase enormously. The same approach was followed as outlined in Section 4.5.2 to develop the calibration for the engine with reduced compression ratio. The derived application parameters are stated in Table B.2.

Figures 4.33 demonstrates that almost all characteristics worsen with a reduction of ε. The ignition delay of the diesel spray depends to a significant extent on the pressure and temperature in the combustion chamber [55]. A reduction of the compression ratio reduces both, prolonging the ignition delay. In order to achieve stable engine operation the diesel injection has to be increased from 2.3 mg to 4 mg. This reduces the NG energy fraction from 79 % to 64 %. While the global air-fuel equivalence ratio remains almost unaffected at approx. 1.6, the air-NG equivalence ratio increases from 2.1 to 2.4 which influences the NG combustion negatively. The unburned species increase from 3.5 % to above 6 %, they comprise of 12 g/kWh HC emissions and 14 g/kWh CO emissions. This is a consequence of the leaner air-NG mixture as also of the reduced pressure and temperature in the combustion chamber. During the expansion stroke when temperature and pressure decrease the oxidation of the fuel and intermediate products comes to a halt earlier due to the lower peak values. The poor diesel ignition and subsequent combustion are observed in the injection timing SOI_{Diesel}. While the diesel injection is advanced by more than 7 °CA, MFB50 occurs later at 5 °CA. The overall combustion duration increases by 10 °CA and the cycle-to-cycle variation is unacceptably high at above 4 %.

A reduction of the compression ratio reduces the efficiency of the engine as the heat-release evolves at a lower average temperature which fundamentally reduces the efficiency of a thermodynamic cycle. It can be studied by means of the Carnot cycle and idealised engine operating cycles [97]. The effects as mentioned cumulate in a reduction of the net indicated efficiency of almost $5\,\%_{Pt.}$. The exhaust gas temperature increases by 40 °C as a consequence of the lower fuel efficiency.

The associated net heat-release rates and cylinder pressure traces are displayed in Figure 4.34. The reduction of the compression ratio is well observed in the pressure evolution. The peak cylinder pressure reduces by 14 bar. The electric diesel injection signal indicates the increase of the ignition delay. Finally, the rise of the heat-release rate is less rapid and also prolonged after 10 °CA. It indicates that not only the combustion of the diesel pilot injection is inferior, but also the subsequent combustion of the air-NG mixture. Presumably, an increase of the piston bowl volume reduces the squish flow. Less charge motion affects the mixture formation of the diesel injection negatively and also the subsequent combustion of the air-NG mixture.

Figures 4.35 and 4.36 display the comparison of the two compression ratios in the load point 2000/11. In contrast to the previous results in the load point 1500/3 the identical calibration can be used in this load point. Thus, the effects resulting exclusively from a reduction of the compression ratio can be analysed. However, this means that in the event of the lower ε the calibration might no longer be optimal. Both measurements are conducted at $\lambda_{global} = 1$,

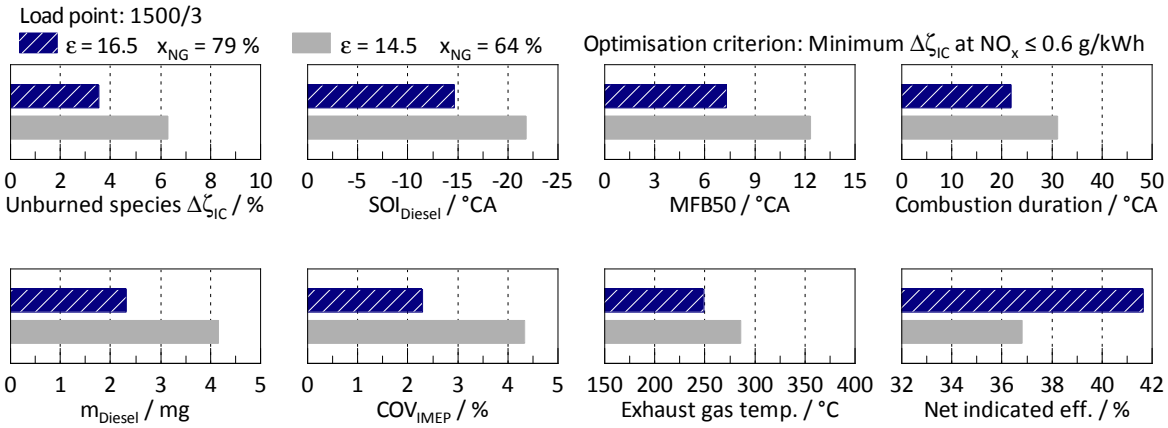

Figure 4.33: The effect of different compression ratios on the DDI combustion in the load point 1500/3.

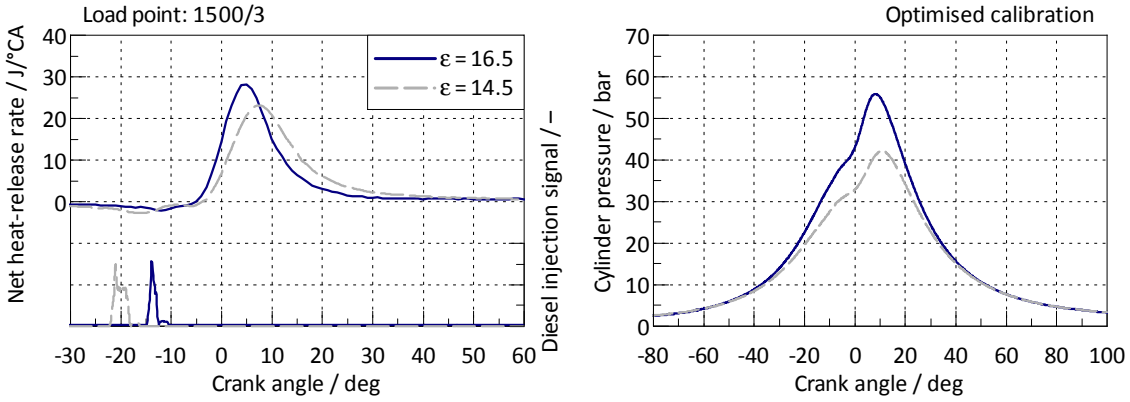

Figure 4.34: The net heat-release rates and the cylinder pressure traces in the load point 1500/3 for the operation with different compression ratios.

MFB50 is set to 7 °CA and the diesel pilot quantity is 2 mg. A full list of the set application parameters is stated in Tables B.1 and B.2.

In general, the trends are similar to the ones observed at 1500/3 however the effects are softened. The ignition delay rises moderately and SOI_{Diesel} must be advanced by 3 °CA to keep MFB50 constant. Due to the higher load the total cylinder mass increases by approx. 30 % compared to 1500/3. This causes the intake manifold pressure to rise by 250 mbar. In addition, the turbulence increases with the higher engine speed. This is both reducing the ignition delay, thus the effect of the compression ratio is less pronounced at 2000/11.

The combustion duration increases by 5 °CA. Again this rise is smaller than at 1500/3. The HC and CO emissions rise by 2 g/kWh resp. 3 g/kWh, which is equivalent to a rise in unburned species from 2.6 % to 3.7 %. The increase can be attributed to the lower combustion temperature at $\varepsilon = 14.5$. Therefore, the oxidation of fuel and intermediate products is inhibited earlier. The net indicated efficiency reduces by 2.5 $\%_{Pt.}$ for the same reasons as stated for the load point 1500/3. The exhaust gas temperature increases by 40 °C.

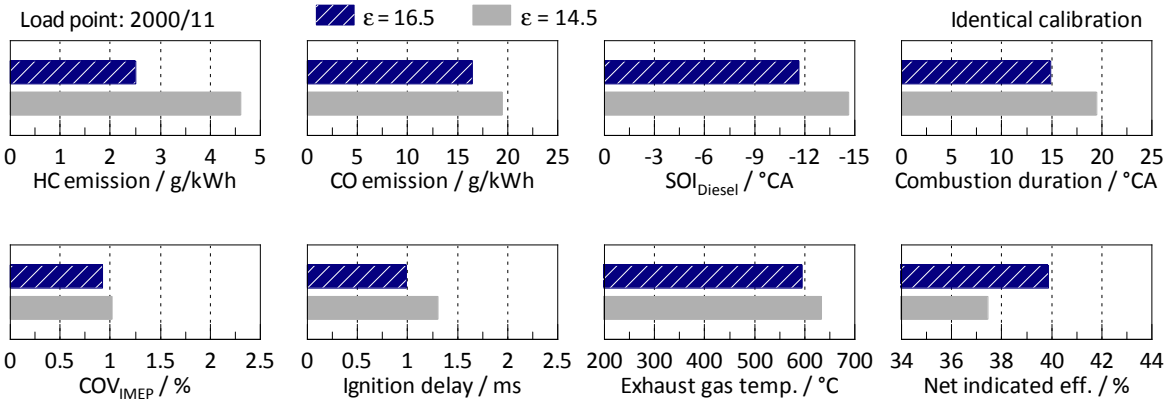

Figure 4.35: The effect of different compression ratios on the DDI combustion process in the load point 2000/11.

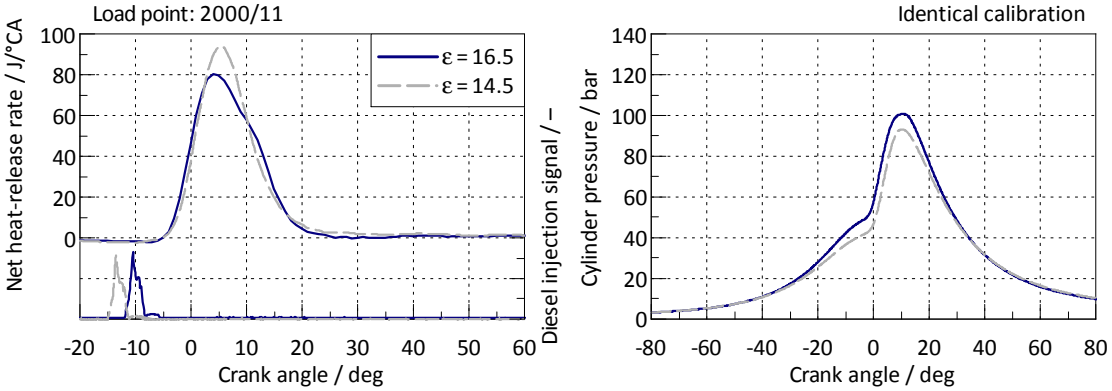

Figure 4.36: The net heat-release rate and the cylinder pressure trace in the load point 2000/11 for different compression ratios.

Figure 4.36 depicts the associated net heat-release rates and the cylinder pressure traces. While the pressure traces exhibit the presumed reduction of the compression pressure and the peak cylinder pressure, the heat-release rate is contradicting at first view. The maximum heat-release rate is higher with reduced ε and at the same time the combustion duration apparently increases by 5 °CA (Figure 4.35). The reason for the prolongation of the combustion duration can be observed between 10 °CA and 17 °CA. With reduced compression ratio the heat-release rate declines faster than with the higher compression ratio. The reason is assumed in the lower cylinder temperature and the reduced squish motion. As a consequence MFB90 is only reached at 20.5 °CA with reduced compression ratio while it is already reached at 15 °CA in the case of $\varepsilon = 16.5$.

The reason for the higher heat-release rate maximum is less obvious. At 2000/11 the charge is stoichiometric and homogeneous. The combustion is dominated by the premixed combustion of air and NG and dependent on flame propagation. It is thus reasonable to review the effects observed in SI engine operation to explain the observed behaviour. In SI engines the heat-release depends on the development of the flame front area which is significantly influ-

enced by the geometry of the combustion chamber [16]. When the flame front approaches the combustion chamber walls the further propagation is limited. This is restricting the flame front area which correlates with the heat-release. If the cylinder pressure evolution is known the flame front area can be calculated [69, 76]. In [76] experiments with a CNG SI engine were performed. Different compression ratios were studied and the same observations were made. With reduced compression ratio the heat-release rate reached a higher maximum and the heat-release was faster overall. The flame front area was calculated and the phenomenon could be traced to a larger flame front area in case of the lower compression ratio. By increasing the clearance volume the flame can extend further which results in a higher heat-release rate. In the investigated case the combustion chamber geometry is different to the experiments in [76], also the ignition source and the ignition sites differ. However, the assumption would appear to be reasonable that with an increased bowl volume the flame front would extend further also in the investigated case.

To conclude, the reduction of the compression ratio reveals that a high compression ratio is vital to the DDI combustion process. In the investigated load points the disadvantages of a reduced compression ratio prevail. At higher load and stoichiometric homogeneous operation the disadvantages are moderate. However, the light load capability of the combustion process deteriorates with a reduced compression ratio. Due to a significant rise of the ignition delay and the associated effects stable engine operation with high efficiency and low losses due to incomplete combustion is prevented if the compression ratio is reduced.

4.5.5 Comparison with Monovalent CNG Spark Ignited Operation

Unthrottled, stoichiometric and homogeneous operation of the DDI concept is intended in large areas of the engine map according to the developed operating strategy displayed in Figure 4.31. Minimum diesel injection quantities are favoured to maximise the CO_2 reduction and they also lead to the best results regarding fuel efficiency and pollutant emissions (see Figure 4.14). This questions the necessity of DF combustion overall. Undoubtedly, the injection system required for DF operation adds cost and complexity in comparison to a conventional diesel engine, but especially in comparison to a CNG spark ignited engine. A homogeneous and stoichiometric air-NG mixture can be ignited with a conventional spark plug also. In addition, the diesel injection quantity would reach an absolute minimum - zero.

Therefore, CNG SI operation was investigated experimentally on the identical base engine to allow for a comparison with the DDI concept. A variant of the cylinder head was manufactured which enables the installation of a spark plug instead of the diesel injector (see Figure 4.10). Conventional Bosch spark plugs of the type ZMR5TPP330 were used. The orientation of the spark plugs was identical to the orientation of the diesel injectors. The direct injection of natural gas was maintained. the CNG SI cylinder head also had only one exhaust valve per cylinder. The differences between DDI combustion with minimum diesel quantities and SI operation are the ignition energy, the number of ignition sites and the location of these ignition sites. A diesel injection of 2.3 mg is a typical quantity used during the investigations of the DDI concept. It introduces approx. 100 J of fuel energy. The spark energy of a spark plug is in the order of magnitude of 100 mJ. The difference in ignition energy is therefore three orders of magnitude. Furthermore, the diesel spray creates six ignition sites inside the piston bowl whereas the spark plug creates only one flame kernel at the top of the combustion

chamber. Another difference is that the spark discharge is in a first approximation independent of the pressure and temperature in the combustion chamber. This means in low load operation stoichiometric and throttled operation becomes feasible as alternative to charge stratification. The experiments with spark plug were mainly conducted to clarify two points:

1. The influence of the ignition source at high loads where the charge is stoichiometric and homogeneous.

2. The efficiency penalty of throttled, stoichiometric CNG SI operation at low loads in comparison to the globally lean and stratified operated DDI concept.

The investigations with spark ignition were conducted with the reduced compression ratio of 14.5. At first, the influence of the ignition source at high loads is reviewed. Some of these results were published earlier in [114]. Figure 4.37 depicts a variation of MFB50 in the load point 1750/15 for spark ignited operation and DDI combustion with a compression ratio of 14.5 and 16.5 respectively. Obviously the stated NG energy fraction x_{NG} of 95 % is valid only for DF combustion. All three measurements were performed at $\lambda_{\mathrm{global}} = 1$ and $\mathrm{SOI}_{\mathrm{NG}} = -300\,^{\circ}\mathrm{CA}$. Furthermore, it is highlighted that the term *ignition delay* is incorrect for SI operation. An *ignition delay* does not exist in SI operation, instead the period between the spark discharge and MFB05 is referred to as an *inflammation phase*. Within this period the flame kernel develops and turns into a turbulent flame. As expected the ignition with the spark plug is inferior to the diesel pilot spray. The inflammation phase is at least 30 % longer than the ignition delay of the diesel spray. Also the combustion duration increases significantly. As a consequence, the spark timing must be advanced by 10 °CA compared to $\mathrm{SOI}_{\mathrm{Diesel}}$ to achieve the same combustion phasing. The shorter combustion duration of the DDI concept is attributed to the multiple ignition sites and the larger ignition energy. The difference between the inflammation phase and the ignition delay cannot be linked to the same causes, because fundamentally different physical processes occur during spark ignition and compression ignition of diesel. The cycle-to-cycle variations are equal between MFB50 of 8 °CA to 13 °CA. At later combustion phasing the variations increase with spark ignition while they are slightly reduced in DDI combustion. This difference is also linked to the significantly higher ignition energy in DDI combustion.

Due to the more rapid combustion and multiple ignition sites more NG can be oxidised while the temperature in the combustion chamber is favourable. This is reflected in the lower HC emission of the DDI concept. The differences in the CO emissions, especially the remarkably lower emission with DDI combustion and $\varepsilon = 14.5$ result from small deviations to the lean in the equivalence ratio. Finally, spark ignition results in an efficiency penalty slightly above $2\,\%_{\mathrm{Pt.}}$. This is a result of the higher HC emission, the longer combustion duration and higher wall heat losses. A loss analysis is stated at the end of this section to quantify the individual losses in dual fuel and spark ignited combustion.

The data presented in Figure 4.37 already indicate that the SI concept is performing worse. Unburned species of 3.5 % on average are above typical values for gasoline SI engines [55]. This is a consequence of the fact that the base engine is not optimised for SI operation. The combustion chamber roof, the intake ports and the piston shape are not designed for SI operation. However, the results demonstrate clearly the influence of the ignition source.

Figures 4.38 and 4.39 demonstrate the results of optimised operation in the load point 2000/11 and the associated indicating data. The application parameters are stated in Table B.3

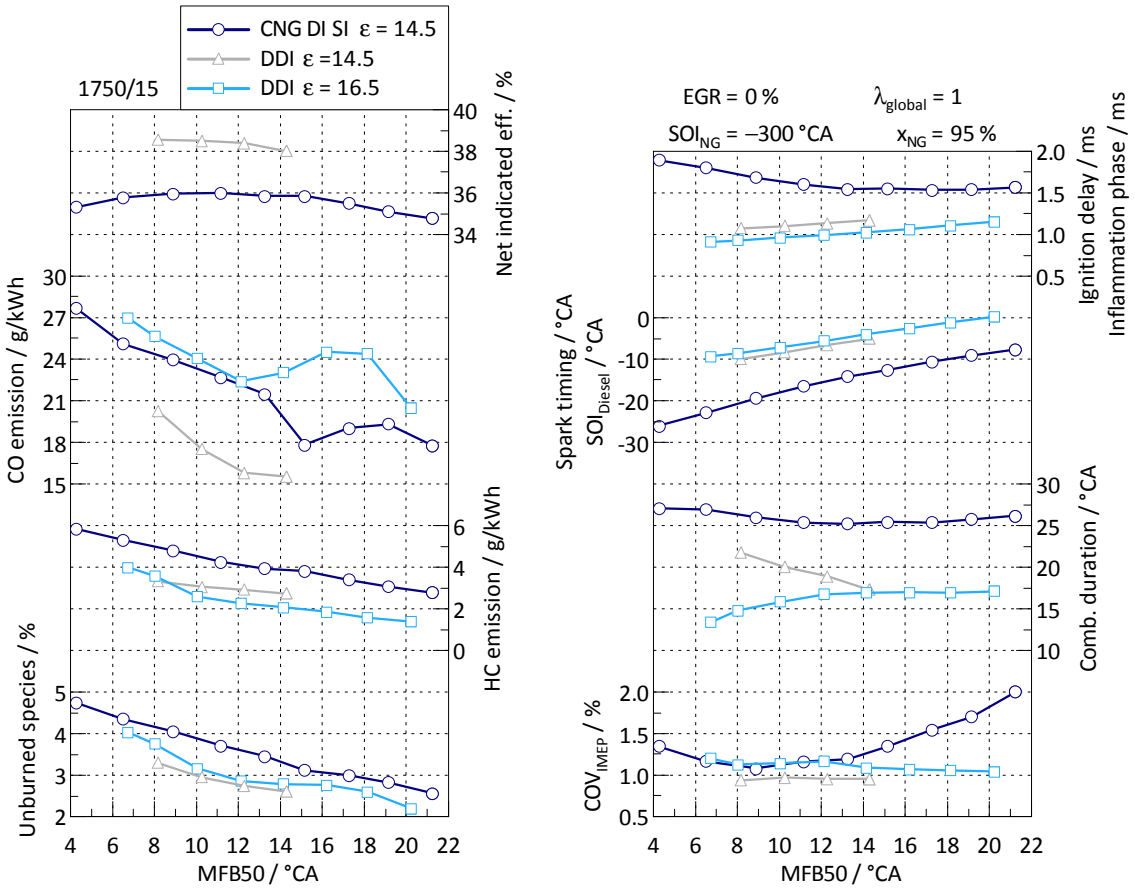

Figure 4.37: Comparison of SI operation and DDI combustion by means of a variation of MFB50 in the load point 1750/15.

in Appendix B. Both the SI operation and the DDI concept with a compression ratio of 14.5 are optimised for maximum fuel efficiency. The results are similar to the findings of Figure 4.37, but the disadvantage of spark ignition is less. The combustion duration increases and the HC and CO emissions rise. The unburned species cumulate to 3.3 % with spark ignition compared to 2.9 % in DF combustion. The cycle-to-cycle variations and the inflammation phase respectively the ignition delay are equal. The exhaust gas temperature is decreased by 40 °C and the penalty in brake thermal efficiency η_e is reduced to 1.5 $\%_{Pt.}$. The gas exchange losses are lower with spark ignition as due to the lower efficiency more charge is required, making a higher intake manifold pressure necessary.

Figure 4.39 displays the net heat-release rates and the cylinder pressure signals. The faster heat-release in DF combustion is clearly evident. This results in the steep incline of the cylinder pressure after TDC while the pressure evolution is very uniform with spark ignition.

Figures 4.40 and 4.41 display a comparison between spark ignition and DDI combustion in the load point 1750/5. Again, both concepts feature a compression ratio of 14.5. The DDI concept is operated globally lean and stratified. x_{NG} is reduced to 80 % to allow for a stable ignition of the diesel spray due to the lower compression ratio. The combustion is optimised for

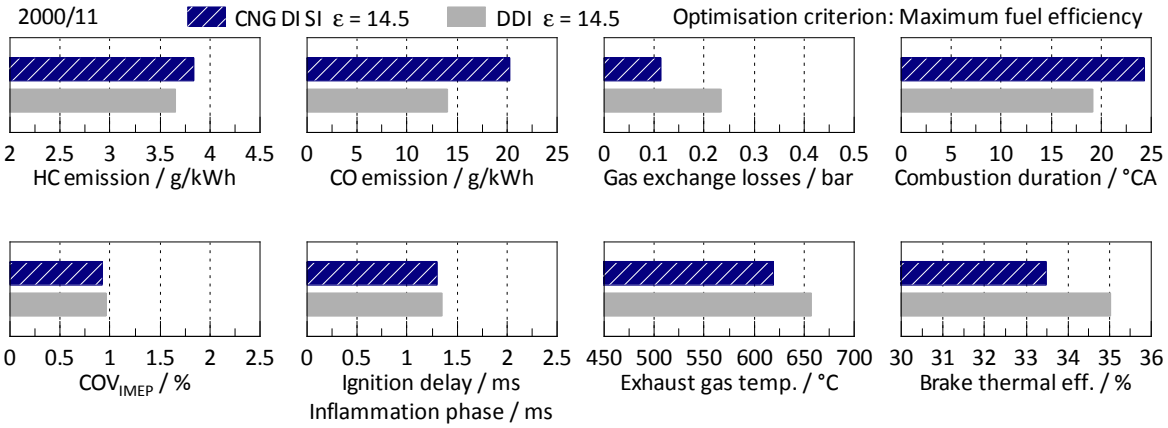

Figure 4.38: Comparison of the optimised calibration of spark ignited operation and DDI combustion in the load point 2000/11.

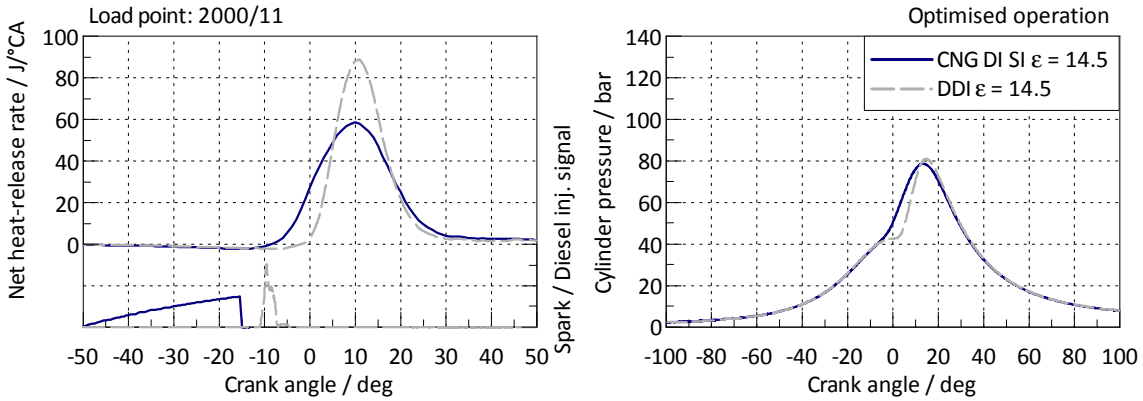

Figure 4.39: The net heat-release rate and the cylinder pressure trace of optimised SI and DDI combustion in the load point 2000/11.

minimum unburned species at diesel-like engine-out NO_x emissions. The SI concept is operated stoichiometrically and homogeneously. It is calibrated for maximum efficiency. The associated application parameters of both concepts are again stated in Table B.3.

As expected the brake thermal efficiency of the spark ignited operation is inferior to the DDI concept. The efficiency is substantially lower by 5 $\%_{Pt.}$. The gas exchange losses contribute to this decline in efficiency. They rise in SI operation as the intake manifold pressure is lowered to 730 mbar to allow for stoichiometric combustion. The charge is diluted by 37 % EGR and a global air-fuel equivalence ratio of 1.3 in DDI combustion. In SI operation only 5 % EGR are deployed and the air-fuel mixture is stoichiometric. As a consequence the exhaust gas temperature rises by 120 °C to 510 °C with SI operation which enables the catalytic oxidation of CH_4 emissions. The NO_x emissions reflect the difference in charge dilution and stoichiometry. The HC and CO emissions are significantly higher and cumulate to unburned species of 3.9 % compared to 1.8 % in the case of the DDI concept. Due to the different mixture preparation

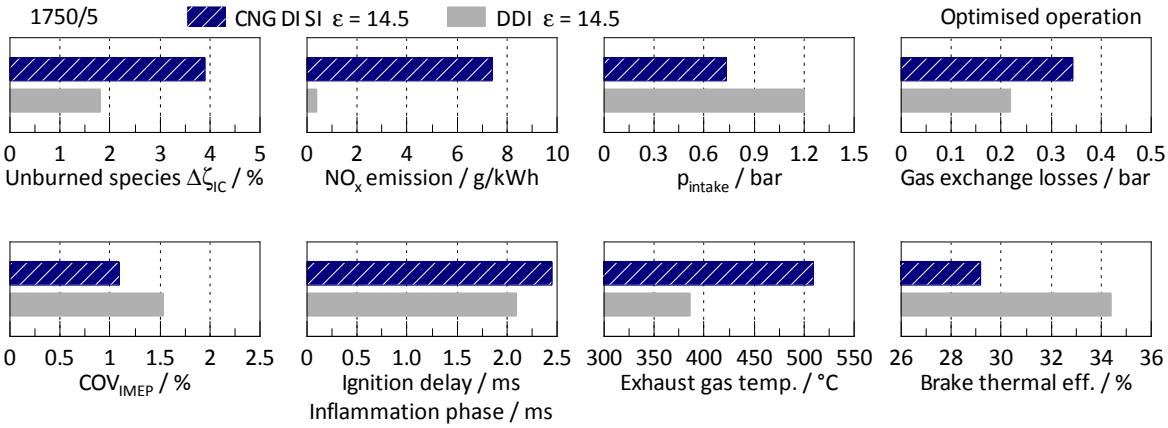

Figure 4.40: Comparison of the optimised spark ignited operation and DDI combustion in the load point 1750/5.

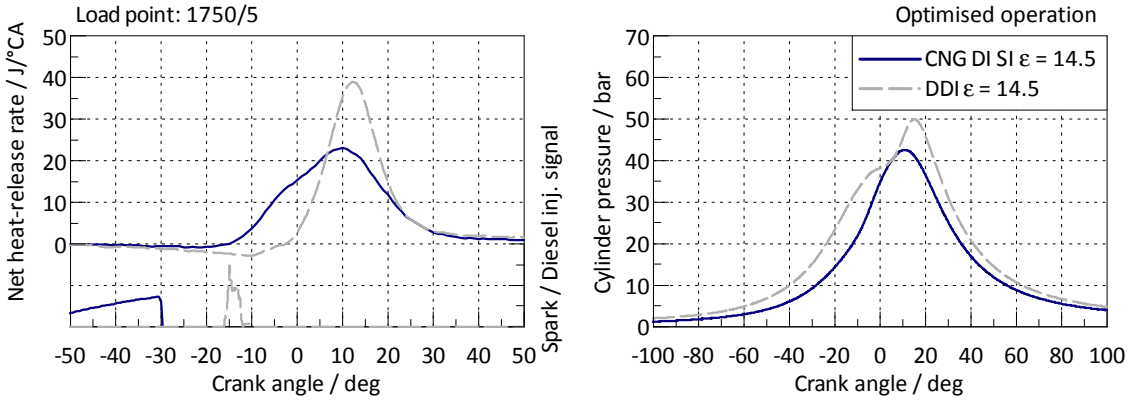

Figure 4.41: The net heat-release rates and the cylinder pressure traces of optimised SI and DDI combustion in the load point 1750/5.

(homogeneous against stratified air-NG mixture) the difference in unburned products cannot be attributed to the different ignition concepts clearly. However, it demonstrates again that the layout of the combustion system is not optimal for SI operation.

Figure 4.41 displays the associated indicating data. It reveals the significantly longer combustion duration in the case of SI operation which is attributed to the lower ignition energy and the single ignition site. The low peak cylinder pressure in SI operation results from the reduced intake manifold pressure.

Finally Figure 4.42 displays a quantification of the losses occurring in SI operation and in the DDI concept for the operation points discussed and depicted in Figures 4.38 to 4.41. The analysis of losses is performed according to the method described in [97]. An in-house software tool given the name *CORA* is used for the execution of the analysis of losses. This tool is the outcome of another PhD thesis at this institute [74]. In the analysis of losses according to Pischinger the theoretical efficiency of a *'perfect engine with real charge'* is first calculated. The

perfect engine with real charge is an engine without friction, wall heat losses, flow losses, gas exchange losses or pressure losses. Furthermore, it exhibits an ideal combustion which follows the efficiency-optimal combustion at constant volume. *'With real charge'* means that at IVC pressure, temperature, mass and composition of the charge equal the charge of the *real engine*. Under these assumptions the efficiency of the *perfect engine* is calculated. Subsequently, the reduction of this theoretical efficiency caused by the individual losses of the *real engine* is calculated by including them stepwise. Thus the individual losses are quantified. If all losses are included, the actual brake thermal efficiency of the *real engine* is derived. The order in which the losses are calculated impacts their distribution, but not their cumulated magnitude. Subsequently, the following losses are considered:

- The loss in efficiency due to incomplete combustion
- The loss in efficiency due to a combustion process deviating from the constant-volume combustion
- The loss in efficiency due to the transfer of heat to the combustion chamber walls
- The loss in efficiency due to the gas exchange
- The loss in efficiency due to friction

Figure 4.42 on the left depicts the analysis of losses for above discussed operation in the load point 1750/5. It reveals that the majority of the difference between CNG spark ignition and the DDI concept results from different charge compositions. In spark ignited operation the charge is stoichiometric and marginal amounts of EGR are used. In the DDI concept the charge is lean and in addition large amounts of EGR are deployed. This results in a different charge mass and different thermodynamic properties of the charge leading to a difference in the efficiency potential of $54.5\,\% - 50.1\,\% = 4.4\,\%_{\mathrm{Pt.}}$. This is confirmed by the measurement results stated in [42]. The effect of stratification was assessed in a CNG DI SI engine. Similar improvements were reported by stratifying the mixture in the load point $\mathrm{n} = 2000\,\mathrm{min}^{-1}$ and $\mathrm{IMEP} = 4\,\mathrm{bar}$.

The increase of unburned species, the longer combustion duration and throttled operation in SI operation (Figure 4.40) lead to an increase of the associated losses compared to the DDI concept as depicted in Figure 4.42. The wall heat losses rise, because the charge is not diluted and the combustion duration is longer. Furthermore, it is observed that the friction losses reduce with spark ignition. This decrease results from the diesel high-pressure pump. The pump is not required in spark ignited operation, thus the piston of the pump was removed to avoid the compression work of the pump. In [42] the net indicated specific fuel consumption was reported to be 215 g/kWh in homogeneous SI operation. The net indicated efficiency of the SI operation depicted in Figure 4.42 left accounts for $29.2\,\% + 4.0\,\% = 33.2\,\%$ which is equivalent to a specific fuel consumption of 221 g/kWh. This gives an idea of the losses resulting from the suboptimal combustion layout for SI operation when compared to the value of 215 g/kWh stated in [42].

The situation is different in the load point 2000/11 which is displayed in the right part of Figure 4.42. Here the charge properties and the air-NG mixture preparation are identical and only the ignition sources differ. Accordingly, the efficiencies of the *perfect engine* are also similar. The difference of $0.6\,\%_{\mathrm{Pt.}}$ results from marginal differences in the stoichiometry and

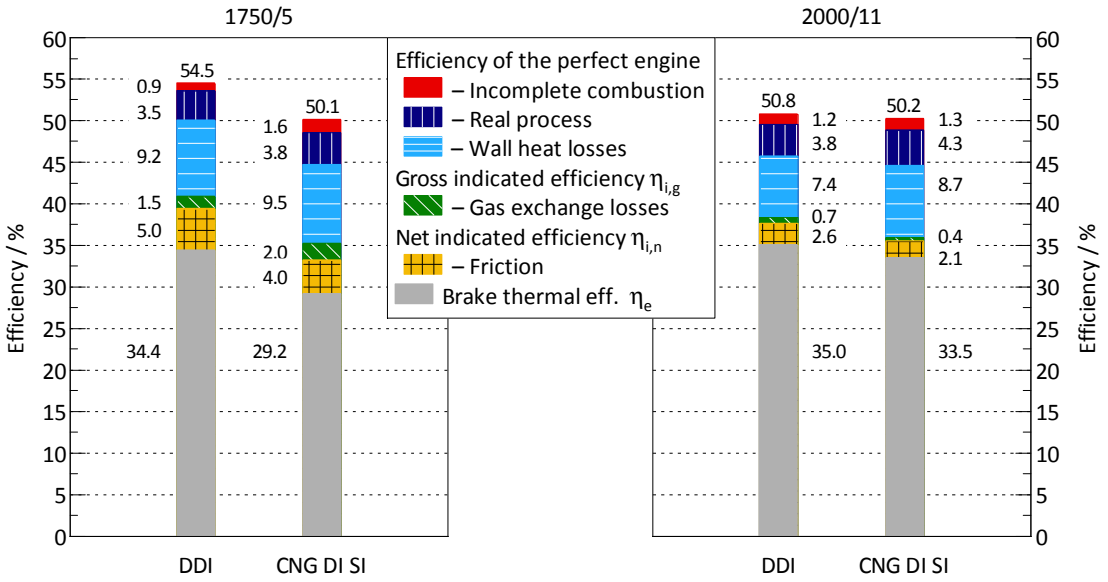

Figure 4.42: Analysis of losses in optimised SI and DDI operation for the load points 1750/5 and 2000/11.

the intake manifold temperature. The majority of the efficiency deficit compared to the DDI concept results from the prolonged combustion duration. Thus, the losses due to a deviation from the constant-volume combustion and the wall heat losses rise. The losses due to incomplete combustion increase too while the gas exchange losses and friction losses are reduced. The friction losses are reduced due to the avoidance of the compression work of the diesel high-pressure pump likewise to the load point 1750/5.

In conclusion and answering the two points stated at the beginning of this section, the following statements can be made: The higher ignition energy by three orders of magnitude and the multiple ignition sites lead to an overall faster combustion and at higher loads to lower cycle-to-cycle variations at late combustion phasing. This is beneficial for the fuel efficiency as the combustion deviates less from the ideal constant-volume combustion and the wall heat losses are reduced. At part load operation the efficiency deficit of throttled and stoichiometric SI operation is significant and amounts to $5\,\%_{\mathrm{Pt.}}$ compared to lean and stratified operation of the DDI concept. As a consequence of the different charge properties the exhaust gas temperature is 120 °C higher reaching 510 °C in SI operation enabling the catalytic oxidation of the CH_4 emissions. Furthermore, the investigations showed that the layout of the combustion system is not optimal for SI operation which adds to the large efficiency deficit. However, the analysis of losses indicates that the deficit results to a large extent from the different charge properties and not from the inferior combustion.

4.5.6 Comparison of Combustion Processes

A comparison of the DDI concept with other combustion processes concludes this chapter on dual fuel combustion with direct fuel injection of NG. The DDI concept with a compression ratio of 16.5 and optimised calibration is compared with the base diesel engine, a gasoline SI engine

and conventional DF combustion with NG port fuel injection. The comparison is conducted in the load points 1500/3 and 2000/11. In addition, an analysis of losses is presented to compare the DDI concept and diesel combustion in detail. The measurements of conventional DF combustion were carried out on the same base engine as explained in Section 4.4. Also the calibration of the conventional DF combustion was optimised for minimum unburned species at low NO_x emission resp. maximum fuel efficiency. The associated application parameters are stated in Appendix B in Table B.1 and B.4. The BMW N20 engine is the chosen gasoline engine for this comparison. It is a turbocharged 4-cylinder engine with a displacement of 2 litres and a compression ratio of $\varepsilon = 10$. It features a valve train with variable valve lift, cam phasing and direct fuel injection [118]. The data originates from an earlier project at this institute. Parts of this comparison were already published in [37, 114].

Figure 4.43 displays the comparison in the load point 1500/3. Both DF concepts and the diesel engine are operated lean. The gasoline engine is operated stoichiometrically. It is well observed that the dual fuel combustion combines characteristics of both diesel and SI combustion. In addition, the advantage of the DDI concept over conventional DF combustion is evident in part load operation. The middle row displays the engine-out emissions. The performance of conventional DF combustion is poor at this light load. The HC emissions reach 25.5 g/kWh. Together with the CO emissions the unburned species cumulate to almost 11 % of the total fuel energy. With the DDI concept the HC emission is reduced enormously by 75 % to 6.6 g/kWh by means of charge stratification. The HC emission almost matches the level of the gasoline engine which is 5 g/kWh. Together with the CO emission the unburned species account for 3.5 % in the DDI concept while they reach 2.8 % in the gasoline engine. The NO_x emission in DF combustion are kept on the level of the diesel engine. In SI operation they are approximately one magnitude larger due to the stoichiometric operation. Furthermore, it becomes apparent that soot is a particular problem of the diesel engine resulting from the non-premixed combustion. Due to the small diesel quantities soot is avoided in DF combustion.

The ignition delay in DF combustion is similar to the diesel engine, while the cycle-to-cycle variations are similar to the gasoline engine. Also the low exhaust gas temperature of only 250 °C and the low gas exchange losses are similar to the diesel engine. The brake thermal efficiency of the DDI concept is higher than that of the other combustion processes in this load point and reaches 33.1 %. It is 4.5 $\%_{\text{Pt.}}$ higher than in conventional DF combustion. This is mainly a consequence of the reduced unburned species. The efficiency of the diesel engine is outmatched by 0.6 $\%_{\text{Pt.}}$ and that of the gasoline engine by 4.1 $\%_{\text{Pt.}}$. The efficiency difference between the DDI concept and the diesel engine is further discussed below by means of an analysis of losses.

The CO_2 emissions are given in the bottom right diagram. They are calculated from the fuel masses assuming complete oxidation. The brake thermal efficiency, the composition of the natural gas and the NG energy fraction influence the CO_2 emission of the DDI concept and thus the feasible CO_2 reduction in comparison to the diesel and the gasoline engine. The often stated CO_2 reduction potential of 25 % is only valid if NG consisted of 100 % methane, if the brake thermal efficiencies were equal and if x_{NG} was 100 %. In the present case, the methane content is 96.7 vol% which negatively influences the CO_2 reduction potential. Although, also the lower heating value of the diesel is below the value stated in Table 2.2. Considering the actual fuel properties during these measurements the CO_2 reduction potential of NG accounts for 25.8 % compared to diesel. In this load point the DDI concept is operated only with 79 %

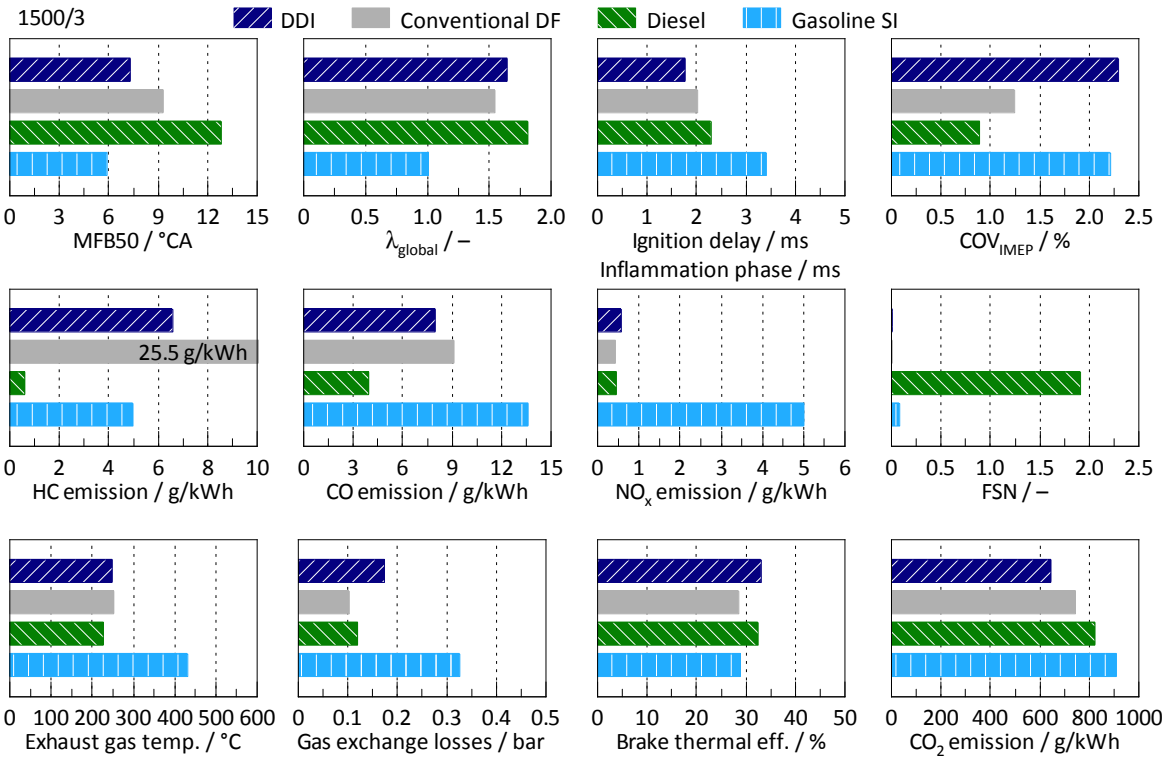

Figure 4.43: Comparison of four different combustion processes in the load point 1500/3.

natural gas. This decreases the reduction potential to 20.3 % if the fuel efficiencies were equal. However, as the DDI engine has a higher efficiency, the actual CO_2 reduction is larger. The calculated CO_2 emission of the DDI concept is 645 g/kWh compared to 823 g/kWh of the diesel engine and 910 g/kWh of the gasoline engine. This corresponds to a CO_2 reduction of 22 % and 29 % respectively.

This data demonstrates clearly the high CO_2 reduction potential at engine-out pollutant emissions comparable to gasoline and diesel engines. However, also the challenge of DF combustion becomes apparent. The HC emissions in this load point accounts for 6.6 g/kWh which is a remarkable achievement in comparison to conventional DF combustion and also in comparison to a modern gasoline engine. However, the exhaust gas temperature is only 250 °C and the HC emissions consist mainly of methane. In addition, the exhaust gas is lean which is part of the reason for the low temperature itself. Temperatures of approx. 450 °C are required for the catalytic oxidation of methane as discussed in Section 4.2.1. Using currently available technology it is thus not possible to convert the CH_4 emissions in part load operation. This is an obstacle preventing compliance with Euro 6 emission limits for diesel or gasoline engines, as no dedicated legislation exists for dual fuel passenger cars. Investigations of exhaust gas aftertreatment using different three-way catalysts were performed in [115] and confirmed the difficulty.

A mitigation strategy was to alter the operating strategy of the DDI concept (Figure 4.31) and extend the diesel operation until the DDI concept can be operated stoichiometrically

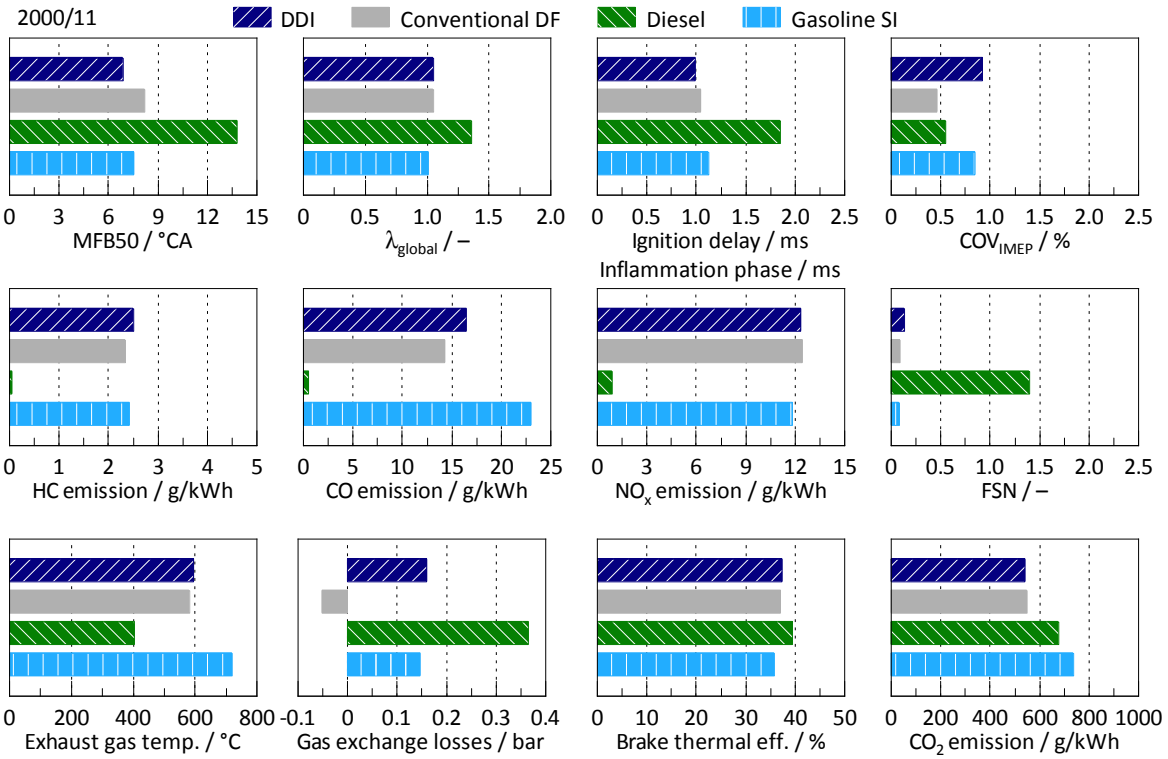

Figure 4.44: Comparison of four different combustion processes in the load point 2000/11.

and homogeneously. However, in view of the common load pattern of passenger car engines (Figure 4.12) especially in urban traffic, this would mean operating the engine in diesel mode to a large extent. The CO_2 reduction would diminish, with the result that the argument for this mitigation strategy would not be compelling.

Figure 4.44 depicts a comparison of the same combustion processes in the load point 2000/11. In this load point both DF concepts and the gasoline engine are operated stoichiometrically and homogeneously. The diesel engine is of course operated lean. It reveals that the ignition delay in DF combustion is similar to the inflammation phase in the gasoline SI engine. This was observed already in Section 4.5.5 where the DDI concept was contrasted with CNG SI operation (Figure 4.38). The cycle-to-cycle variations are comparable between all combustion processes. The pollutant emissions of both DF concepts and the gasoline engine are very similar since all three combustion processes are operated stoichiometrically and EGR is not deployed. The CO emission of the gasoline engine is higher, but this results from small differences in the stoichiometry between the gasoline engine and the DF concepts. The CO emission responds very sensitively around $\lambda_{\text{global}} = 1$ to lean and rich excursions. It is also observed that the HC and CO emissions of conventional DF combustion are slightly lower than the emissions of the DDI concept. The difference in combustion phasing certainly has an influence, but it is assumed that the mixture homogenisation is improved with NG PFI compared to direct injection. In general, it is observed that in this load point the results of conventional DF combustion and the DDI concept are almost identical, since both concepts are operated homogeneously and

stoichiometrically. The exhaust gas temperature of both DF concepts almost reaches 600 °C, which allows for the oxidation of the CH_4 emissions. The brake thermal efficiency of the diesel engine is higher by 2.1 $\%_{\mathrm{Pt.}}$ compared to the DDI concept. The efficiency of the gasoline engine is 1.6 $\%_{\mathrm{Pt.}}$ lower than that of the DDI concept.

The CO_2 emission of the DDI concept calculated from the fuel mass is 542 g/kWh, that of the diesel engine is 676 g/kWh and that of the gasoline engine is 736 g/kWh. At this operating point the natural gas energy fraction x_{NG} of the DDI concept is 94 %. Under the assumption of equal brake thermal efficiencies this would result in a CO_2 reduction potential of 24.2 % compared to the diesel engine. Incorporating the difference in the fuel efficiencies results in a CO_2 reduction of 20 % compared to the diesel engine and 26 % compared to the gasoline engine. The comparison with conventional combustion processes demonstrates that starting from medium loads DF combustion is a feasible alternative to conventional combustion processes with high fuel efficiency and a reduction of the CO_2 emission between 20 % and 26 %.

In conclusion Figure 4.45 shows an analysis of losses for the diesel engine and the DDI concept in the two load points discussed to better understand the distribution of the individual losses of the combustion processes. In the load point 1500/3 the diesel engine and the DDI concept are operated globally lean and approx. 40 % EGR is used in both cases. The efficiencies of the perfect engine are almost identical at 58 % and 57.8 % which represents the general efficiency potential. The larger amount of unburned species of the DDI concept reflects in the losses due to incomplete combustion. However, the majority of the efficiency difference results from the wall heat losses and losses due to the deviation from the constant-volume combustion. The longer combustion duration and a retarded combustion phasing of the diesel engine increase these losses. The gas exchange of the DDI concept is inferior compared to the diesel engine, because in order to recirculate these high amounts of exhaust gas the pressure difference between exhaust and intake manifold must be actively increased. The net indicated efficiency of the DDI concept is higher compared to the diesel engine by more than 2 $\%_{\mathrm{Pt.}}$. However, this gain is compensated in part by the higher friction losses of the DDI concept. They result from a higher diesel rail pressure p_{Diesel}. While the DDI concept is operated in this load point at a diesel injection pressure of 800 bar, the diesel engine is operated at 450 bar. By definition, the power demand of the auxiliaries is included in the friction. Therefore, the higher power demand of the diesel high-pressure pump increases the friction of the DDI concept and reduces the gain in brake thermal efficiency to 0.6 $\%_{\mathrm{Pt.}}$.

The situation is different in the load point 2000/11. The diesel engine is operated globally lean and with 26 % EGR. The DDI concept is operated homogeneously, stoichiometrically and without EGR. Due to this difference in the charge properties the efficiencies of the perfect engine differ by 3.6 $\%_{\mathrm{Pt.}}$ in favour of the diesel engine. The wall heat losses of the DDI concept are also higher due to the stoichiometric charge which results in a higher combustion temperature. However, also in this load point the combustion of the DDI concept is considerably faster resulting in lower losses due to the deviation from the constant-volume combustion. Additionally, the friction losses are smaller, as the DDI concept is operated at a diesel rail pressure of 400 bar in this load point while the diesel engine is operated at above 1000 bar. The penalty in brake thermal efficiency of the DDI concept is thus reduced to 2.1 $\%_{\mathrm{Pt.}}$, but the advantage of lean combustion is not fully compensated.

When comparing the losses in load point 1500/3 and 2000/11 it is revealed that for both combustion processes the wall heat losses reduce with higher engine speed while the losses

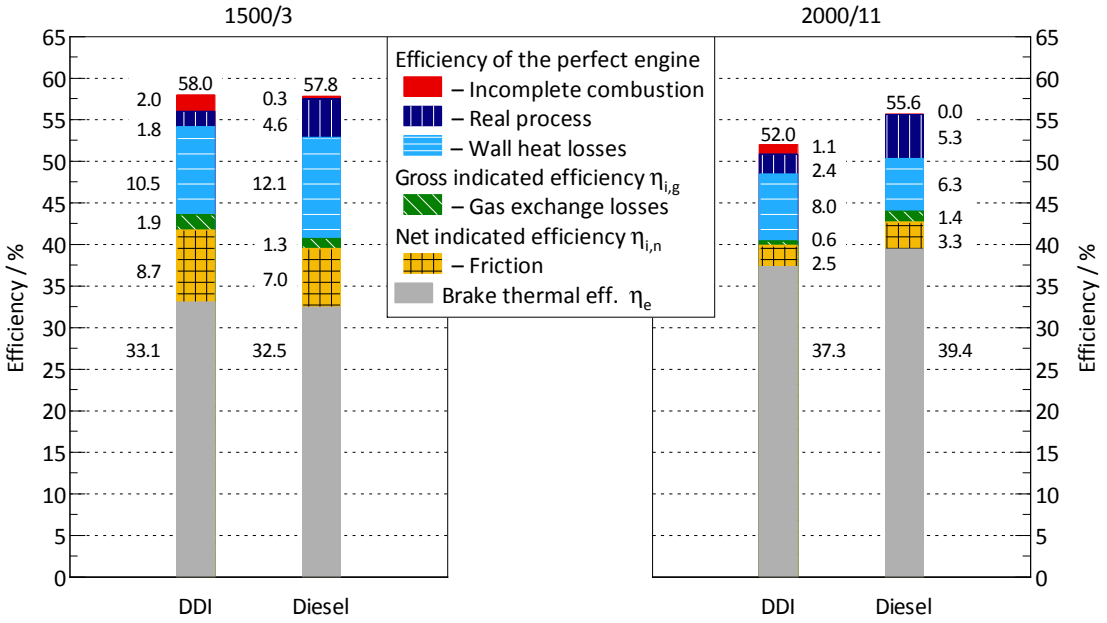

Figure 4.45: Analysis of losses in the load points 1500/3 and 2000/11 conducted for the diesel engine and the DDI concept.

of the real process increase. This is an effect of the higher engine speed. The combustion evolves faster at $n = 2000\,min^{-1}$ absolutely in the time domain, and therefore the wall heat losses reduce. However, the deviation from the constant-volume combustion increases when the heat-release rate is scaled with the engine speed and plotted against the crank angle as Figure 4.46 illustrates. The graphs display the gross heat-release rate of the DDI concept at 1500/3 and 2000/11. The diagram on the left shows the heat-release rate in the time domain. It is scaled in such a way that the heat-release rate at 1500/3 appears identical in the time domain and in the crank angle domain.

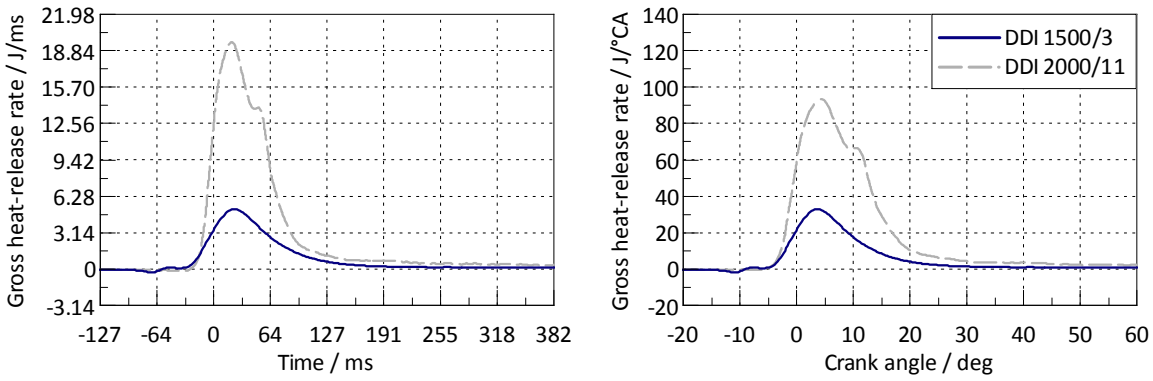

Figure 4.46: The gross heat-release rate of the DDI concept in the load points 1500/3 and 2000/11 plotted against the time and the crank angle.

4.6 Summary

In this thesis natural gas-diesel dual fuel combustion was investigated experimentally on the engine test bench. The challenge of this combustion process is a high CH_4 emission in part load operation which results from over-lean air-NG mixtures. It was revealed that these emissions can be attributed to a fundamental trade-off between the ignition conditions of the diesel spray and that of the air-NG mixture. A novel dual fuel concept was developed to reduce the high CH_4 emissions in part load operation. The proposed concept is termed DDI – *Dual Direct Injection* and features low-pressure direct injection of natural gas. Thus, charge stratification becomes feasible which reduces the local air-NG equivalence ratio and improves the combustion of the air-NG mixture, while the ignition conditions of the diesel spray are not diminished. This allows for a significant reduction of the CH_4 emission.

The influence of the most important application parameters, as also the influence of the compression ratio on the combustion were investigated experimentally. It was shown that a high compression ratio is mandatory for the investigated concept to ensure a short ignition delay and fast and stable combustion. The calibration of the DDI concept was optimised in four load points between $n = 1500\,min^{-1}$ / $BMEP = 3\,bar$ (1500/3) and $n = 1750\,min^{-1}$ / $BMEP = 15\,bar$ (1750/15). At light engine loads the charge is globally lean and the combustion was optimised for minimum unburned species at low NO_x emissions. At higher loads stoichiometric operation is favourable and the combustion was optimised for maximum brake thermal efficiency. With this information an operating strategy was developed for the most relevant area of the engine operating map. At idling and very light loads conventional diesel operation is proposed. At part load lean and stratified dual fuel combustion is favourable and at higher loads homogeneous and stoichiometric DF combustion is suggested. Depending on the operating point unburned species between 2 % and 3.5 % of the fuel energy are achieved. If the NO_x emission is not limited unburned species as low as 1 % are achieved in lean operation. These values are in the range of modern gasoline SI engines which are reported to emit HC emissions in the range of 1 % and 2.5 % of the fuel energy [55].

In a next step the engine was adapted to CNG spark ignited operation to determine the efficiency potential of the DDI concept in comparison to a conventional CNG SI engine. In part load operation the efficiency benefit of the DDI concept reaches $5\,\%_{Pt.}$, because it is operated globally lean while the SI engine is operated stoichiometrically. At higher loads when both concepts are operated stoichiometrically the efficiency advantage still accounts for $1.5\,\%_{Pt.}$ due to a faster combustion and reduced wall heat losses.

Finally, the DDI concept was compared with conventional diesel and gasoline engines and conventional dual fuel combustion with NG port fuel injection. At part load operation when the charge is lean the HC emissions of conventional DF combustion are reduced significantly by up to 75 % from 25.5 g/kWh to 6.6 g/kWh with the DDI concept. This is a consequence of the fuel stratification and results in an increase of the brake thermal efficiency by $4.5\,\%_{Pt.}$. At higher loads both the DDI concept and the conventional dual fuel concept are operated stoichiometrically and the results are comparable. The comparison with the diesel and the gasoline engine demonstrates that overall the engine-out pollutant emissions of the DDI concept are on the level of modern gasoline engines. However, the exhaust gas is lean in part load operation which creates a large challenge for the exhaust gas aftertreatment. At light loads the fuel efficiency of the DDI concept outperforms the diesel engine. At higher loads when the

DDI concept is operated stoichiometrically the efficiency is between diesel and gasoline engines. Due to the high fuel efficiency and the utilisation of NG a CO_2 reduction between 20 % and 29 % can be achieved with the DDI concept in comparison to diesel and gasoline engines.

The biggest unsolved challenge also with the DDI concept is the exhaust gas aftertreatment of the remaining HC emissions in part load operation. The HC emissions consist to more than 90 % of methane which requires an exhaust gas temperature of approx. 450 °C for catalytic oxidation [48]. At high loads, during stoichiometric operation of the DDI concept the exhaust gas temperature reaches 600 °C and the conversion is no problem. However, in part load operation when the charge is globally lean and high amounts of EGR are used the exhaust gas temperatures reaches only 300 °C. This is clearly below the threshold for methane oxidation. Together with the HC emission itself, the exhaust gas aftertreatment of methane is the limiting factor for a further promotion of dual fuel combustion, especially for passenger car applications. The average load of passenger car engines is low, which means their engines are operated to great extent under operating conditions very critical for the exhaust gas aftertreatment. Using the technology presented, however, dual fuel combustion could already be an attractive option for applications in which the average load is substantially higher and the load pattern less dynamic. An example are large engines for marine applications where DF engines are the state of the art [124].

4.6.1 Suggestions for Future Work

Further research and deepened understanding is required in many of areas of dual fuel combustion. Firstly, the combustion fundamentals are not well understood yet, the transition from non-premixed combustion to premixed flame propagation, the sources and the formation of the pollutant emissions, as also the location of the ignition sites and the parameters influencing it all require further investigation.

Secondly, more application-oriented advances in the exhaust gas aftertreatment of methane are required for the utilisation of DF engines in dynamic applications. Also a further reduction of the engine-out HC emissions is required to expand the operating area to lighter loads and to mitigate the difficulty of methane aftertreatment.

Thirdly, the investigations of the DDI concept need to be expanded to higher engine speeds and a detailed investigation of the full load potential is necessary. Furthermore, the optimal charge motion and the optimal design of the combustion chamber need to be studied in more detail.

5 Natural Gas Spark Ignited Operation

5.1 Introduction

As outlined in Chapter 1 this second part of the thesis is a numerical investigation. It consists of 1D engine simulations to define the thermodynamic layout of a homogeneously and stoichiometrically operated heavy duty NG engine and to assess the efficiency potential of several introduced novel technologies in heavy duty engines. This task was part of the EU project *HDGAS* which received funding from the European Union's Horizon 2020 Programme under grant agreement number 653391. The base engine was the FPT Cursor 13 diesel engine with a displacement of 12.9 litre. The crank case and fundamental geometrical dimensions are identical with this engine. The cylinder head, the timing drive and everything attached to the cylinder head are newly developed components. The developed engine features a lot of new technology in heavy duty engines compared to those available on the market. The engine comprises direct injection of LNG of up to 50 bar, Corona ignition, a waste gate turbocharger with fixed turbine size and cooled high-pressure EGR. Furthermore, two overhead cam shafts with cam phasers are deployed to allow for variable valve timing.

As stated earlier current heavy duty NG engines on the market are derivations of diesel engines. These engines feature swirl charge motion, a flat combustion chamber roof and vertical valves. Sometimes one cam shaft is used which does not allow for the implementation of cam phasing. While such a layout is optimal for diesel engines it is detrimental for SI engines and results in penalties in the fuel efficiency. Usually homogeneous SI engines make use of a tumble charge motion for improved mixture formation and combustion stability as also an acceleration of the combustion [9, 73, 82]. Since in the HDGAS project the cylinder head was newly developed a combustion chamber design optimal for SI operation was realised. This means two overhead cam shafts are used, the valves are angular and the combustion chamber features a pent roof design. In combination with an appropriate intake port design and a flat piston this creates a tumble charge motion in the cylinder. It is for the first time that such a layout is realised on a modern heavy duty NG SI engine and that a modern heavy duty NG engine is designed dedicatedly for NG operation.

The aim was to thus realise a 10 % reduction in GHG emissions in the WHTC and 10 % higher torque and rated power in comparison to existing heavy duty NG engines of the model year 2013. Figure 5.1 shows the full load target of the HDGAS engine. In [39, 46] homogeneous and stoichiometric concepts were regarded as the best solution for heavy duty NG engines which fulfil the Euro 6 emission standards due to the easier exhaust gas aftertreatment compared to lean concepts. Some of the technologies implemented in the HDGAS engine were also suggested in [39] to increase the fuel efficiency of stoichiometric heavy duty NG engines. Table 5.1 states fundamental dimensions and characteristics of the developed engine.

The development work was divided between the project partners. At the IVT the 1D engine simulations were conducted to perform the thermodynamic layout of the engine and to

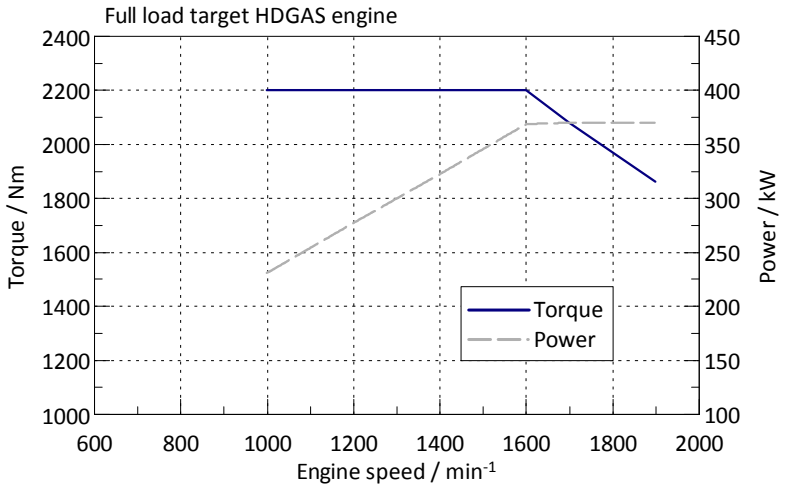

Figure 5.1: Target torque and power of the HDGAS engine at full load operation.

Table 5.1: Parameters of the heavy duty NG engine developed in the HDGAS project.

Cylinder	6
Displacement	12.88 dm^3
Bore / Stroke	135 mm / 150 mm
Compression ratio	13
Valves per cylinder	4
Rated power	370 kW at 1600 min^{-1}...1900 min^{-1}
Rated torque	2200 Nm at 1000 min^{-1}...1600 min^{-1}

define key components of the engine. The group of Prof. Angelo Onorati at Politecnico di Milano (PoliMi) was responsible for the 3D CFD simulation of the in-cylinder charge motion and the mixture formation. BorgWarner supplied the high-frequency Corona ignitors. AVL Graz conducted the single-cylinder engine (SCE) measurements and supported the whole development with their expertise. FPT was responsible for the design of the single-cylinder and the multi-cylinder engine as well as the calibration of the multi-cylinder engine. Finally, IVECO was responsible for the vehicle integration and built the demonstrator vehicle.

The 1D simulations were performed to investigate different EGR layouts, to choose a suitable turbocharger and to assess the efficiency potentials of several of the introduced technologies. The influence of EGR in combination with a waste gate turbocharger was analysed in full load and part load operation. Early and late Miller valve timing was investigated in the presence of external EGR and compared to conventional valve timing. In this context also the interdependencies between turbine size, EGR, valve timing, gas exchange work and fuel efficiency were examined. Furthermore, the potential of cam phasing was investigated in combination with EGR and indications for an operating strategy were given. Subsequently, insights gained during these investigations are presented and the individual and combined potentials of these

technologies to raise the fuel efficiency are discussed.

In Section 5.2 the methodology followed during the development of the HDGAS engine is outlined. Details of the model building and performed method development are given in Section 5.3. The results of the usage of EGR and the interaction with the turbocharger, the different valve timing concepts and cam phasing are discussed in Section 5.4. Furthermore, a comparison of the simulation results with measurements of the SCE is given in Section 5.4. Finally, the findings are summarised in Section 5.5.

5.2 Methodology

The 1D simulations performed consider the entire process of the combustion engine. These start with the induction of air through the air filter, incorporate all following steps and end with the exhaustion of the exhaust gases through the muffler.

The gas flow is simulated in one dimension only. Once all valves are closed, the compression, combustion and expansion of fuel and air in the cylinder are modelled by a zero-dimensional approach. The combination of zero- and one-dimensional elements is typical in so-called 1D engine simulations. It is evident that for this reason the simulation cannot reproduce all the effects occurring in a combustion engine. For example, it cannot account for three-dimensional effects of the flow field nor can it account for the effect of the injection timing on the mixture formation or combustion stability. Yet the simplicity of the model reduces the computational time drastically and therefore makes it a powerful tool in the development process of a combustion engine. The inaccuracies of the model are met with factors which in part incorporate the effects which cannot be described physically. However, the exact values of these factors are mostly unknown. This creates the need to calibrate the model against measurement data and fine-tune the model for good accuracy.

At the time of the simulations no measurement data of the HDGAS engine was available since the 1D simulations were performed at the beginning of the development process. An adapted approach was thus chosen. As mentioned above the HDGAS engine builds on the crank case of the FPT Cursor 13 diesel engine. A CNG fuelled prototype of this engine (Cursor 13 CNG) exists. This prototype features CNG PFI, spark ignition, a waste gate turbocharger and the swirl charge motion of the diesel engine. EGR is not used. In a first step a 1D model of this Cursor 13 CNG engine was built and calibrated with measurement data. The model was validated with a second independent set of measurement data. Subsequently, this calibrated and validated model was adapted to meet the layout of the HDGAS engine. With this approach the attempt was made to increase the predictability of the model even though measurement data was not available at the time when the investigations were performed. After completion of the simulations, the findings were validated with measurements on the single-cylinder engine test bench conducted by AVL Graz.

The full load operation of the engine was simulated at nine engine speeds between 600 $\mathrm{min^{-1}}$ and 1900 $\mathrm{min^{-1}}$. Furthermore, the part load operation was simulated at an engine speed of 1200 $\mathrm{min^{-1}}$ and 100 kW brake power. This load is equivalent to BMEP = 7.8 bar or a brake torque of 800 Nm. It is the typical operating point of a heavy duty long-haul truck on the highway and is therefore most relevant for the fuel efficiency. The simulations were performed with the commercial software *AVL BOOST* v2013.2.

5.3 Model Building

In this section the initial model of the Cursor 13 CNG engine is presented and the modelling of certain components is discussed. The results of the model validation are displayed. Subsequently, the adaptation of the model to the layout of the HDGAS engine is discussed. Especially, the consideration of EGR and its effects on the combustion are reviewed.

5.3.1 Cursor 13 CNG Model

Figure 5.2 depicts the created model of the Cursor 13 CNG engine. The six cylinders (C1 – C6), the six CNG injectors (I1 – I6) in front of the intake ports, the waste gate turbocharger (TC1), the intercooler (CO1) and the throttle valve (TH1) are recognisable. Two PID controllers regulate the boost pressure and the intake manifold pressure by actuating the throttle valve and the waste gate. The dimensions of the pipes were provided by FPT. The compressor operating map and the turbine characteristics were provided by the supplier to model the turbocharger. They are displayed in Figure 5.3. The turbine measurement data is displayed in black in the right diagram. It is approximated with a polynomial and a spline to ensure a continuous trend. The fit is directly implemented in the model. The efficiency of the compressor which is also an input to the model is calculated offline and iteratively for each load point. Since steady-state simulations were performed a turbocharger model was chosen which computes the energy balance at the turbocharger shaft without considering the inertia and the turbocharger speed. The output of this turbocharger model is the compressor pressure ratio. After the simulation is completed the calculated compressor pressure ratio and the mass flow are used to interpolate

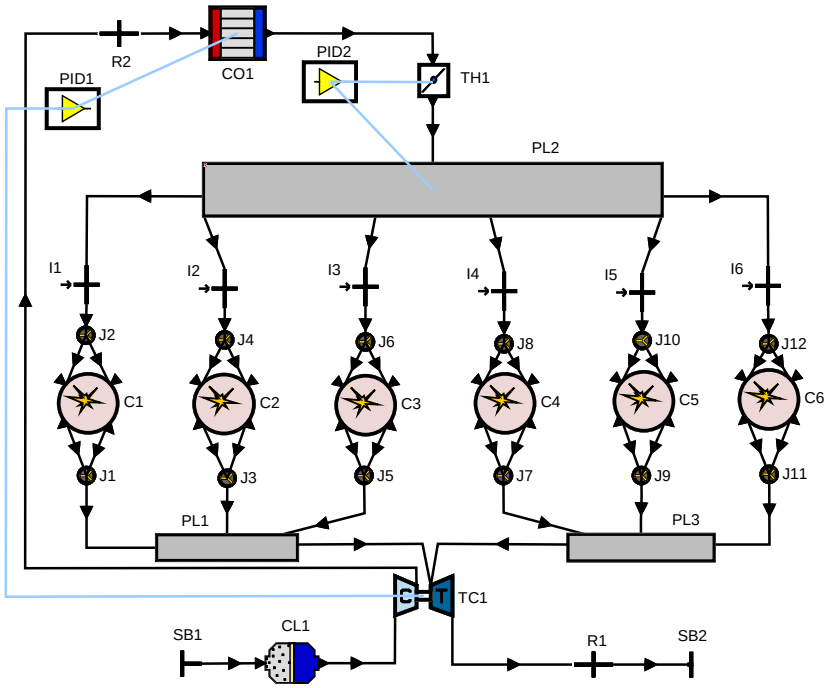

Figure 5.2: 1D simulation model of the FPT Cursor 13 CNG engine created with *AVL BOOST* v2013.2.

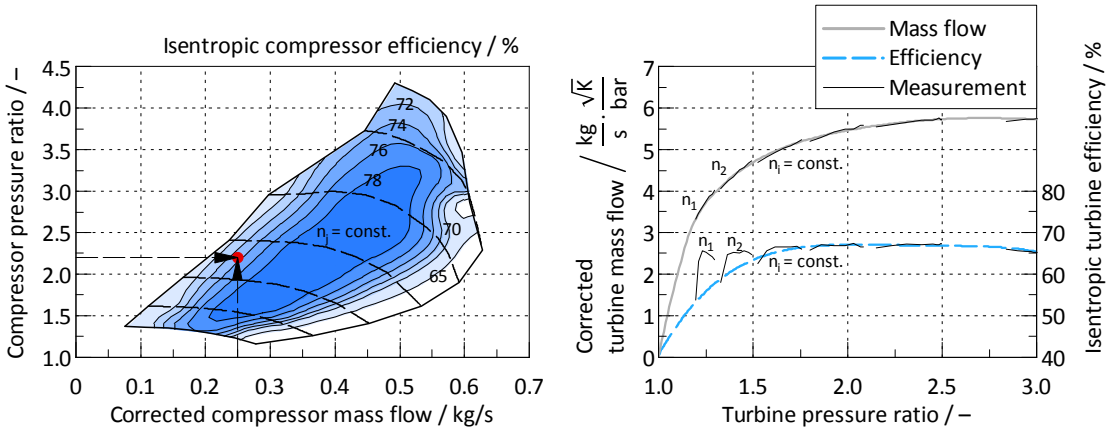

Figure 5.3: The compressor map provided (left) and the turbine characteristics together with their approximation (right).

the compressor efficiency in the operating map as demonstrated in the left graph of Figure 5.3. This efficiency is adopted in the model and the simulation is rerun. The procedure is repeated until the mass flow, the pressure ratio and the efficiency of the compressor converge. The heat-release rate is another necessary input of the model. It was calculated from the provided measurement data. The wall heat transfer is calculated according to the model of Woschni and Huber [59, 133]. The engine friction was calculated from the measurement data. The flow coefficients of the intake and exhaust ports in dependency of the valve lift were provided by FPT. Also the flow coefficient of the throttle valve in dependency of the throttle angle was provided.

Validation

Figure 5.4 displays the model fit for selected quantities and full load operation. Dataset 1 was used to calibrate the model. Dataset 2 was used to validate the model. The trends of the intake manifold pressure of dataset 1 and 2 differ, because the measurements were conducted with turbochargers of different sizes. In case of dataset 1 the waste gate is closed below engine speeds of 1200 min^{-1}. In the case of dataset 2 the waste gate is closed below 1000 min^{-1}. No degree of freedom exists with a closed waste gate to influence the intake manifold pressure and the fit of the model is particularly visible to the observer. A good agreement between simulation and measurement is found in case of dataset 1. The relative deviation is below 5 %. The maximum relative deviation in case of dataset 2 is 10 %. The trends are captured well, but especially the temperature and pressure before the turbine deviate. This indicates inaccuracies in the turbocharger models. Potential sources of deviation are that the turbocharger characteristics (Figure 5.3) are recorded on turbocharger test beds with stationary gas flows, but the gas dynamics of the engine are highly transient. In addition, the model does not account for the inertia of the turbocharger and the provided engine measurement data results from two different measurement campaigns which can also lead to discrepancies.

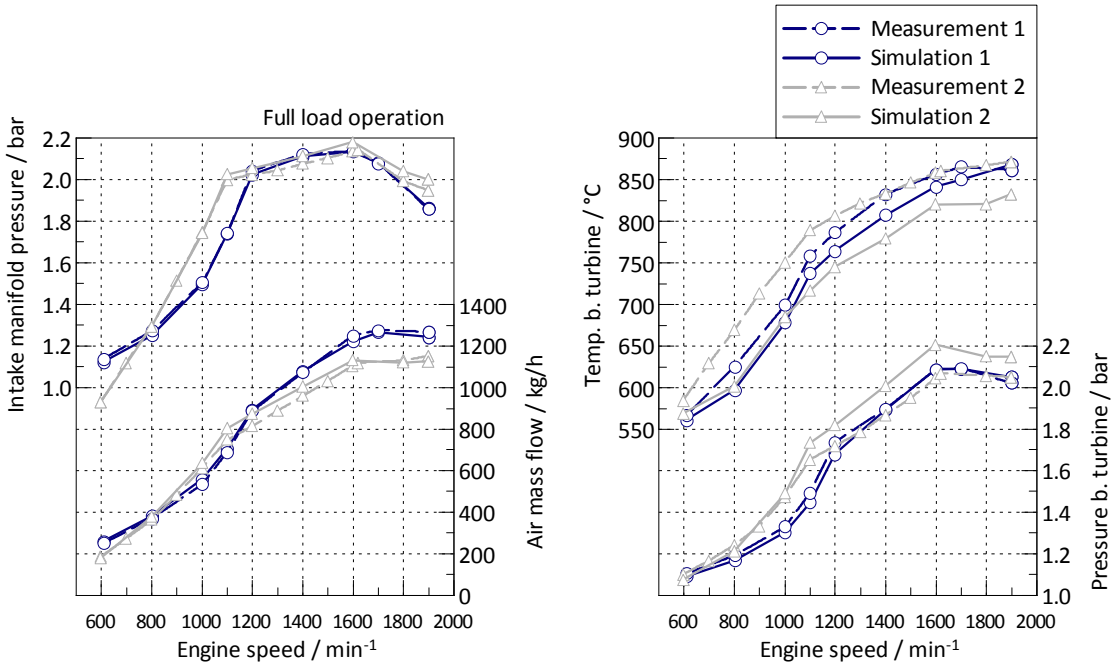

Figure 5.4: Fit of the 1D simulation model of the Cursor 13 CNG engine for two independent sets of measurement data.

5.3.2 HDGAS Model

After the calibration and validation of the model of the Cursor 13 CNG engine (Figure 5.2), the model was adapted to the specifications of the HDGAS engine. Figure 5.5 displays the final model of the HDGAS engine. The changes made from the Cursor 13 CNG model are versatile and are listed below:

- The dimensions of the pipes were adapted to the geometry of the HDGAS engine.
- The injectors (I1 – I6) for CNG port fuel injection were removed and replaced by direct injection.
- Exhaust gas recirculation was added. Different layouts were investigated as detailed in the results section. In Figure 5.5 the final layout with a split EGR cooler (CO2, CO3), reed valves (R6, R7) and an EGR valve (R4) is displayed. A PID controller (PID3) was added to control the amount of EGR.
- The new intake and exhaust port design was considered by different flow coefficients calculated and provided by PoliMi by means of 3D CFD simulations.
- Another PID controller (PID4) was added to the existing PID1 for the actuation of the waste gate. Depending on the operating mode either the boost pressure was controlled (PID4) or the engine torque (PID1).

– A method was developed to implement the efficiency map of the compressor to circumvent the offline interpolation of the compressor efficiency described in the previous section.

– At full load operation a correlation between the amount of EGR and MFB50 was implemented to account for the influence of EGR on the knock limit.

– The influence of EGR on the heat-release rate was considered.

The implementation of the last two points is explained in more detail in the next section. The model of the wall heat losses remained unchanged. The influence of the Corona ignition on the combustion was not considered, because no measurement data existed to estimate the influence on the combustion duration.

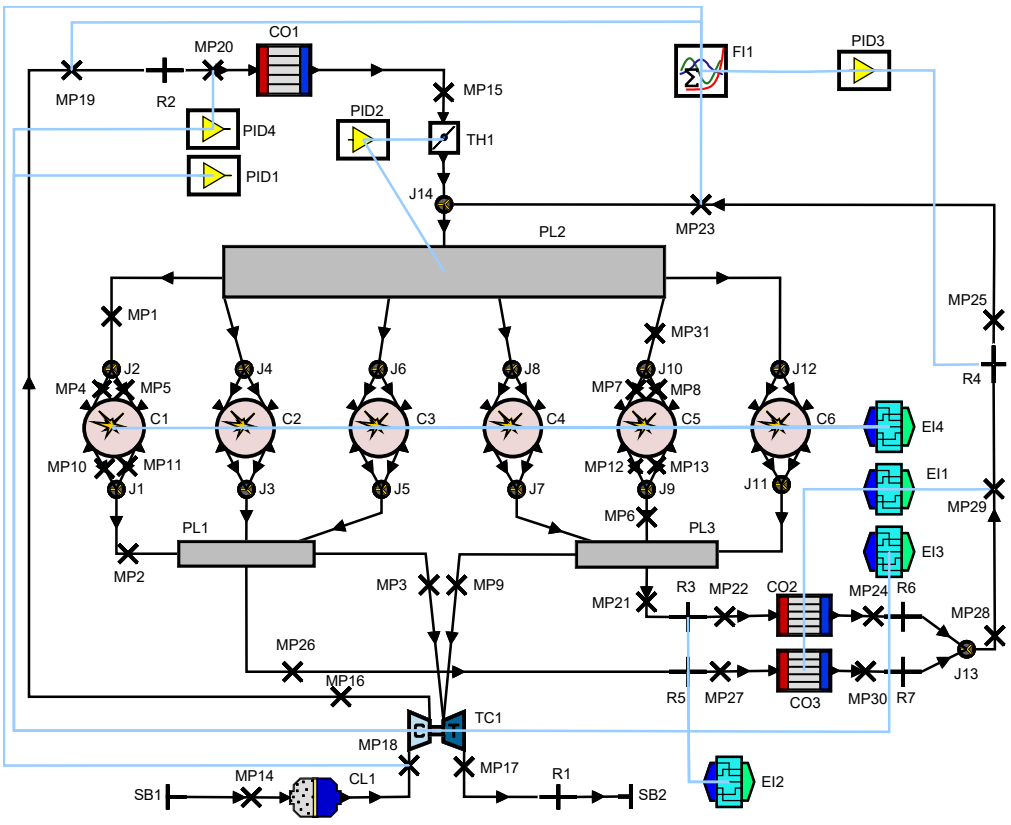

Figure 5.5: The 1D simulation model of the HDGAS engine created with *AVL BOOST* v2013.2.

5.3.3 Consideration of the Influence of EGR on the Heat-Release Rate

In the 1D simulation the combustion of the air-fuel mixture is considered by a 0D-model which solves the first law of thermodynamics for a control volume identical to the combustion chamber. The work transfer to the piston, the wall heat losses and the energy released due to the combustion are considered in this model. The evolution of the heat-release rate over degree crank angles (the 'shape' of the heat-release rate) is an input parameter to this model.

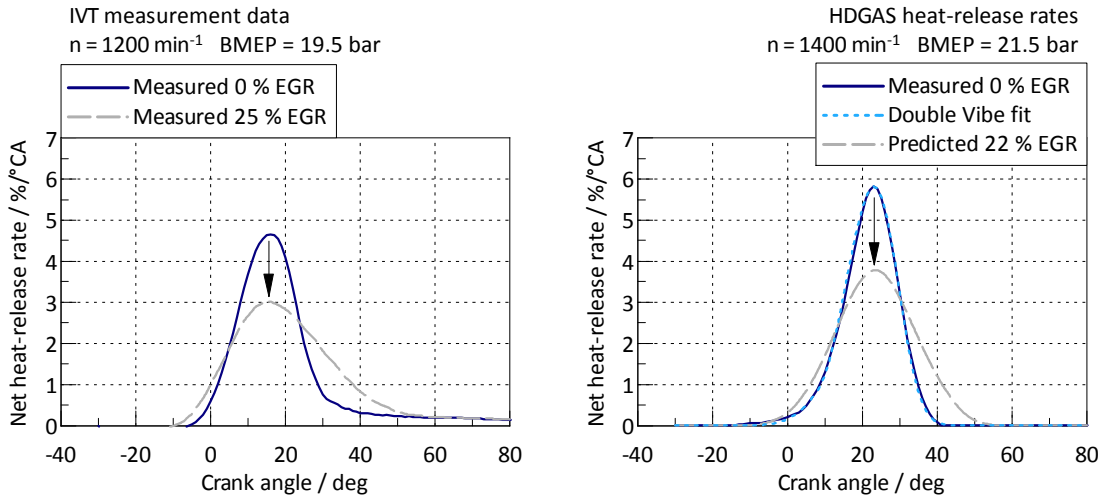

Figure 5.6: Influence of EGR on the net heat-release rate of the SCE engine (left) and transfer to the heat-release rates deployed in the 1D simulations (right).

EGR has a significant influence on the heat-release rate, it is therefore important to consider this effect. The Cursor 13 CNG prototype engine does not feature EGR in order to study the effect. Thus, another approach was chosen to estimate the influence of EGR.

Measurement data is available at the institute of a spark ignited single-cylinder CNG engine with 2 litre displacement and a compression ratio of 12.5. This engine was operated with and without EGR. The effect of EGR on the heat-release rate was studied by reviewing these measurement data and the findings were transferred to the HDGAS simulation model.

Figure 5.6 on the left depicts measurement data of the single-cylinder engine referred to on an exemplary basis. The engine is operated stoichiometrically and homogeneously. The diagram shows the net heat-release rates with 0 % and 25 % EGR at full load operation at an engine speed of 1200 min^{-1}. Since only the shape of the heat-release rate is of interest the normed heat-release rate in %/°CA is plotted. This means that in both cases the area under the trace is equal to 100 %. The maximum heat-release rate reduces considerably from 4.6 %/°CA to 3 %/°CA by the addition of EGR which is a reduction of 35 %. At the same time the combustion is prolonged since the area under the curve is constant. Therefore, the reduction of the maximum HRR alone can be used as an indicator for the influence of EGR on the HRR. The prolongation of the combustion is an automatic consequence of the postulation that the integral of the HRR is constant.

An EGR target was specified for each simulated load point based on the experience of the project partners. A corresponding reduction of the maximum heat-release rate was defined for each load point by reviewing the measurement data of the single-cylinder engine. Table 5.2 states the EGR target for each load point and the defined reduction of the net heat-release rate. Figure 5.6 on the right illustrates how the heat-release rate was altered. The measured heat-release rate of the Cursor 13 CNG engine is the model input for simulations without EGR. This heat-release rate is approximated with a double vibe fit. In a second step this fit is altered in order to achieve the reduction specified in Table 5.2. The heat-release rates generated in this way serve as input for the simulations with EGR.

Table 5.2: The EGR target and the defined reduction of the maximum heat-release rate.

Engine speed min^{-1}	Torque Nm	EGR target %	Reduction maximum HRR %
600	max.	8	−14
800	max.	10	−17
1000	2200	11	−19
1100	2200	12.5	−21
1200	2200	18	−30
1400...1900	2200...1860	22	−35
1200	800	20	−25

An uncertainty in the deployed heat-release rates remains of course, both with and without EGR. The combustion chamber geometry, the charge motion, presumably the turbulence level and the ignition source differ between the Cursor 13 CNG prototype engine, the single-cylinder engine at the institute and the HDGAS engine under development. However, since at the time of the simulations no measurement data of the HDGAS engine was available this approach is valid to estimate the influence of EGR on a heavy duty NG SI engine.

Furthermore, the influence of EGR on the knock limit was estimated again by reviewing the SCE measurement data. It was found that by the addition of EGR and incorporating a safety margin to the actual knock limit, MFB50 = 14 °CA is feasible for the single-cylinder engine. An algorithm was implemented in the simulation which linearly interpolates between MFB50 = 14 °CA if the EGR target is achieved and the MFB50 of the Cursor 13 CNG engine at 0 % EGR which is around 20 °CA. The heat-release rate is shifted accordingly.

5.4 Simulation Results

In this section the findings of the simulations are presented. The effects of EGR in part load and full load operation in combination with a waste gate turbocharger are discussed. Early and late Miller valve timing in the presence of external EGR is reviewed and compared to conventional valve timing. Finally, cam phasing is investigated together with EGR and in combination with the standard and the early Miller valve lift profiles. The section is concluded by a comparison of the simulation results and measurements of the HDGAS single-cylinder engine conducted by AVL Graz.

5.4.1 Exhaust Gas Recirculation in the Context of an SI Engine with Waste Gate Turbocharger

Theory

EGR is state of the art generally in all passenger car and many heavy duty diesel engines. It is used to reduce the engine-out NO_x emissions of diesel engines by lowering the combustion

temperature and the oxygen concentration. By contrast, EGR has previously scarcely been used in stoichiometrically operated SI engines, as the engine-out NO_x emissions are effectively reduced by the three-way catalyst creating no need for EGR from an emissions perspective. It was used in some engines instead for dethrottling during part load operation. As today's PC gasoline engines are generally turbocharged and the new emission legislation focuses on RDE, EGR has again received attention for SI engines. Fuel enrichment is commonly used in passenger car gasoline SI engines to safeguard the turbocharger at full load from too high exhaust gas temperatures. Fuel enrichment must be avoided, however, with the introduction of the RDE legislation. Thus, new concepts such as EGR are considered to reduce the exhaust gas temperature [24, 26, 121] and first series applications in passenger car gasoline SI engines were reported [56, 61, 90].

Similarly, EGR is also considered for stoichiometrically operated turbocharged NG heavy duty engines to raise the fuel efficiency and to reduce the thermal strain of the turbocharger to ensure the required durability [2, 39, 99]. Detailed studies were published [46, 68] and a series application was reported [57]. The effects of EGR are manifold and are summarised for heavy duty natural gas SI engines below.

By adding cooled exhaust gas to the fresh charge the air-fuel mixture is diluted. Thus, the combustion temperature decreases as more inert mass is present in the cylinder. As a consequence the wall heat losses reduce which raises the fuel efficiency. A reduction of the combustion temperature implies that the exhaust gas temperature is also lowered. Hence, EGR is a viable measure to meet the temperature limit of the turbocharger, which is a critical constraint in stoichiometric engine concepts. The limit is in the range of 800 °C for a modern turbocharger designed for heavy duty NG engines. Furthermore, EGR influences the caloric properties of the cylinder charge during compression. The specific heat capacity of exhaust gas is higher than of fresh charge which decreases the isentropic exponent of the cylinder charge. This results in a reduced work demand during compression. In addition, the reduced combustion temperature increases the isentropic exponent during expansion. Both effects cumulate in an increase of the fuel efficiency of the engine [97].

At full load operation cooled EGR is a measure to reduce the knocking probability, again by reducing the combustion temperature. Thereby the maximum torque can be raised. Alternatively, the compression ratio can be increased or MFB50 can be advanced, both measures influence the fuel efficiency positively. Finally, the addition of exhaust gas requires a higher intake manifold pressure to keep the amount of fresh charge constant. During part load operation of SI engines this means the engine is dethrottled and the gas exchange losses are reduced. Also at full load operation EGR affects the gas exchange losses of an engine with waste gate turbocharger positively. The relations are less obvious and therefore are explained subsequently by means of the simulation results.

Layout

As stated in the previous section an EGR target was defined for the HDGAS engine at full load operation in dependence of the engine speed (Table 5.2). Different EGR layouts were investigated to achieve this target. Figure 5.7 displays the four investigated EGR layouts, they comprise of:

a Exhaust gas recirculated from three cylinders and one cooler.

b Exhaust gas recirculated from all six cylinders and one cooler.

c Exhaust gas recirculated from all six cylinders and a split cooler for reduced flow resistance.

d Addition of reed valves to eliminate back flow and utilise even small pressure peaks.

Figure 5.8 shows the achieved amount of EGR and the EGR target at full load. The simulations were performed with the finalised waste gate turbocharger of the HDGAS engine. The turbocharger was chosen in order to meet the low-end torque and the EGR target at $n = 1000\,min^{-1}$. The feasible amount of EGR increases from layout **a** to layout **d**. The influence of the reed valves at lower engine speeds is especially remarkable. In order to recirculate exhaust gas a positive pressure gradient between the exhaust manifold and the intake manifold is required. This prerequisite is, however, in conflict with the requirements for an optimal gas exchange. The pressure gradient between exhaust and intake manifold should be as small as possible or even negative for minimum gas exchange losses. Therefore, with variants **a** to **c** no exhaust gas can be recirculated below engine speeds of $1000\,min^{-1}$ as the pressure gradient is either negative or too small. The reed valves enable the utilisation of small pressure peaks to promote EGR even if on average the pressure gradient is negative. However, also with layout **d** the target is not met between $1100\,min^{-1}$ and $1400\,min^{-1}$. A smaller turbine would facilitate higher amounts of EGR, yet at the cost of higher gas exchange losses as the exhaust manifold pressure rises. It was decided that the EGR achieved with layout **d** is sufficient due to these correlations.

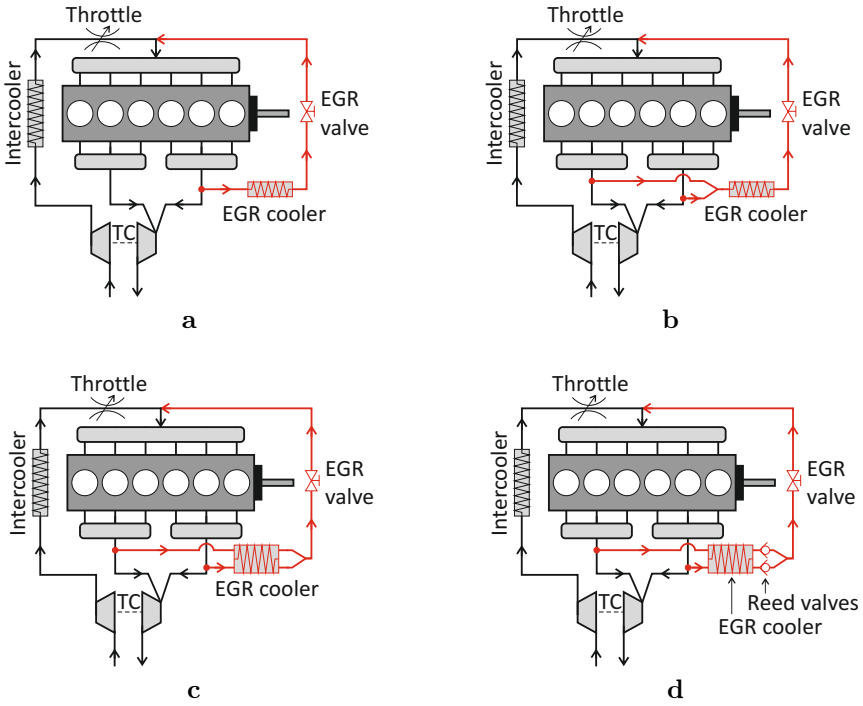

Figure 5.7: The four investigated EGR layouts for the HDGAS engine.

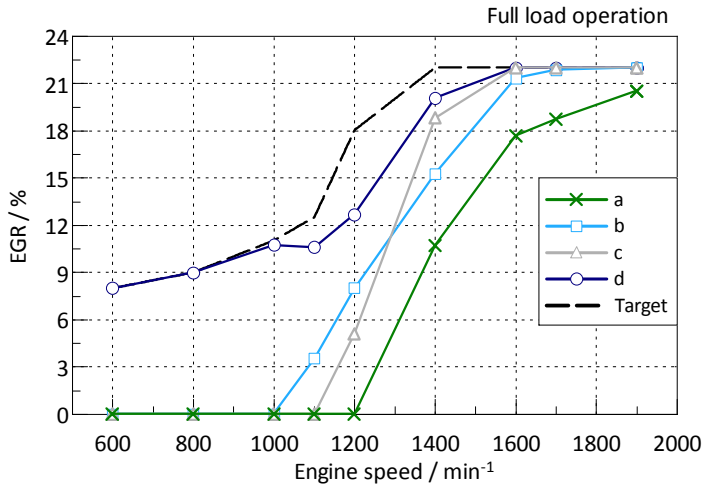

Figure 5.8: The EGR target at full load and the achieved amount of EGR with each EGR layout (Figure 5.7).

Part Load Operation

The influence of EGR on the HDGAS engine is quantified by the comparison of simulation results with and without EGR. The results with EGR refer to layout **d**. Figure 5.9 displays results in the part load operating point $n = 1200\,\mathrm{min}^{-1}$ and $\mathrm{BMEP} = 7.8\,\mathrm{bar}$. In the following this load point is abbreviated as 1200/7.8. Note that the origin of the bar charts is unequal to zero in some cases for a better perceptibility of the differences. The EGR target in this load point is 20 %. It is achieved without problems due to the throttled operation. MFB50 is set to 12 °CA in both cases and the effect of EGR on the heat-release rate is considered as explained in Section 5.3.3.

The intake manifold pressure p_{intake} must be raised by almost 200 mbar in the case with EGR in order to maintain the load. The exhaust manifold pressure p_{exhaust} remains almost unaffected. This results in a reduction of the gas exchange losses by 200 mbar or one third.

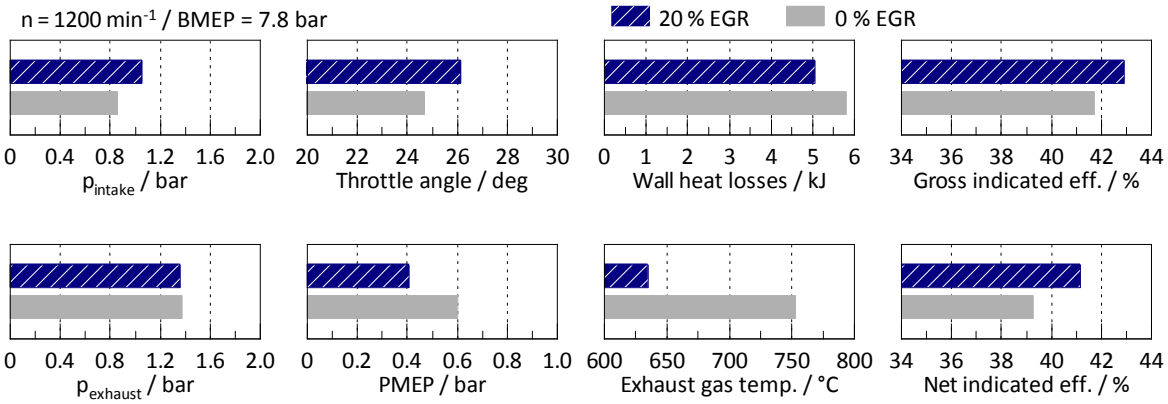

Figure 5.9: The influence of EGR in part load operation.

As explained above charge dilution leads to a reduction of the combustion temperature. As a consequence the wall heat losses reduce by 13 % and the exhaust gas temperature decreases by 120 °C from 750 °C to 630 °C. The changes in the wall heat losses, the caloric properties of the charge and the heat-release rate cumulate in an increase of the gross indicated efficiency $\eta_{i,g}$ by 1.2 $\%_{Pt.}$ to 42.9 %. The total of the described effects result in an increase of the net indicated efficiency $\eta_{i,n}$ even by 1.9 $\%_{Pt.}$ to 41.5 %. With a friction mean effective pressure (FMEP) of 1 bar, this results in a brake thermal efficiency η_e of 36.9 %.

Full Load Operation

The influence of EGR at full load operation is displayed in Figure 5.10. In the top left part the torque, the EGR rate and the set MFB50 are depicted. The results with EGR represent variant **d** of Figure 5.7. MFB50 is adjusted in dependence of the amount of EGR to account for the knocking probability as explained in Section 5.3.3. In the bottom left diagram the influence on the gas exchange is displayed. The addition of EGR requires a higher intake manifold pressure to maintain the load. Therefore, the waste gate is closed more (described by the ratio of the mass flow across the turbine to the total exhaust gas mass flow) to provide a higher boost pressure. This entails also an increase of the exhaust manifold pressure, but the increase of the intake manifold pressure is larger. The reason is that the turbocharger efficiency is rising as the operating points are shifted towards more favourable areas in the compressor operating map as demonstrated in Figure 5.11 As a result, the gas exchange losses decrease by up to 350 mbar in the engine speed range from 1000 min^{-1} to 1900 min^{-1}. At 600 min^{-1} and 800 min^{-1} the engine torque reduces with EGR, because not enough boost pressure can be provided to keep the mass of fresh charge constant. This also reflects in the gas exchange losses which are slightly higher with EGR at 600 min^{-1} and 800 min^{-1}. However, PMEP is still negative which indicates that also during the gas exchange work is transferred from the gas to the piston.

In the right diagram the effect on the exhaust gas temperature is displayed. Without EGR the temperature reaches up to 940 °C considerably exceeding the limit of 800 °C. By the introduction of EGR the exhaust gas temperature is lowered by 190 °C to 750 °C. Although the reduction is not only caused by EGR, also the advancement of MFB50 reduces the exhaust gas temperature. The wall heat losses are reduced by approximately 8 %. The large difference at 600 min^{-1} and 800 min^{-1} results from the different load in these two operating points. Both the gross and net indicated efficiency increase by approximately 2.5 $\%_{Pt.}$ by the addition of EGR. However, the difference in MFB50 also contributes to it. The small differences in efficiency below 1000 min^{-1} are contributed to the different load, the comparably small amount of EGR and similar MFB50.

Finally, Figure 5.11 displays the location of the operating points in the compressor operating map. EGR shifts the operating points towards higher compressor pressure ratios as higher boost pressures are required. For the present engine and turbocharger this results in an increase of the compressor efficiency. In conclusion, the positive effects of EGR on SI engines stated in literature are clearly confirmed for heavy duty natural gas SI engines with a waste gate turbocharger. In part load as well as full load operation the efficiency of the engine is raised while the exhaust gas temperature is lowered which is vital for the turbocharger at full load operation.

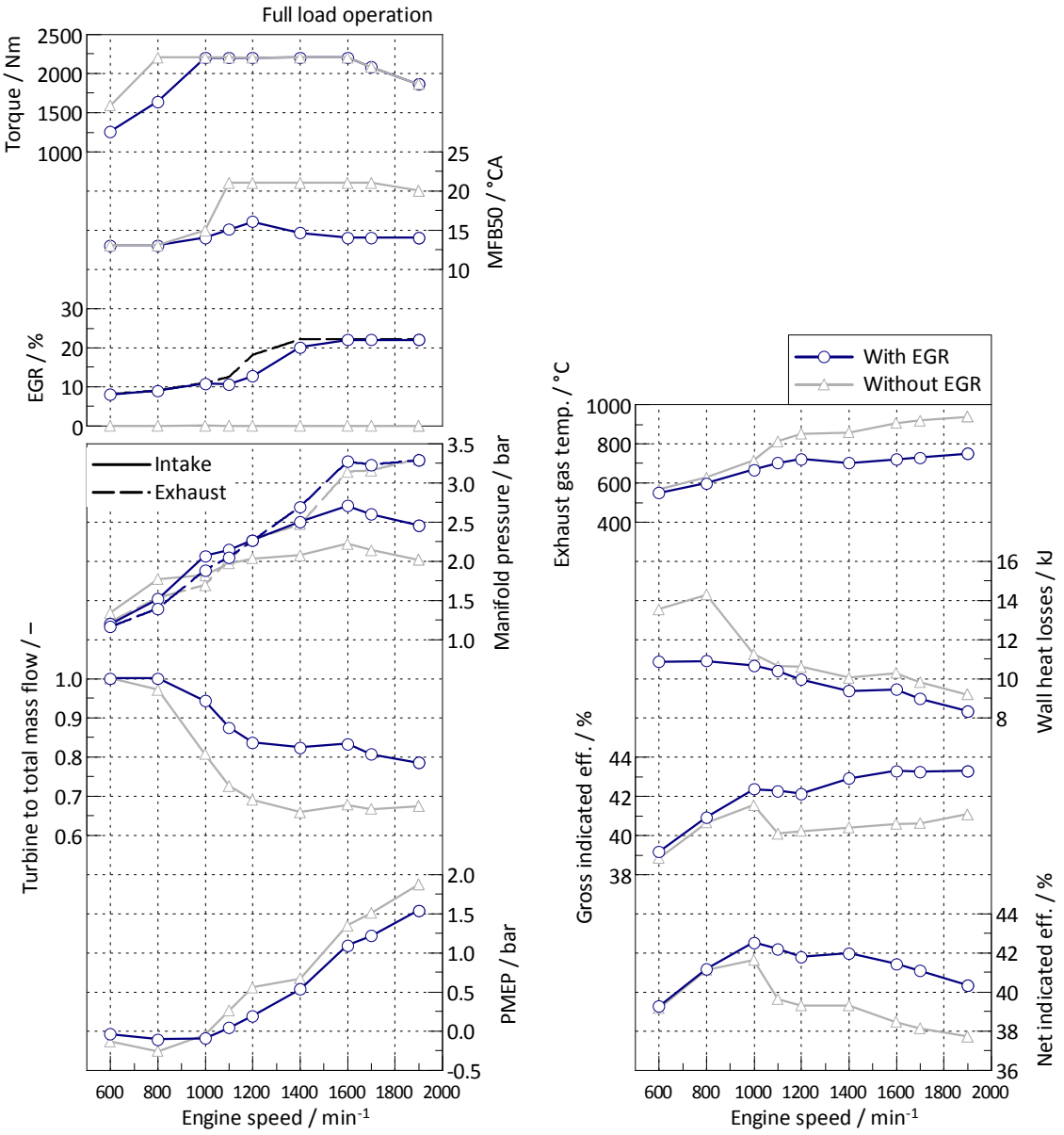

Figure 5.10: The influence of EGR at full load operation.

5.4.2 Early and Late Miller Valve Timing

Apart from conventional valve timing which is optimised for maximum volumetric efficiency, the early and late Miller Cycle were investigated. The latter one is also referred to as Atkinson Cycle. They are characterised by an early, respectively late intake valve closing (IVC). Subsequently, a short introduction to the theory behind the Miller Cycle is given. Afterwards the layout of the valve lift profiles is discussed and the results in full load and part load operation are presented.

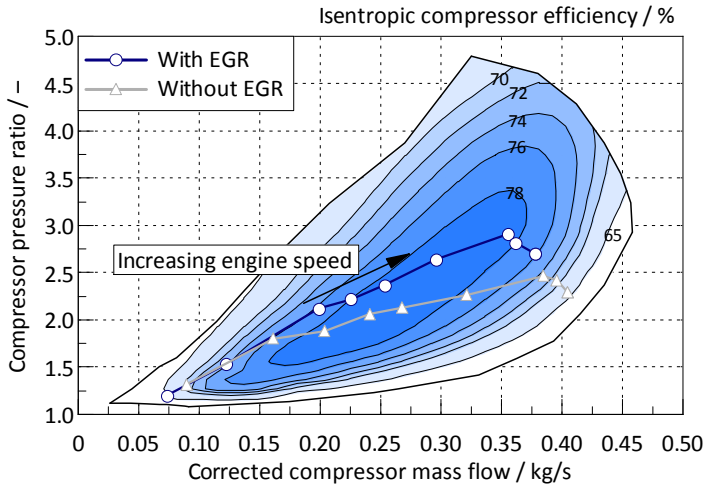

Figure 5.11: The compressor operation map and the influence of EGR on the operating points.

Theory

Early Miller timing is characterised by an early IVC while late Miller timing makes use of late IVC. From a thermodynamic point of view both processes are identical. The differences which still exist in practice are discussed later. The effects of and motivation for Miller timing are manifold. An excellent overview of the various effects is given in [107]. Figure 5.12 depicts an idealised process of the early Miller Cycle in comparison to conventional valve timing in part load operation. With conventional valve timing IVC is in BDC and the compression starts in point 2. In the early Miller Cycle the intake valve already closes in point 1b'. The cylinder charge is overexpanded to point 2 and then again compressed. The compression above intake conditions starts only in point 1b'. The early IVC reduces the volumetric efficiency and therefore the gas exchange losses of a stoichiometric engine in part load operation. The gas exchange work of conventional valve timing is represented by the hatched area. With Miller timing, if IVC is optimal (as in Figure 5.12) the gas exchange work vanishes, as the volumetric efficiency is reduced exactly to such an extent that throttling is not required.

A second effect important in the context of this work is the charge temperature. With Miller timing the charge temperature is reduced. The right graph of Figure 5.12 displays the cylinder temperature in part load operation. Due to the overexpansion of the cylinder charge after point 1b', the charge has a lower temperature in point 2 than with conventional valve timing. At full load operation due to the reduced volumetric efficiency a higher boost pressure is required with Miller timing than with conventional valve timing. This can be interpreted as an outsourcing of compression [107], since the compression of charge in the cylinder is reduced while the compression of air by the turbine is increased. As a consequence the temperature after the compressor is higher which opens up the possibility for better charge cooling. Therefore, also in full load operation the charge temperature is reduced which positively affects the conflict between knocking, MFB50, the compression ratio and the maximum attainable load.

The described effects are valid for early as also late Miller timing. Differences arise when considering the turbulence of the cylinder charge. Since the maximum acceleration of the valves

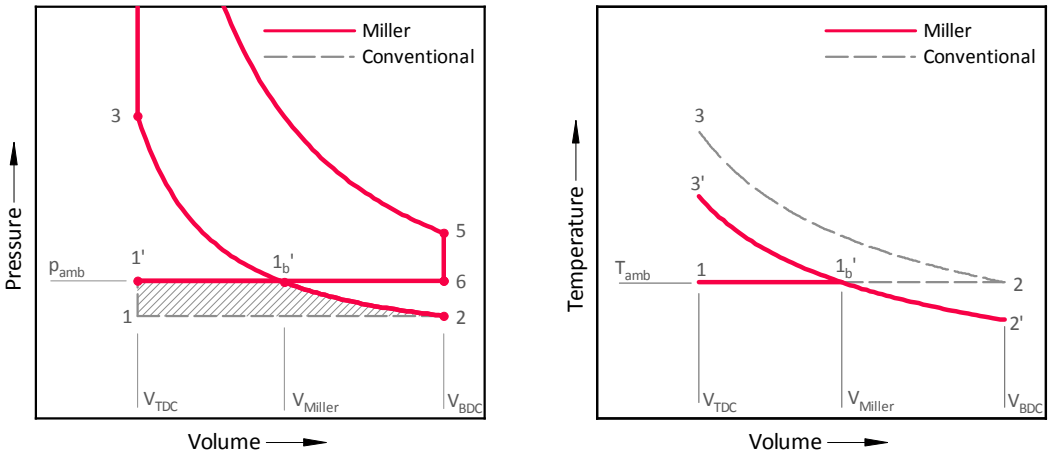

Figure 5.12: The pressure and temperature evolution of the Miller Cycle and conventional valve timing for an idealised process in part load operation [107].

is limited early IVC also entails a reduced valve lift. Furthermore, the inflow of air which is a source of turbulence is stopped early before BDC. Both effects cause a reduced turbulence level at firing TDC. In contrast, late Miller timing sustains a higher turbulence intensity. As cylinder charge is pushed back into intake duct, however, the flow losses are in reality higher. A more elaborate discussion of Miller timing is given in [107].

Layout

The investigated valve lift profiles are depicted in Figure 5.13. The conventional valve timing is denoted as *Standard*. All three intake valve lift profiles were combined with the same exhaust valve lift profile. Table 5.3 states the specifications of the individual valve lift profiles. φ_i and φ_e are the intake resp. exhaust cam phasing angles. They are defined as the angles between TDC and the maximum of the valve lift curves and are positive by definition.

Figure 5.14 displays the volumetric efficiency at full load operation and the ratio of turbine to total mass flow. The late Miller cam profile was designed in such a way that at $n = 1000\,min^{-1}$ (the engine speed at which the low-end torque is specified) the volumetric efficiency is approximately equal to early Miller timing. Thereby, the ratio of turbine to total mass flow is also identical which means the low-end torque is achieved with the same safety margin. At higher engine speeds the volumetric efficiency of late Miller timing is considerably higher than with early Miller timing due to the gas dynamics which change with the engine speed and the inertia of the gas flow.

Full Load Operation

Figure 5.15 depicts the influence of early and late Miller timing at full load operation. It reveals that the effects are limited compared to the introduction of EGR which was discussed in Section 5.4.1. Furthermore, the effect of late Miller timing is smaller than the one of early Miller timing as the volumetric efficiency is less reduced. In the simulation model the temperature at the intercooler outlet is kept constant. This means that the potential of additional charge

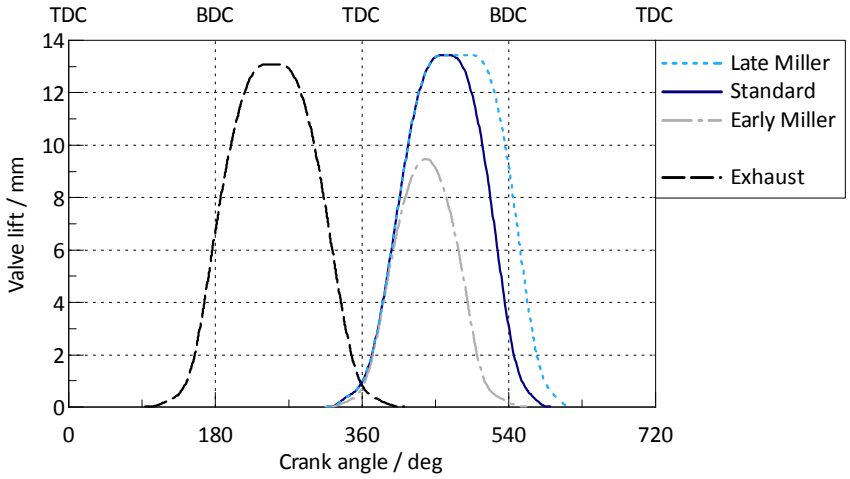

Figure 5.13: The investigated valve lift profiles of standard, early and late Miller timing.

Table 5.3: Specifications of the investigated valve lift profiles.

	Duration[1] °CA	IVC[1] °CA	EVO[1] °CA	φ_i °CA	φ_e °CA	max. lift mm
Intake						
Standard	218	566	–	103	–	13.4
Early Miller	165	522	–	78	–	9.5
Late Miller	247	595	–	117	–	13.4
Exhaust	232	–	136	–	109	13.1

[1] at 0.5 mm valve lift

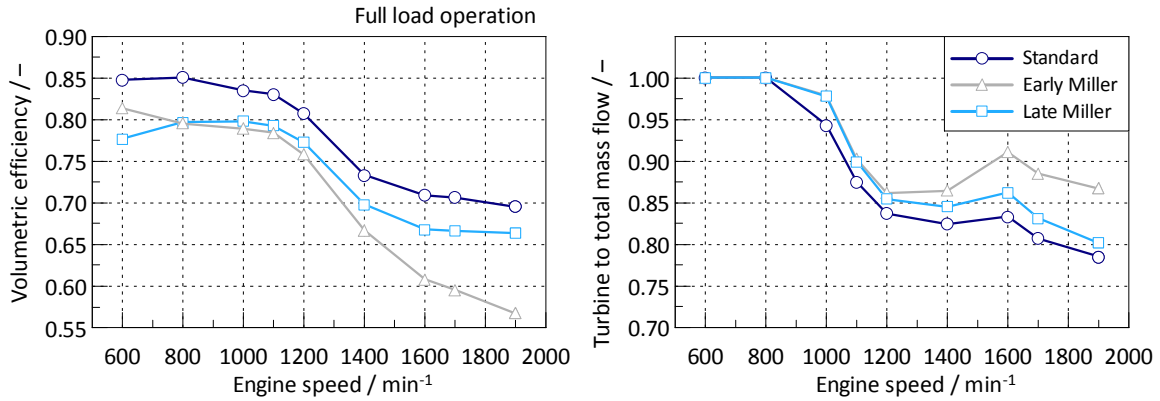

Figure 5.14: The volumetric efficiency and the ratio of turbine to total mass flow for the investigated valve lift profiles at full load operation.

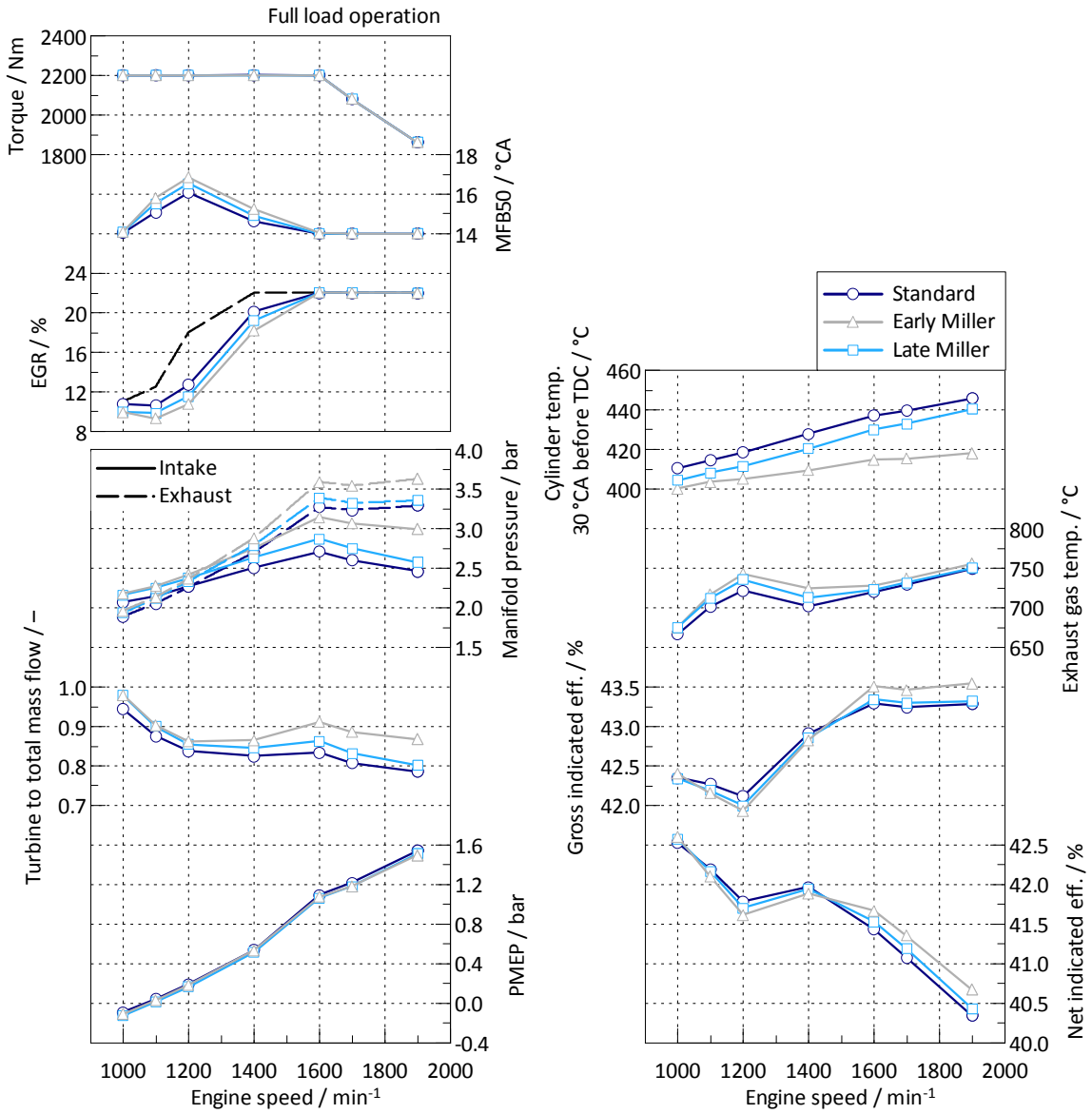

Figure 5.15: The effect of early Miller, late Miller and standard timing at full load operation.

cooling is completely utilised with Miller timing since the temperature at the intercooler inlet is higher. In the right graph of Figure 5.15 the cylinder temperature 30 °CA before firing TDC is displayed. This is just before the start of combustion. With early Miller timing the cylinder temperature is lowered by 10 °C to 28 °C. This positively affects the knocking probability. The decrease is smaller with late Miller timing and remains constant at approx. 7 °C.

The intake manifold pressure must be raised by more than 400 mbar with early Miller timing and by 150 mbar with late Miller timing. This requires a closing of the waste gate which is indicated by an increase in the ratio of turbine to total mass flow. However, unlike the introduction of EGR (Figure 5.10) the exhaust manifold pressure also rises considerably.

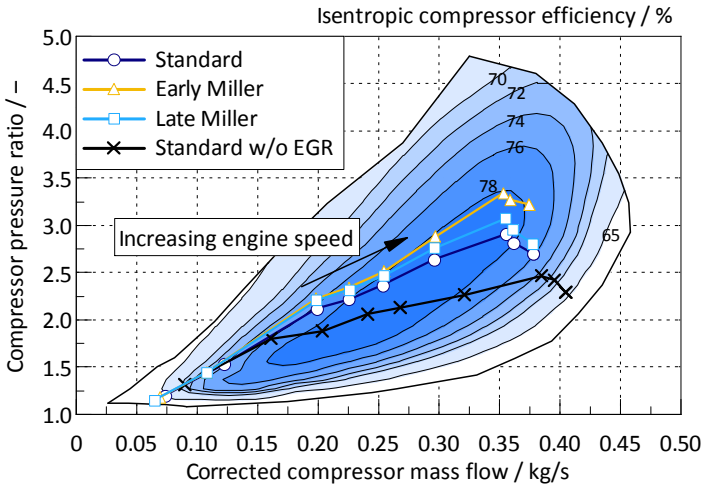

Figure 5.16: The compressor operating map and the operating points at full load with different valve timing concepts.

Therefore, the reduction of the gas exchange losses is lower. The reason is the turbocharger efficiency as demonstrated in Figure 5.16. By the introduction of EGR the operating points of the compressor are shifted towards areas of higher compressor efficiency. By Miller timing the efficiency remains approximately constant. It cannot be raised further as the maximum efficiency has already been reached. As a consequence, there is a stronger increase in the exhaust manifold pressure.

It is worth mentioning that the gas exchange losses are calculated from BDC to BDC independent of the valve timing. This more or less arbitrary partition of the engine cycle into a low-pressure and a high-pressure cycle can cause artefacts when IVC deviates considerably from BDC. Parts of the gas exchange can be assigned to the high-pressure cycle and vice versa. However, when the whole engine cycle of 720 °CA is considered, these artefacts dissolve and the IMEP remains unaffected.

Even though the changes in the pressure gradient between exhaust and intake manifold are small, they affect the feasible amount of EGR as displayed in the top left graph of Figure 5.15. The changing level of EGR softens the influence of the valve timing on the gas exchange work and affects MFB50. The influence on the exhaust gas temperature is below 30 °C and results from the increase of the exhaust manifold pressure and the differences in EGR and combustion phasing.

The effect of Miller timing on the gross indicated efficiency is ambivalent. Between 1000 min^{-1} and 1400 min^{-1} it is reduced by up to 0.2 $\%_{\mathrm{Pt.}}$ compared to standard timing. This results from the retarded MFB50 which influences the brake torque and the reduced EGR which affects the wall heat losses. At higher engine speeds early Miller timing facilitates an increase of the gross indicated efficiency by approximately 0.2 $\%_{\mathrm{Pt.}}$. EGR and MFB50 are equal which means the higher efficiency is caused by the reduced charge temperature. The improvement by late Miller timing is below 0.1 $\%_{\mathrm{Pt.}}$, because the difference in volumetric efficiency is too small compared to standard timing.

The influence of Miller timing on the net indicated efficiency is slightly larger, because

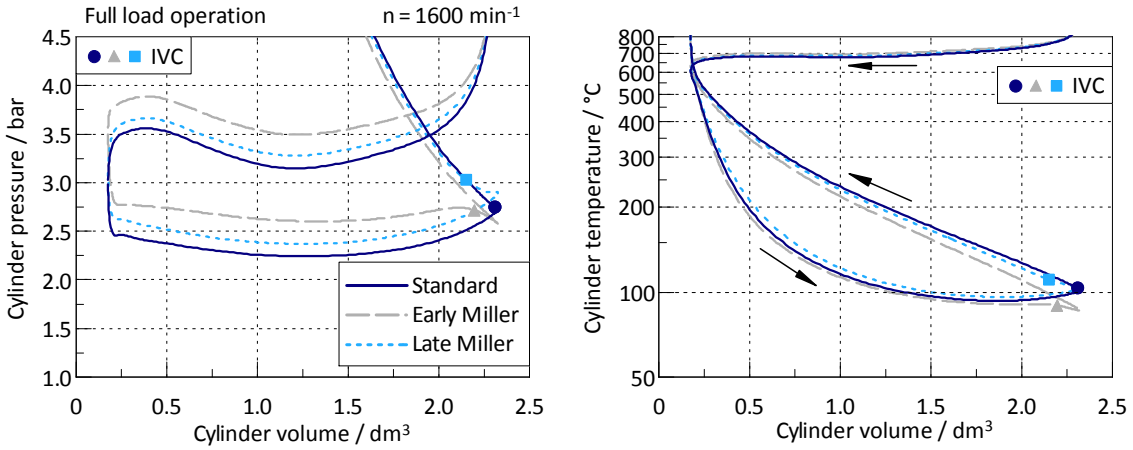

Figure 5.17: The p-V and T-V diagrams for early Miller, late Miller and standard timing at full load operation and $n = 1600\,min^{-1}$.

the positive effect on the gas exchange losses is included. Early Miller timing increases the efficiency by $0.3\,\%_{Pt.}$ above $1400\,min^{-1}$. Late Miller timing increases the efficiency by $0.1\,\%_{Pt.}$ above $1400\,min^{-1}$. At $1400\,min^{-1}$ and below the reduction of the gas exchange work and the wall heat losses cannot compensate the negative influence on EGR and MFB50.

Finally, Figure 5.17 depicts the p-V and T-V diagrams at $n = 1600\,min^{-1}$. IVC is defined at 1 mm effective valve lift and added in the graphs. The overexpansion in the case of early Miller timing, the higher intake manifold pressure and the cooler charge are well observed.

Part Load Operation

In part load operation Miller timing enables dethrottling of the engine. Figure 5.18 depicts simulation results of early Miller, late Miller and standard timing in the load point 1200/7.8. All three variants are operated with 20 % EGR and MFB50 is set to 12 °CA. As the volumetric efficiency is reduced with Miller timing, the intake manifold pressure is raised by 60 mbar respectively 80 mbar. The throttle valve is opened to achieve this rise. Since the waste gate remains fully closed at these low pressures also the exhaust manifold pressure remains unchanged. Consequently, the PMEP which quantifies the gas exchange losses reduces by 60 mbar respectively 70 mbar. The exhaust gas temperature is not significantly influenced. The wall heat losses decrease by approx. 2 % and in accordance the gross indicated efficiency increases slightly by Miller timing. The increase in net indicated efficiency accounts for $0.3\,\%_{Pt.}$ and $0.4\,\%_{Pt.}$ mainly due to the reduction in gas exchange work. Figure 5.19 shows the associated p-V and T-V diagrams. The reduction of the gas exchange work is well observed. The reduction of the charge temperature at BDC is also recognisable.

Finally, Figure 5.20 displays crank angle resolved simulation results for the three valve lift profiles. It displays the intake and exhaust manifold pressure, the cylinder pressure, the mass flow over intake and exhaust valves and the valve lift profiles. In the case of early Miller valve timing the overexpansion of the cylinder charge can be observed by a reduction of the cylinder pressure at 540 °CA which equals BDC. The exhaustion of fresh charge after BDC in the case

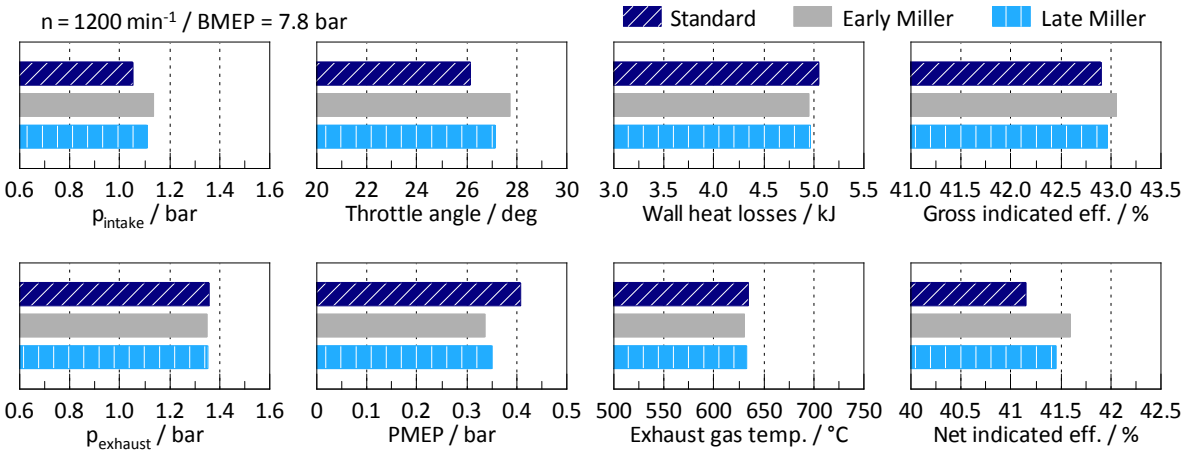

Figure 5.18: The effect of early Miller, late Miller and standard timing on the part load operation in the load point 1200/7.8.

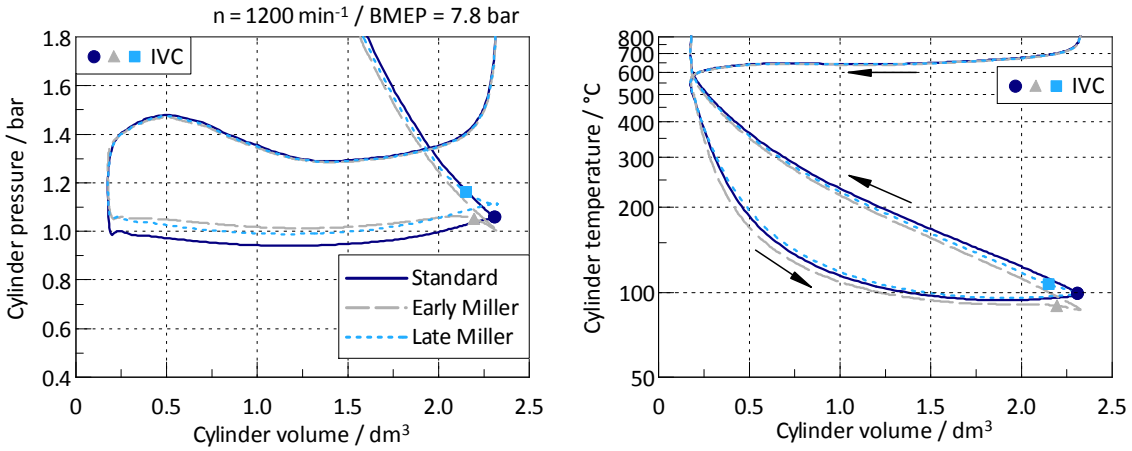

Figure 5.19: The p-V and T-V diagram in part load operation (1200/7.8) for early Miller, late Miller and standard valve timing.

of late Miller timing is well observable too. It also entails a later rise of the cylinder pressure compared to standard valve timing.

Conclusion

The potential of early and late Miller timing to reduce the gas exchange losses at full load operation is limited. However, in combination with intercooling the charge temperature at the end of the compression stroke can be reduced by up to 28 °C. This positively affects the trade-off between knocking, MFB50, compression ratio and the maximum attainable load. In part load operation the gas exchange losses are reduced distinctly resulting in an increase in net indicated efficiency by up to $0.4\,\%_{\mathrm{Pt.}}$ at BMEP = 7.8 bar. Miller timing is a practical method to raise the part load efficiency and at the same time improve the full load operation.

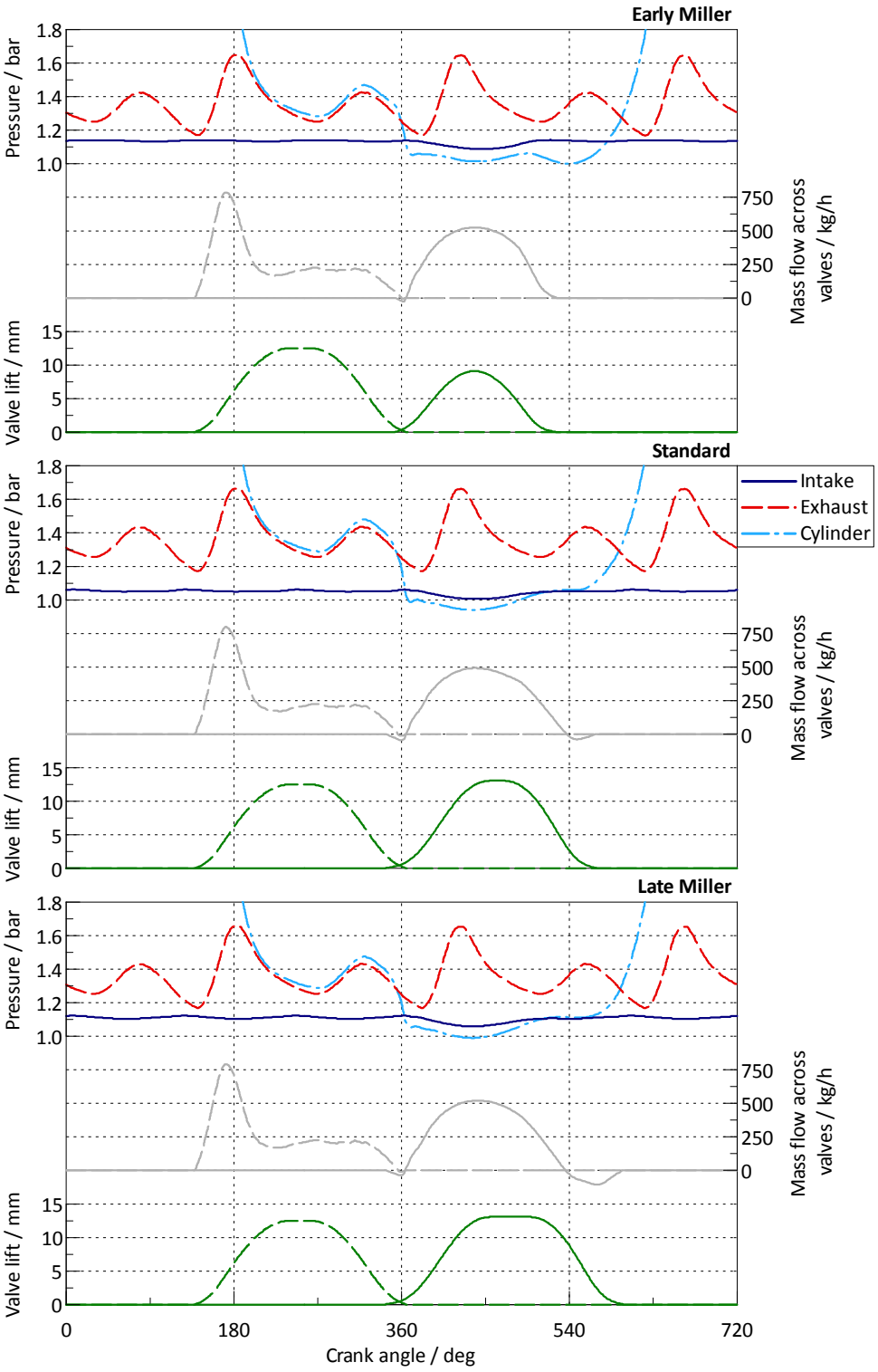

Figure 5.20: Crank angle resolved simulation results which are characteristic for the gas exchange in the part load operating point 1200/7.8.

5.4.3 Variable Valve Timing

Ultimately, the potential of cam phasing was investigated and indications for an operating strategy were derived. The investigations were conducted for the standard and early Miller cam profiles at full load and also part load operation in combination with external EGR. Hydraulically actuated cam phasers are installed on both cam shafts of the HDGAS engine. They rotate the cam shafts relatively to the crank shaft and thereby influence the valve timing during the operation of the engine. A more detailed description of the functionality of cam phasers and available realisations is given in [30]. Figure 5.21 displays the effect of cam phasing on the valve timing. The valve lift curves can be shifted relative to TDC and set optimal for each operating point.

The angle between the maximum of the valve lift curve and TDC is referred to as intake cam phasing angle φ_i resp. exhaust cam phasing angle φ_e. For the standard cam profile and fixed valve timing these angles are $\varphi_\mathrm{i} = 103\,°\mathrm{CA}$ and $\varphi_\mathrm{e} = 109\,°\mathrm{CA}$. Subsequently, the short notation I 103 / E 109 is often used to state a specific valve timing.

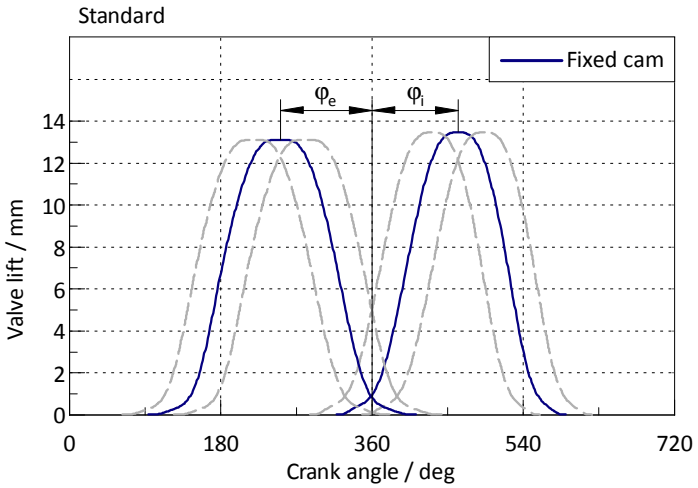

Figure 5.21: The effect of cam phasing on the valve timing for the standard cam profile.

The piston of the HDGAS engine includes valve pockets to allow for considerable valve lifts at TDC. Thereby the effects of a large valve overlap can also be assessed. A maximum valve lift of 5 mm is permissible at TDC which ensures a clearance between valves and piston of 1.5 mm. Figure 5.22 illustrates the situation of maximum valve lift at TDC.

Methodology

Figure 5.23 depicts the load points in which cam phasing was investigated. At part load operation a load sweep at $n = 1200\,\mathrm{min^{-1}}$ was analysed at BMEPs of 3 bar, 5 bar, 7.8 bar and 12 bar. Full load simulations at engine speeds of $600\,\mathrm{min^{-1}}$, $800\,\mathrm{min^{-1}}$, $1000\,\mathrm{min^{-1}}$, $1200\,\mathrm{min^{-1}}$, $1600\,\mathrm{min^{-1}}$ and $1900\,\mathrm{min^{-1}}$ were conducted.

In each operating point variations of the intake and exhaust cam phasing angles were performed according to the domain stated in Figure 5.24. The valve timing of fixed cams (as investigated in the previous section) is marked green. The minimum cam phasing angles (I 45 / E 78

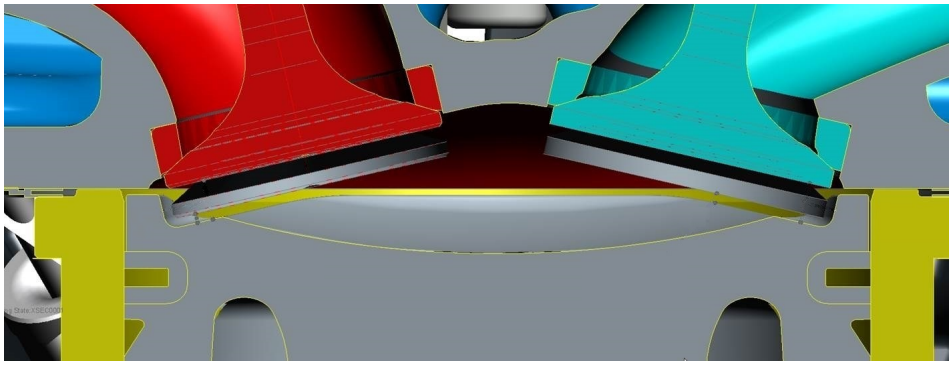

Figure 5.22: The minimum clearance between piston and valves at TDC at the maximum permissible valve lift of 5 mm.

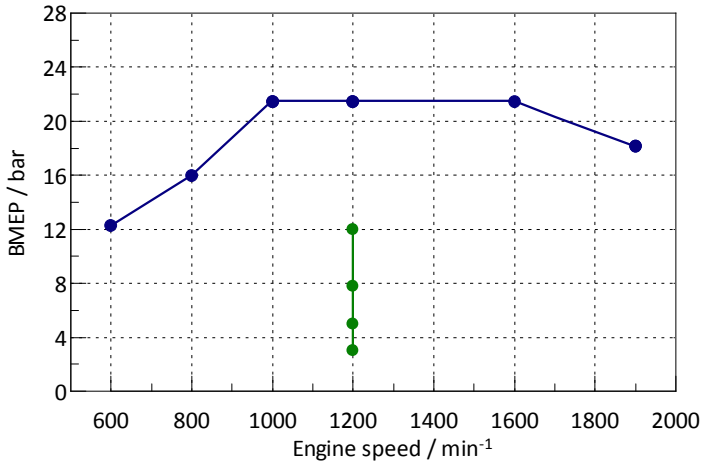

Figure 5.23: Load points in which cam phasing was assessed; Green: part load operation, blue: full load operation.

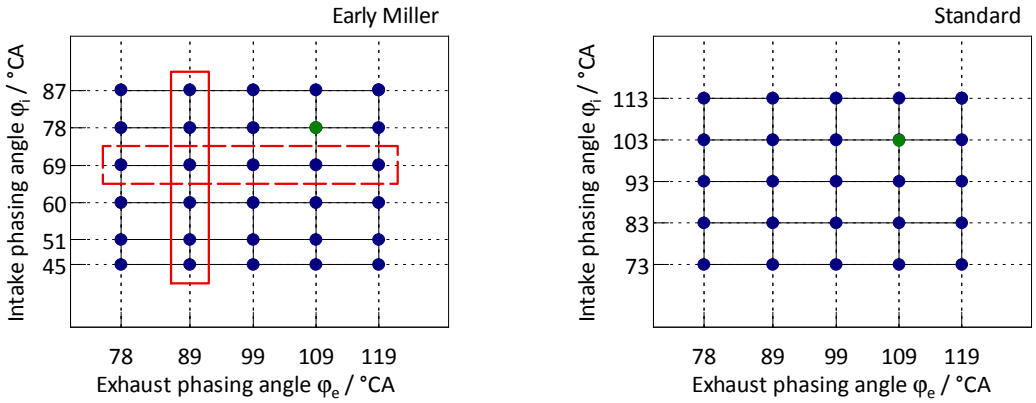

Figure 5.24: Domain of the simulated intake and exhaust cam phasing angles for early Miller and standard cam profiles (green: timing of the fixed cams).

resp. I 73 / E 78) are defined in accordance to the mechanical limit of 5 mm valve lift at TDC. Once the simulations were completed sweeps of constant intake resp. exhaust cam phasing angle (as indicated in the left graph of Figure 5.24) were plotted to investigate and demonstrate the effects of cam phasing.

Part Load Operation

The effects of cam phasing and the derivation of the operation strategy are discussed in detail for the early Miller cam profile. Subsequently, the potential of cam phasing at part load operation is discussed by reviewing the whole load sweep at $n = 1200\,\mathrm{min}^{-1}$ for both the early Miller and the standard cam profiles.

Figure 5.25 shows a variation of the intake cam phasing angle φ_i at BMEP = 3 bar for constant exhaust cam phasing angles and the early Miller cam profile. The total amount of EGR consists of internal and external EGR. The external EGR is recirculated from the exhaust manifold and cooled while the internal EGR consists of residual gas which remains in the combustion chamber. The internal EGR is thus considerably hotter than the external EGR. The total fraction of exhaust gas in the cylinder is kept constant at 24 %. The MFB50 is also kept constant at 13 °CA. The fixed valve timing is marked by the solid blue circle.

The intake cam phasing angle φ_i adjusts two important quantities of the valve timing, the valve overlap and IVC. The amount of internal EGR rises considerably with reducing intake cam phasing angle. The top and middle graph of Figure 5.26 illustrate the mechanisms behind this. The graphs display crank angle resolved data of I 45 / E 109 and I 78 / E 109 (i.e. a reduction of φ_i). Due to the low load the intake manifold pressure is below the exhaust manifold pressure. Reducing φ_i increases the valve overlap and results in a backflow of exhaust gas from the exhaust ducts into the intake ducts as the negative mass flow across the valves indicates. Simultaneously, IVC is advanced reducing the time for the inflow. The intake manifold pressure must be raised by opening the throttle valve in order to reach the target load. The exhaust manifold pressure remains almost unaffected. These dependencies are also well observed in Figure 5.25. As a consequence, the gas exchange work reduces considerably by up to 200 mbar compared to fixed valve timing, raising the net indicated efficiency by $1.3\,\%_\mathrm{Pt.}$.

The exhaust cam phasing angle φ_e also adjusts the valve overlap and more importantly it defines exhaust valve opening (EVO). A reduction of φ_e further increases the internal EGR as Figure 5.25 displays. The gas exchange losses are reduced by 220 mbar and the efficiency is raised by $1.4\,\%_\mathrm{Pt.}$ compared to the fixed valve timing. The combinations of smallest φ_i and φ_e (e.g. I 45 / E 78) are violating the condition of constant EGR since the internal EGR alone exceeds 24 %. They are therefore not displayed in Figure 5.25. The middle and bottom graph of Figure 5.26 illustrate the effect of a reduction of the exhaust cam phasing angle. The valve overlap further increases and the backflow of exhaust gas is prolonged reducing the time available for the inflow of fresh charge. The intake manifold pressure must therefore be raised further and the gas exchange work is reduced.

The second important effect is the adjustment of the EVO. It balances the conflicting goals of low gas exchange work and high gross indicated efficiency $\eta_\mathrm{i,g}$. Late EVO improves the utilisation of the cylinder pressure and therefore increases $\eta_\mathrm{i,g}$. However, the pressure level during the subsequent exhaust stroke is higher, which raises the gas exchange work. By contrast, early EVO results in a poor utilisation of the cylinder pressure, but the pressure level during

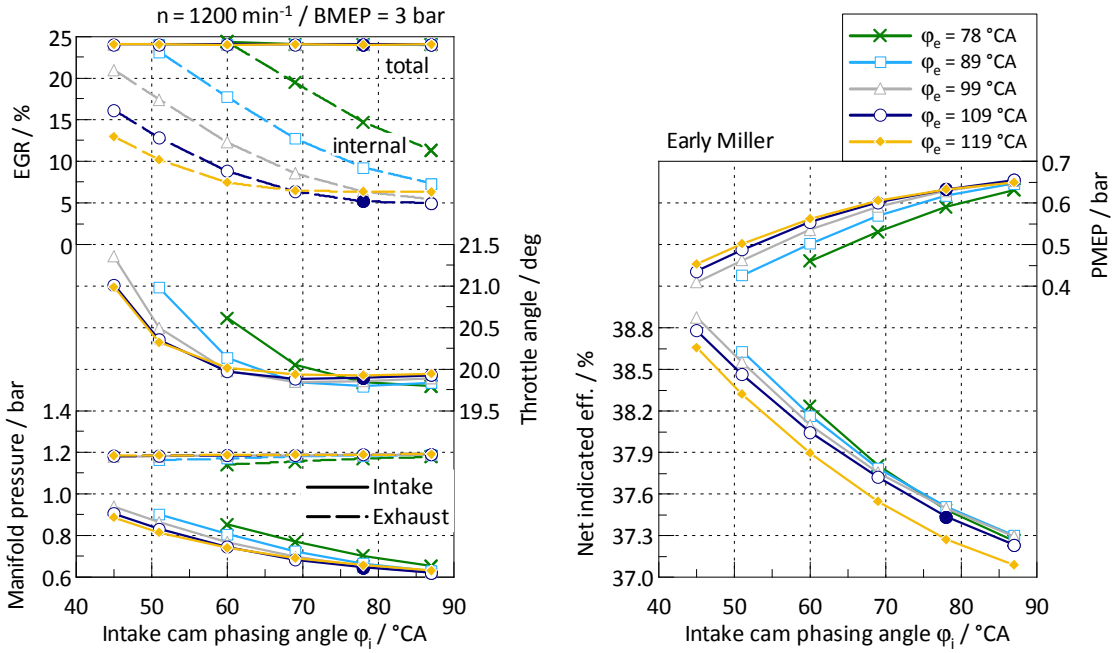

Figure 5.25: Variation of the intake cam phasing angle φ_i at $n = 1200\,min^{-1}$ / BMEP = 3 bar, constant exhaust cam phasing angles and the early Miller valve lift profile.

the exhaust stroke is lower leading to smaller gas exchange work. The optimum EVO depends on engine speed and load and is characterised by the maximum net indicated efficiency. For the current load point and with the set boundary conditions the optimum EVO occurs at $\varphi_e = 99\,°CA$.

Finally, Figure 5.27 displays the p-V and T-V diagrams for the same valve timings as in Figure 5.26. It illustrates the significant decrease of the gas exchange loop. In the case of I 45 / E 78 the temperature at BDC is higher compared to the other variants due to the large amount of internal EGR which raises the charge temperature by approx. 30 °C.

Figure 5.28 displays a variation of the intake cam phasing angle at BMEP = 7.8 bar. The relations are similar to the ones at BMEP = 3 bar, but the trends soften. Since the load is higher the gas exchange losses are smaller already with fixed cams (solid blue circle). A reduction of φ_i advances IVC and reduces the time available for the inflow of charge. The intake manifold pressure must be raised to maintain the load and as a result the gas exchange work decreases. The valve overlap also increases, but as the pressure difference between exhaust and intake is substantially smaller the amount of internal EGR does not increase significantly. Ultimately, at $\varphi_i = 51\,°CA$ the pressure gradient between exhaust and intake manifold is too small to recirculate the desired amount of exhaust gas and the EGR target can no longer be met. As a result, the gas exchange work remains constant and the net indicated efficiency reduces as the wall heat losses increase.

To illustrate the influence of the exhaust cam phasing angle lines of constant φ_i are plotted in Figure 5.29. Small exhaust cam phasing angles are equivalent to a late EVO which leads to an increase in gross indicated efficiency as a high cylinder pressure is sustained longer.

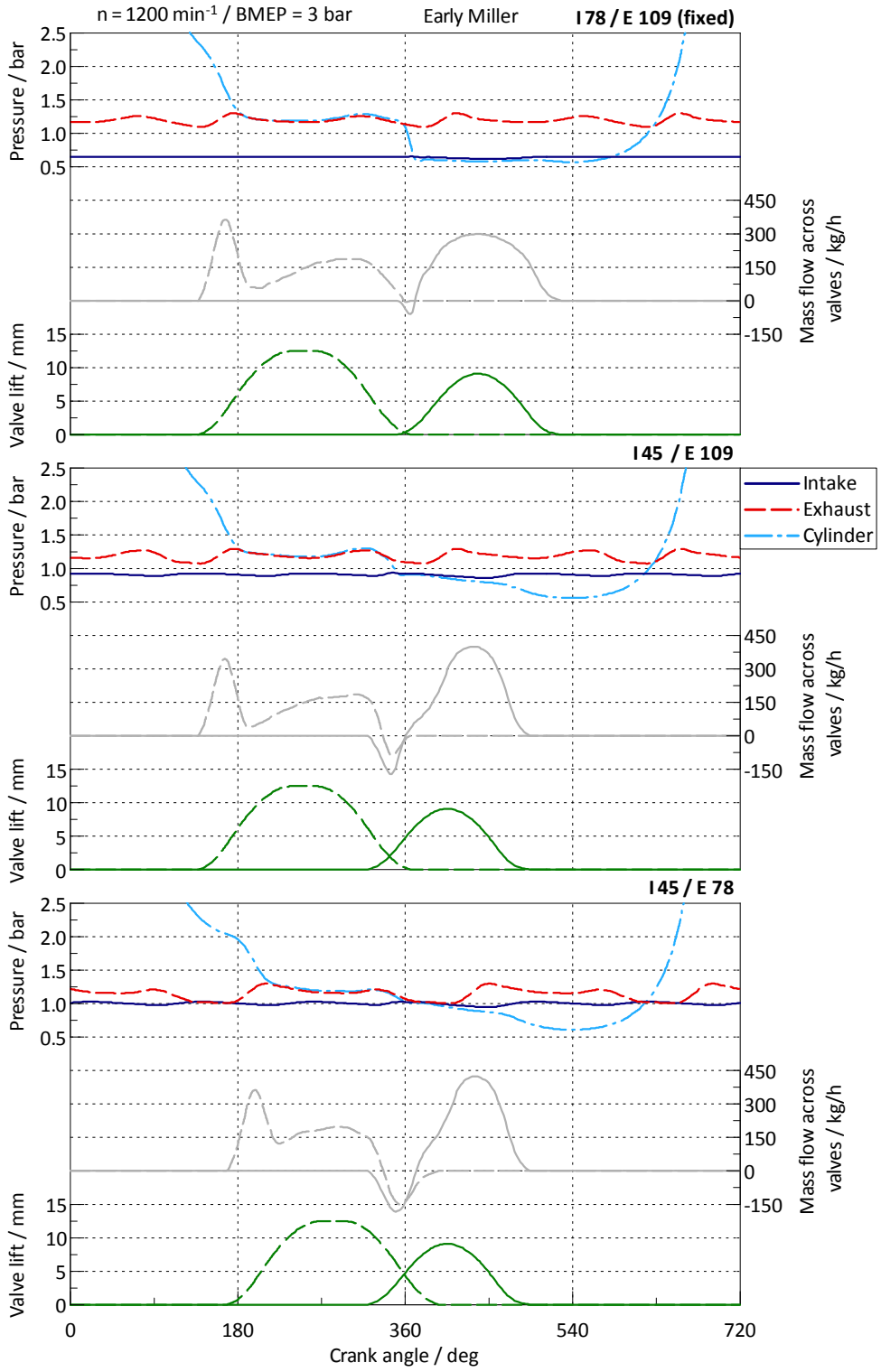

Figure 5.26: Crank angle resolved simulation results for the early Miller cam profile with three different combinations of cam phasing angles in the load point n = 1200 min^{-1} / BMEP = 3 bar.

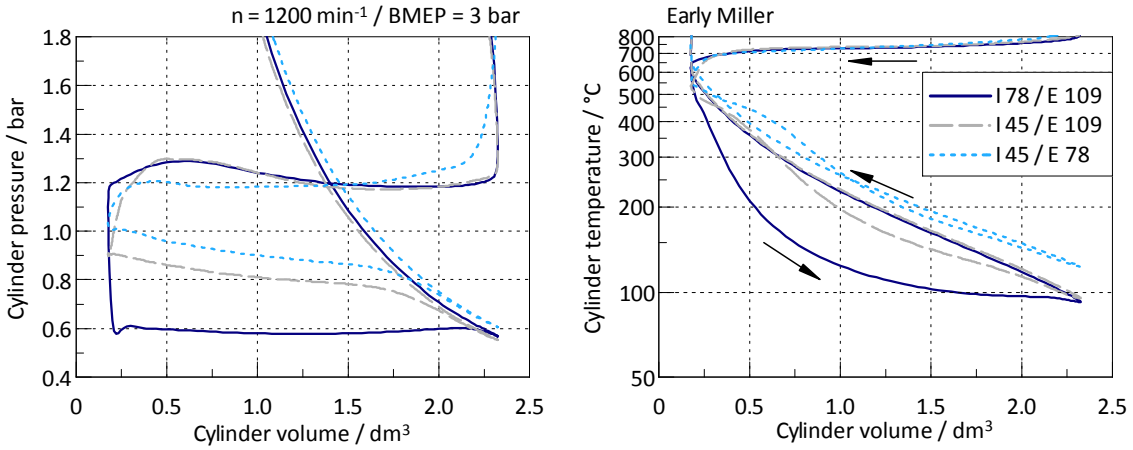

Figure 5.27: The p-V and T-V diagram of the early Miller cam profile with three different combinations of cam phasing angles in the load point $n = 1200\,\mathrm{min^{-1}}$ / BMEP = 3 bar.

However, the gas exchange work increases too as the pressure is higher during the following exhaust stroke. The optimum between high gross indicated efficiency and low gas exchange losses is flat and occurs at $\varphi_e = 109\,°\mathrm{CA}$ in this load point. Figure C.1 in Appendix C states additional crank angle resolved data for a better traceability of the described effects.

Figure 5.30 shows a variation of φ_i at BMEP = 12 bar. The effect of cam phasing on the net indicated efficiency vanishes almost entirely. Improvements in the gas exchange work are offset by a reduction in gross indicated efficiency as the decreasing EGR negatively affects the wall heat losses. The maximum position of the throttle valve is 85 °. At small intake cam phasing angles unthrottled operation is already achieved in this load point. Furthermore, it is notable that the intake manifold pressure exceeds the exhaust manifold pressure. External EGR is feasible only because of the reed valves installed in the EGR ducts. Internal EGR is no longer feasible as the pressure gradient reverses. Instead of a backflow of exhaust gas during the valve overlap scavenging occurs. Scavenging refers to fresh charge which directly flows into the exhaust duct and escapes the combustion. Along with this residual gases are also expelled. In Figure 5.30 scavenging is observable at $\varphi_i = 51\,°\mathrm{CA}$ as with increasing valve overlap (decreasing φ_e) the internal EGR approaches zero.

Under some operating conditions scavenging can be desirable, for example to improve the response of the turbocharger. However, in stoichiometric operation scavenging must be avoided as it results in lean exhaust gas. It affects the lambda control and the exhaust gas aftertreatment negatively. Therefore, $\varphi_i = 51\,°\mathrm{CA}$ is excluded for the derivation of the operating strategy. Figure C.2 in Appendix C states crank angle resolved quantities which demonstrate scavenging at $\varphi_i = 51\,°\mathrm{CA}$.

Figure 5.31 on the left demonstrates the operating strategy of cam phasing with the early Miller cam profile for a load sweep at $n = 1200\,\mathrm{min^{-1}}$. The operating strategy was derived on the basis of the preceding investigations. The criterion for optimisation was maximum fuel efficiency under the condition of a maximum residual gas fraction in the cylinder of 24 %. Furthermore, scavenging was avoided. In the right graph the operating strategy for the standard cam profile is displayed. It was developed in the same manner as detailed for the early

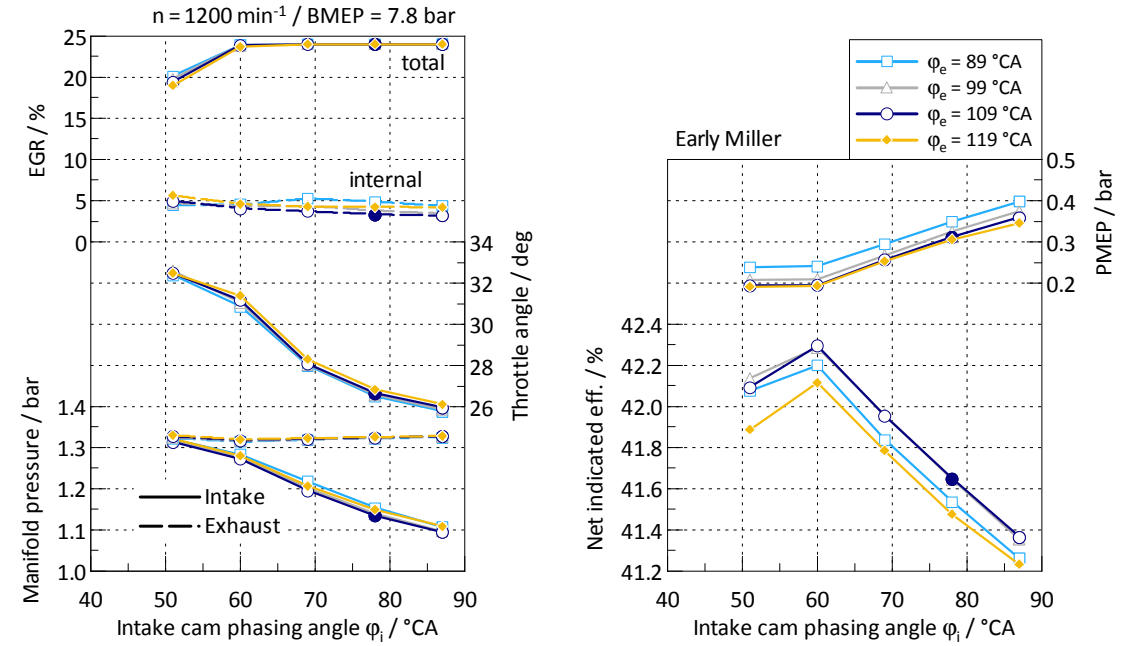

Figure 5.28: Variation of the intake cam phasing angle φ_i at $n = 1200\,min^{-1}$ / BMEP = 7.8 bar for different exhaust cam phasing angles and the early Miller cam profile.

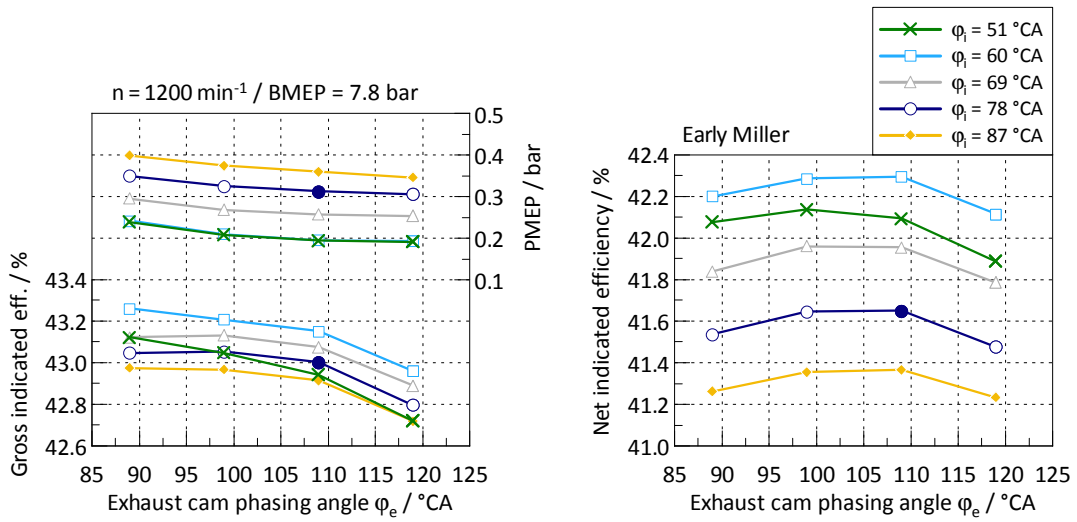

Figure 5.29: Variation of the exhaust cam phasing angle φ_e at $n = 1200\,min^{-1}$ / BMEP = 7.8 bar for different intake cam phasing angles and the early Miller cam profile.

Miller profile. Independent of the cam profile it reveals that at low loads a large valve overlap is advantageous. With increasing load the optimal valve overlap decreases. This is caused in part by scavenging which is prevented by these operating strategies. Furthermore, the exhaust cam phasing angle φ_e of the fixed timing is well suited and there is no need for adjustment at higher loads.

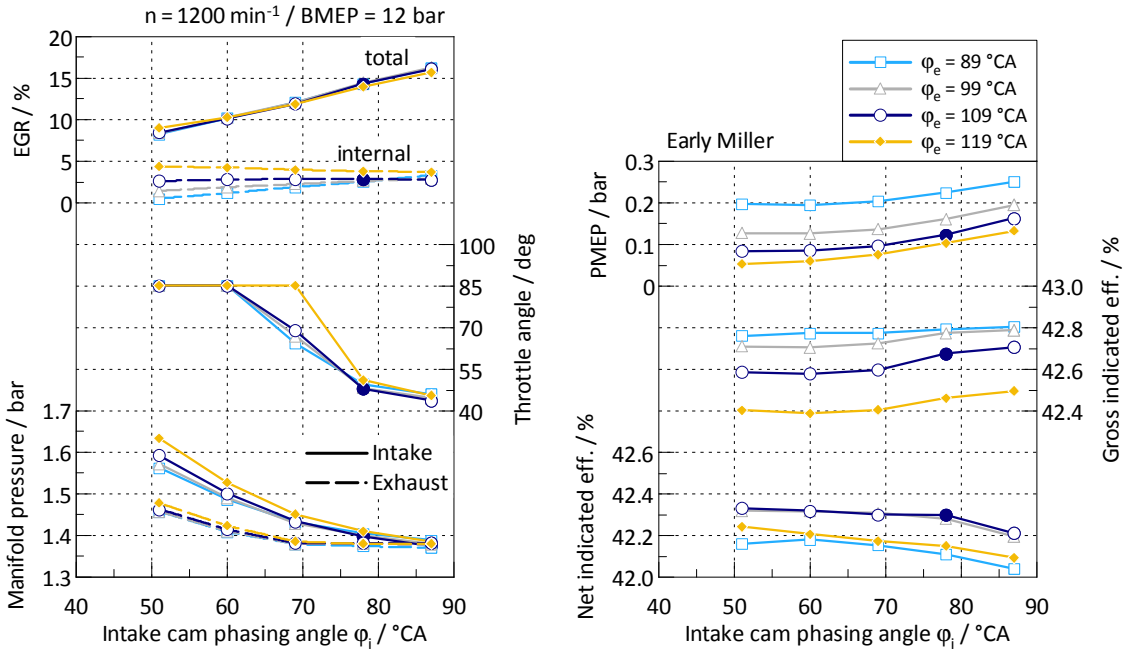

Figure 5.30: Variation of the intake cam phasing angle φ_i at $n = 1200\,min^{-1}$ / BMEP = 12 bar for different exhaust cam phasing angles and the early Miller cam profile.

Figure 5.32 shows the effect of the stated operating strategies on the gas exchange losses and the net indicated efficiency. While cam phasing increases the part load efficiency considerably in combination with the early Miller profile, it remains without significant effect in combination with the standard valve lift profile. In the case of the Miller cam profile the net indicated efficiency increases by 1.4 $\%_{Pt.}$ at BMEP = 3 bar. With increasing load this efficiency benefit reduces to less than 0.1 $\%_{Pt.}$ at BMEP = 12 bar. The improvement results from a reduction of the gas exchange work. In the case of the standard cam profile the efficiency gain is in the range of 0.1 $\%_{Pt.}$. The reduction of the gas exchange losses is compensated by an increase in the wall heat losses as detailed below.

Figure 5.33 states loss analyses for the early Miller and standard profiles with and without cam phasing to explain the different results obtained with these two cam profiles. The loss analyses are conducted according to the method described in [97]. The efficiency of the ideal engine remains unchanged by the introduction of cam phasing with the early Miller cam profile. The wall heat losses increase by 0.2 $\%_{Pt.}$ but the reduction of the gas exchange losses by 1.6 $\%_{Pt.}$ overcompensates this, resulting in the stated increase of the net indicated efficiency by 1.4 $\%_{Pt.}$. The wall heat losses rise, because high amounts of internal EGR are used which raise the charge temperature. However, the effect remains limited as early IVC causes a reduction of the charge temperature in part load operation (as detailed in Section 5.4.2). In comparison to the fixed Miller timing IVC is advanced by 33 °CA with cam phasing. Thereby, much of the temperature increase caused by internal EGR is compensated.

The situation is different with the standard cam profile. Also in this case large amounts of internal EGR are deployed with cam phasing. However, the associated temperature rise is not

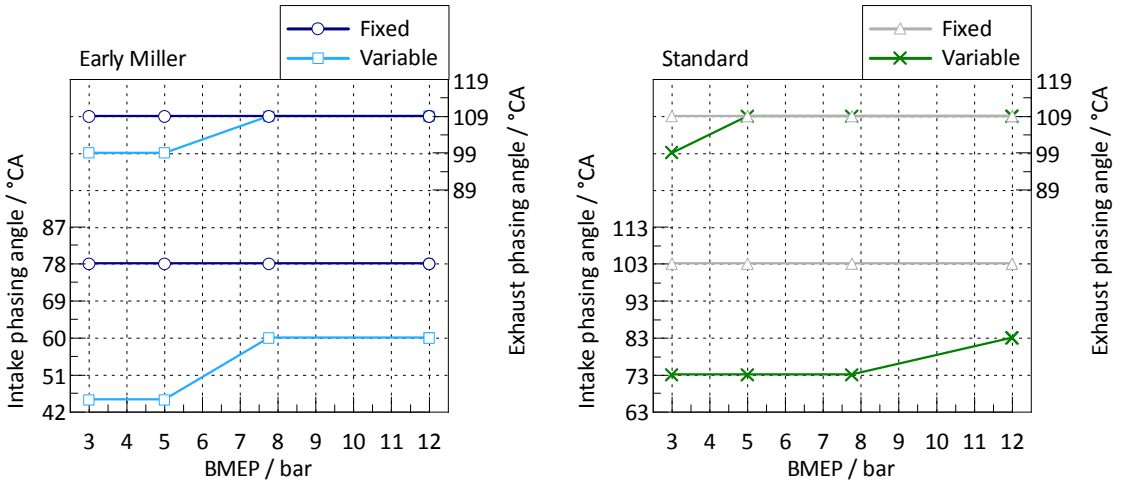

Figure 5.31: Cam phasing operating strategy for early Miller (left) and standard (right) valve lift profiles for a load sweep at $n = 1200\,min^{-1}$.

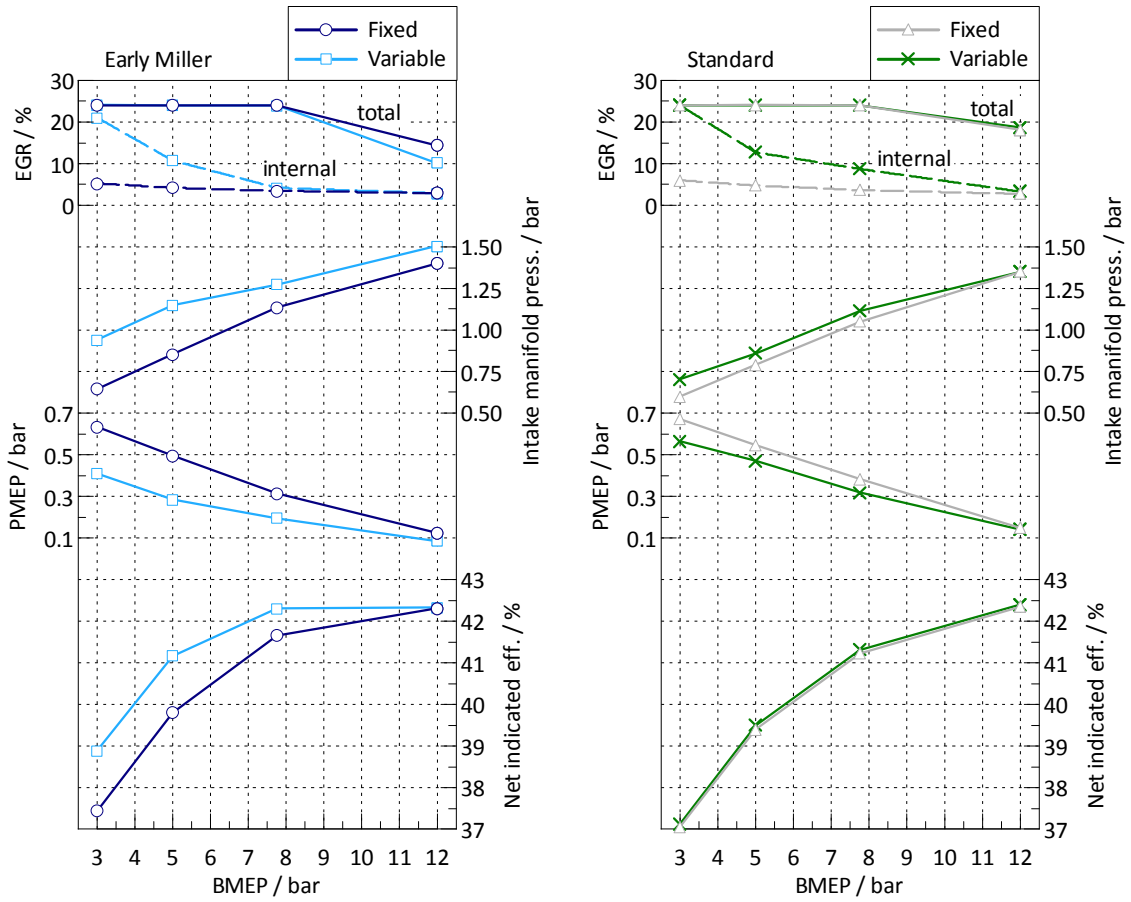

Figure 5.32: The effects of cam phasing in combination with early Miller (left) and standard (right) cam profiles for a load sweep at $n = 1200\,min^{-1}$.

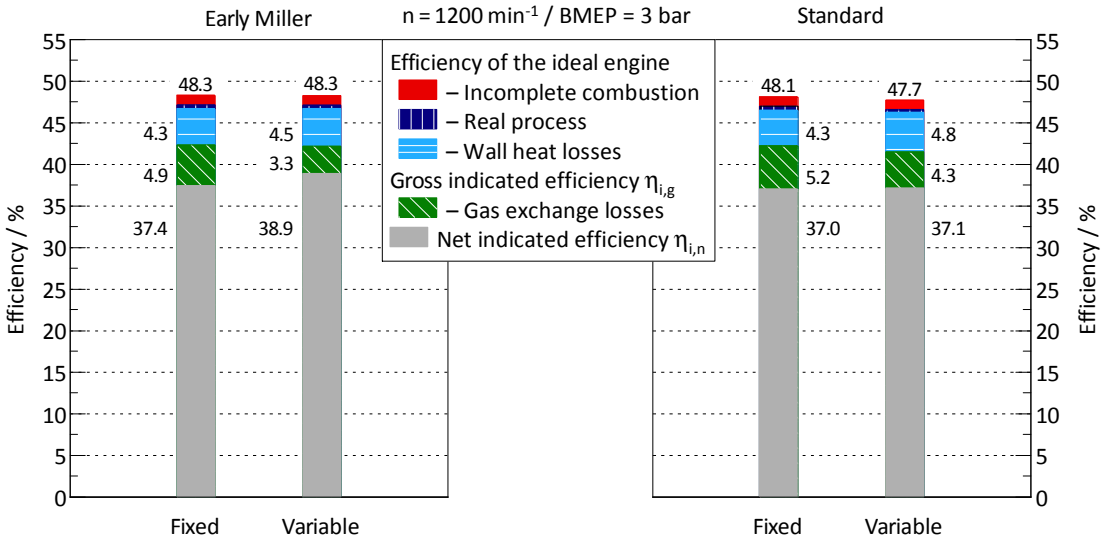

Figure 5.33: Loss analysis in the load point 1200 / 3 for the operation with and without cam phasing. Left: Early Miller cam profile, right: standard cam profile.

compensated as IVC cannot be advanced far enough to make use of the same effect as with the Miller cam profile. As a result, the charge temperature is higher, decreasing the efficiency of the ideal engine by 0.4 $\%_{\mathrm{Pt.}}$. Additionally, the wall heat losses rise by 0.5 $\%_{\mathrm{Pt.}}$. This almost diminishes the efficiency gain due to the reduction of the gas exchange work.

In the literature experimental studies on cam phasing in naturally aspired gasoline SI passenger car engines exist [72, 98]. The maximum load of naturally aspired engines is considerably lower and the engine speed range is larger compared to the investigated heavy duty engine. In addition these studies make use of conventional cam profiles and do not use early Miller cam profiles in combination with cam phasing. Therefore, a comparison of the results is not possible in all aspects. Nevertheless, also in these studies it was concluded that a large valve overlap is the most effective method to reduce the gas exchange work during part load operation. At very light loads it was reported that the overlap must be reduced to limit the cycle-to-cycle variations which rise with increasing residual gas content. In [78] cam phasing was investigated experimentally with conventional and early Miller cam profiles on a boosted gasoline SI passenger car single-cylinder engine in part load operation. The derived operating strategy is similar to the one presented. High valve overlaps at low engine loads are favoured and with increasing load the valve overlap is reduced. In addition, the same observation was made that cam phasing with early Miller cam profiles is more effective than with conventional profiles. This documents that in turbocharged heavy duty SI engines similar trends and relations exist as in turbocharged passenger car SI engines in relation to cam phasing.

Full Load Operation

The effects of cam phasing at full load operation are only discussed for the early Miller cam profile, because the relations and the conclusions drawn are identical to the ones with the standard cam profile. The operating strategy for cam phasing at full load was derived in the

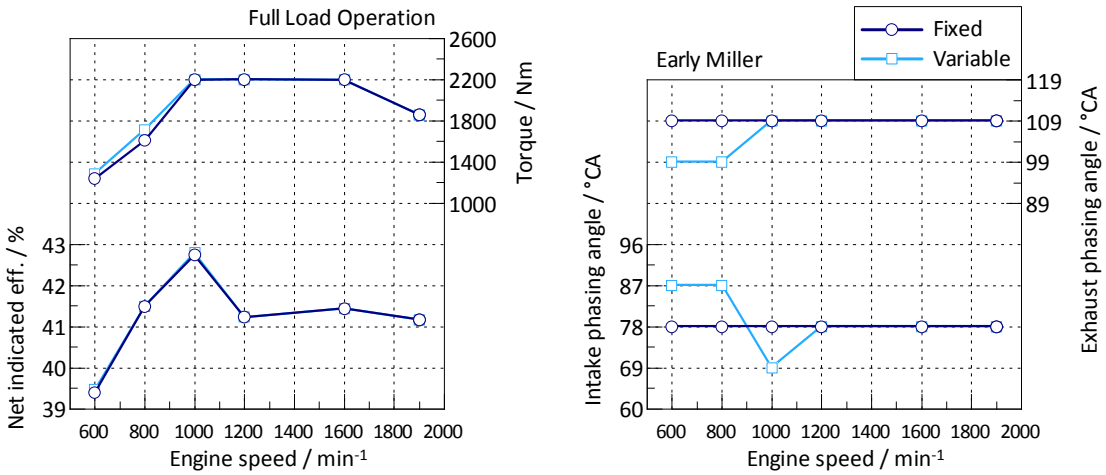

Figure 5.34: Right: Derived operating strategy of cam phasing at full load operation in combination with the early Miller cam profile. Left: The effect of cam phasing on the engine torque and the net indicated efficiency.

same way as it was described in detail for part load operation. The criterion for optimisation was again maximum fuel efficiency.

Figure 5.34 on the right depicts the derived operating strategy and on the left its effect on the engine torque and the net indicated efficiency. From $n = 1200\,\text{min}^{-1}$ onwards the fixed timing is optimal and therefore no benefit is generated by cam phasing. Even below $n = 1200\,\text{min}^{-1}$ the effect of cam phasing is very limited. The torque at $n = 600\,\text{min}^{-1}$ is raised by 50 Nm and by 105 Nm at $800\,\text{min}^{-1}$. The net indicated efficiency increases by less than $0.1\,\%_{\text{Pt.}}$. Nevertheless, the mechanisms of cam phasing at full load operation are described below, because in combination with a waste gate turbocharger some notable phenomena occur.

In general, two cases need to be distinguished. Load points in which the torque is not limited or the maximum torque is not achieved yet and load points in which the torque is limited. At $600\,\text{min}^{-1}$ and $800\,\text{min}^{-1}$ the rated torque of 2200 Nm is not achieved while at $1000\,\text{min}^{-1}$ the rated torque is already reached without cam phasing. These two cases require different strategies which also reflects in the operation strategy. There is a shift from large intake cam phasing angles to small angles once the rated torque is achieved.

At first the case of unlimited torque is discussed. Figure 5.35 depicts a variation of the intake cam phasing angle at $600\,\text{min}^{-1}$. The amount of external EGR is constant at 8 % and the waste gate is fully closed as the rated torque of 2200 Nm is not reached. A prolongation of IVC (i.e. an increase of φ_{i}) increases the volumetric efficiency. This results in an increase of the torque. However, a second effect is amplifying the torque increase. In a stoichiometric engine an increase in fresh charge results in higher peak temperatures and pressures. Therefore also the exhaust gas temperature increases which raises the specific enthalpy of the exhaust gas. More boost pressure can be generated even though the waste gate position remains unchanged (fully closed). As a consequence, the torque rises further and the gas exchange work is reduced also. Notice that the gas exchange loop even inverts and work is released during the gas exchange (indicated by negative values of PMEP). Consequently, the net indicated efficiency increases.

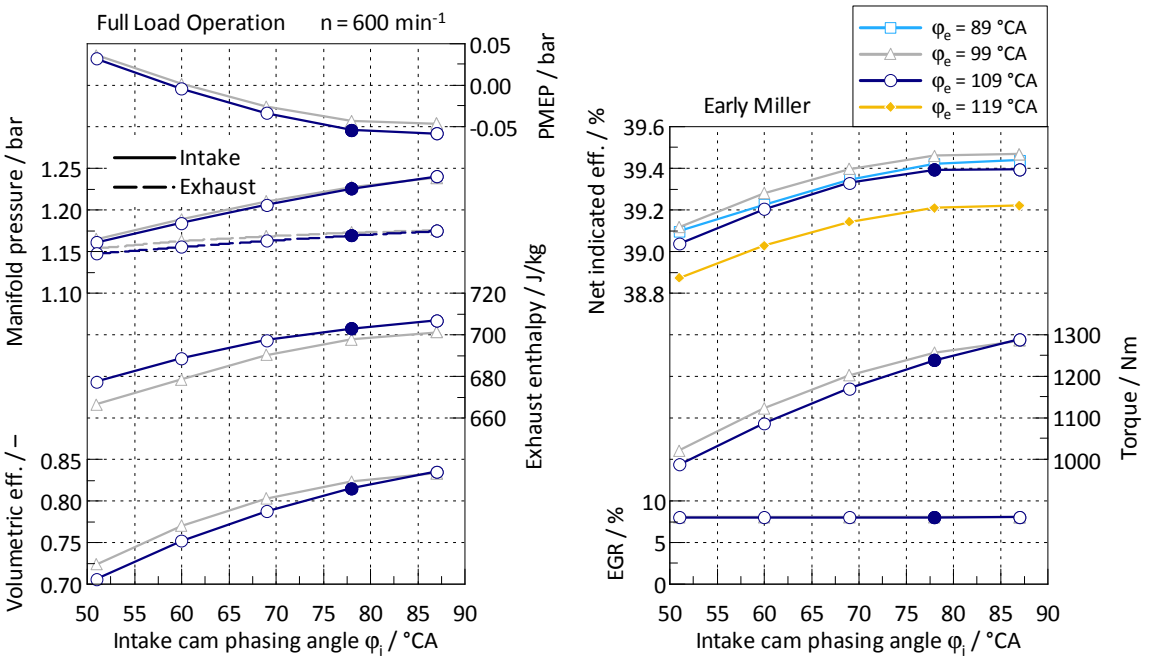

Figure 5.35: Variation of the intake cam phasing angle at full load operation at $n = 600\,\mathrm{min^{-1}}$ in combination with the early Miller cam profile.

Varying the exhaust cam phasing angle, the already discussed trade-off exists between low gas exchange work and high utilisation of the cylinder pressure. φ_e is set to find the best compromise between these two conflicting goals.

Figure 5.36 states crank angle resolved results. It displays the larger mass flow across the intake valves (i.e. higher volumetric efficiency) with increasing φ_i. A large valve overlap has to be avoided at full load for another reason. Depending on the pressure gradient between intake and exhaust manifold large valve overlaps lead to either scavenging (indicated by the black circle) or internal EGR. Scavenging must be avoided for the reasons stated and internal EGR facilitates knocking due to the increase in charge temperature and must also be avoided. Overall, at $n = 600\,\mathrm{min^{-1}}$ cam phasing results in an increase of the torque by 50 Nm and a rise in net indicated efficiency by $0.1\,\%_{\mathrm{Pt.}}$ compared to fixed timing.

The relations invert if the torque is constrained. Figure 5.37 states a variation of φ_i at $n = 1000\,\mathrm{min^{-1}}$. While at $600\,\mathrm{min^{-1}}$ and $800\,\mathrm{min^{-1}}$ an increase in φ_i leads to an increase in net indicated efficiency, at $1000\,\mathrm{min^{-1}}$ a reduction in φ_i increases the fuel efficiency. The mechanisms behind this trend reversal are elaborated below. Note that the gas exchange loop is also positive in this operating point and more negative values of PMEP are favourable. A reduction of φ_i reduces the volumetric efficiency as IVC is advanced. A higher intake manifold pressure is required to maintain the load which requires the waste gate to close. Due to the relatively good turbocharger efficiency the increase in intake manifold pressure is stronger than the increase in exhaust manifold pressure. This reduces the gas exchange work (resp. increases the work delivered to the crank shaft during the gas exchange as PMEP is negative) and increases the net indicated efficiency.

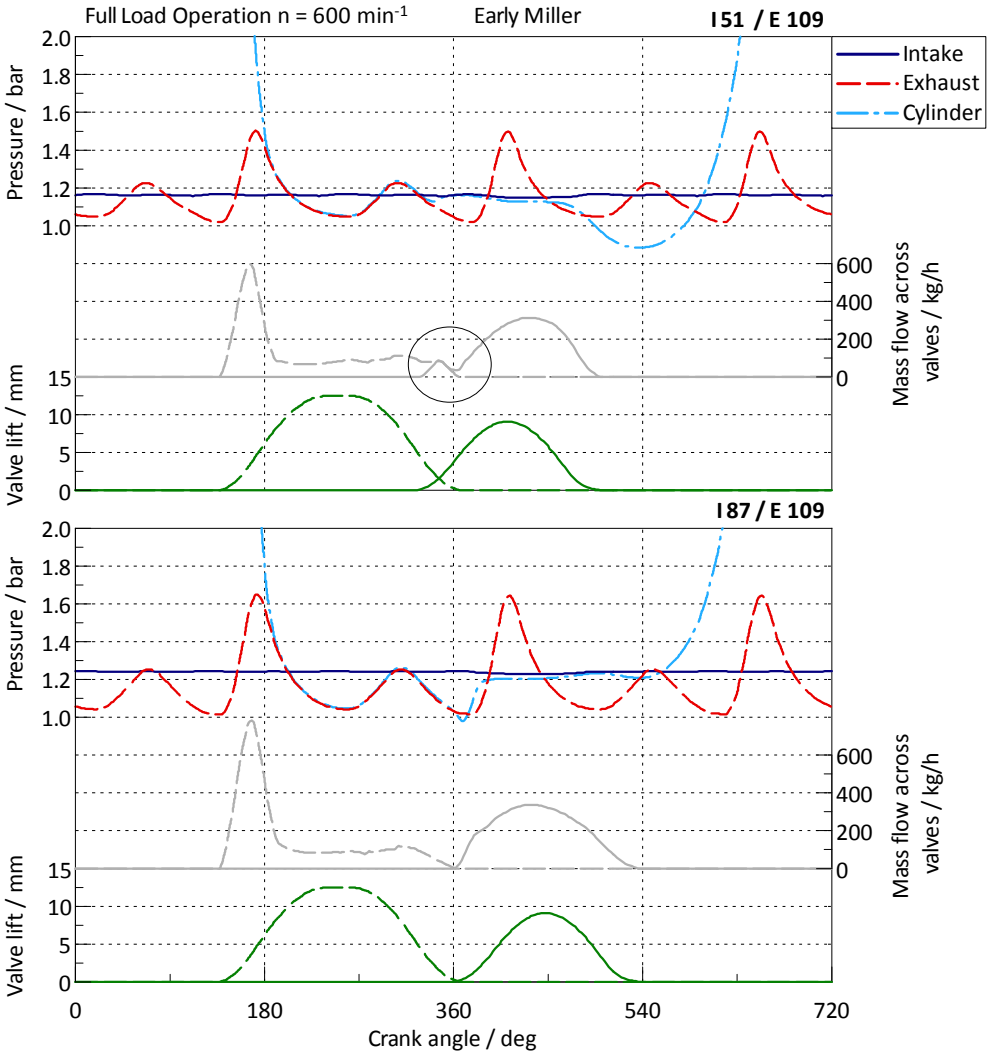

Figure 5.36: Crank angle resolved data for two different valve timings at full load operation at $n = 600\,\mathrm{min}^{-1}$ in combination with the early Miller valve lift profiles.

Although, this effect is softened by a reduction of external EGR. The further increase of the positive pressure gradient between intake and exhaust manifold constrains the recirculation of exhaust gas. If the amount of EGR remained constant, the reduction in PMEP would be larger. Figure 5.38 depicts crank angle resolved data for the valve timing I 60 / E 109 and I 87 / E 109. The earlier IVC in case of I 60 / E 109 and the resulting higher intake manifold pressure are notable. Furthermore, scavenging already occurs as indicated by the black circle. Therefore this configuration and smaller φ_i were excluded in the operation strategy (see Figure 5.34) and I 69 / E 109 was chosen instead. For the exhaust cam phasing angle the relations are identical to the ones at $n = 600\,\mathrm{min}^{-1}$. The fixed timing of $\varphi_\mathrm{e} = 109\,°\mathrm{CA}$ proves to be optimal.

The results of cam phasing at full load operation of a natural gas heavy duty engine are generally unedifying. The improvements are limited to engine speeds below the low-end torque

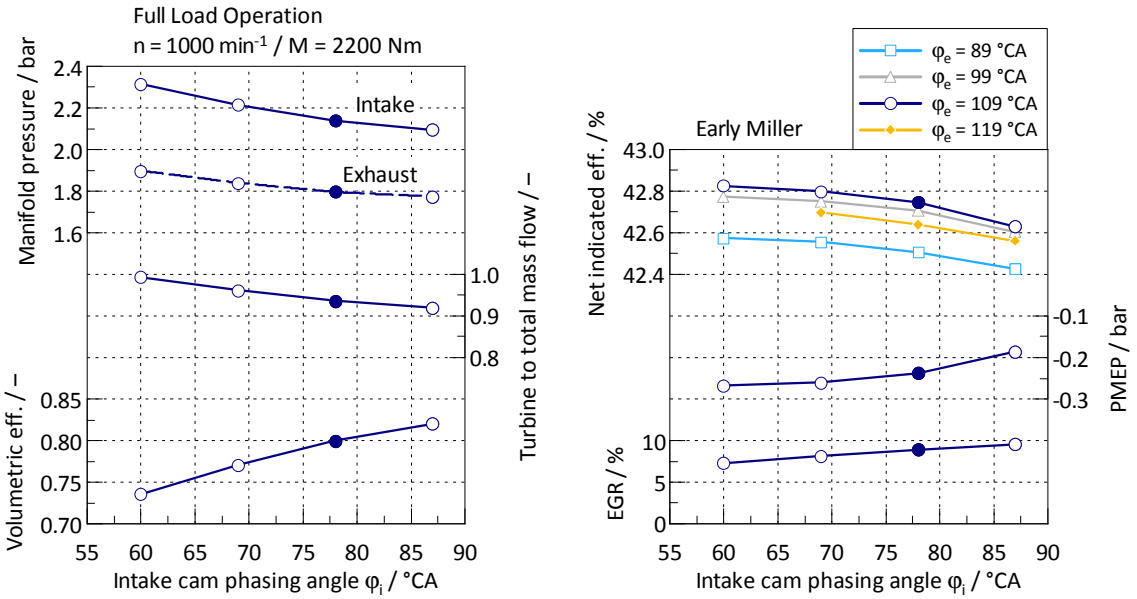

Figure 5.37: Variation of the intake cam phasing angle at full load operation at $n = 1000\,min^{-1}$ in combination with the early Miller cam profile.

($n = 1000\,min^{-1}$). At these engine speeds, the torque can be raised by up to 6 % by increasing the volumetric efficiency. At higher engine speeds the fixed timing is revealed to be optimal. One reason is that in heavy duty engines the ratio between maximum speed and idling speed is approx. 4 while in passenger car gasoline engines this ratio is approx. 10. The gas dynamics thus show much greater variation in passenger car engines than in heavy duty engines as they scale linearly with the engine speed. As a result it is easier to cover the whole engine speed range satisfactorily with a fixed valve timing in heavy duty engines than in a passenger car engine. This results in a smaller potential of cam phasing at full load operation in comparison to passenger car engines.

Conclusion

It was proved that cam phasing on both cam shafts is a leverage to further increase the part load efficiency for the given engine configuration, even if external EGR is already applied. A Miller cam profile is a prerequisite, however, for achieving a further efficiency increase in the presence of external EGR. By advancing IVC the volumetric efficiency is reduced. Therefore, a higher intake manifold pressure is required which reduces the gas exchange losses. Advancing IVC also increases the valve overlap. If the total amount of EGR is kept constant, external EGR is replaced by internal EGR. This raises the charge temperature as internal EGR is not cooled. With early Miller timing additional charge cooling is achieved by overexpanding the charge which compensates the temperature increase of internal EGR. This effect cannot be achieved with the standard cam profile. As a consequence wall heat losses increased with the standard cam profile and detrimental charge properties compensate the reduction of the gas exchange work. The exhaust cam phasing angle is adjusted for optimal EVO in each operating

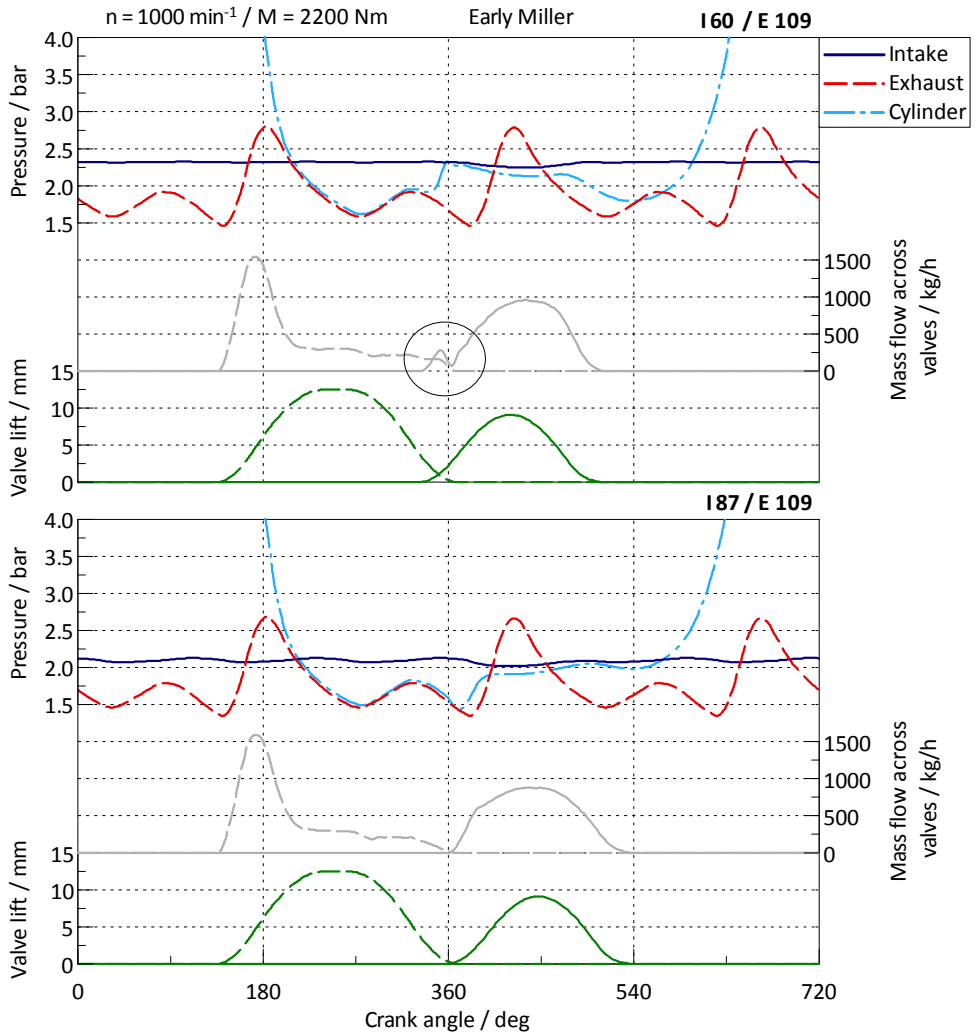

Figure 5.38: Crank angle resolved data for two different valve timings at full load operation at $n = 1000\,\mathrm{min}^{-1}$ in combination with early Miller cam profile.

point. Early EVO leads to a low utilisation of the cylinder pressure, but also reduces the gas exchange losses. Late EVO increases the work gained during the combustion stroke, but also the gas exchange work.

At BMEP = 3 bar the net indicated efficiency is increased by 1.4 $\%_{\mathrm{Pt.}}$ with early Miller cam profiles. With increasing load and decreasing gas exchange losses this efficiency potential reduces towards almost zero at BMEP = 12 bar. A comparison of the derived operating strategy with literature on cam phasing in gasoline SI passenger car engines revealed that the relations in heavy duty and passenger car engines are similar. A large valve overlap is the most effective method to reduce the gas exchange losses during part load operation. The residual gas tolerance at light loads must be considered though.

The analysis further proved that cam phasing is not a measure to increase the fuel efficiency at full load operation for the investigated engine concept. Due to the small engine speed

range of heavy duty engines the fixed timing is optimal for the majority of engine speeds. The torque can be increased by up to 6 % in operating points with fully closed waste gate. This is achieved by adjusting IVC for optimal volumetric efficiency. Furthermore, at higher engine speeds when the waste gate is open the gas exchange losses can be slightly reduced by increasing the utilisation of the waste gate turbocharger. However, as the gas exchange work is marginal in relative terms at full load operation this does not increase the fuel efficiency to any considerable extent.

5.4.4 Single-Cylinder Engine Measurements

After the 1D simulations were completed, measurements on the single-cylinder engine were conducted by AVL Graz. The gas exchange of a multi-cylinder engine and a SCE is not comparable as the gas dynamics differ. The cross-cylinder influence is not reproduced in the SCE, the turbocharger dynamics are missing and also the intake and exhaust layouts usually differ. However, SCE measurements provide a good opportunity to investigate the combustion. A few selected results from the SCE measurements are presented where a comparison with the 1D simulations is possible and meaningful.

Figure 5.39 displays the influence of EGR on the heat-release rate as measured on the SCE for three load points. The predicted heat-release rates used in the 1D simulations are depicted too. The derived estimates of the influence of EGR on the HRR are quite reasonable on a relative level (see Table 5.2 in Section 5.3.3). However, on an absolute level the predicted HRR is too optimistic at low engine speeds and light loads. The reason seems to be the different charge motion of the HDGAS engine and the Cursor 13 CNG prototype. As described in Section 5.3.3 the measured heat-release rates of the Cursor 13 CNG engine (which does not utilise EGR) were the basis to develop the HRRs with EGR. The HDGAS engine features tumble charge motion while the Cursor 13 CNG engine features a swirl-based combustion process. Swirl motion in combination with a squish flow increases the flow velocity significantly around TDC. This potentially results in the faster heat-release than the tumble charge motion of the HDGAS engine.

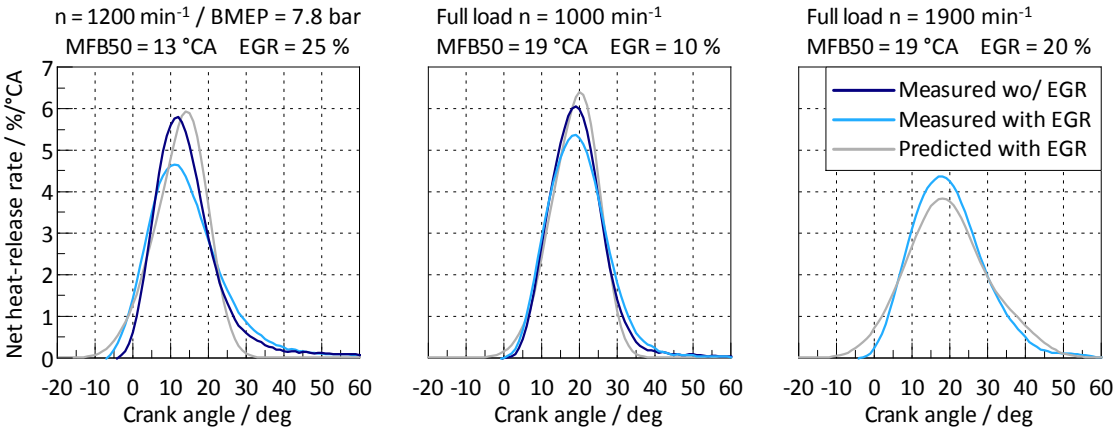

Figure 5.39: Influence of EGR on the heat-release rate of the HDGAS engine in three load points and the predicted HRRs deployed in the 1D simulations.

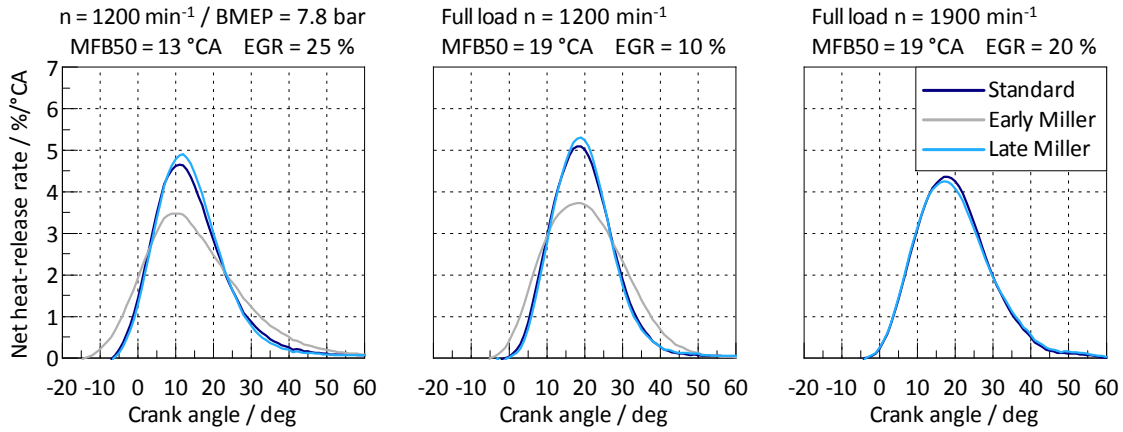

Figure 5.40: Influence of standard, early Miller and late Miller cam profiles on the measured heat-release rates in three load points.

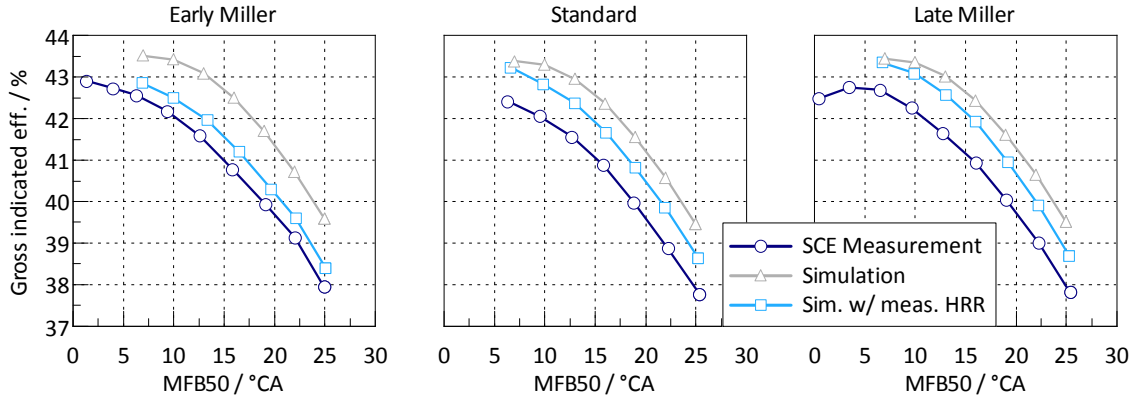

Figure 5.41: Comparison of the gross indicated efficiency of SCE measurements and 1D simulations for a variation of MFB50 in the load point $n = 1200\,\mathrm{min}^{-1}$ / BMEP = 7.8 bar using 25 % EGR. The results are stated for standard, early Miller and late Miller cam profiles.

Furthermore, at the time of the 1D simulations there was no information available on how the different valve lift profiles affect the combustion by influencing the turbulence intensity. Figure 5.40 depicts the measured heat-release rates in three load points for standard, early Miller and late Miller valve lift profiles. While the heat-release rates of the measurements with standard and late Miller valve lift profiles are almost identical, the deteriorating effect of early Miller timing on the heat-release rate is pronounced. A significant amount of turbulence is created during the flow of fresh charge through the intake valves. Due to the early IVC caused by early Miller timing the turbulence intensity is decreased notably which condenses in a slower flame front propagation and therefore a slower heat-release rate. Late Miller timing circumvents this problem by late IVC which reflects in the faster evolution of the heat-release rate. These measurement results are in-line with 3D CFD simulations in literature [64, 106].

Finally, Figure 5.41 states a comparison of SCE measurements and 1D simulation results in

the load point 1200/7.8 with 25 % EGR. The gross indicated efficiency is stated for a variation of MFB50 and all three valve lift profiles. The gross indicated efficiency is chosen, because the net indicated efficiency incorporates the gas exchange which is not representative for the reasons stated above. The simulations over-predict the efficiency by approx. 1.5 $\%_{\mathrm{Pt.}}$ independent of the valve lift profile. The deviation results to a large extent from the deployed heat-release rates which were expected to be faster than they turned out to be (Figures 5.39 and 5.40). The influence of the HRR was confirmed by deploying the measured HRRs and rerunning the simulations. The efficiency gap thereby reduces to less than 1 $\%_{\mathrm{Pt.}}$ in absolute terms and 2 % or below in relative terms. The remaining deviations result from inaccuracies in the model of the wall heat losses. Furthermore, the flow coefficients of the valve flow rely on 3D CFD simulations and are not measured. This is another potential source for divergence. Engine-out HC and CO emissions are no major source of divergence, because the simulation considers 3 % of the fuel energy as unburned. This is in good agreement with the measurement results. The results show overall that the trends are captured very well.

5.5 Summary

In the framework of the HDGAS project four new engine concepts were developed for heavy duty natural gas engines. The Institute of Internal Combustion Engines and Thermodynamics joined forces with FPT Industrial, AVL Graz and the research group of Prof. Angelo Onorati at Politecnico di Milano to develop a novel stoichiometrically operated spark ignited natural gas engine, which fulfils the Euro 6 emission legislation. The target was to achieve a 10 % reduction in GHG emissions in the WHTC and 10 % higher torque and rated power compared to heavy duty natural gas engines of the model year 2013. In order to accomplish this ambitious target novel engine technologies were applied and the engine was designed dedicatedly for natural gas SI operation. Available heavy duty NG engines are derivations of diesel engines, due to the relatively small market penetration of NG vehicles. These engines are originally designed and optimised for diesel operation which results in penalties when they are converted for NG operation. Therefore, a modern heavy duty NG engine was developed dedicatedly for an SI combustion process for the first time in the HDGAS project. The cylinder head features angular valves with two overhead cam shafts, a pent roof combustion chamber and tumble charge motion. In addition, NG direct injection was introduced as also cooled high-pressure EGR at part load and full load operation. Furthermore, Corona ignition, cam phasing on both cam shafts and a waste gate turbocharger were deployed.

The 1D simulations were conducted at the beginning of the project to define the thermodynamic layout of the engine and to assess the efficiency potential of the combination of EGR with Miller timing and cam phasing. At the time of the simulations the engine did not exist in hardware form. The simulation was thus calibrated with measurement data of a Cursor 13 CNG prototype engine of FPT. Subsequently, the simulation model was adapted to the requirements of the HDGAS engine. A study was performed with available measurement data at the institute to assess and predict the influence of EGR on the heat-release rate which the model requires as input.

With the calibrated simulation model different layouts for EGR were investigated. The simulations revealed a trade-off between the amount of exhaust gas which can be recirculated at full load and the gas exchange losses. High amounts of EGR require a larger pressure gradient

between exhaust and intake manifold (realised by a smaller turbine of the turbocharger) and therefore cause higher gas exchange work. Reed valves proved as an effective means to increase the feasible amount of EGR without raising the gas exchange work. At full load operation EGR caused a reduction of the exhaust gas temperature by 190 °C. It is thus an effective means to limit the exhaust gas temperature and to maintain the temperature limit of critical engine components. Furthermore, for a given turbine size EGR reduces the gas exchange work, the wall heat losses and the knocking probability which allows for an earlier combustion phasing. At full load EGR led to an increase in net indicated efficiency by approx. 2.5 $\%_{\mathrm{Pt.}}$. In part load operation EGR enables a dethrottling of the engine and also reduces the wall heat losses. In the load point typical for highway driving an increase of the net indicated efficiency by 1.9 $\%_{\mathrm{Pt.}}$ was achieved.

The effect of early and late Miller timing in combination with EGR was studied in comparison to standard valve timing, designed for optimum volumetric efficiency. At full load operation the effect of Miller timing on the gas exchange work is small, but the charge temperature close to TDC was reduced by up to 28 °C which reduces the knocking probability. At part load operation the gas exchange work is reduced which resulted in an increase in net indicated efficiency by 0.4 $\%_{\mathrm{Pt.}}$. Miller timing is thus a practical solution to raise the part load efficiency and at the same time improve the operation at full load.

Furthermore, the influence of cam phasing in the presence of EGR and a waste gate turbocharger was investigated. In part load operation the gas exchange losses are reduced by advancing IVC which decreases the volumetric efficiency. In addition, external EGR is replaced by internal EGR as the valve overlap increases. In combination with the early Miller cam profile a significant increase in fuel efficiency of up to 1.4 $\%_{\mathrm{Pt.}}$ at BMEP = 3 bar was achieved. With the standard cam profile no improvement was realised as the shift from external to internal EGR increases the wall heat losses which compensated the reduction in gas exchange work. In combination with the early Miller cam profile this increase can be avoided by additional charge cooling. At full load operation the volumetric efficiency can be optimised by cam phasing which increases the torque for a given waste gate mass flow. If no rise in torque is desired and the waste gate is open a reduction in volumetric efficiency reduces the gas exchange losses as the utilisation of the turbocharger increases. The overall effect at full load is minor, however, as the engine speed range of heavy duty engines is small and therefore the gas dynamics do not differ as significantly as they do in passenger car engines. A comparison with literature on cam phasing in gasoline SI engines revealed that the relations in heavy duty and passenger car engines are similar. A large valve overlap is the most effective method to reduce the gas exchange losses during part load operation.

In overall terms the combination of cooled high-pressure EGR, early Miller timing and cam phasing resulted in an increase in net indicated efficiency of 3 $\%_{\mathrm{Pt.}}$ or a reduction of the specific fuel consumption of 7.2 % in the important load point relevant for highway driving. EGR has the biggest influence (1.9 $\%_{\mathrm{Pt.}}$) followed by cam phasing (0.7 $\%_{\mathrm{Pt.}}$) and Miller timing (0.4 $\%_{\mathrm{Pt.}}$). At full load operation the net indicated efficiency was raised by up to 3.4 $\%_{\mathrm{Pt.}}$ by the introduction of these technologies. This corresponds to a reduction of the specific fuel consumption of 8.4 %. The reduction is caused mainly by the introduction of EGR and advancing the combustion phasing due to a reduced knock probability. Early Miller timing and cam phasing have only a small effect on the fuel efficiency at full load operation.

Measurements on the single-cylinder engine conducted by AVL Graz confirmed the influence

of EGR on the heat-release rate. Furthermore, they revealed that the influence of the valve lift profile on the heat-release rate is significant, as it influences the turbulence intensity and therefore the propagation of the flame front.

The performed 1D simulations verify that the target of 10 % higher torque is achieved by the utilisation of a suitable turbocharger. Furthermore, the simulations confirm that the introduced technologies (EGR, Miller timing and cam phasing) provide significant leverage to increase the fuel efficiency. Their deployment in future heavy duty NG engines is thus recommended. The final assessment if the target of a 10 % reduction in GHG emissions in the WHTC is achieved needs to be performed on the engine test bench since not all effects of the introduced technologies can be evaluated by means of 1D simulations and the WHTC includes a wider range of load points.

6 Conclusion

In this thesis two different natural gas engine concepts were investigated. The motivation for these investigations is the need to limit the anthropogenic GHG emissions which facilitate global warming. Natural gas consists mainly of methane and thus has a lower carbon-intensity than gasoline or diesel (H/C-ratio of 3.8 vs. 1.9 [19, 97]). Using NG as fuel the tank-to-wheel CO_2 emission can be reduced by 25 % compared to gasoline and diesel if the fuel efficiency remains unchanged.

In the first part of this work a novel concept for natural gas-diesel dual fuel combustion for passenger car engines was investigated experimentally on the engine test bench. Dual fuel combustion is a proven concept for large engines in marine applications and for power generation. In these applications the average load is high and the dynamics are low. The challenge in dual fuel combustion is a high emission of unburned CH_4 at part load operation due to an over-lean air-NG mixture. It was demonstrated that these emissions can be attributed to a fundamental trade-off between the ignition conditions of the diesel spray and that of the air-NG mixture. Conventional dual fuel concepts feature port fuel injection of natural gas. The novelty of the investigated concept is low-pressure direct injection of NG which enables a stratification of the air-NG mixture. Thus, the local air-NG equivalence ratio can be reduced without diminishing the ignition conditions of the diesel spray. This allows for a significant reduction of the CH_4 emission in part load operation. The concept is named DDI – *Dual Direct Injection*.

The most important application parameters of the DDI concept were identified and their influence on the combustion was investigated. Furthermore, the influence of the compression ratio was analysed. It revealed that a high compression ratio is vital for the DDI concept to ensure a short ignition delay and stable and fast combustion. Based on these results, the calibration of the DDI concept was optimised in four load points between 3 bar and 15 bar BMEP. The combustion was optimised for minimum unburned species and during lean operation additionally for NO_x emissions on the level of the diesel engine which served as basis for these experiments. With the information on optimised operation an operating strategy was developed for the engine operating map. Diesel operation is proposed during idling and at very light engine loads. At part load lean and stratified dual fuel operation is suggested while at higher loads stoichiometric and homogeneous operation is feasible and also preferred. Depending on the operating point the unburned species of the DDI concept account for 2 % to 3.5 % of the fuel energy which is in the range of modern gasoline engines. In part load operation the total HC emission of conventional dual fuel combustion is significantly reduced by 75 % with the DDI concept due to the fuel stratification. This results in an increase of the brake thermal efficiency by $4.5\,\%_{\mathrm{Pt.}}$.

The engine was adapted to CNG spark ignition to compare the DDI concept with conventional stoichiometric and homogeneous CNG SI operation. In part load operation the efficiency benefit of the DDI concept reaches $5\,\%_{\mathrm{Pt.}}$ due to the lean operation. At higher loads when both concepts

are operated stoichiometrically the efficiency advantage still accounts for 1.5 $\%_{Pt.}$ due to a faster combustion and reduced wall heat losses.

The DDI concept was also compared to conventional diesel and gasoline engines. This demonstrated that the overall engine-out pollutant emissions of the DDI concept are on the level of modern gasoline engines, but with the difference of lean exhaust gas. At part load operation the fuel efficiency of the DDI concept outmatches the diesel engine. At higher loads when the DDI concept is operated stoichiometrically the efficiency is at a level between that of diesel and gasoline engines. Due to the high fuel efficiency and the utilisation of natural gas CO_2 savings between 20 % and 29 % can be achieved with the DDI concept compared to diesel and gasoline engines.

The biggest unsolved challenge of the DDI concept is the exhaust gas aftertreatment of the remaining CH_4 emissions as the exhaust gas temperatures are low during part load operation. CH_4 is a particularly stable molecule and temperatures of approx. 450 °C are required for the catalytic oxidation. At high loads during stoichiometric operation of the DDI concept exhaust gas temperatures of 600 °C are achieved. However, during part load operation exhaust gas temperatures of only 300 °C are realised due to the lean operation and the high amounts of EGR. This is clearly below the threshold for methane oxidation and prohibits a catalytic oxidation. Even though significant progress in the reduction of CH_4 emissions was achieved with the DDI concept the difficult exhaust gas aftertreatment of methane using current technology prevents a further promotion of dual fuel combustion especially for passenger car applications. Despite this dual fuel combustion with the presented technology could already be an attractive option for applications with higher average load and a less dynamic load pattern than in passenger car applications.

In the second part of this thesis the thermodynamic layout of a novel monovalent and stoichiometric natural gas SI engine for heavy duty commercial vehicles was performed by means of 1D simulations. This task was part for the EU project HDGAS in which four different natural gas engine concepts were developed. The stimulus of this project was that on the market available heavy duty NG engines are derivations of diesel engines. In NG operation this results in penalties in fuel efficiency since the base engines are developed and optimised for non-premixed combustion of diesel, a fundamentally different combustion process compared to natural gas spark ignited operation. Therefore, in HDGAS a modern heavy duty NG engine was developed, for the first time dedicatedly optimised for SI operation from the beginning. A cylinder head specifically designed for SI operation featuring a pent roof combustion chamber and tumble charge motion was introduced as also NG direct injection. Furthermore, cam phasing on both cam shafts, Corona ignition, cooled high-pressure EGR and a waste gate turbocharger were deployed. By means of these novel technologies in heavy duty engines a 10 % reduction in GHG emissions in the WHTC and 10 % higher torque and rated power should be achieved in comparison to heavy duty NG engines of the model year 2013.

The 1D simulations were conducted in order to define the EGR layout, to perform the turbocharger matching and to assess the efficiency potential of several of the introduced technologies. The influence of EGR during part load and full load operation was investigated. Early and late Miller timing were analysed in combination with external EGR and compared to conventional valve timing. Finally, the efficiency potential of cam phasing in combination with EGR and Miller timing was assessed and indications for an operating strategy were derived.

It revealed that EGR decreases the combustion temperature, improves the charge properties and leads to a dethrottling of the engine during part load operation. This resulted in an improvement in net indicated efficiency by 1.9 $\%_{\mathrm{Pt.}}$ in the part load operating point relevant for highway driving. At full load operation the net indicated efficiency was increased by 2.5 $\%_{\mathrm{Pt.}}$. However, this rise is not only contributed to EGR but also to an advanced combustion phasing due to the reduced knocking probability. Furthermore, the exhaust gas temperature was reduced by 190 °C. EGR is therefore an effective means to limit the exhaust gas temperature and to reduce the thermal strain of critical engine components.

Early and late Miller valve timing further increased the net indicated efficiency by up to 0.4 $\%_{\mathrm{Pt.}}$ during part load operation due to a reduction of the volumetric efficiency which leads to dethrottling of the engine. At full load operation the charge temperature close to TDC could be reduced by up to 28 °C which influences knocking and the wall heat losses positively. The effect on the gas exchange remained small at full load operation.

Finally, cam phasing in combination with early Miller valve lift profiles and EGR led to a significant increase in fuel efficiency during part load operation. The net indicated efficiency was raised by 1.4 $\%_{\mathrm{Pt.}}$ at BMEP = 3 bar due to a dethrottling of the engine. The efficiency gain decreases with increasing load. At full load operation the effects were minor due to the small engine speed range of heavy duty engines. The gas dynamics thus do not differ as strongly as they do in passenger car engines, which reduces the effect of variabilities.

In overall terms the 1D simulations performed verified that the target of 10 % higher torque is achieved by the utilisation of a suitable turbocharger. Furthermore, the simulations confirmed that the introduced technologies (EGR, Miller timing and cam phasing) provide significant leverage for increased fuel efficiency. Their deployment in future heavy duty NG engines is thus recommended. In the important part load operating point relevant for highway driving the net indicated efficiency was raised by 3 $\%_{\mathrm{Pt.}}$ which corresponds to a reduction in specific fuel consumption of 7.2 %. At full load operation the net indicated efficiency was raised by up to 3.4 $\%_{\mathrm{Pt.}}$ which is equivalent to a a reduction in specific fuel consumption of 8.4 %. The final assessment if the target of a 10 % reduction in GHG emissions in the WHTC is achieved needs to be performed on the engine test bench since it is not possible to evaluate all technologies and effects by means of 1D simulations and the WHTC includes a wider range of load points.

In conclusion, this work demonstrates that NG is a viable and attractive option to reduce the tank-to-wheel CO_2 emission of vehicles in the short and medium-term until renewable energy sources become available on a large scale.

Bibliography

[1] Ardey, N., Stütz, W., Hiemesch, D., Kaufmann, M., "Die neuen Drei- und Vierzylinder-Dieselmotoren von BMW", MTZ – Motortechnische Zeitschrift, vol. 75, issue 7, 2014, doi:10.1007/s35146-014-0386-5

[2] Arnberger, A., Andersen, J., Wieser, K., Schreier, H., "Combustion concepts for commercial gas engines with highest efficiency", 10th Int. MTZ Conference – Heavy-Duty-, On- and Off-Highway Engines, Speyer, 2015

[3] Balzer, C., Kofod, M., Koot, M., Wilbrand, K., "Natural gas for cleaner mobility", 4th International Engine Congress, Baden-Baden, 2017

[4] Bank, R., Etzien, U., Buchholz, B., Harndorf, H., "Methane Catalysts at an Upstream Turbine Position", MTZ industrial, vol. 5, issue 1, 2015, doi:10.1007/s40353-015-0503-z

[5] Baratta, M., Spessa, E., Mairone, P., "Numerical investigation of turbolag reduction in HD CNG engines by means of exhaust valve variable actuation and spark timing control", Int. Journal of Automotive Technology, vol. 11, issue 3, 2010, doi:10.1007/s12239-010-0037-x

[6] Baratta, M., Rapetto, N., Spessa, E., Fuerhapter, A., et al., "Numerical and Experimental Analysis of Mixture Formation and Performance in a Direct Injection CNG Engine", SAE Technical Paper, 2012-01-0401, 2012, doi:10.4271/2012-01-0401

[7] Baratta, M., Misul, D., Xu, J., Fuerhapter, A., et al., "Development of a High Performance Natural Gas Engine with Direct Gas Injection and Variable Valve Actuation," SAE Int. Journal of Engines, vol. 10, issue 5, 2017, doi:10.4271/2017-24-0152

[8] Barba, C., Dyckmans, J., Förster, J., Schnekenburger, T., "Natural gas-Diesel dual fuel for commercial vehicle engines", 4th International Engine Congress, Baden-Baden, 2017

[9] Baretzky, U., Pfeffer, T., Kuntz, P., Ullrich, W., "Optimierte Entwicklungsmethode zur Verbesserung der Gemischaufbereitung für den Audi R8 FSI® Motor für Le Mans", 25th International Vienna Motor Symposium, Vienna, 2004

[10] Barnstedt, D., Eichlseder, H., Schaffer, K., Fasch, S., et al., "Entwicklung eines Wasserstoff/Diesel DualFuel-Motors für den Einsatz in Nahverkehrs-Nutzfahrzeugen", 10th Conference on Gas-Powered Vehicles, Stuttgart, 2015

[11] Bartholomew, C. H., Farrauto, R. J., "Fundamentals of industrial catalytic processes", John Wiley & Sons, 2006, ISBN 978-0-471-45713-8

[12] van Basshuysen, R. (ed.), "Erdgas und erneuerbares Methan für den Fahrzeugantrieb", Springer Vieweg, 2015, ISBN 978-3-658-07158-5

[13] Besch, M. C., Israel, J., Thiruvengadam, A., Kappanna, H., et al., "Emissions Characterization from Different Technology Heavy-Duty Engines Retrofitted for CNG/Diesel Dual-Fuel Operation", SAE Int. Journal of Engines, vol. 8, issue 3, 2015, doi:10.4271/2015-01-1085

[14] Boden, T. A., Marland, G., Andres, R. J., "Global, Regional, and National Fossil-Fuel CO_2 Emissions",Carbon Dioxide Information Analysis Center, Oak Ridge, 2016, doi:10.3334/CDIAC/00001_V2016

[15] Boßdorf-Zimmer, B., Krinke, S., Lösche-ter Horst, T., "Die Well-to-Wheel-Analyse Umwelteigenschaften mess- und planbar machen", MTZ – Motortechnische Zeitschrift, vol. 73, issue 2, 2012

[16] Boulouchos, K., "IC-Engines and Propulsion Systems II", Lecture Notes, ETH Zürich, Zurich, 2013

[17] Bourhis, G., Solari, J.-P., Dauphin, R., De Francqueville, L., "Fuel Properties and Engine Injection Configuration Effects on the Octane on Demand Concept for a Dual-Fuel Turbocharged Spark Ignition Engine", SAE Technical Paper, 2016-01-2307, 2016, doi:10.4271/2016-01-2307

[18] Bundesamt für Energie, "Energieetikette für Personenwagen: Umweltkennwerte 2016 der Strom- und Treibstoffbereitstellung", Bern, 2017

[19] Cerbe, G., Lendt, B. (eds.), "Grundlagen der Gastechnik", Hanser, 2016, ISBN 978-3-446-44965-7

[20] Demmelbauer-Ebner, W., Andersen, J., Mangold, R., "CNG as ideal supplement to e-traction aiming at CO_2-neutral mobility?", 4th International Engine Congress, Baden-Baden, 2017

[21] De Ojeda, W., "Effect of Variable Valve Timing on Diesel Combustion Characteristics," SAE Technical Paper, 2010-01-1124, 2010, doi:10.4271/2010-01-1124

[22] Deutsches Institut für Normung, "Automotive fuels – Compressed natural gas – Requirements and test methods", DIN standard, 51624, 2008

[23] Di Blasio, G., Belgiorno, G., Beatrice, C., Fraioli, V., et al., "Experimental Evaluation of Compression Ratio Influence on the Performance of a Dual-Fuel Methane-Diesel Light-Duty Engine", SAE Int. Journal of Engines, vol. 8, issue 5, 2015, doi:10.4271/2015-24-2460

[24] Dingelstadt, R., Ewert, S., Werz, M., Tremble, P., "Potenziale der Abgasrückführung beim Ottomotor", MTZ – Motortechnische Zeitschrift, vol. 75, issue 9, 2014, doi:10.1007/s35146-014-0510-6

[25] Dronniou, N., Kashdan, J., Lecointe, B., Sauve, K., et al., "Optical Investigation of Dual-fuel CNG/Diesel Combustion Strategies to Reduce CO_2 Emissions", SAE Int. Journal of Engines, vol. 7, issue 2, 2014, doi:10.4271/2014-01-1313

[26] Duchaussoy, Y., Lefebvre, A., Bonetto, R., "Dilution Interest on Turbocharged SI Engine Combustion", SAE Technical Paper, 2003-01-0629, 2003, doi:10.4271/2003-01-0629

[27] Edenhofer, O., Pichs-Madruga, R., Sokona, Y., Minx, J. C., et al. (eds.), "Climate Change 2014: Mitigation of Climate Change. Contribution of Working Group III to the Fifth Assessment Report of the Intergovernmental Panel on Climate Change", Cambridge University Press, 2014, ISBN 978-1-107-05821-7

[28] Edwards, S. P., Frankle, G. R., Wirbeleit, F., Raab, A., "The Potential of a Combined Miller Cycle and Internal EGR Engine for Future Heavy Duty Truck Applications," SAE Technical Paper, 980180, 1998, doi:10.4271/980180

[29] Eichlseder, H., Schaffer, K., Leitner, D., Klell, M., et al., "Potential of Synergies in a Vehicle for Variable Mixtures of CNG and Hydrogen", SAE Technical Paper, 2009-01-1420, 2009, doi:10.4271/2009-01-1420

[30] Eichlseder, H., Klüting, M., Piock, W. F., "Grundlagen und Technologien des Ottomotors", Springer Wien, 2008, doi:10.1007/978-3-211-47104-3

[31] Eichlseder, H., Grabner, P., Hadl, K., Hepp, C.,et al., "Dual-Fuel-Konzepte für mobile Anwendungen", 34th International Vienna Motor Symposium, Vienna, 2013

[32] European Committee for Standardization, "Gas infrastructure - Quality of gas - Group H", EN standard, 16726:2015, 2015

[33] European Environment Agency, "Monitoring of CO2 emissions from passenger cars – Regulation 443/2009", https://www.eea.europa.eu/data-and-maps/data/co2-cars-emission-11, 2016, accessed on 27.2.2017

[34] European Environment Agency, "Monitoring CO_2 emissions from new passenger cars and vans in 2015", EEA report 27/2016, 2016, doi:10.2800/85593

[35] European Parliament, "Regulation (EC) No 443/2009 of the European Parliament and of the Council of 23 April 2009 setting emission performance standards for new passenger cars as part of the Community's integrated approach to reduce CO_2 emissions from light-duty vehicles", EU regulation, 443/2009, 2009

[36] Fasching, P., Sprenger, F., Eichlseder, H., "Experimental Optimization of a Small Bore Natural Gas-Diesel Dual Fuel Engine with Direct Fuel Injection," SAE Int. Journal of Engines, vol. 9, issue 2, 2016, doi:10.4271/2016-01-0783

[37] Fasching, P., Sprenger, F., Granitz, C., "A holistic investigation of natural gas-diesel dual fuel combustion with dual direct injection for passenger car applications", Automotive and Engine Technology, 2017, doi:10.1007/s41104-017-0018-4

[38] Fasching, P., Sprenger, F., Preuhs, J. F., Hoffmann, G., et al., "The challenges of natural gas direct injection and its application to a natural gas-diesel dual-fuel concept", 16th Symposium – The Working Process of the Internal Combustion Engine, Graz, 2017

[39] Figer, G., Seitz, H. F., Graf, G., Schreier, H., "Nutzfahrzeug-Gasmotoren mit Dieseleffizienz", MTZ – Motortechnische Zeitschrift, vol. 75, issue 10, 2014, doi:10.1007/s35146-014-0573-4

[40] Flierl, R., Temp, A., Wegmann, A., Barrois, A., et al., "Simultane Verbrennung – Methan-Benzin- und Methan-Diesel-Mischbetrieb", MTZ – Motortechnische Zeitschrift, vol. 72, issue 10, 2011, doi:10.1365/s35146-011-0175-3

[41] Florea, R., Neely, G. D., Abidin, Z., Miwa, J., "Efficiency and Emissions Characteristics of Partially Premixed Dual-Fuel Combustion by Co-Direct Injection of NG and Diesel Fuel (DI^2)" SAE Technical Paper, 2016-01-0779, 2016, doi:10.4271/2016-01-0779

[42] Friedrich, W., Grzeszik, R., Wensing, M., "Mixture Formation in a CNG-DI Engine in Stratified Operation", SAE Technical Paper, 2015-24-2474, 2015, doi:10.4271/2015-24-2474

[43] Fürhapter, A., Certic, M., Philipp, H., Rössler K., et al.,"Potential of CNG Direct Injection for Passenger Car Propulsion", 5th Conference on Gas-Powered Vehicles, Berlin, 2010

[44] Garcia, P., Tunestal, P., "Experimental Investigation on CNG-Diesel Combustion Modes under Highly Diluted Conditions on a Light Duty Diesel Engine with Focus on Injection Strategy", SAE Int. Journal of Engines, vol. 8, issue 5, 2015, doi:10.4271/2015-24-2439

[45] Garcia Valladolid, P., Tunestal, P., "Effects of Intake Manifold Conditions on Dual-Fuel CNG-Diesel Combustion in a Light Duty Diesel Engine Operated at Low Loads", SAE Technical Paper, 2016-01-0805, 2016, doi:10.4271/2016-01-0805

[46] Geiger, J., Umierski, M., Simm, P., Heuser, P., "Der Erdgasmotor als Nutzfahrzeugantrieb – Trends und Herausforderungen bei der Entwicklung", 8th Conference on Gas-Powered Vehicles, Stuttgart, 2013

[47] Getzlaff, J., "Erdgas als Kraftstoff für Kfz-Verbrennungsmotoren", Habilitation treatise, Brandenburgische Technische Universität Cottbus-Senftenberg, Cottbus, 2005

[48] Gremminger, A., Deutschmann, O., Grunwaldt, J.-D., "Untersuchung der Wirkmechanismen bei katalytischer Methanreduktion", FVV-Frühjahrstagung, Heft R566, Projekt 1134, Magdeburg, 2014

[49] Hall, C. M., Sevik, J., Pamminger, M., Wallner, T., "Hydrocarbon Speciation in Blended Gasoline-Natural Gas Operation on a Spark-Ignition Engine", SAE Technical Paper, 2016-01-2169, 2016, doi:10.4271/2016-01-2169

[50] Hall, J., Bassett, M., Hibberd, B., Streng, S., "Heavily Downsized Demonstrator Engine Optimised for CNG Operation", SAE Int. Journal of Engines, vol. 9, issue 4, 2016, doi:10.4271/2016-01-2363

[51] Harrington, J., Munshi, S., Nedelcu, C., Ouellette, P., et al., "Direct Injection of Natural Gas in a Heavy-Duty Diesel Engine", SAE Technical Paper, 2002-01-1630, 2002, doi:10.4271/2002-01-1630

[52] Haslacher, R., "Entwicklung optischer Messverfahren zur Analyse von Brennverfahren für PKW-Gasmotoren", Phd thesis, Technische Universität Graz, Graz, 2011

[53] Hepp, C., Krenn, M., Wasserbauer, J., Eichlseder, H., "Dual Fuel Compression Ignition Combustion Concept for Gasoline and Diesel", SAE Technical Paper, 2014-01-1319, 2014, doi:10.4271/2014-01-1319

[54] Heuser, B., Kremer, F., Pischinger, S., Rohs, H., et al., "An Experimental Investigation of Dual-Fuel Combustion in a Light Duty Diesel Engine by In-Cylinder Blending of Ethanol and Diesel", SAE Int. Journal of Engines, vol. 9, issue 1, 2016, doi:10.4271/2015-01-1801

[55] Heywood, J. B., "Internal Combustion Engine Fundamentals", McGraw-Hill, 1988, ISBN 0-07-100499-8

[56] Hirose, I., "Mazda 2.5L SKYACTIV-G Engine with New Boosting Technology", 37th International Vienna Motor Symposium, Vienna, 2016

[57] Hoffmann, K., Benz, M., Weirich, M., Herrmann, H.-O., "Der neue Erdgasmotor für mittelschwere NFZ von Mercedes-Benz", MTZ – Motortechnische Zeitschrift, vol. 75, issue 11, 2014, doi:10.1007/s35146-014-0569-0

[58] Hofherr, T., "Potenzialbetrachtung effizienzsteigender Maßnahmen sowie Abgasnachbehandlungsmöglichkeiten eines direkteinblasenden Erdgasmotors für die PKW-Anwedung", PhD thesis, Technische Universität Wien, Vienna, 2015

[59] Huber, K., "Der Wärmeübergang schnellaufender, direkt einspritzender Dieselmotoren", PhD thesis, Technische Universität München, Munich, 1990

[60] Husted, H. L., Karl, G., Schilling, S., Weber, C., "Direct Injection of CNG for Driving Performance with Low CO_2", 23rd Aachen Colloquium Automobile and Engine Technology, Aachen, 2014

[61] Hwang, I., Lee, H., Park, H., Hwang, K., et al., "Hyundai-Kia's Highly Innovative 1.6L GDI Engine for Hybrid Vehicle", 37th International Vienna Motor Symposium, Vienna, 2016

[62] IFA-Museum Nordhausen am Harz e.V., "Die 100-jährige Geschichte des IFA-Industrieparks Nordhausen", Website, http://www.ifa-museum-nordhausen.de/geschichte/motoren.php, accessed on 7.3.2017

[63] Ishiyama, T., Kang, J., Ozawa, Y., Sako, T., "Improvement of Performance and Reduction of Exhaust Emissions by Pilot-Fuel-Injection Control in a Lean-Burning Natural-Gas Dual-Fuel Engine", SAE Int. Journal of Fuels and Lubricants, vol. 5, issue 1, 2012, doi:10.4271/2011-01-1963

[64] Karch, M., Budack, R., Adam, S., Wurms, R., et al., "Der neue Audi 2.0l TFSI – Herausforderungen bei der Brennverfahrensentwicklung", 15th Symposium – The Working Process of the Internal Combustion Engine, Graz, 2015, ISBN 978-3-85125-425-9

[65] Karim, G. A., "Combustion in Gas Fueled Compression: Ignition Engines of the Dual Fuel Type", Journal of Eng. for Gas Turbines and Power, vol. 125, issue 3, 2003, doi:10.1115/1.1581894

[66] Keeling, C. D., Piper, S. C., Bacastow, R. B., Wahlen, M., et al., "Exchanges of Atmospheric CO_2 and $^{13}CO_2$ with the Terrestrial Biosphere and Oceans from 1978 to 2000. I. Global aspects", SIO Reference Series, no. 01-06, San Diego, 2001.

[67] Khosravi, M., Rochussen, J., Yeo, J., Kirchen, P., et al., "Effect of Fuelling Control Parameters on Combustion Characteristics of Diesel-Ignited Natural Gas Dual-Fuel Combustion in an Optical Engine", ASME 2016 Internal Combustion Engine Division Fall Technical Conference, ICEF2016-9399, Greenville, 2016, doi:10.1115/ICEF2016-9399

[68] Knorr, H., Weidner, M., Barciela, B., "Gekühlte Abgasrückführung bei aufgeladenen, stöchiometrisch betriebenen Erdgas-Nutzfahrzeugmotoren - ein Schlüssel zur Wirkungsgradsteigerung", 2nd International Engine Congress, Baden-Baden, 2015

[69] Koch, T., "Numerischer Beitrag zur Charakterisierung und Vorausberechnung der Gemischbildung und Verbrennung in einem direkteingespritzten, strahlgeführten Ottomotor", PhD thesis, ETH Zürich, Zurich, 2002

[70] Königsson, F., "Advancing the Limits of Dual Fuel Combustion", PhD thesis, Royal Institute of Technology, Stockholm, 2014, ISBN 978-91-7501-427-2

[71] Kraftfahrt-Bundesamt, "Fahrzeugzulassungen (FZ) – Neuzulassungen von Kraftfahrzeugen nach Umwelt-Merkmalen, Jahr 2015", FZ 14, Flensburg, 2016

[72] Kramer, U., Phlips, P., "Phasing Strategy for an Engine with Twin Variable Cam Timing", SAE Technical Paper, 2002-01-1101, 2002, doi:10.4271/2002-01-1101

[73] Krebs, R., Böhme, J., Dornhöfer, R., Wurms, R., et al., "Der neue Audi 2,0T FSI Motor – Der erste direkteinspritzende Turbo-Ottomotor bei Audi", 25th International Vienna Motor Symposium, Vienna, 2004

[74] Krenn, M., "Methoden für die thermodynamische Analyse und Simulation der Dual Fuel Verbrennung in Großmotoren", PhD thesis, Technische Universität Graz, Graz, 2015

[75] Kuzuoka, K., Kamio, J., Hashimoto, K., "Effect of Mixture Stratification and Fuel Reactivity on Dual-Fuel Compression Ignition Combustion Process for SI-Based Engine", SAE Technical Paper, 2016-01-2304, 2016, doi:10.4271/2016-01-2304

[76] Lämmle, C., "Numerical and Experimental Study of Flame Propagation and Knock in a Compressed Natural Gas Engine", PhD thesis, ETH Zürich, Zurich, 2005

[77] Lesche, F., "Iveco Stralis Natural Power in long-haul transport", 11th Conference on Gas-Powered Vehicles, Potsdam, 2016

[78] Li, Y., Zhao, H., Stansfield, P., Freeland, P., "Adaptation of a Dual Continuous Variable Cam Phasing System to a 4-Valve, 4-Cylinder Engine - Thermodynamic Benefits and Engine Hardware Requirements," SAE Technical Paper, 2006-01-0408, 2006, doi:10.4271/2006-01-0408

[79] Luef, R., Hadl, K., Eichlseder, H., "Experimentelle Untersuchungen von Erdgas-Diesel Brennverfahren an einem modernen PKW-Dieselmotor", 8. VDI-Tagung Innovative Fahrzeugantriebe, Dresden, 2012, ISBN 978-3-18-092183-9

[80] MacFarling Meure, C., Etheridge, D., Trudinger, C., Steele, P., et al., "Law Dome CO_2, CH_4 and N_2O ice core records extended to 2000 years BP", Geophysical Research Letters, vol. 33, issue 14, 2006, doi:10.1029/2006GL026152

[81] Magnusson, I., Manente, V., "Evaluation and optimisation of combustion concept for heavy duty gas engines", THIESEL 2012 – Conference on Thermo- and Fluid Dynamic Processes in Direct Injection Engines, Valencia, 2012,

[82] Mährle, W., Krauss, M., Luttermann, C., Klauer, N., "High Precision Injection in Verbindung mit Aufladung am neuen BMW Twin-Turbo-Ottomotor", MTZ – Motortechnische Zeitschrift, vol. 68, issue 4, 2007, doi:10.1007/BF03227396

[83] Manns, H. J., Brauer, M., Dyja, H., Beier, H., et al., "Diesel CNG - The Potential of a Dual Fuel Combustion Concept for Lower CO_2 and Emissions", SAE Technical Paper, 2015-26-0048, 2015, doi:10.4271/2015-26-0048

[84] Patychuk, B., Wu, N., McTaggart-Cowan, G., Hill, P., et al., "Intake and Exhaust Valve Timing Control on a Heavy-Duty, Direct-Injection Natural Gas Engine," SAE Technical, Paper 2015-01-0864, 2015, doi:10.4271/2015-01-0864

[85] May, I., Pedrozo, V., Zhao, H., Cairns, A., et al., "Characterization and Potential of Premixed Dual-Fuel Combustion in a Heavy Duty Natural Gas/Diesel Engine" SAE Technical Paper, 2016-01-0790, 2016, doi:10.4271/2016-01-0790

[86] McTaggart-Cowan, G., Mann, K., Huang, J., Singh, A., et al., "Direct Injection of Natural Gas at up to 600 Bar in a Pilot-Ignited Heavy-Duty Engine", SAE Int. Journal of Engines, vol. 8, issue 3, 2015, doi:10.4271/2015-01-0865

[87] Melaika, M., Dahlander, P., "Experimental Investigation of Methane Direct Injection with Stratified Charge Combustion in Optical SI Single Cylinder Engine", SAE Technical Paper, 2016-01-0797, 2016, doi:10.4271/2016-01-0797

[88] Neusser, H.-J., Szengel, R., Kirsch, U., Worm, J., "Der Neue Dreizylinder-Erdgasmotor von Volkswagen", MTZ – Motortechnische Zeitschrift, vol. 74, issue 4, 2013, doi:10.1007/s35146-013-0073-y

[89] Noah, U., "Using CNG and LNG in heavy commercial vehicles", 9th Conference on Gas-Powered Vehicles, Potsdam, 2014

[90] Ohta, Y., Fushiki, S., Matsuo, S., "The New PRIUS Powertrain: The New 1.8L ESTEC 2ZR-FXE Engine with the New Generation Hybrid System", 37th International Vienna Motor Symposium, Vienna, 2016

[91] Ott, T. M., "Hybrid-Electric Vehicle with Natural Gas-Diesel Engine", PhD thesis, ETH Zürich, Zurich, 2013

[92] Otten, R., "Mobility in times of the turnaround in energy policy – the Audi A4 Avant g-tron", 11th Conference on Gas-Powered Vehicles, Potsdam, 2016

[93] Ottinger, N., Veele, R., Xi, Y., Liu, Z. G., "Desulfation of Pd-based Oxidation Catalysts for Lean-burn Natural Gas and Dual-fuel Applications", SAE Int. Journal of Engines, vol. 8, issue 4, 2015, doi:10.4271/2015-01-0991

[94] Pachauri, R. K., Meyer, L. A. (eds.), "Climate Change 2014: Synthesis Report. Contribution of Working Groups I, II and III to the Fifth Assessment Report of the Intergovernmental Panel on Climate Change", Intergovernmental Panel on Climate Change, Geneva, 2015, ISBN 978-92-9169-143-2

[95] Pamminger, M., Sevik, J., Scarcelli, R., Wallner, T., et al., "Evaluation of Knock Behavior for Natural Gas - Gasoline Blends in a Light Duty Spark Ignited Engine", SAE Int. Journal of Engines, vol. 9, issue 4, 2016, doi:10.4271/2016-01-2293

[96] Pischinger, R., "Bombenversuche über Gasverbrennungen", Habilitation treatise, Technische Universität Graz, Graz, 1968

[97] Pischinger, R., Klell, M., Sams, T., "Thermodynamik der Verbrennungskraftmaschine", Springer Wien, 2009, ISBN 978-3211-99276-0

[98] Poepperl, M., Hedrich, G., Heusler, H., Koehler, D., et al., "Adaptation of a Dual Continuous Variable Cam Phasing System to a 4-Valve, 4-Cylinder Engine - Thermodynamic Benefits and Engine Hardware Requirements," SAE Technical Paper, 2006-01-0408, 2006, doi:10.4271/2006-01-0408

[99] Rinkens, T., Biwer, C., Geiger, J., "Safeguarding the reliability of natural gas engines for commercial vehicles", 3rd International Engine Congress, Baden-Baden, 2016

[100] Rochussen, J., Yeo, J., Kirchen, P., "Effect of Fueling Control Parameters on Combustion and Emissions Characteristics of Diesel-Ignited Methane Dual-Fuel Combustion", SAE Technical Paper, 2016-01-0792, 2016, doi:10.4271/2016-01-0792

[101] Rood Werpy, M., Santini, D., Burnham, A., Mintz, M., "Natural Gas Vehicles: Status, Barriers, and Opportunities", Argonne National Laboratory, Report ANL/ESD/10-4, 2010

[102] Rößler, K., Otto, F., Preuhs, J.-F., Farah, P., "Direct Injection of Natural Gas for Passenger Cars – Prospects and Challenges", 7th Conference on Gas-Powered Vehicles, Potsdam, 2012

[103] Salaun, E., Apeloig, J., Grisch, F., Yvonnet, C.-E., et al., "Optical Investigation of Ignition Timing and Equivalence Ratio in Dual-Fuel CNG/Diesel Combustion", SAE Technical Paper, 2016-01-0772, 2016, doi:10.4271/2016-01-0772

[104] van Sambeek, J., "Diesel blend 2.0 – the Prins dual-fuel system", 9th Conference on Gas-Powered Vehicles, Potsdam, 2014

[105] Schlatter, S., "Experimental and Numerical Characterization of Enhanced Ignition Systems for Large Bore Gas Engines", PhD thesis, ETH Zürich, Zurich, 2015

[106] Schutting, E., Neureiter, A., Fuchs, C., Schatzberger, T., et al., "Miller- und Atkinson-Zyklus am aufgeladenen Dieselmotor", MTZ – Motortechnische Zeitschrift, vol. 68, issue 6, 2007, doi:10.1007/BF03227416

[107] Schutting, E., Dumböck, O., Kraxner, T., Eichlseder, H., "Thermodynamic consideration of the Miller cycle on the basis of simulation and measurements", 3rd International Engine Congress, Baden-Baden, 2016

[108] Seboldt, D., "Untersuchungen zum Potenzial der CNG-Direkteinblasung zur Reduktion von HC-Emissionen in Gasmotoren", Phd thesis, Universität Stuttgart, 2017, doi:10.1007/978-3-658-17906-9

[109] Serrano, D., Obiols, J., Lecointe, B., "Optimization of Dual Fuel Diesel-Methane Operation on a Production Passenger Car Engine - Thermodynamic Analysis", SAE Technical Paper, 2013-01-2505, 2013, doi:10.4271/2013-01-2505

[110] Sevik, J., Pamminger, M., Wallner, T., Scarcelli, R., et al., "Performance, Efficiency and Emissions Assessment of Natural Gas Direct Injection compared to Gasoline and Natural Gas Port-Fuel Injection in an Automotive Engine", SAE Int. Journal of Engines, vol. 9, issue 2, 2016, doi:10.4271/2016-01-0806

[111] Singh, A., Anderson, D., Hoffman, M., Filipi, Z. et al., "An Evaluation of Knock Determination Techniques for Diesel-Natural Gas Dual Fuel Engines", SAE Technical Paper, 2014-01-2695, 2014, doi:10.4271/2014-01-2695

[112] Smaling, R., Mohr, D., Eckroth, D., Desai, A., et al., "Development of an On-Road Heavy Duty Natural Gas Engine", 37th International Vienna Motor Symposium, Vienna, 2016

[113] Sprenger, F., Fasching, P., Kammerstätter, S., "Experimentelle Untersuchung von Erdgas-Diesel Brennverfahren mit äußerer und innerer Gemischbildung für Pkw-Anwendungen", 15th Symposium – The Working Process of the Internal Combustion Engine, Graz, 2015, ISBN 978-3-85125-425-9

[114] Sprenger, F., Fasching, P., Eichlseder, H., "Erdgas-Diesel Dual-Direct-Injection – Ein alternatives Brennverfahren zur signifikanten CO_2-Reduzierung", 10. Tagung Diesel- und Benzindirekteinspritzung 2016, Berlin, 2016, ISBN 978-3-658-15327-4

[115] Sprenger, F., "Entwicklung eines Erdgas-Diesel Dual-Fuel-Brennverfahrens zur signifikanten CO_2-Reduktion bei Pkw-Motoren", PhD thesis, Technische Universität Graz, Graz, 2017

[116] Stålhammar, P., Erlandsson, L., Willner, K., Johannesson, S., "Demonstration och utvärdering av dual-fuel-tekniken", Swedish Gas Technology Centre – SGC, Report SGC 233, Malmö, 2011, isrn:SGC-R-233-SE

[117] Steinert, R., Prümm, W., Köllner, O., "MAN EURO VI Gas Engines for Commercial Vehicles", 7th Conference on Gas-Powered Vehicles, Potsdam, 2012

[118] Steinparzer, F., Klauer, N., Kannenberg, D., Unger, H., "Der Neue Aufgeladene 2,0-l-Vierzylinder-Ottomotor von BMW", MTZ – Motortechnische Zeitschrift, vol. 72, issue 12, 2011, doi:10.1365/s35146-011-0202-4

[119] Streng, S., Wieske. P., Warth, M., Hall, J., "Monovalenter Erdgasbetrieb und Downsizing für niedrigste CO_2-Emissionen", MTZ – Motortechnische Zeitschrift, vol. 77, issue 7-8, 2016, doi:10.1007/s35146-016-0069-5

[120] Suzuki, Y., Tsujimura, T., Mita, T., "The Performance of Multi-Cylinder Hydrogen / Diesel Dual Fuel Engine", SAE Int. Journal of Engines, vol. 8, issue 5, 2015, doi:10.4271/2015-24-2458

[121] Takaki, D., Tsuchida, H., Kobara, T., Akagi, M., et al., "Study of an EGR System for Downsizing Turbocharged Gasoline Engine to Improve Fuel Economy", SAE Technical Paper, 2014-01-1199, 2014, doi:10.4271/2014-01-1199

[122] Takasaki, K., Imhof, D., Ishibashi, R., Tsuru, D., et al., "Fundamental Study on GI (Natural Gas High-Pressure Injection) Combustion with Visualization Method", 14th Symposium – The Working Process of the Internal Combustion Engine, Graz, 2013, ISBN 978-3-85125-295-8

[123] Taniguchi, S., Masubuchi, M., Kitano, K., Mogi, K., "Feasibility Study of Exhaust Emissions in a Natural Gas Diesel Dual Fuel (DDF) Engine", SAE Technical Paper, 2012-01-1649, 2012, doi:10.4271/2012-01-1649

[124] Troberg, M., Portin, K., Jarvi, A., "Update on Wärtsilä 4-stroke Gas Product Development", 27th CIMAC World Congress, paper no. 406, Shanghai, 2013

[125] Tsuru, D., Kikunaga, S., Koga, T., Takasaki, K., et al., "Application of large-sized RCEM to a study on combustion in dual fuel gas engine operation", 4th Rostock Large Engine Symposium, Rostock, 2016

[126] Umetrics AB, "Modde v9.1", User manual, 2011

[127] United Nations Framework Covention on Climate Change, "The Paris Agreement", http://unfccc.int/paris_agreement/items/9485.php, accessed on 27.2.2017

[128] Unitrove Limited, "Gas Calculation Tools", http://unitrove.com/engineering/tools/gas, accessed on: 12.7.2017

[129] U.S. Department of Energy, "Alternative Fuels Data Center", http://www.afdc.energy.gov/fuels/prices.html, accessed on: 27.2.2017

[130] Volvo Group, "Volvo Trucks first to market gas-powered truck for long-haul operations", press release, Gothenburg, 31.5.2011

[131] Weisheit, P., "Natural Gas Strategy at Volkswagen", 9th Conference on Gas-Powered Vehicles, Potsdam, 2014

[132] Willems, W., Kramer, U., Maas, H., "Alternative fuels of today for sustainable mobility of tomorrow", 4th International Engine Congress, Baden-Baden, 2017

[133] Woschni, G., "Einfluß von Rußablagerungen auf den Wärmeübergang zwischen Arbeitsgas und Wand im Dieselmotor", 3rd Symposium – The Working Process of the Internal Combustion Engine, Graz, 1991

[134] Wunderlich, K., Merdes, N., Waltner, A., Vent, G., et al., "The New Mercedes-Benz CNG Engine Generation as Part of the BlueDIRECT Engine Family M270/M274", 22nd Aachen Colloquium Automobile and Engine Technology, Aachen, 2013

[135] Yeo, J., Rochussen, J., Kirchen, P., "Application of an In-Cylinder Local Infrared Absorption Fuel Concentration Sensor in a Diesel-Ignited Dual-Fuel Engine", SAE Technical Paper, 2016-01-2310, 2016, doi:10.4271/2016-01-2310

[136] Zaccardi, J.-M., Serrano, D., "A Comparative Low Speed Pre-Ignition (LSPI) Study in Downsized SI Gasoline and CI Diesel-Methane Dual Fuel Engines", SAE Int. Journal of Engines, vol. 7, issue 4, 2014, doi:10.4271/2014-01-2688

[137] Zhang, H., Chiu, J., Bartel, J., "Late Intake Valve Closing with Throttle Control at Light Loads for a Lean-Burn Natural Gas Engine", SAE Technical Paper, 1999-01-3485, 1999, doi:10.4271/1999-01-3485

[138] Zoldak, P., Sobiesiak, A., Wickman, D., Bergin, M., "Combustion Simulation of Dual Fuel CNG Engine Using Direct Injection of Natural Gas and Diesel", SAE Int. Journal of Engines, vol. 8, issue 2, 2015, doi:10.4271/2015-01-0851

Appendix

A Test Bench Facilities

A.1 Measurement Devices

- **Engine torque transducer:** HBM T40B; $M = \pm 1\,kNm$
- **Indicating system:**
  - **Crank angle encoder:** AVL 365C
  - **Cylinder pressure transducers:** Piezoelectric relative pressure sensors AVL GH14DK and AVL GH13G; Pressure range: 250 bar
  - **Intake pressure transducer:** Piezoresistive absolute pressure sensor Kistler 4045A5; Pressure range: 0 bar...5 bar
  - **Exhaust pressure transducer:** Piezoelectric relative pressure sensors AVL GU21C (cooled)
  - **Charge amplifier:** AVL MicroIFEM
  - **Data acquisition:** AVL IndiSet Advanced, Type 642
  - **Quartz cooling system:** AVL ZP 91.00/1-4
- **Exhaust gas measurement:**
  - **Air-fuel equivalence ratio:** ETAS Lambda meter LA4
  - **Particulate matter:** AVL Smoke meter 415S
  - **Exhaust gas analysers:**
    - AVL SESAM i60 FT:
      - FTIR: Thermo Fisher Scientific Antaris IGS for CH_4, NO_x, CO, etc.
      - FID: AVL FID i60 HH for THC
      - IRD and PMD: AVL COMBI i60 CO_2/O_2 for O_2 and CO_2 in the intake manifold
    - AVL Emission bench CEB II:
      - CLD: ECO PHYSICS CLD 700 RE ht for NO_x
      - FID: ABB Multi-FID 14 EGA for THC
      - NDIR: ABB Advance Optima Uras 14 EGA for CO and CO_2
      - PMD: ABB Advance Optima Magnos 16 EGA for O_2

- **Fuel mass flow measurement:**
  - Diesel: Emerson Micro Motion Coriolis Flow Sensor CMFS010M
  - CNG: Emerson Micro Motion Coriolis Flow Sensor CMF010P
- **Blow-by measurement device:** AVL Blow By Meter 442
- **Pressure transducers:** Absolute and relative pressure transducers with different measurement range PMA P30 and P40
- **Temperature measurement:** Type K thermocouples and PT100 resistance thermometers
- **Gas Chromatograph:** Daniel Danalyzer Model 2350

A.2 Infrastructure

- **Coolant conditioning:** Coolant conditioning unit AVL 553
- **Oil conditioning:** Oil conditioning unit AVL 554
- **Boost air conditioning:** In-house development
- **NG injector control:** AVL Engine Timing Unit 427
- **NG injector driver:** Hoerbiger Provebo

B Application Parameters

Here the associated application parameters are given of the measurements as given in Section 4.5.2, 4.5.4, 4.5.5 and 4.5.6.

Table B.1: The application parameters for the optimised operation with the standard compression ratio of $\varepsilon = 16.5$.

Load point	1500/3	1750/5		2000/11
Optimisation criterion	$\Delta\zeta_{\mathrm{IC}}$ & NO_x	$\Delta\zeta_{\mathrm{IC}}$	$\Delta\zeta_{\mathrm{IC}}$ & NO_x	η_{e}
m_{Diesel} / mg	2.3	2.3	2.3	2.1
x_{NG} / %	79	85	86	94
$\mathrm{SOI}_{\mathrm{NG}}$ / °CA	–70	–80	–80	–300
$\mathrm{SOI}_{\mathrm{Diesel}}$ / °CA	–14.7	–11.6	–23.7	–11.7
p_{Diesel} / bar	800	800	400	400
p_{NG} / bar	16	16	16	16
p_{intake} / mbar	1000	1000	1200	1200
Swirl flap / % 0 %...fully open	55	70	50	0
EGR / %	43	22	40	0
EGR cooler bypassed	yes	yes	no	–
MFB50 / °CA	7.5	6.0	7.0	7.0
$\lambda_{\mathrm{global}}$ / –	1.64	1.55	1.37	1.05
λ_{NG} / –	2.09	1.81	1.59	1.12

Table B.2: The application parameters for the operation with a reduced compression ratio of $\varepsilon = 14.5$.

Load point	1500/3	2000/11
Optimisation criterion	$\Delta\zeta_{\mathrm{IC}}$ & NO_x	–
m_{Diesel} / mg	4.2	1.9
x_{NG} / %	64	95
$\mathrm{SOI}_{\mathrm{NG}}$ / °CA	–100	–300
$\mathrm{SOI}_{\mathrm{Diesel}}$ / °CA	–21.8	–14.6
p_{Diesel} / bar	400	400
p_{NG} / bar	16	16
p_{intake} / mbar	1000	1250
Swirl flap / % 0 %...fully open	40	0
EGR / %	40	0
EGR cooler bypassed	yes	–
MFB50 / °CA	12.5	7.0
$\lambda_{\mathrm{global}}$ / –	1.60	1.03
λ_{NG} / –	2.44	1.07

Table B.3: The application parameters for the comparison of spark ignition and DDI combustion with a compression ratio of $\varepsilon = 14.5$.

Load point	1750/5		2000/11	
Operating mode	CNG DI SI	DDI	CNG DI SI	DDI
Optimisation criterion	η_e	η_e & NO_x	η_e	η_e
m_{Diesel} / mg	0	3.4	0	2.2
x_{NG} / %	100	80	100	94
SOI_{NG} / °CA	–300	–75	–340	–300
SOI_{Diesel} / °CA	–	–15.8	–	–10.7
Spark timing / °CA	–29.5	–	–15	–
p_{Diesel} / bar	–	400	–	400
p_{NG} / bar	16	16	16	16
p_{intake} / mbar	730	1200	1300	1275
Swirl flap / % 0 %...fully open	20	30	50	30
EGR / %	5	37	0	0
EGR cooler bypassed	yes	yes	–	–
MFB50 / °CA	9.5	12.5	11	12
λ_{global} / –	1.02	1.31	1.02	1.06
λ_{NG} / –	1.02	1.63	1.02	1.13

Table B.4: The application parameters of conventional dual fuel combustion with PFI of natural gas and a compression ratio of $\varepsilon = 16.5$.

Load point	1500/3	2000/11
Optimisation criterion	$\Delta\zeta_{\mathrm{IC}}$ & NO_x	η_{e}
m_{Diesel} / mg	2.5	2.7
x_{NG} / %	79	92
$\mathrm{SOI}_{\mathrm{NG}}$ / °CA	–360	–360
$\mathrm{SOI}_{\mathrm{Diesel}}$ / °CA	–15.2	–8.8
p_{Diesel} / bar	400	400
p_{NG} / bar	8	8
p_{intake} / mbar	1000	1180
Swirl flap / % 0 %...fully open	55	0
EGR / %	39	0
EGR cooler bypassed	yes	–
MFB50 / °CA	9.3	8.2
$\lambda_{\mathrm{global}}$ / –	1.55	1.05
λ_{NG} / –	1.94	1.14

C Crank Angle Resolved Simulation Results

Here additional crank angle resolved simulation results are presented, which aid the perception of the correlations discussed in Section 5.4.3.

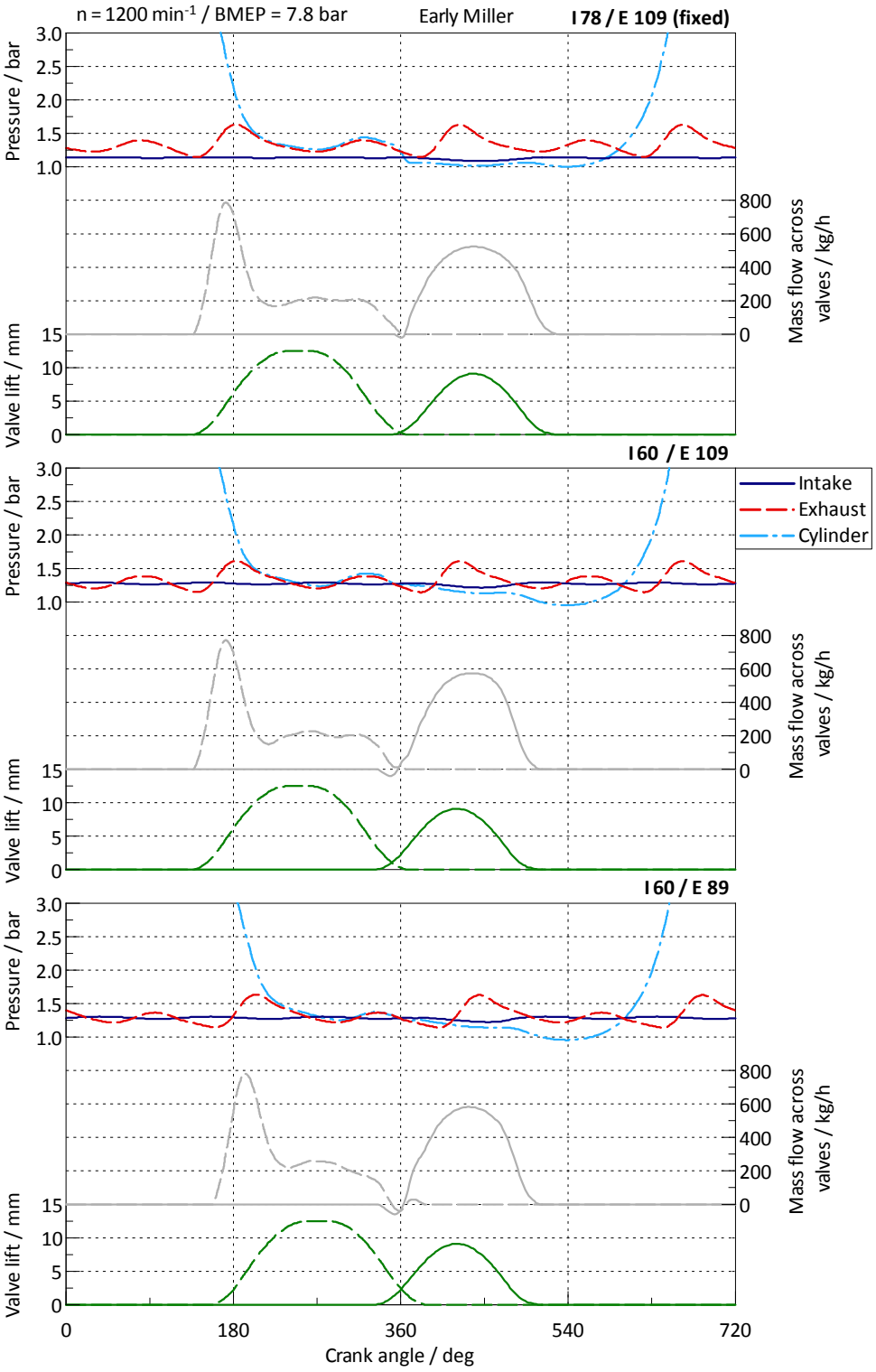

Figure C.1: Crank angle resolved simulation results with the early Miller cam profile and three combinations of cam phasing angles in the load point $n = 1200\,min^{-1}$ / BMEP = 7.8 bar.

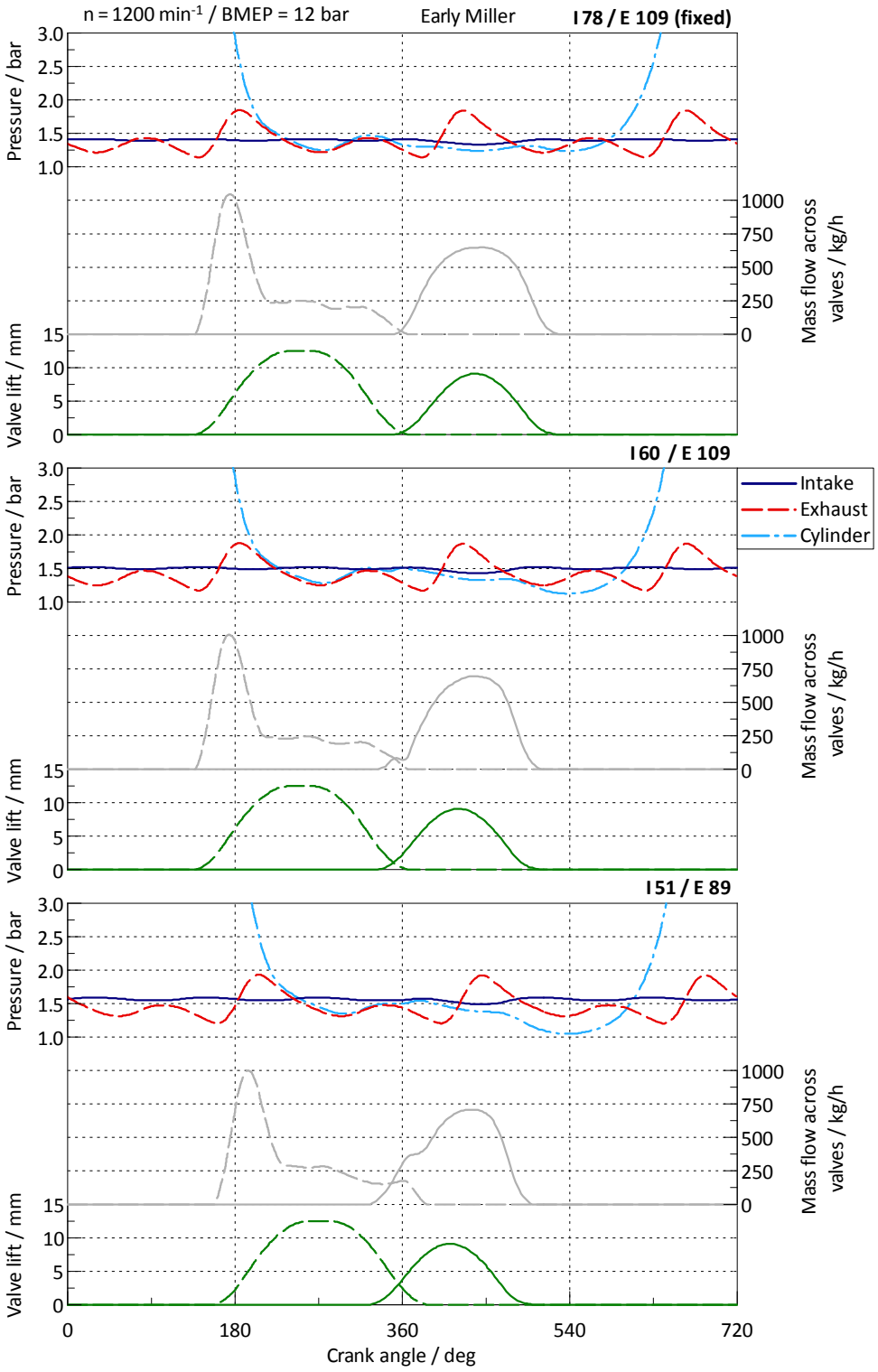

Figure C.2: Crank angle resolved data of simulations with the early Miller cam profile and three different combinations of cam phasing angles in the load point n = 1200 min^{-1} / BMEP = 12 bar.

D List of Publications

- Sept. 2017: Fasching, P., Sprenger, F., Preuhs, J. F., Hoffmann, G., Piock, W. F., "The challenges of natural gas direct injection and its application to a natural gas-diesel dual-fuel concept", 16th Symposium – The Working Process of the Internal Combustion Engine, Graz, 2017
- Sept. 2017: Golini, S., Fasching, P., Hasenbichler, G., Arnberger, A., "Natural Gas Engines for Long-Haulage Applications: Current Approach and Future Developments", 16th Symposium – The Working Process of the Internal Combustion Engine, Graz
- July 2017: Fasching, P., Sprenger, F., Granitz, C., "A Holistic Investigation of Natural Gas-Diesel Dual Fuel Combustion with Dual Direct Injection for Passenger Car Applications", Automotive and Engine Technology, doi:10.1007/s41104-017-0018-4
- Dec. 2016: Fasching, P., "Development of a New Generation of Natural Gas engines for Heavy Duty Vehicles for CO_2-Reduction", Article in the annual report of the Institute of Internal Combustion Engines and Thermodynamics, Technische Universität Graz, Graz
- Nov. 2016: Sprenger, F., Fasching, P., Eichlseder, H., "Erdgas-Diesel Dual-Direct-Injection: Ein alternatives Brennverfahren zur signifikanten CO_2-Reduzierung", 10. Tagung Diesel- und Benzindirekteinspritzung, Berlin, ISBN 978-3-658-15327-4
- April 2016: Redtenbacher, C., Kiesling, C., Wimmer, A., Sprenger, F., Fasching, P., Eichlseder, H.,"Dual Fuel Brennverfahren - Ein zukunftsweisendes Konzept vom Pkw- bis zum Großmotorenbereich?", 36. Internationales Wiener Motorensymposium, Wien
- April 2016: Fasching, P., Sprenger, F., Eichlseder, H., "Experimental Optimization of a Small Bore Natural Gas-Diesel Dual Fuel Engine with Direct Fuel Injection", SAE Int. Journal of Engines, vol. 9, issue 2, 2016-01-0783, doi:10.4271/2016-01-0783
- Sept. 2015: Sprenger, F., Fasching, P., Kammerstätter, S., "Experimentelle Untersuchung von Erdgas-Diesel Brennverfahren mit äußerer und innerer Gemischbildung für Pkw-Anwendungen", 15th Symposium – The Working Process of the Internal Combustion Engine, Graz